Rewiring of proline metabolism through increased expression of mitochondrial pyrroline-5-carboxylate reductase sustains colorectal cancer.

Thesis submitted for the degree of
Doctor of Philosophy at the University of Leicester

By
Saif AL AQBI
BVM&S (Hons), MSc.Path.
Department of Cancer Studies and Molecular Medicine
University of Leicester

December 2018

Abstract

Rewiring of proline metabolism through increased expression of mitochondrial pyrroline-5-carboxylate reductase sustains colorectal cancer

Saif AL AQBI

Proline is non-essential amino acid and its metabolism has been linked to cancer progression. Pyrroline-5- carboxylate reductase (PYCR) enzymes catalyze the NAD(P)H-dependent conversion of the precursor pyrroline-5-carboxylate to proline. There are three PYCR isoforms mitochondrial PYCR1 and PYCR2, and cytosolic PYCRL. Analysis of colorectal cancer (CRC) datasets indicated that PYCR1is overexpressed in cancer compared to normal tissue and we could confirm robust expression of PYCR1 in numerous CRC cell lines. In addition, analysis of primary cells isolated from surgically resected cancers and scoring of tissue microarray (TMA) confirmed the robust increase in PYCR1 protein expression in both adenoma and cancer lesions. To investigate the functional meaning of the PYCR1 expression, we used siRNA technology. Knockdown of PYCR1 enzyme decreased cell number by reducing both cell proliferation and survival in a variety of CRC cell lines. Indeed, loss of PYCR1 protein enhanced expression of the cell cycle inhibitor p21 and substantially reduced expression of cyclin D1 and D3. Additionally, depletion of PYCR1 protein enhanced apoptosis that measured by AnnexinV/PI staining. Notably, the addition of proline was unable to compensate for PYCR1-deficiency, indicating that production of proline is not responsible for the pro-tumorigenic activity of PYCR1.

In summary, our findings indicate that proline metabolism is necessary to sustain colorectal carcinogenesis and that PYCR1 is a potential target for anti-cancer therapies.

Acknowledgement

This thesis is the culmination of both personal and professional challenges I have overcome with the help of many wonderful individuals whom I have encountered throughout my journey. Firstly, I would like to express my deepest gratitude to my supervisors, Dr Alessandro Rufini and Professor Karen Brown, for all their guidance and help that have made this project a reality. Moreover, my great appreciation is extended to Dr Mafalda Pires Damaso, Dr Hong Cai, Dr Ni Ni Moe Myint, Dr. Jennifer Higgins and Dr Salim F. Kadhim for their contributions to the successful completion of the preclinical studies. I am also thankful to Dr Peter Greaves and Dr Kevin West for their help with the pathological assessment of samples. Additionally, I would like to offer my appreciation to Dr Catherine Andreadi, Dr Lynne Howells, and Professor Andreas Gescher for their guidance on various aspects of my project. I would also like to mention the wonderful support I received from Ms. Karen Kulbicki, Ms. Nalini Foreman and Ms. Maria Szpek for their help and encouragement throughout my project. I am also very grateful to all my wonderful colleagues Ankur, Con and Gintare for their constant help and friendship that have made this a memorable experience. Last but not least, I feel blessed to have the unwavering support and confidence from my wife, Zena Madhag, and my children, Ali, Fatimah and Jaffar to guide me through this PhD journey until the end. Finally, I would like to express my sincere gratitude to my sponsor, Iraqi ministry of higher education and scientific research and University of Kufa for their supporting to my study.

List of contents

List of Figures

Chapter One

Chapter Two

Chapter Three

Chapter Four

Chapter Five

List of Tables

Chapter One

Chapter Two

Chapter Four

Chapter Five

Chapter Eight

List of Abbreviation

ABC	Avidin-Biotin Complex
ACC	Acetyl-CoA carboxylase
Acetyl-CoA	Acetyl coenzyme A
ACLY	ATP citrate lyase
ACS	American Cancer Society
ACTB	Actin
ADI	Arginine deiminase
AMP	Adenosine monophosphate
AMPK	AMP- activated protein kinase
APC	Adenomatous polyposis coli
APS	Ammonium persulfate
Ascl2	Achaete-Scute complex homologue 2
ASCT	Alanine-serine-cysteine transporter 2 (ASCT2)
ASL	Argininosuccinate lyase
ASNS	Asparagine synthetase
ASS	Argininosuccinate synthetase
ATP	Adenosine triphosphate
BCA	Bicinchoninic acid
ß-catenin	Beta- catenin
β-TrCP	Beta-transducing repeat containing protein
BER	Base excision repair
BMP	Bone morphogenic protein
bp	Base pair
BPTES	Bis-2-(5-phenylacetamide-1, 2, 4-thiadiazol-2-yl) ethyl sulphide
BSA	Bovine serum albumin

°C	Celsius / centigrade
Cat#	Catalogue number
CBC	Crypt base columnar
CBCs	Crypt base columnar stem cells
CBP	CREB-Binding Protein
CDKs	Cyclin-dependent kinases
CIMP	CpG islands hypermethylation phenotype
CIN	Chromosomal instability
CK1α	Casein kinase1alpha
CO_2	Carbon dioxide
cDNA	Complementary DNA
COX	Cyclooxygenase
CPS-I	Carbamoyl phosphate synthetase
CRC	Colorectal cancer
CRD	Cysteine-rich domain
CSM	Confocal scanning microscopy
C_T	Cycle threshold
ΔC_T	Delta cycle threshold
$\Delta\Delta C_T$	Delta delta cycle threshold
DAB	3, 3′-diaminobenzidine
DAPI	4′, 6-diamidino-2-phenylindole
DHFR	Dihydrofolate reductase
DMEM	Dulbecco's Modified Eagle's Medium
DMSO	Dimethyl sulfoxide
DNA	Deoxyribonucleic acid
dNDP	Deoxyribonucleoside diphosphates
DPX	Distyrene, a plasticizer and xylene
DVL	Dishevelled segment polarity
E14	Exon 14
EA	Essential amino acid

EC	Endogenous control
ECL	Enhanced Chemiluminescence Luminol
ECM	Extracellular matrix
ECMC	Experimental cancer medicine centre
EDTA	Ethylene diamine tetra-acetic acid
EdU	5-ethynyl-2'-deoxyuridine
EGF	Epithelial growth factor
EGFR	Epidermal growth factor receptor
EMT	Epithelial mesenchymal transition
ER	Estrogen receptor
ETC	Electron transport chain
FACS	Fluorescence-activated cell sorting
FAD	Flavin adenine dinucleotide
FAM	Fluorescence acronym modification dye
FAP	Familial adenomatous polyposis
FAS	Fatty acid synthase
FCS	Fetal calf serum
FDA	Female deleted *Apc* gene mice 1 (target, *Lgr5-Cre+*)
FDB	Female deleted *Apc* gene mice 2 (target, *Lgr5-Cre+*)
FDC	Female deleted *Apc* gene mice 3 (target, *Lgr5-Cre+*)
FFPE	Formalin-fixed, paraffin embedded
FH	Fumarate hydratase
FITC	Fluorescein isothiocyanate
FNA	Female negative mice 1 (control, *Lgr5-Cre-*)
FNB	Female negative mice 2 (control, *Lgr5-Cre-*)
FNC	Female negative mice 3 (control, *Lgr5-Cre-*)
FZD	Frizzled
G1	Gap 1 Phase
G2	Gap 2 Phase
GDH	Glutamate dehydrogenase

GLS	Glutaminase enzyme
GLUT-1/3	Glucose transporter
GM	Geometric mean
GOI	Gene of interest
GSAL	Glutamate semialdehyde
GSK3-ß	Glycogen synthase kinase 3 beta
GTP	Guanosine Triphosphate
H_2O_2	Hydrogen peroxide
H&E	Haematoxylin and eosin
HCEC	Human colon epithelial cell
HIF-1	Hypoxia-inducible factor 1
HNPCC	Hereditary non-polyposis colorectal cancer
HPs	Hyperplastic polyps
hrs	Hours
IDH	Isocitrate dehydrogenase
IF	Immunofluorescence
IHC	Immunohistochemistry
IMS	Industrial methylated spirit
IP	Intraperiton
ISCs	Intestinal stem cells
KRAS	Kirsten rat sarcoma viral oncogene homolog
LEF	Lymphoid enhancer factor
Lgr5	Leucine-rich repeat- containing G-protein coupled receptor
LOH	Loss of heterozygosity
LPS2	Liposarcoma
LRP5/6	Low-density lipoprotein receptor-media related Protein 5/6
L-THFA	L-tetrahydro-2-furoic acid
mg	Milligram
µg	Microgram

µL	Microliter
µM	Micromolar
M	Molar
M Cells	Microfold cells
MAML-1	Mastermind-like-1
MAPK	Mitogen-activated protein kinase
MDA	Male deleted *Apc* gene mice 1 (target, *Lgr5-Cre+*)
MDB	Male deleted *Apc* gene mice 2 (target, *Lgr5-Cre+*)
MDC	Male deleted *Apc* gene mice 3 (target, *Lgr5-Cre+*)
MEM	Minimum Essential Medium Eagle
MGB	Minor groove binder
mL	Millilitre
MLH1	MutL homolog 1
mM	Millimolar
MMPs	Matrix metalloproteinase
MMR	Miss-match repaired genes
MNA	Male negative mice 1 (control, *Lgr5-Cre-*)
MNB	Male negative mice 2 (control, *Lgr5-Cre-*)
MNC	Male negative mice 3 (control, *Lgr5-Cre-*)
MPs	Mixed polyps
MSH2	MutS homolog 2
MSI	Microsatellite instability
MSS	Microsatellite stable
mTOR	Mechanistic target of rapamycin
MYC	Myelocytomatosis Viral Oncogene Homolog
NADPH	Nicotinamide adenine dinucleotide phosphate

NDP	Non-digital zoomer program
NDPs	Ribonucleoside diphosphates
NEAA	Non- essential amino acid
NICD	Notch intracellular domain
OAT	Ornithine aminotransferase
Olfm4	Olfactomedin 4
OXPHOS	Oxidative phosphorylation
P	Phosphorylation processes
PBS	Phosphate buffered saline
PBS-T	Phosphate buffered saline- TWEEN®20
PBS-Triton	Phosphate buffered saline – Triton
P5C	Pyrroline-5-carboxylate
P5CS	P5C synthase
P5CDH	Pyrroline-5- carboxylate dehydrogenase
PCR	Polymerase chain reaction
PDH	Pyruvate dehydrogenase
PDK1	Pyruvate dehydrogenase kinase1
PGE2	Prostaglandin E2
PHGDH	Phosphoglycerate dehydrogenase
PI	Propidium iodide
PIK3C	Phosphatidylinositol-4,5- bisphosphate 3 -kinase catalytic subunit alpha
PIL	Personal licence
PI3K/AKT	Phosphoinositol 3- kinase/protein kinase B
PMS2	Postmeiotic segregation increased 2
POX	Proline oxidase
PRF	Pre-clinical research facility
PRODH	Proline dehydrogenase
PS	Phosphatidylserine

PSAT1	Phosphoserine aminotransferase 1
PSPH	Phosphoserine phosphatase
PYCR	Pyrroline-5-carboxylate reductase
RG	Reference gene
RIF	Rabbit immunoglobulin fraction
RLT	RNA later-like buffer
RNA	Ribonucleic acid
RNR	Ribonucleotide reductase
rpm	Round per minute
ROS	Reactive oxygen species
RRM2B	Ribonucleotide reductase small subunits B
RT	Room temperature
RT reaction	Reverse transcriptase reaction
RT-qPCR	Reverse transcriptase- quantitative PCR
S	S Phase (cell cycle)
SCO2	Synthesis of cytochrome c oxidase
SEM	Standard error of mean
SDH	Succinate dehydrogenase
SDS	Sodium dodecyl sulfate
SHMT	Serine hydroxymethyltransferase
siRNA	Small interfering RNA
SMAD	Mother against decapentaplegic
SSAs	Sessile serrated adenomas
TA	Transit-amplifying T-cell factor 4
TAC	Transit-amplifying cell
TCA	Tricarboxylic acid cycle
TCF4/LEF	T-cell factor4/lymphoid enhancer factor
TEMED	N, N, N′, N′-tetramethylethylenediamine
TFAM	Mitochondrial transcription factor A
TGFβ	Transforming growth factor-beta

TIGAR	TP53- induced glycolysis regulator
TMA	Tissue microarray
TMP	Thymidine monophosphate
TNM	Tumour, Node, Metastasis
TP53	Tumour protein 53
TSAs	Traditional serrated adenomas
TYMS	Thymidylate synthase
UMP	Uridine monophosphate
V	Volt
WB	Western blot
WHO	World Health Organization
Wnt	Wingless/Integration-1
Wt	Wilde type
w/v	Weight to volume

List of Conference Abstracts

- **Saif AL AQBI**, Constantinos Alexandrou, Ni Ni Moe Myint, Mafalda Pires Damaso, Jennifer Higgins, Ankur Karmokar, Giuseppe Sica, Karen Brown and Alessandro Rufini. Role of proline biosynthesis in colorectal cancer development. Poster presentation. Therapeutic Interventions for Cancer Prevention – The Way Forward. Bristol, United Kingdom, 18th-19th of July 2016.

- **Saif AL AQBI**, Constantinos Alexandrou, Ni Ni Moe Myint, Mafalda Pires Damaso, Jennifer Higgins, Ankur Karmokar, Giuseppe Sica, Kevin West, Lynne Howells, Anne Thomas, Karen Brown and Alessandro Rufini. The role of proline biosynthesis in colorectal cancer development. Poster presentation. 1st Crick International Cancer Conference. The Francis Crick Institute, London, United Kingdom, 24th of September 2017.

Chapter One: Introduction

1. Introduction

1.1 The large intestine Anatomy, Physiology and Histology

Anatomically, the large intestine consists of four main parts: appendix, cecum, colon and rectum. Similarly, the colon is divided into four parts. These are the ascending, transverse, descending and the sigmoid colon (Anders, 2011) (Figure 1.1). Physiologically, the large intestine has an important role in water and vitamin absorption in addition to the storing and expulsion of faecal waste.

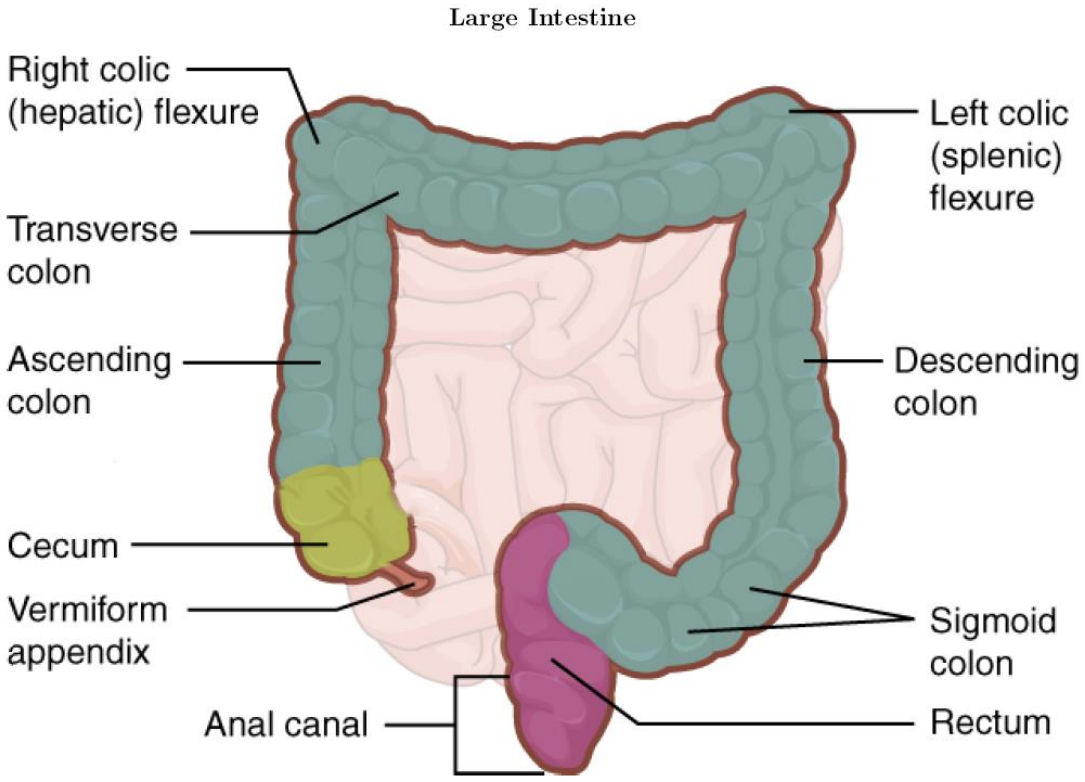

Figure 1.1. Human large intestine parts (Appendix, Cecum, Colon and Rectum). Anatomically, the colon is divided into four parts, ascending, transverse, descending and sigmoid colon. The ascending part of the colon connects dorsally with Caecum (Figure taken from Browne, 2014).

Histologically, from the inner lumen to outer surface, the large intestine contains four layers including mucosa, submucosa, muscular layer (muscularis) and adventitia (serosa) (Mohan, 2010) (Figure 1.2).

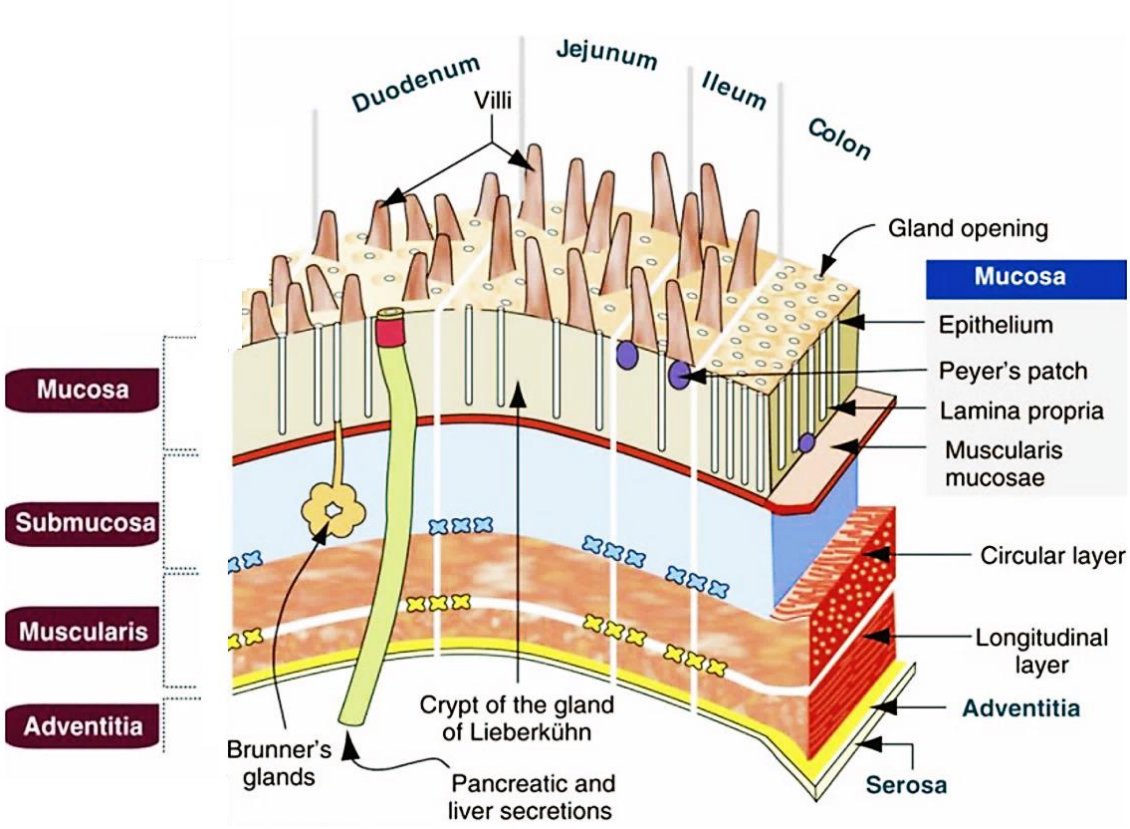

Figure 1.2. The histological layers of Human intestine. The four histologic layers of the colon are mucosa, submucosa, muscular layer (muscularis) and adventitia (serosa). (Figure taken from Gelberg, 2014).

Mucosa is the part of the large intestine located proximally to the lumen and it is composed of intestinal epithelium and the underlying stromal components (Figure 1.3).

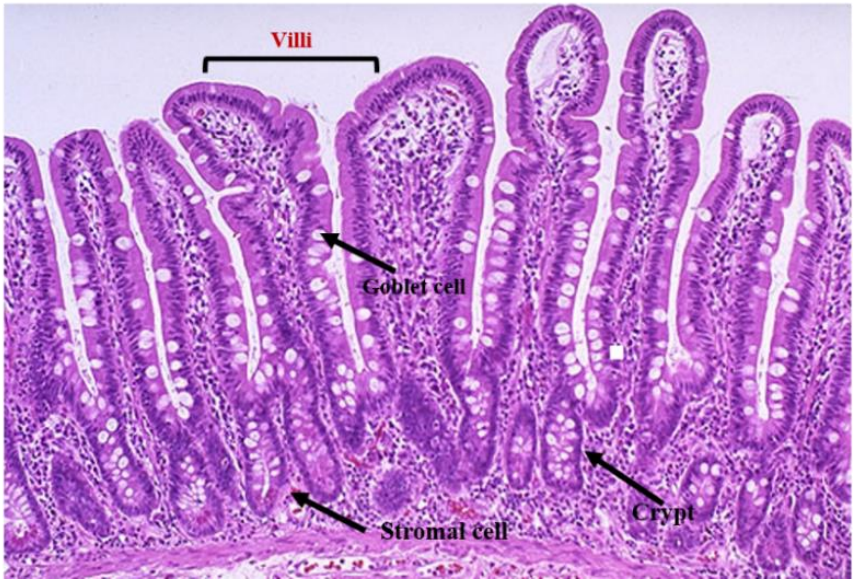

Figure 1.3. Histological section for intestinal mucosa. (A) Intestinal section stained with haematoxylin and eosin (H&E) stain as it appears under light microscope. Villi, crypts, stromal cells and goblet cells are indicated. (Figure taken from Kabiri et al., 2014).

Microscopically, the mucosa can be divided into villi and crypts. Colon epithelial cells connect together to form the epithelial sheets which make the colon surface (villus). The villus contains two types of differentiated epithelia, absorptive (enterocytes) and secretory, which includes goblet cells for mucus secretion, enteroendocrine cells, which secret hormones such as catecholamine to regulate the intestinal activity. An additional secretory differentiated type cells of the villus are tuft cells, which are involved in inflammation and tumour formation and play an important role in regulating prostaglandin formation through cyclooxygenase (COX) enzymes (Carulli et al., 2014) (Figure 1.4). Finally, another differentiated epithelial cell type in the intestinal villi is microfold (M) cells, which lie over specialized lymphoid follicles in the intestinal mucosa, known as Payer's patches. The M cells contribute to the processing of microbial antigens and systemic immune response. (Clevers, 2013 and Ohno, 2015).

Crypts are multiple epithelial invaginations located at the base of intestinal villi (Clevers, 2013) (Figure1.4). Approximately 2000 cells arrange together to form the intestinal crypt

and about 15 highly-proliferating intestinal stem cells (ISCs), also known as crypt base columnar (CBC) stem cells, are present at the crypt's base (Potten et al., 1992, Bach et al., 2000 and Clevers,2013). In addition, a specialized non-proliferating cell type intercalates with ISCs at intestinal crypt region, these cells are called Paneth cells. The main function of Paneth cell is supporting the intestinal immunity through secretion of anti-pathogenic enzyme , mainly lysozyme and defensins (Sato et al., 2011 and Gassler, 2017) and to support the division and maintenance of the crypt stem cell pool (Sato et al., 2011).

Several protein biomarkers have been shown to identify in ISCs, such as leucine-rich repeat- containing G-protein coupled receptor 5 (Lgr5), achaete-Scute complex homologue 2 (Ascl2) and olfactomedin 4 (Olfm4) (Barker, 2014, Van der Flier et al., 2009). Indeed ISCs are also called lgr5+ cells. The important characteristic of stem cells is their ability to self-renew and maintains crypt-villus units. Upon division, ISCs generate transit-amplifying cells (TAC), which are also located in the crypt. TACs have a limited ability to divide and migrate upwards toward to villus where they differentiate into the different specialized cells and substitute the dead cells in the intestinal villi (Medema and Vermeulen, 2011) (Figure 1.4). The homeostasis of the intestinal stem cells in the crypt is controlled by Paneth cells and the underlying stromal cells, including fibroblasts, percryptal myofibroblasts, endothelial cells, and smooth muscle cells (Powell et al., 2011). Paneth cells and percryptal myofibroblasts both secrete paracrine signalling that promote division of the ISCs (Powell et al., 1999, Kosinski et al., 2007 and Adegboyega et al., 2002 and Gassler, 2017). These paracrine factors include several ligands of the Wingless/Integration-1 (Wnt) signalling pathway, such as Wnt3a, that is responsible for regulating stem cell activity and self-renewal in the intestinal crypts (Snippert et al., 2010).

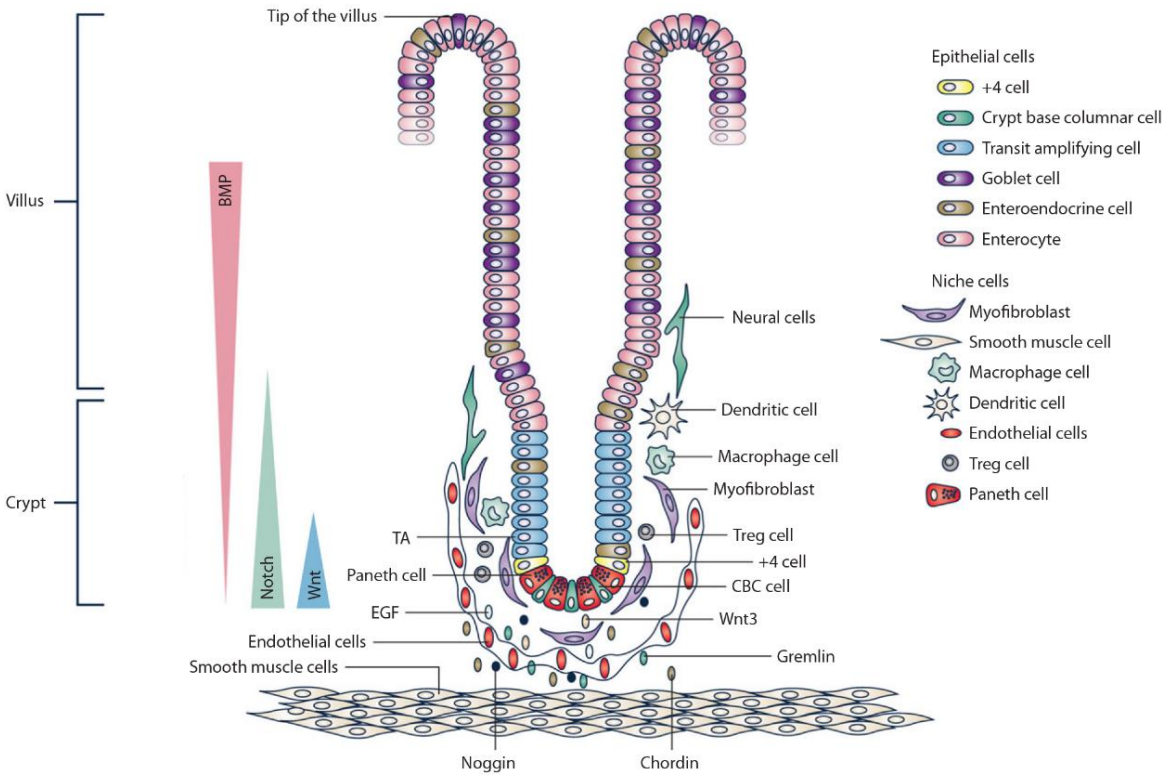

Figure 1.4. The cell types and molecular pathways in the intestinal crypt and villi. The crypts are invaginations of the epithelial lining in the intestine. The ISCs, also known as crypt base columnar cells (CBC), are situated at the base of the crypt (green cells), and interspersed between the secretory Paneth cells (Red cells). ISCs are regulated by paracrine interaction with local myofibroblasts and Paneth cells. These stem cells divide and migrate upwards out of the base of the crypt to become TACs and then differentiated specialized cells in the villi: enteroendocrine cells, goblet cells and enterocyte cells. This differentiation process is controlled through a decreasing gradient of Wnt signalling towards the lumen, counterbalance by BMP signalling. (Figure taken from Sailaja et al., 2016).

1.2 Signalling pathways regulating the homeostasis of the intestinal stem cells

The intestine is one of the most rapidly regenerating organs in the living body. This property is controlled by ISCs (Carulli et al., 2014, Potten, 1977 and Buczacki et al., 2013). Three main signalling pathways control development and regulation of ISC: the Wingless/integration-1(Wnt) signalling pathway, the Bone Morphogenetic Pathway (BMP) and the Notch pathway (Kuhnert et al., 2004) (Figure 1.4).

Many studies have outlined the importance of Wnt signalling pathway in the maintenance of ISCs self-renewal in case of its activity at the highest level (Shah and Zuckerman 2011). Indeed, Wnt/β-catenin pathway includes a group of signal transduction proteins that transduce the signals from cell surface into the nucleus to control the expression of genes involved in cellular proliferation, survival and determination of cell fate (Fearnhead, 2001, Clevers and Nusse, 2012). Three types of Wnt signalling have been described: the canonical Wnt pathway, the noncanonical planar cell polarity pathway, and the noncanonical Wnt/calcium pathway (Kosinski et al., 2007 and Gregorieff et al., 2005). The maintenance of ISCs and crypt homeostasis are controlled by the canonical pathway that relies on the transcriptional programme elicited by nuclear ß-catenin bound to the T-cell factor/lymphoid enhancer factor (TCF4/LEF) transcriptional factors (Cavallo et al., 1998, Behrens et al., 1996, Fevr et al., 2007 and Van de Wetering et al., 2002).

The signalling cascade of the canonical Wnt pathway is activated by the binding of the Wnt ligands, which are 40kDa lipidated proteins, to the membrane heterodimeric complex composed of frizzled (FZD) and the lipoprotein receptor-related proteins (LRPs) 5/6 (Figure 1.5) (Bhanot et al., 1996, Pinson et al., 2000 and He et al., 2000). The FZD receptor contains a large extracellular cysteine-rich domain (CRD) with a hydrophobic groove that allows Wnt ligands to bind through its lipid moiety (Clevers and Nusse, 2012).

At the inactive, OFF phase (that is in absence of Wnt ligands) super molecular destruction complex is formed in the cytoplasm via binding of adenomatous polyposis coli (APC) protein, casein kinase1α (CK1α), glycogen synthase kinase 3 beta (GSK3-ß), dishevelled segment polarity (DVL) and Axin scaffolding protein. This complex recruits and phosphorylates ß-catenin. Subsequently, phosphorylated b-catenin is targeted from proteasomal degradation though ubiquitination mediated by the transducing repeats-containing protein (β-TrCP). This constant degradation of β-catenin stops the

transcriptional activation of target genes (Aberle et al., 1997, Fearnhead et al., 2001, Clevers and Nusse, 2012 and MacDonald et al., 2009) (Figure 1.5).

The binding between Wnt ligands and FZD/LRP5/6 receptor leads to activation of the Wnt pathway (ON phase) and promotes phosphorylation of cytoplasmic tail of LRP by GSK3-ß and CK1. This results in recruitment of the scaffolding protein Axin to LRP6 with the sequential inactivation of the destruction complex (Wu et al., 2009 and Fearnhead et al., 2001) (Figure1.5). In these circumstances, ß-catenin is not phosphorylated and is not targeted for degradation, rather it rapidly accumulates in the cytoplasm and translocates to the nucleus, where it binds TCF/LEF and regulates expression of Wnt-target genes, including the stem cell markers Lgr5 and olfm4 and the oncogene Myelocytomatosis Viral Oncogene Homolog (*MYC*) and Cyclin D1 (Fearnhead et al., 2001, MacDonald et al., 2009 and Novak and Dedhar, 1999, He et al., 1998, Tetsu and McCormick, 1999, MacDonald et al., 2009 and Wu et al., 2009).

As described above, the APC protein is one of the main components of destruction complex, and contributes to control the amount and activity of ß-catenin (Xing et al., 2003). Notably, inactivating mutations targeting the *APC* gene are highly common in colorectal cancer (CRC) and *APC* is therefore regarded as a typical tumour suppressor gene (Vermeulen et al., 2010 and Henderson, 2000).

Indeed, the Wnt signalling pathway promotes the proliferation of ISCs (Korinek et al., 1998, Kuhnert et al., 2004, Pinto and Clevers, 2005, and Yamagishi, et al., 2016), and the uncontrolled activation of this pathway results in the developing of wide range of CRCs (Korinek et al., 1997). Under normal physiological conditions, the Wnt pathway at the bottom of the intestinal crypts is activated by the concerted actions of Paneth cells and pericryptal myofibroblasts. Paneth cells secrete different Wnt ligands, whereas myofibroblasts secrete also the Wnt agonists R-spondins, which are ligands of the Lgr5 receptors expressed on the surface of the ISCs (Barker et al., 2007, Carmon et al., 2011, De Lau et al., 2011, Kim et al., 2005 and Clevers and Bevins, 2013). As TAC progress upwards, the progressive decrease in Wnt activators stimulates exit from the cell cycle and differentiation.

The Notch signalling pathway is activated by binding of the Notch ligands (such as Delta or Jagged) to the Notch receptor, resulting in the formation of an active Ɣ-secretase

complex. In turn, this complex cleaves the Notch receptor transmembrane domain, leading to release of the Notch intracellular domain (NICD), which translocates to the nucleus to bind the transcriptional regulators, suppressor of hairless (also known as CSL, LAG-1 CBF-1 or RBP-J), mastermind-like-1 (MAML-1) and p300/CREB-Binding Protein (CBP) (Qiao and Wong 2009). The Notch signalling pathway modulates ISCs dynamics in relation to both enterocytes and intestinal secretory cells (Fre et al., 2005). The importance of Notch signalling has been confirmed using an inducible gut-specific Notch-mutant mouse model. Notch pathway was shown to regulate ISCs by repressing of transcription of cyclin-dependent kinases (CDKs) inhibitors, thus promoting proliferation and inhibiting differentiation (Riccio et al., 2008).

Another signalling pathway that plays an important role in regulating ISCs fate is the BMP pathway. BMP signalling prevents stem cell proliferation and self-renewal. This pathway is activated by BMP protein ligands binding to their cognate receptors. Subsequently, the signals are transduced to the nucleus via phosphorylation of mothers against decapentaplegic (SMAD) proteins 3 and 4 (Figure 1.4), this leads to inhibition of proliferation through transcriptional repression of *c-Myc* and up-regulation of a cyclin-dependent kinase inhibitor ($p15^{INK4B}$) (Derynck and Zhang 2003, Hardwick et al., 2008 and Shi and Massagué 2003). At the base of the intestinal crypt, myofibroblasts secret several BMP antagonists such as gremlin 1,2 and chordin-like1, which inhibit BMP pathway activation within the ISCs niche. This helps to balance self- renewal and differentiation within the intestine (Kosinski et al., 2007 and Whissell et al., 2014). In addition, Bmpr1a (a BMP receptor) deficient mice, or mice that showed overexpression of Noggin (a BMP inhibitor) showed an increased proliferation of ISCs and enhanced crypt fission (He et al., 2004 and Haramis 2004), remarking the anti-proliferative role of BMP in the gut.

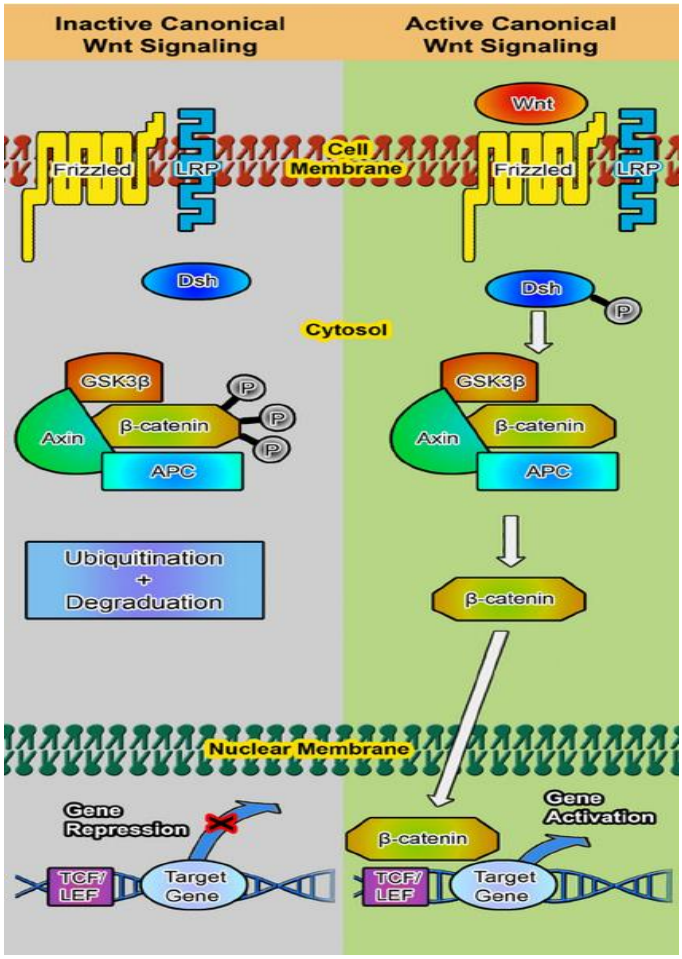

Figure 1.5. An overview of the canonical Wnt signalling pathway. In the Wnt canonical pathway, in the absence of Wnt ligand, the destruction complex (formed by CK1, APC, GSK3-β and Axin) phosphorylates β-catenin, targeting it for proteasome-mediated degradation. This prevents the expression of β-catenin target genes. Wnt ligands binding to FZD/LRP5/6 receptors results in inactivation of the destruction complex, leading to accumulation and nuclear translocation of β-catenin. Within the nucleus, β-catenin will form a complex with the transcription factors of the LEF/TCF family, leading to target genes transcription. P=phosphorylation. (Figure taken from Zhang et al., 2014).

1.3 Cancer definition

Cancer is defined as a sequence of molecular events that essentially modify the normal properties of living cells. In summary, the normal control systems that inhibit overgrowth and invasion of other tissues are inactivated in cancer cells and in the meantime, there is activation in oncogenes that involved in stimulation of the cellular proliferation (Pierotti et al., 2003). This abnormalities support cancer cell division and growth in the presence of signals which normally inhibit cell growth (Schneider, 2001). According to the World Health Organization (WHO), cancer is considered the second leading cause of death around the world with 8.8 million death cases in 2015 and with nearly one out six deaths resulting from cancer (WHO, 2015).

1.4 Hallmarks of cancer

All cancers arise from genetic alterations that enable malignant transformation (Hanahan and Weinberg 2000). These alterations modify six physiological processes required to develop invasive cancers, known as the hallmarks of cancer (Hanahan and Weinberg 2011). Originally, they included sustaining proliferative signalling, evading growth suppressors, resisting cell death, enabling replicative immortality, inducing angiogenesis, and activating invasion and metastasis. However, in the last decade, four new hallmarks of cancer have been proposed: reprogramming of energy metabolism, genome instability and mutation, evading immune destruction and tumour-promoting inflammation. (Hanahan and Weinberg, 2011) (Figure 1.6).

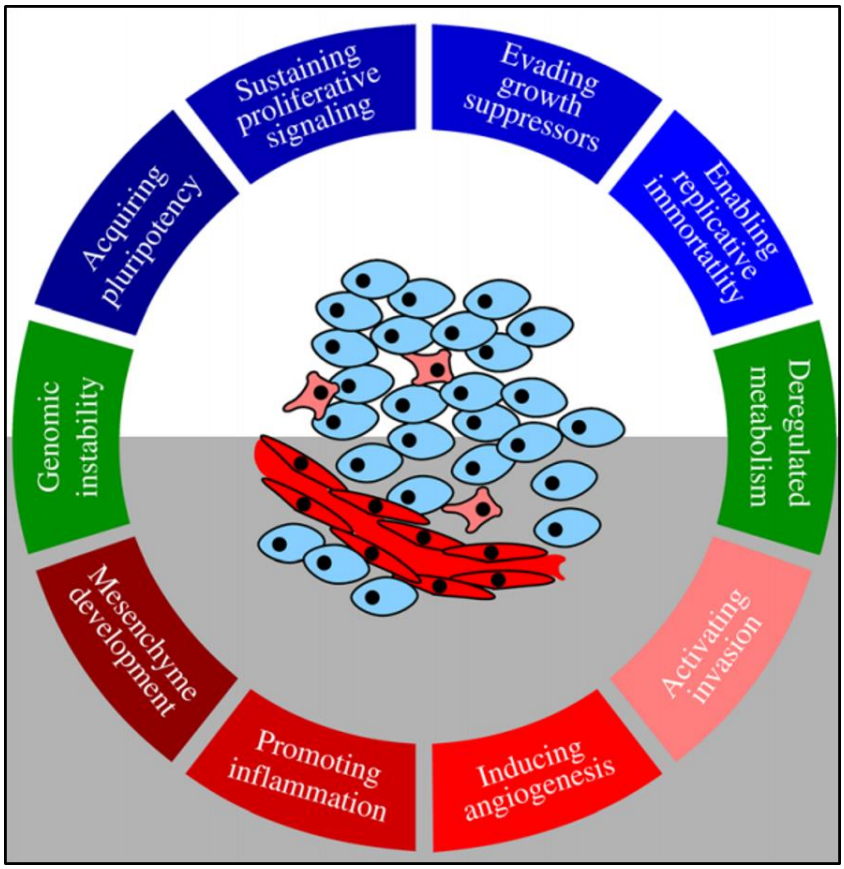

Figure 1.6. The Hallmarks of Cancer. The diagram shows the hallmarks of cancer as outlined by Weinberg and Hannah (Figure taken from Markert and Vazquez, 2015).

1.5 Colorectal cancer

1.5.1. Statistics and incidence

CRC arises from the epithelial layer of colon and rectum (American Cancer Society (ACS), 2017). According to the world health organization, CRC ranks as the third most common cancer worldwide with a reported number of deaths reaching 639,000 in 2004 (WHO,2009).

In the UK, CRC is the fourth most commonly diagnosed cancer and, with over 40,000 new cases each year, it accounts for approximately 12% of all new cancer cases. Typically, CRC cases are more common in males than females (55 % males versus 45% females). In addition, CRC is classified as the second cause of cancer–related deaths in the UK, accounting for 10% of all cancer deaths (Cancer Research UK, 2016) (Figure1.7).

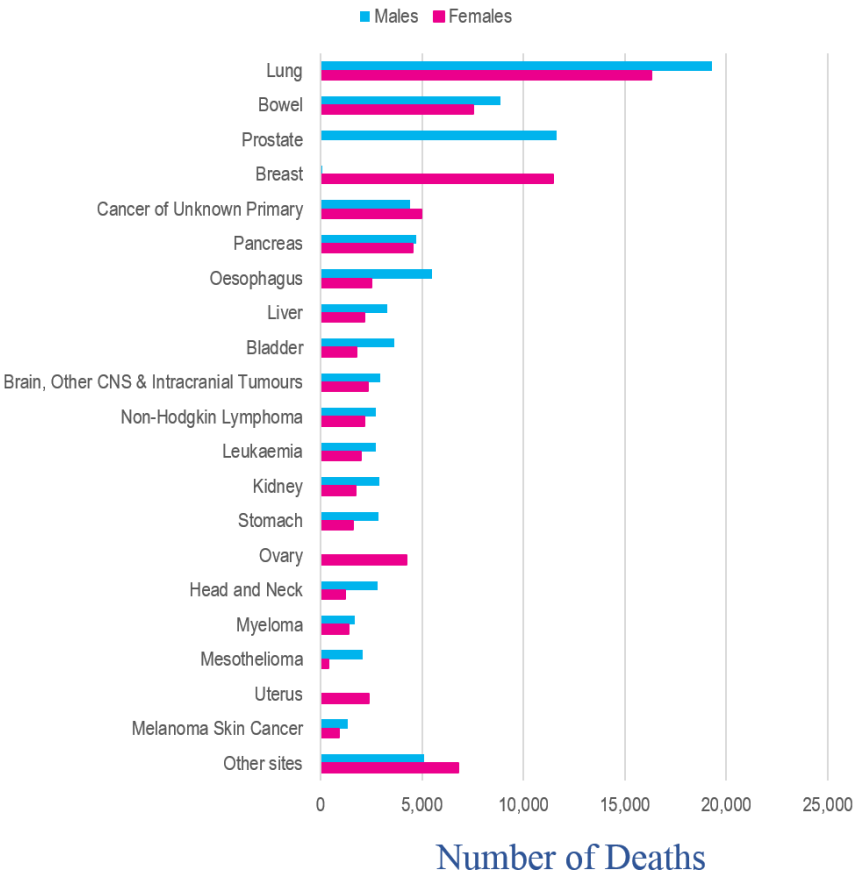

Figure 1.7. Bowel Cancer is the second cancer –related death in the UK in 2016. Number of deaths per year in the UK (Figure taken from Cancer Research UK website, 2016).

In England, the survival rate for CRC remains strongly related to stage at diagnosis. Five-year net survival for bowel cancer is highest for patients diagnosed at stage I, and lowest for those diagnosed at stage IV. The data of 2014 in England show that approximately 98% of patients diagnosed at stage I survived their disease for at least five years, versus 40% of patients diagnosed at stage IV (Cancer Research UK, 2014) (Figure 1.8). This discrepancy becomes even more remarkable with the 5-year survival rate. 90% of patients with stage I CRC survive 5 years after diagnosis, but survival drops dramatically to 14% in patients with metastatic disease. However, in case of stage IV disease with limited, respectable metastatic spread, the removal of the tumours by surgical operation can result in prolonged survival (American cancer society, 2017, Kanas et al., 2012 Gupta and Massagué, 2006 and Spano et al., 2012).

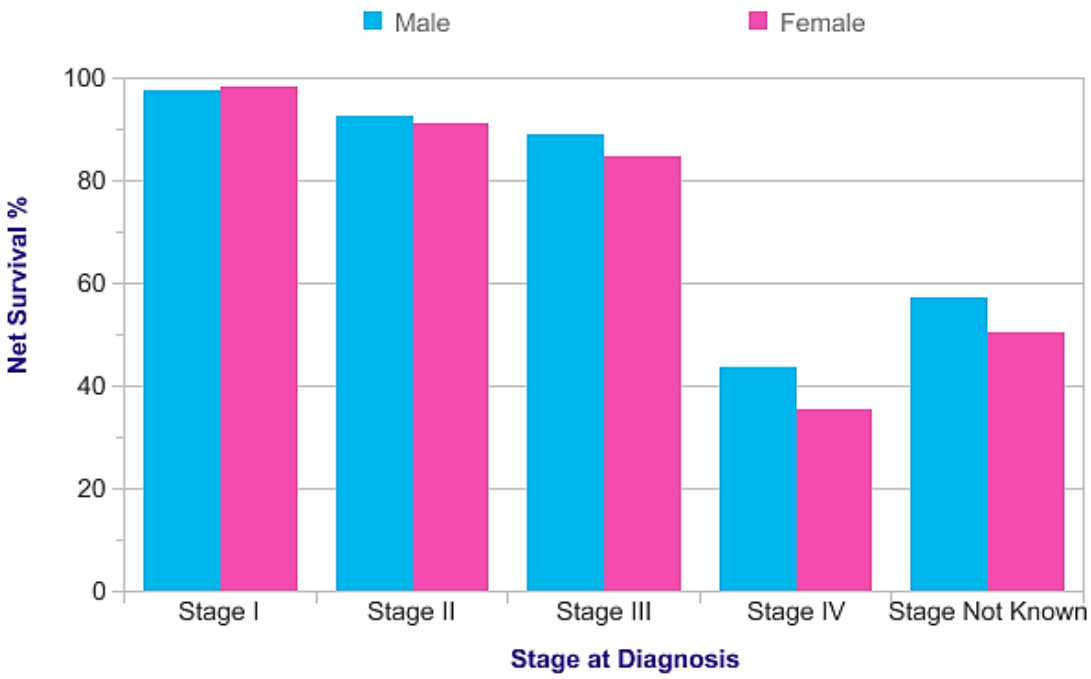

Figure 1.8. The 5-year survival rate of CRC according to stage at diagnosis. The graph reports percentages of survival male and female patients diagnosed with different stages of CRC (Figure taken from Cancer Research UK website, 2014).

1.6 Risk factors

Age is a major risk factor in CRC incidence In the UK, between 2012 and 2014, 44% of CRCs were diagnosed in patients aged 75 and over (Cancer Research UK, 2015). At ages 50-54, the incidence rate of CRC increases and peaks at around 75-79 years (Figure 1.9) (Cancer Research UK, 2015).

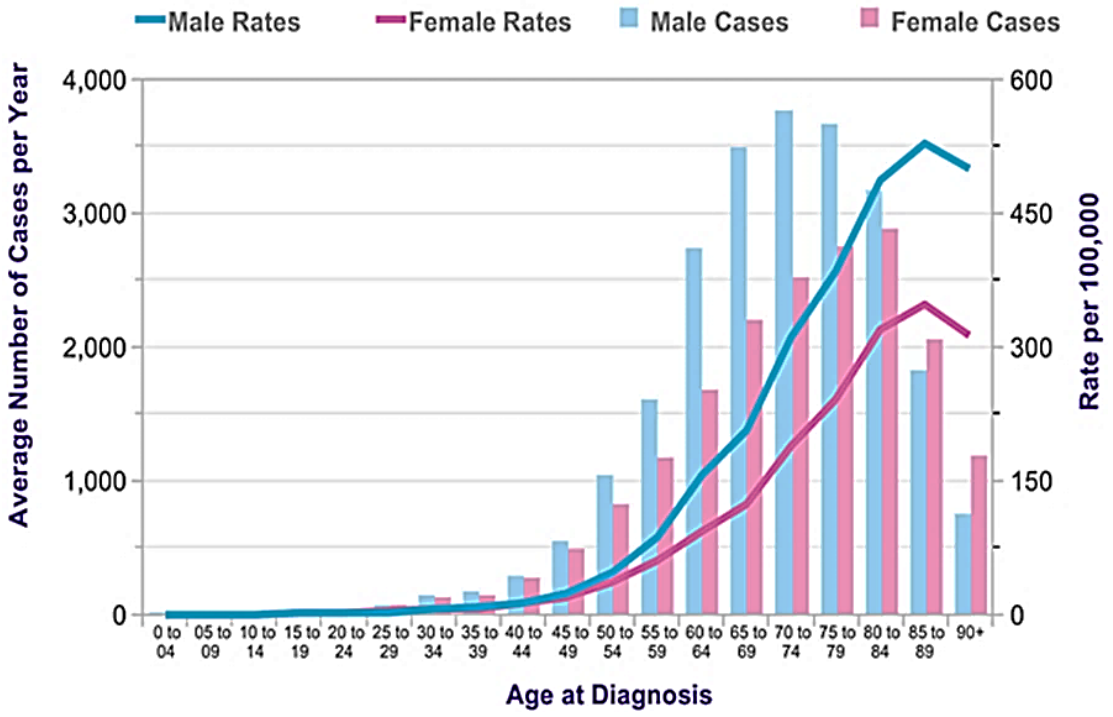

Figure 1.9. Age is a risk factor in CRC. The graph reports the number (bars) and incidence (lines) of CRC cases per year according to age, and sex groups (Figure taken from Cancer Research UK website, 2015).

Genetic predisposition and environmental conditions also affect the risk of developing CRC. Despite this, the vast majority of CRC develop spontaneously; some studies have suggested that about 20% of CRC cases can be attributed to genetic factors (Lichtenstein et al., 2000). Different hereditary polyposis syndromes are known to develop because of genetic alterations. The major CRC hereditary syndromes are familial adenomatous polyposis (FAP) and hereditary non-polyposis colorectal cancer (HNPCC) or Lynch syndrome (Figure 1.10). In addition, Juvenile Polyposis Coli and Peutz-Jeghers syndromes are also included among the inherited CRC, although they are rare (Cunningham et al., 2010).

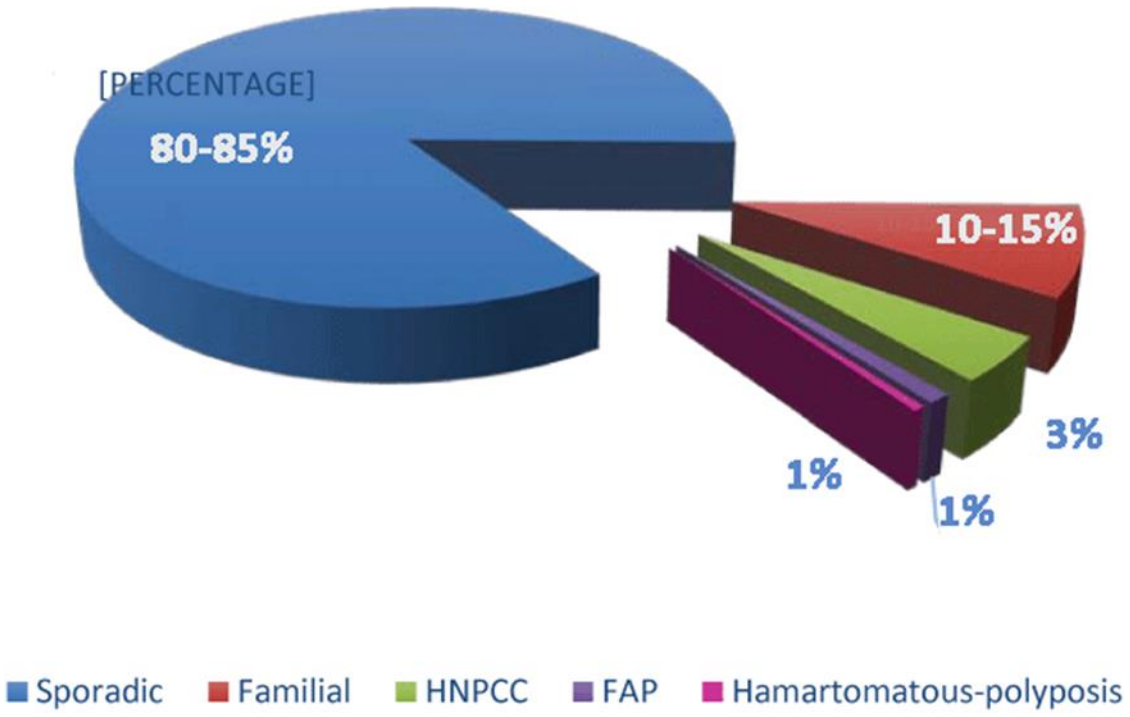

Figure 1.10. The percentages incidence of colorectal cancer (CRC) types. (Figure taken from Fredericks et al., 2015).

Dietary habits also affect risk of CRC. Diets rich in animal fat and saturated fat have been associated with increased risk of developing CRC (Hursting, et al., 1990, Miller, et al., 1983 and Giovannucci et al., 1992).

Other studies showed that heterocyclic amines, generated during the cooking of red meat, have a clear positive correlation with the risk of CRC incidence (Steck et al., 2014, Chao et al., 2005, Butler et al., 2003 and Rao et al., 2001). Indeed, the World Health Organization recommends to moderate consumption of red meat in order to decrease the chances of developing CRC (WHO, 2015).

On the other hand, several studies showed that some dietary regiments might help to reduce colorectal tumorigenesis. These include increasing the intake of vegetables, high fibre food, fruits and fish (Giovannucci et al., 1992, Howe et al., 1992 and, Satia et al., 2004).

Finally, the risk of developing CRC is also affected by lifestyle choices. For example, smoking, obesity and lack of physical activity are important risk factors for the development of CRC (Nöthlings et al., 2009, Friedenreich, and Orenstein 2002, Almendingen 2001, Tiemersma et al., 2003 and Giovannucci et al., 1993).

1.7 Colorectal cancer staging

There are two main CRC staging methodologies: the Tumour, Node, Metastasis (TNM) system and the Dukes system. The most widely used system is the TNM, which uses a scale from 0 to 4 to rank the tumour size and a 0 to 3 scale to rank the lymph node spreading. The absence or presence of distant metastasis is indicated by an M0 or M1, respectively. The Dukes staging system is an older system for CRC staging that is still commonly used. In this case, tumour progression is ranked from 0 to 4 according (Table 1.1 and Figure 1.11). Additionally, a tumour-grading system is also applied to describe the aggressiveness of primary cancer. Three grades are distinguished; Grade 1 refers to slow growing tumour with high similarity to the original colon tissue, Grade 2 indicates moderately differentiated tumours and, finally, Grade 3 identifies poorly differentiated, aggressive tumours (Mori, 2010).

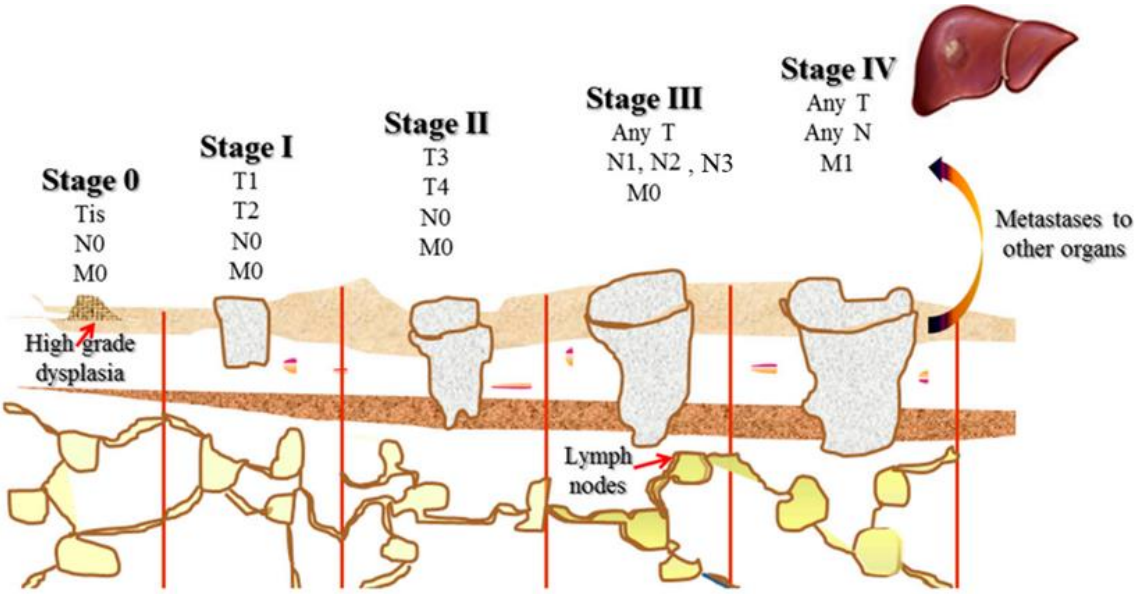

Figure 1.11. CRC TNM stages. The different stages of CRC according to the TNM classification system. Stage 0 refers to benign tumour (Adenoma) (Figure taken from Lin et al., 2015).

Stage	TNM	Dukes	Description
Stage 0	Tis,N0,M0	A	Carcinoma in situ
Stage 1a	T1,N0,M0	A	Tumour invades submucosa
Stage 1b	T2,N0,M0	A	Tumour invades muscularis propria
Stage 2a	T3, N0, M0	B	Tumour invades through muscularis propria into pericolorectal tissues
Stage 2b	T4, N0, M0	B	Tumour penetrates through the surface of the peritoneum and invades other parts of the bowel or surrounding organs
Stage 3a	T1,N1-3,M0	C	Tumour invades the submucosa with metastases 1-3 lymph nodes
Stage 3b	T2, N1-3, M0	C	Tumour invades muscularis propria with metastases 1-3 lymph nodes
Stage 3c	T3, N1-3, M0	C	Tumour invades through muscularis propria into pericolorectal tissues with metastases 1-3 lymph nodes
Stage 3d	T4, N1-3, M0	C	Tumour penetrates through the surface of the peritoneum and into other parts of the bowel or surrounding organs with metastases in 1-3 lymph nodes
Stage 3e	T(any size),N2,M0	C	A tumour of any size, and there are metastases in 4 or more local lymph nodes
Stage 4	T (any size), N (any node involvement), M1	D	A tumour of any size, with any number of lymph nodes involved, and distant metastases to another organ.

Table 1.1. CRC staging comparison between TNM and Dukes systems. (Table taken from Obrocea et al., 2011, Akkoca et al., 2014 and Mori, 2010).

1.8 The adenoma – carcinoma sequences: adenomas as precursors of CRC

CRCs develop from progressive accumulation of genetic and epigenetic alterations, which support the transformation of normal colonic epithelium into benign adenomatous polyps and then adenocarcinoma (Yamagishi et al., 2016). Therefore, all CRC lesions initiate as polyp (benign tumour), before progressing to malignant cancer (Fleming et al., 2012 and Shussman and Wexner, 2014).

Colon polyps can be pedunculated if they appear as mushroom-like growths, which attach to the surface of the mucosa by a long, thin stalk, or sessile flat lesions lying on the mucosal surface (Shussman and Wexner, 2014). Histologically, polyps are categorized into two main types, either traditional or serrated adenomatous polyps (Figure 1.12). Similarly, based on the same distinction, there are two main pathways to CRC: the traditional or classical pathway and the serrated pathway.

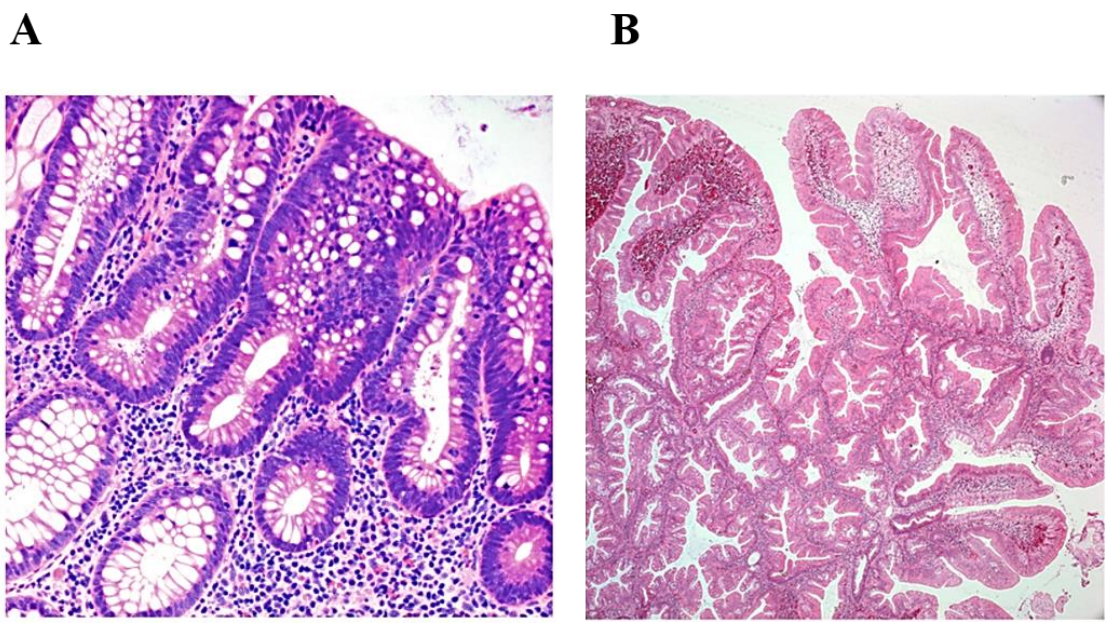

Figure 1.12. Histopathological sections show two types of colon adenomas. **(A)** Traditional adenoma **(B)** Serrated adenoma (Figure taken from Fleming et al., 2012 and Rex et al., 2012).

Depending on their histological features, traditional adenomas are classified into three main classes: tubular adenomas, tubulovillous adenomas and villous adenomas. This classification is mainly based on a percentage of villous components in adenoma tissue. For instance, in tubular adenomas, the percentage of villous component is less than 25%, while tubulovillous adenomas contain an intermediate villous component (25-75%). Finally, villous adenomas contain more than 75% of villous component (Fleming et al., 2012). If adenomas appear large in size (more than 1 cm) and contain high-grade dysplasia then these are classified as advanced adenomas (Heitman et al., 2009).

Serrated polyps are hyperplastic pathological changes often diagnosed in the proximal right-sided colon. These lesions are characterized by an infolding of crypt epithelium that gives the tissue a saw-toothed appearance (i.e. serrated) in the longitudinal section or a stellate appearance in cross-section. These polyps comprise a heterogeneous set of lesions grouped into three categories: sessile serrated adenomas (SSAs), traditional serrated adenomas (TSAs) and hyperplastic polyps (HPs) (Haque et al., 2014). HPs are the most predominant serrated lesion accounting for around 80-90% of serrated polyps (Yamane et al., 2014). Based on genetic profile, three types of molecular alterations have been diagnosed in serrated pathway: *BRAF* gene mutations, microsatellite instability (MSI) and CpG islands hypermethylation phenotype (CIMP) (Patai et al., 2013 and Murcia et al., 2016).

Furthermore, some histopathological classifications include a mixed serrated polyp group. Essentially, this term gathers lesions that display combined histologies of both traditional and serrated polyps with variable grades of dysplasia (East et al., 2015).

As mentioned, the two distinct adenoma subtypes broadly correspond to distinct pathways implicated in CRC development: the traditional and serrated pathways. In 1990, Vogelstein and Fearon proposed a model for CRC development based on the adenoma-carcinoma sequence originating from the traditional adenomatous polyps and responsible for 80 to 90% of all CRCs (Fearon and Vogelstein 1990) (Figure 1.13).

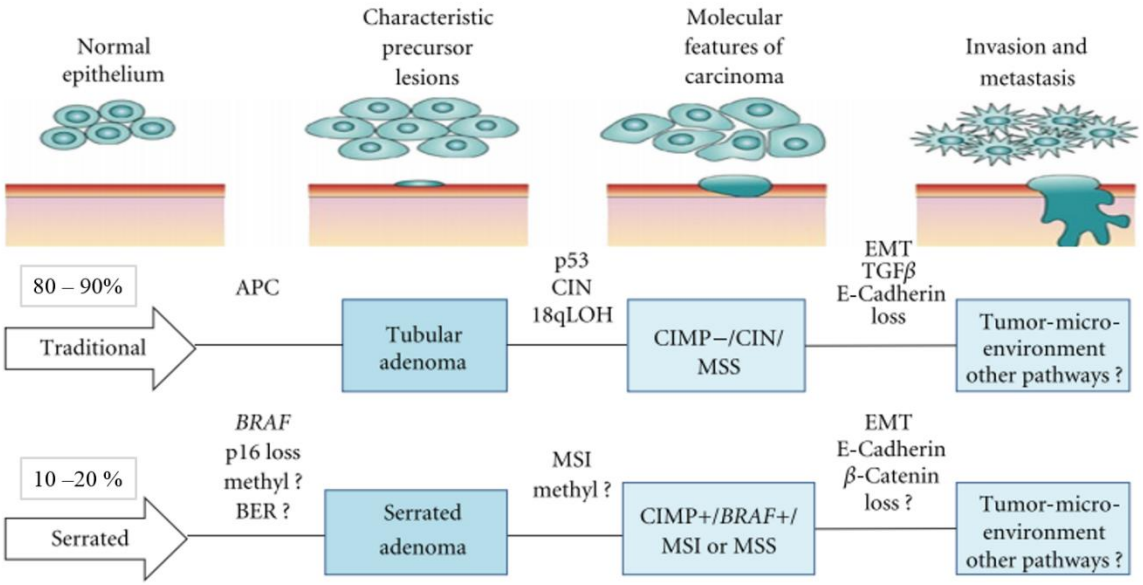

Figure1.13. The adenoma-carcinoma sequence: a genetic overview of CRC development (Figure taken from Pancione et al., 2012).

Accordingly, these tumours arise as a result of serial mutations affecting the tumour suppressor gene *APC*, followed by gain-of-function alterations in the oncogene Kirsten rat sarcoma viral oncogene homolog (*KRAS*) and finally the tumour protein 53 (*TP53*) gene (Carethers and Jung 2015, Fearnhead et al., 2002, Worthley and Leggett 2010 and Yamagishi et al., 2016). According to this model, colorectal tumorigenesis is therefore initiated by activation of the Wnt pathway by loss of the *APC* gene. In some cases, *p53* mutations have been proposed to mark the transition from an adenoma to a carcinoma (Hao, 2002). Once a carcinoma has developed, the tumour begins to invade the surrounding stroma with genomic instability promoting further mutations and tumour progression (Walther et al., 2009). Additionally, several biological functions are regulated by *p53* gene such as DNA damage response, apoptosis and senescence (Resnick and Inga, 2003). Therefore, mutations in *p53* are commonly found in tumours and lead to altered metabolic pathways, faulty cell cycle control, defective apoptosis and inefficient DNA repair (Li et al., 2012). Indeed an additional feature of this pathway is the widespread chromosomal instability (CIN) and aneuploidy enabled by the loss of *p53* function (Pino and Chung, 2014).

CIN creates gene deletions, duplications and chromosomal rearrangements. Approximately, 70 -85% of sporadic CRCs are characterized by CIN (Pino and Chung, 2010).

CIN is also responsible for loss of heterozygosity (LOH) at tumor suppressor gene loci (Grady and Carethers, 2008). Mutation of the phosphatidylinositol-4, 5-bisphosphate 3-kinase catalytic subunit alpha (*PIK3CA*) and Sma-and Mad-related protein 4 (*SMAD4*) are also commonly observed in this subtype of CRC (Yamagishi, et al., 2016, De Sousa et al., 2013 and Rad et al., 2013). Of note, germline mutations in the *APC* gene are responsible for the previously mentioned FAP syndrome (Cetta et al., 2000).

BRAF mutations, microsatellite instability (MSI) and CpG island methylator phenotype (CIMP) are the main genetic alterations that characterize the serrated neoplasia, which is responsible for 10 to 20% of CRCs.

BRAF is a proto-oncogene coding for a serine/threonine kinase of the Mitogen Activated Protein Kinase (MAPK) pathway. This pathway, which is activated in response to pro-growth stimuli, such as engagement of receptor tyrosine kinases (RTKs), acts to promote proliferation and survival and is often altered in cancer (McCain, 2013). In the vast majority of cases *BRAF* mutations results in the substitution of a glutamate for a valine in position 600. This causes the constitutive activation of this kinase and consequently of the downstream MAPK (Chalovich and Eisenberg, 2013). *BRAF* mutations have been described in melanoma, lung cancer and hairy cell leukaemia, as well as in 10% to 15% of CRCs (Chat-Uthai et al., 2018).

Another genomic alteration frequently observed in serrated lesions is microsatellite instability (MSI). Microsatellites (MS) are regions of DNA with tandem repeats of short sequences containing one to four nucleotides (Markowitz et al., 1995 and Gemayel et al., 2012). MS are prone to replication error during DNA replication, which are corrected by the Mismatch Repair pathway (MMR) (Ogino and Goel, 2008, Armaghany et al., 2012 and Murphy et al., 2006).

The MMR is a complex DNA repair process characterized by numerous genes such as MutL homolog1 (*MLH1*), MutS homolog1 (MSH1), MutS homolog2 (*MSH2*), MutS homolog6 (*MSH6*) and postmeiotic segregation increased2 (*PMS2*). MSI is caused by defective *MMR*. Methylation-driven silencing of *MSH1* or somatic mutations of *MMR* genes are common causes of MSI (Richman, 2015). Notably, MSI tumours are

characterized by a high mutational burden and this might explain why they have a good prognosis (Nebot-Bral et al., 2017).

MSI cancers are indeed characterized by a strong immune infiltration and it is currently thought that the neo-antigens generated by MSI are responsible for mounting an anti-tumour immune response (Passardi et al., 2017). In fact, in the USA the FDA has recently approved immunotherapy for the treatment of MSI metastatic tumours (Boyiadzis et al., 2018). Of note, germline alterations in MMR and the associated MSI are the hallmarks of the inherited Lynch syndrome.

CIMP is an altered epigenetic pattern commonly observed in serrated carcinogenesis (Toyota et al., 1999 and Samowitz et al., 2005). Typically, DNA is methylated at cytosine bases that precede a guanine (CpG site) and CpG islands represent genomic loci enriched in CpG sequences. CIMP manifests when a widespread methylation affects CpG islands in the tumour genome (Ahuja et al., 1997 and Toyota et al., 1999). Around 30% – 40% of sporadic proximal CRCs appear as CIMP-positive, in comparison to 3%–12% of distal CRCs (Hawkins et al., 2002, Van et al., 2002 and Barault et al., 2008).

CIMP-positive CRCs often have MSI due to methylation of the *MLH1* promoter and are commonly accompanied by *BRAF* mutations (Chen et al., 2017). It should be noted, however, that CIMP is not solely observed in serrated tumours, as 50% of CIMP tumours are categorized as CIN (Samowitz et al., 2005 and Nosho et al., 2008). Furthermore, CIMP-positive tumours are divided into two main categorises, CIMP-high, which are related to *BRAF* mutations and *MLH1* methylation, and CIMP-low, which are related to *KRAS* mutations (Shen et al., 2007 and Suehiro et al., 2008).

1.9 Tumour suppressor genes and oncogenes regulate cancer metabolism

Normally, the main controllers of tissue homeostasis and monitors of growth signals in the living cells are proto-oncogenes and tumour suppressor genes. Indeed, these genes have an ultimate potential to regulate the cell growth and division. Therefore, any genetic modifications or mutations in those can lead to constitutively active growth signalling which stimulates cells to proliferate. Because of this unbounded proliferation, the tumour cell undergoes a rewiring of metabolic pathways within the tissues from which they originated (Dang 2012). This metabolic reprogramming supports tumour cells by providing them with a constant supply of energy, biomass elements and redox potential

and allows cancer cells to survive and proliferate in hostile conditions and under stringent selective pressure. Increase in cell size and DNA replication are essential requirements of proliferating cancer cells, which necessitate constant biosynthesis of proteins, lipids and nucleotides as well as maintenance of an energy reservoir (Ward and Thompson 2012). The molecular events that underlie metabolic reprogramming during tumorigenesis are complex and include modifications induced by oncogenes and tumour suppressor genes. Several oncogenic signalling pathways, such as those involving hypoxia-inducible factor 1 (HIF-1), mechanistic target of rapamycin (mTOR), AMP-activated protein kinase (AMPK) and phosphoinositol 3- kinase/protein kinase B (PI3K/AKT), have all been shown to contribute towards the rewiring of metabolism in cancer cells (Semenza, 2010a ; Shaw and Cantley, 2006 ; Guertin and Sabatini, 2007 ; Shackelford and Shaw, 2009 and Wise et al., 2008).

For instance, HIF-1 is a master regulator of cancer cells' response to low levels of oxygen. The levels of this transcription factor increase in many types of cancer in hypoxia conditions, an increase mediated by protein stabilization through prolyl hydroxylation (Semenza, 2010b). Generally, highly proliferating tumour cells show a hypoxic microenvironment because of increasing oxygen consumption and limited blood supply. This condition triggers metabolic reprogramming (Vaupel et al., 2001). Metabolically, the main effect of HIF-1 is to initiate the shift from mitochondrial respiration and oxidative phosphorylation to anaerobic glycolysis through stimulating the expression of glucose transporter (GLUT-1 and GLUT-3) and expression of glycolytic enzymes such as hexokinase (Semenza, 2011 and Brahimi et al., 2007).

A master regulator of cellular metabolism in normal tissue and cancer is the mTOR pathway, and approximately 80% of human tumours show activation of this pathway (Menon, S. and Manning, 2009 and Guertin and Sabatini, 2007). mTOR is a serine threonine kinase, which participates in two different multi-protein complexes: the mTOR complex 1 (mTORC1) and the mTOR complex 2 (mTORC2). While mTORC2 is a main regulator of the PI3K/AKT pathway, mTORC1 regulates directly essential metabolic pathways. mTORC1 is composed of mTOR, regulatory-associated protein of mTOR (Raptor), mammalian lethal with SEC13 protein 8 (MLST8) and the recently identified Proline-rich AKT1 substrate 1 (PRAS40) and DEP domain-containing mTOR-interacting protein (DEPTOR) (Zoncu et al., 2011). This complex is activated in response to growth

factors or amino acid availability. With regard to nutrients, this pathway senses the intracellular level of amino acids, especially arginine and leucine, and when amino acids are abundant, the mTOR kinase stimulates protein translation, nucleotide biosynthesis and lipid metabolism, all activities that can support cellular proliferation (Kim et al., 2008, Sancak et al., 2010 and Zoncu and Sabatini, 2011).

Additionally, *c-MYC* oncogene also influences cellular metabolism. Several human cancers exhibit *c-MYC* deregulation, which in turn triggers tumourigenesis via transcriptional modulation of many target genes (Lin et al., 2012). In terms of metabolism, some *c-Myc*-target genes are involved in glucose metabolism, nucleotide, lipid, amino acid and protein synthesis (Li and Simon, 2013 and Dang 2013). Furthermore, mitochondrial biogenesis is also regulated by *c-Myc* gene via stimulating the expression of genes involved in mitochondrial structure and function, such as mitochondrial transcription factor A (*TFAM*). This gene encodes a protein necessary for mitochondrial transcription and mitochondrial DNA replication (Li, 2005). It has been reported that the proto-oncogene *c-MYC* is a Wnt/ß- catenin target essential for CRC development (Rennoll, 2015 and Sansom et al., 2007). *c-MYC* overexpression is usually diagnosed in CRC specimens (Erisman et al., 1985).

Tumour suppressor genes also regulate metabolic pathways. For example, *TP53* plays an important role in regulation of glycolysis and oxidative phosphorylation (OXPHOS) phases via transcriptional regulation of its target genes *TP53*- induced glycolysis regulator (*TIGAR*) and synthesis of cytochrome c oxidase (*SCO2*), respectively. The glycolysis is negatively regulated by *TP53* through activation of *TIGAR* (an inhibitor of the fructose-2, 6-bisphosphate). In contrast, OXPHOS process is positively regulated through *TP53*-mediated transcription of *SCO2* (a member of the COX-2 assembly involved in the electron-transport chain) (Madan et al., 2011 and Bensaad et al., 2006). These functions are considered part of the anti-tumour activity of *TP53*, which stimulates glucose OXPHOS and hinders glycolysis.

1.10 Metabolic reprogramming supports tumour initiation and progression

As mentioned, during tumorigenesis, cancer cells rewire a wide range of metabolic pathways to satisfy the metabolic demands associated with the high proliferation rates (LaMonte et al., 2013). These demands are classified into three main categories: bioenergetics, such as generation of ATP; production of biochemical intermediates required for the synthesis of macromolecules, such as fatty acids for lipid synthesis, nucleotides for nucleic acids synthesis, amino acids for protein synthesis; and maintenance of reductive capacity, mostly in the form of nicotinamide adenine dinucleotide phosphate (NADPH) to neutralize increased reactive oxygen species (ROS) (Cairns et al., 2011). Metabolic reprogramming is considered a hallmark of cancer necessary for cancer initiation and progression (Furuta et al., 2010 and Liu et al., 2015a).

In 1929, the German physiologist Otto Warburg was the first scientist to discover and characterise one of the most important characteristics of cancer metabolism, which is aerobic glycolysis. In this pathway, cancer cells use large quantities of glucose and excrete it as lactate even in the presence of oxygen, which is why this phenomenon was termed "aerobic" glycolysis, also known as "the Warburg effect". The reason for this increased glycolytic flux is unclear, as, in most cases, tumours display a functional mitochondrial function (Sonveaux et al., 2008). It has been suggested that metabolic pathways branching from glycolysis, such as the pentose phosphate pathway or serine biosynthesis might be indeed the reason for the increased glycolytic flux (Faubert et al., 2017). However, recent data also indicate that normal and cancer tissues metabolize lactate though the TCA cycle, suggesting that lactate is not a "waste" product of glycolysis (Hui et al., 2017, Furuta et al., 2010 and Warburg 1956).

Interestingly, the expression of certain genes that directly regulate the rate of key metabolic pathways is drastically altered at different stages of tumour progression and several enzymes and proteins involved in metabolism show dramatically upregulation in cancer versus normal cases (Sreedhar and Zhao, 2017). For instance, cancer cells need to uptake a high level of glucose, and therefore upregulation of glucose transporters, such as GLUT1 is a common event in cancers (Asano et al., 1991). Similarly, overexpression of the monocarboxylate transporters (MCT1-4) is necessary for extrusion of cytosolic lactate (Pinheiro et al., 2014).

Moreover, several cancers show upregulation of pyruvate dehydrogenase kinase1 (PDK1). PDK1 is a negative regulator for pyruvate dehydrogenase (PDH), and it prevents conversion of pyruvate into acetyl-CoA via PDH enzyme (Kim et al., 2006 and McFate et al., 2008). This reduces acetyl-CoA entering into the Krebs cycle in the mitochondria, and promote an aerobic glycolysis and possibly reduces ROS production in cancer cells. (Papandreou et al., 2006).

In addition to the Warburg effect, several metabolic pathways undergo reprogramming in tumour cells, including lipogenesis and nucleotides synthesis pathways (De Berardinis and Chandel, 2016). Metabolic reprogramming of lipogenesis pathway is classified as one of most significant alterations in tumour cells. Three genes in this pathway play a key role in tumour progression: ATP citrate lyase (ACLY), acetyl-CoA carboxylase (ACC) and fatty acid synthase (FAS) (Menendez and Lupu, 2007). ACLY converts citrate to cytosolic acetyl-CoA, which is a key precursor of fatty acids, while ACC converts acetyl-CoA to malonyl-CoA that serves as a substrate for FAS to produce fatty acids (Turyn et al., 2003). Nucleotides are not solely components of DNA and RNA, but they are also cofactors for the biosynthesis of CoA and NAD or support cell signalling in the case of Adenosine Triphosphate (ATP) and Guanosine Triphosphate (GTP) (Tong et al., 2009). Increased nucleotide biosynthesis is common in cancer cells and plays an important role in tumorigenesis (Furuta et al., 2010). Several enzymes involved in nucleotide metabolism are upregulated in many cancer types such as thymidylate synthase (TYMS), ribonucleotide reductase (RNR), and dihydrofolate reductase (DHFR). Among these enzymes, the highest expression levels were identified for both RNR and TYMS, which have been shown to be directly involved in tumour initiation (Mannava et al., 2012, Foekens et al., 2001 and De Miglio et al., 2004). RNR is necessary for deoxy ribonucleotides synthesis via reduction of ribonucleoside diphosphates (NDPs) to deoxyribonucleoside diphosphates (dNDPs). Instead, TYMS, a folate dependent enzyme, generates thymidine monophosphate (TMP) via methylation of uridine monophosphate (UMP) (Dong et al., 2000). Of note, DHFR and TYMS are the main targets of anti-folate drugs such as methotrexate and pemetrexed, which are widely used chemotherapeutic compounds. However, in addition to the metabolic pathways outlined above, metabolism of nonessential amino acids (NEAA) has also been extensively linked to tumour metabolic reprogramming (Liu et al., 2015b).

1.11 Regulation of NEAA metabolism in cancer cells

The requirement of cancer cells for amino acids increases to support their rapid proliferation. Based on their metabolism, in humans two groups of amino acids have been distinguished: essential amino acids (EA) and NEAA. EA cannot be synthesized by the body and must be supplied through nutritional intake. This category includes histidine, isoleucine, leucine, lysine, methionine, phenylalanine, threonine, tryptophan and valine. NEAAs are produced by living body and they include arginine, glutamine, tyrosine, cysteine, glycine, proline, serine, ornithine, alanine, asparagine and aspartate (Horovitz and Paşca, 2017). Amino acids are essential building blocks for protein synthesis, but they are also intermediate metabolites that fuel other biosynthetic reactions (Tsun and Possemato, 2015). For example, aspartate and glycine contribute to the biosynthesis of nucleotides; serine is tightly associated with folate metabolism though production of 5, 10 methylene-tetrahydrofolate, aspartate and glutamate are very important for fuelling the TCA cycle through transaminase reactions, a process known as anaplerosis (Lane and Fan, 2015 and Labuschagne et al., 2014).

Recent work has outlined a striking reliance of cancer cells on the metabolism of NEAA, paving the way to the identification of new potential approaches to cancer therapy. The NEAA glutamine has a pivotal role in supporting cancer growth and progression. Together with glucose, glutamine is a major source of energy and carbons for cancer cells (Curi et al., 2005 and De Berardinis et al., 2008).

Furthermore, glutamine is the main nitrogen source. Many specialised transporters such as Na+-dependent neutral amino acid transporter alanine-serine-cysteine transporter 2 (ASCT2), enable glutamine uptake by cancer cells and are upregulated in many tumours (Cormerais et al., 2018). Once inside the cells, glutamine is metabolized by the action of one of the two glutaminases enzymes (GLS1 and GLS2) which deaminate glutamine to produce glutamate and ammonia. Glutamate enters the tricarboxylic acid (TCA) cycle via its conversion to α-ketoglutarate by the action of glutamate dehydrogenase (GDH) or transaminases.

Glutamine metabolism contributes to the maintenance of an active TCA- cycle in cancer cells and its metabolism has been widely investigated as a potential target for anti-cancer therapies. Many tumours show overexpression of GLS, and inhibition of GLS isozymes

(GLS1 and GLS2) impairs tumour growth (Lobo et al., 2000, Gao et al., 2009 and Wang et al., 2010). GLS inhibitors, such as compound 968 and Bis-2-(5-phenylacetamide-1, 2, 4-thiadiazol-2-yl) ethyl sulphide (BPTES), demonstrated encouraging results in delaying tumour growth (Robinson et al., 2007 and Le et al., 2012).

Additionally, another important non-essential amino acid for cancer cells growth is arginine. Arginine supports multiple cellular metabolic pathways such as urea cycle, biosynthesis of nucleotides, proline, glutamate and nitric oxide (Kuo et al., 2010). L-citrulline and aspartic acid are the main intermediate substrates that are converted into argininosuccinate via the action of argininosuccinate synthetase (ASS) enzyme in the urea cycle. ASS is the rate- limiting enzyme for de novo arginine biosynthesis. Subsequently, argininosuccinate is converted into L- arginine and fumarate by argininosuccinate lyase (ASL). Fumarate enters the tricarboxylic acid cycle (TCA), linking arginine metabolism with glucose energy metabolism. Several human cancers, such as CRC, malignant melanoma and hepatocellular carcinoma, display loss of ASS expression, typically through promoter methylation. This event renders cancer cells unable to synthesise arginine and reliant on its external supplementation, a phenotype known as arginine auxotrophy (Phillips et al., 2013, Keshet, and Erez, 2018 and Haines et al., 2011). Deprivation of arginine from culture medium halts proliferation of ASS-deficient tumour cells (Scott et al., 2000 and Alexandrou et al., 2018). Therefore, these cancers are susceptible to arginine deprivation therapy utilizing recombinant arginine degrading enzymes such as arginine deiminase (ADI) and arginase (Feun et al., 2015). Regulated forms of these enzymes are being tested extensively in clinical trials in a wide range of cancers (Fung and Chan, 2017 and Feun et al., 2012).

Asparagine is another NEAA with an important role in promoting proliferation of cancer cells (Krall et al., 2016). Asparagine plays a critical role as exchange factor for other amino acids: intracellular asparagine levels enable cancer cells to uptake amino acids such as glycine, serine, arginine and histidine. Through this role, asparagine regulates mTORC1 activity and protein synthesis (Knott et al., 2018). Beyond regulation of mTOR, asparagine can also participate in nucleotides biosynthesis and serine metabolism via its regulation of serine levels uptake from the extracellular environment (Krall et al., 2016 and Richards and Schuster, 1998). Additionally, knockdown of asparagine synthetase (ASNS) in cancer cell lines such as HeLa (cervical cancer), A431 (epidermoid

carcinoma), Hs578T (breast cancer) and MDAMB231 (breast cancer), leads to reduced proliferation in absence of asparagine from the culture media (Richards and Kilberg, 2006). These findings indicate that intracellular asparagine level supports cancer cell proliferation (Zhang et al., 2014 and Krall et al., 2016).

Serine is another NEAA whose metabolism supports tumorigenesis. Serine is synthesised from a three-step biosynthesis pathway branching from glycolysis. The glycolytic intermediate 3-phosphoglycerate is converted to 3-phosphohydroxypyruvate by phosphoglycerate dehydrogenase (PHGDH). The sequential actions of phosphoserine transaminase1 (PSAT1) and phosphoserine phosphatase (PSPH) converts 3-phoshohydroxypyruvate to serine (Sun et al., 2016). The downstream metabolism of serine is also extremely important. Serine can be converted to glycine by the action of serine hydroxymethyltransferase (SHMT) and in this process SHMT uses tetrahydrofolate as cofactor generating 5,10-methylenetetrahydrofolate in the process. This compound is part of the one-carbon/folate metabolism, which is a metabolic pathway that serves to activate and transfer 1C units for biosynthetic processes including nucleotide synthesis and homocysteine remethylation (Locasale, 2013).

In addition, glycine is a component of glutathione linking serine metabolism to redox homeostasis. A loss of function screen established that certain breast cancers have phosphoglycerate dehydrogenase (PHGDH) gene amplification and depend on endogenous production of serine to sustain proliferation (Possemato et al., 2011). Similar results were obtained in melanoma where substantial amounts of glucose-derived carbons are fuelled into serine biosynthesis (Locasale et al., 2011). In addition, serine metabolism also contributes to redox balance by glutathione production (Vučetić et al., 2017). Interestingly, it has been reported that c-*Myc* promotes transcription of serine biosynthesis enzymes (Sun et al., 2015).

1.12 Proline metabolism in cancer initiation and progression

1.12.1 Proline metabolism

Proline is a NEAA with a unique structure as the alpha amino nitrogen group is contained within the pyrrolidine ring. This makes proline different from other NEAAs and the only proteinogenic amino acid (sometimes called an imino acid) with the amine group bound to two carbon atoms to form a ring-like structure known as pyrrolidine ring (Figure 1.14) (Phang, 1985, Phang et al., 2008a and Kawakami et al., 2012).

Additionally, because of its peculiarity, proline plays a distinctive and irreplaceable role in influencing the chemical and physical properties of proteins and mediating molecular recognition and signalling (Hong-qi et al., 1982 and Mehansho et al., 1983). Indeed, the interactions between different proteins are often based on proline-dependent recognition motifs (Adams, 1970, Adams and Frank, 1980 and Phang, 1985).

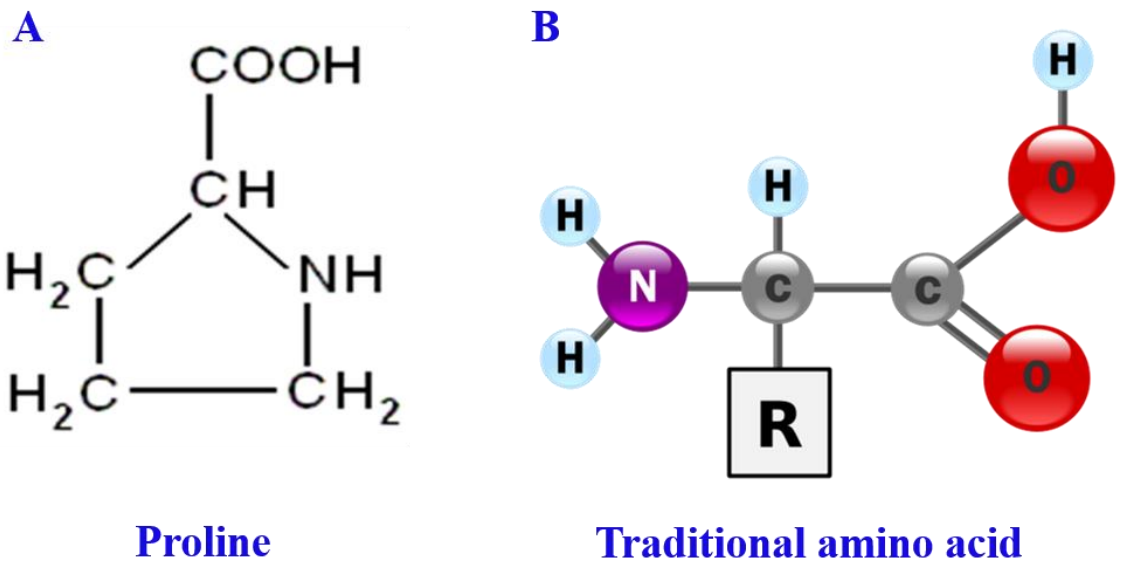

Figure 1.14. The chemical structure of proline. Proline structure in **(A)** compared to traditional amino acid structure in **(B)**. The amine (NH) group in proline is bound to two-carbon molecules leading to a ring-like structure, (Figure taken from Kawakami et al., 2012).

Another implication of the proline unique ring structure is that its metabolism cannot be performed by the pyridoxal-phosphate-dependent transaminases that metabolize primary amino acids. Instead, a specific set of enzymes has evolved to enable the biosynthesis and catabolism of proline (Phang et al., 2010).

There are two main routes to proline biosynthesis that initiate with ornithine or glutamate, respectively. Both metabolites are converted to a common proline precursor: L-glutamate-γ- semialdehyde (GSAL), an intermediate that spontaneously cyclizes to pyrroline-5-carboxylate (P5C) (Figure 1.15) (Tanner, 2017). Ornithine δ-aminotransferase (OAT) catalyzes GSAL formation from ornithine, whereas P5C synthase (P5CS) forms GSAL from glutamate (Fichman et al., 2015). Finally, reduction of P5C to proline is catalysed by NAD (P)H-dependent pyrroline-5-carboxylate reductases (PYCRs).

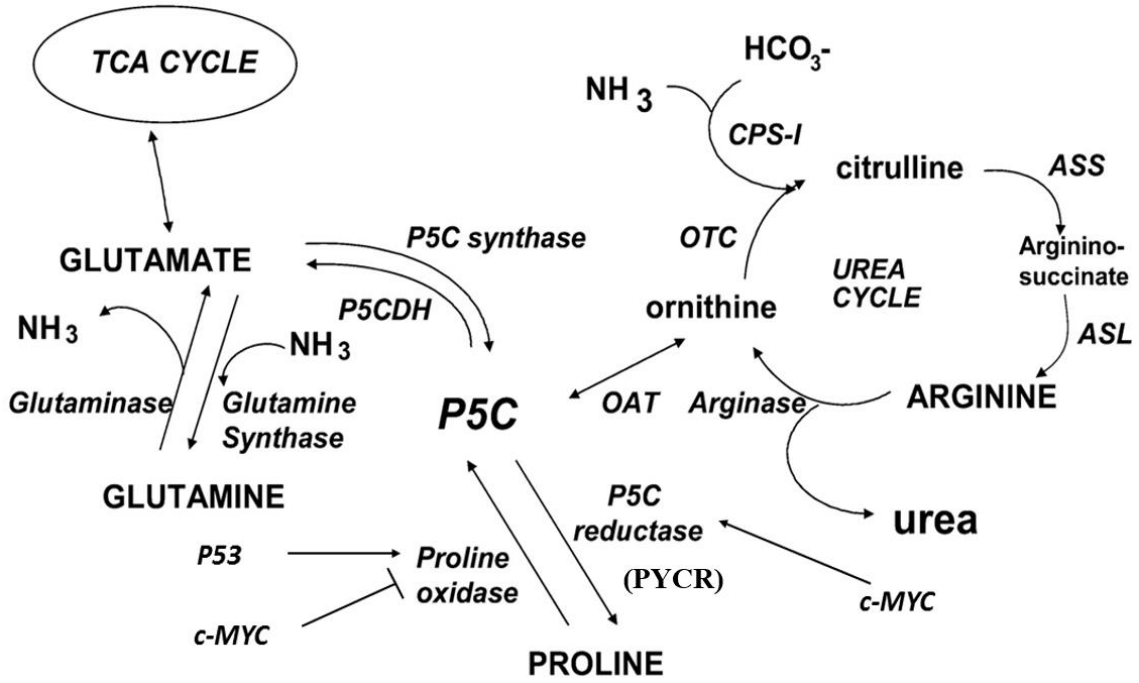

Figure 1.15. Metabolic pathway of proline and related amino acids. OAT: Ornithine aminotransferase, **ASL,** argininosuccinate lyase**, ASS,** argininosuccinate synthase, **CPS-I**, carbamoyl phosphate synthetase, **P5C:** Pyrroline-5-carboxylate, **P5CDH:** P5C dehydrogenase (Figure taken from Bertolo and Burrin, 2008).

In humans, three isozymes of PYCR have been distinguished: PYCR1, PYCR2 and PYCRL (PYCR3) (Dougherty et al., 1992, Hu et al., 2008 and Wu et al., 2008). These three isozymes are encoded by three different genes, localized at three different chromosomal locations (Table 1.2) (Phang, 1985 and Dougherty et al., 1992). The PYCR1 gene is located on chromosome 17q25.3 and it encodes two protein isoforms, the first one contains 319 residues and the second isoform contains 316 amino acids. The PYCR2 gene is located on chromosome 1q42.12 and it encodes two isoforms of 320 and 246 amino acids (Dougherty et al., 1992 and Phang, 1985). The PYCR3, initially identified in melanoma cells, is localized on chromosome 8q24.3, and it encodes two isoforms, a 286 aa and a 266 aa protein (De Ingeniis et al., 2012). Moreover, PYCR1 and PYCR2 enzymes are localized in the mitochondria, whereas PYCR3 is cytosolic. It has been suggested that PYCR1 might preferentially localize in mitochondrial outer membrane or mitochondrial transmembrane space, while the PYCR2 resides in the mitochondrial matrix (De Ingeniis et al., 2012). This compartmentalization might also have functional implication in the enzyme cofactor specificity. Mitochondrial PYCRs preferentially use NADH, but the cytosolic PYCRL requires NADPH as co-factor (De Ingeniis et al., 2012). In this regard, it is commonly accepted that cytosolic proline synthesis (ornithine route) oxidizes the NADPH as a cofactor and relies on PYCR3, whereas mitochondrial proline synthesis (glutamate route) preferentially oxidizes the NADH cofactor (De Ingeniis et al., 2012).

Recently, the high-resolution crystal structures of PYCR1 in complex with the proline analogue L-tetrahydro-2-furoic acid (L-THFA)and NAD(P)H has been determined (Christensen et al., 2017) (Figure 1.16).

PYCR1 has two main domains (Figure 1.16. A). The N-terminal domain contains a Rossmann fold for binding to NAD (P) H. The C-terminal domain has numerous α-helices and elaborates in oligomerization and binding of substrate. Two PYCR1 monomers combine through their C-terminal domains to form a functional dimer (Figure 1.16.B). Five dimers assemble further around a central axis to form a complex claaled pentamer-of-dimers decamer (Figure 1.16. C).

The cylindrical decamer, PYCR1 fold and the interlocking dimer have also been observed in the P5CRs structure that isolated from microrganisms (Nocek et al., 2005). The reason

for the decameric structure remains unclear, although it might accelerate proline production as part of a metabolon.

Enzyme	Gene Name	Gene ID	Map Location	Isozyme	Amino Acids No.
PYCR1	PYCR1	5831	17q25.3	PYCR1.1	319
				PYCR1.2	316
PYCR2	PYCR2	29920	1q42.12	PYCR2.1	320
				PYCR2.2	246
PYCRL/3	PYCRL	65263	8q24.3	PYCRL.1	286
				PYCRL.2	266

Table 1.2. : Human PYCR Isozymes. Summary of the PYCRs genes, showing gene ID, chromosomal localization and main isoforms. (Adapted from Hu and Hou, 2014).

The catabolic breakdown of proline takes place in the mitochondria and is initiated by the inner mitochondrial membrane enzyme proline dehydrogenase (PRODH or POX), which oxidase proline back to P5C (Liu and Phang 2013). Using the flavin adenine dinucleotide (FADH) as cofactor. P5C can then go back to ornithine via OAT or to glutamate via pyrroline-5- carboxylate dehydrogenase (P5CDH) (Bertolo and Burrin 2008 and Liu, and Phang 2013) (Figure 1.15). Two genes code for PRODH enzymes: PRODH1 (chromosome22q11.21) and PRODH2 (chromosome 19q13.12) (Tanner et al., 2018). The mitochondrial degradation of proline via PRODH results in direct electron donation to the electron transport chain (ETC) through FADH to generate either ATP or reactive oxygen species (ROS) (Adams, 1970, Adams and Frank, 1980 and Liu et al., 2005).

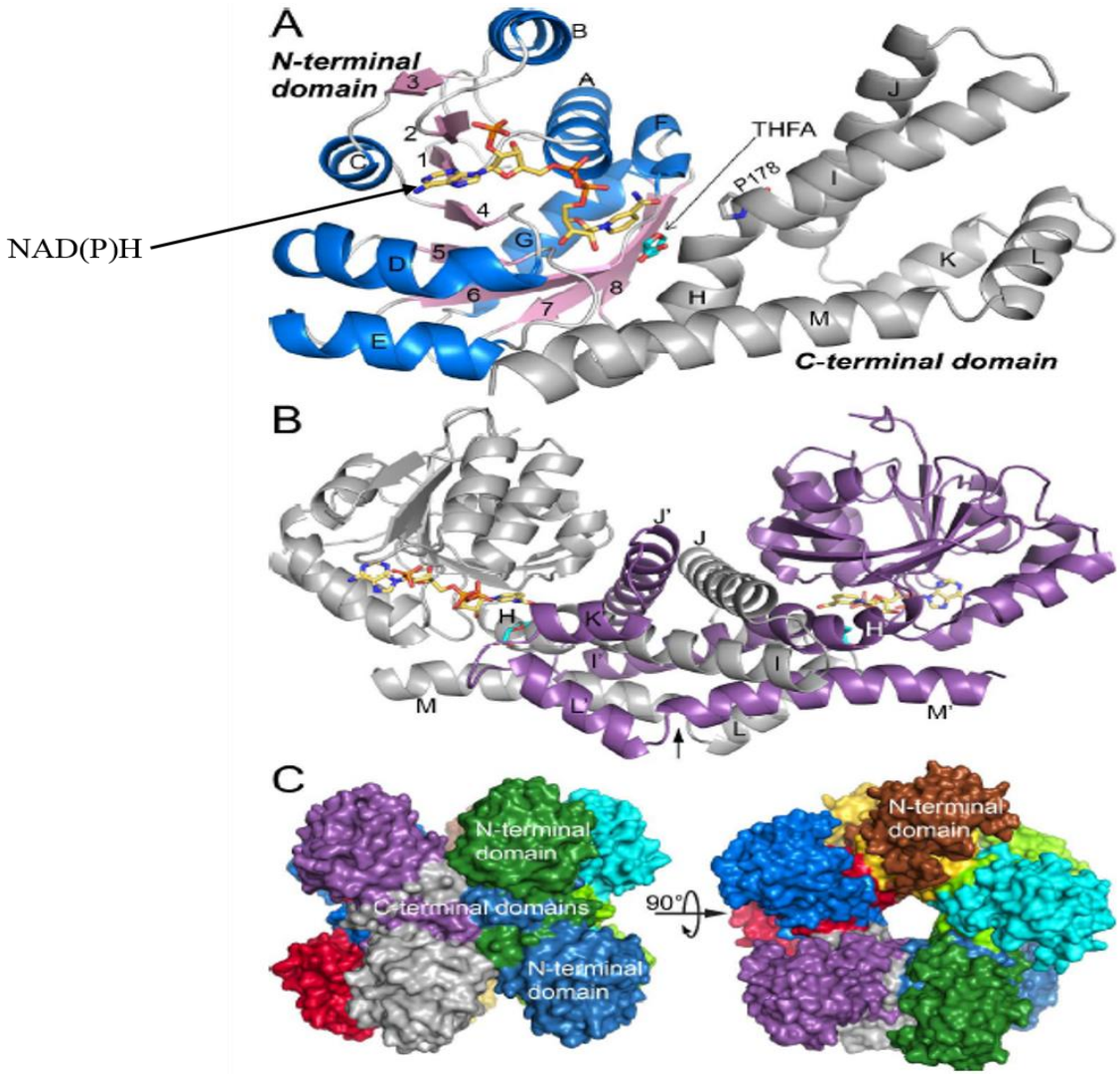

Figure 1.16. PYCR1 structure. (A) The 3D structure of the PYCR1 monomer as appear in the ternary complex with NADPH and the proline/P5C analogue L-THFA (The N-terminal NAD (P) H-binding domain has coloured according to the secondary structure, with β-strands as pink and α-helices as blue. The C-terminal oligomerization domain shows gray colour. The β-strands have been labelled as 1-8 and the α-helices have labelled as A-M. **(B)** The molecular structure of PYCR1 dimer. The α-helices of the C-terminal domain have been labelled as H-M for the gray monomer and H´-M´ related to the purple monomer. The arrow represents the 2-fold axis of the dimer. **(C)** The pentamer-of dimers decamer for PYCR1, through each chain shows different colour aria (Figure taken from Tanner et al., 2018).

1.12.2 Proline sources in the tumour microenvironment

In addition to the dietary intake, proline can be supplied to living cells via degradation of collagen by matrix metalloproteinase (MMPs) and prolidase. Collagen constitutes 80% of extracellular matrix (ECM) proteins components and hydroxyproline and proline amount to more than 25 % of the amino acid residues in collagen. Therefore, ECM is a major source of proline (Phang et al., 2010 and Dtxit et al., 1977). In tumours, MMPs are upregulated and contribute to cancer progression and invasion (Stallings and Radisky, 2007, Deryugina and Quigley, 2006, Kakkad et al., 2010 and Stevenson et al., 2013). The concentration of proline is increased in tissues isolated from different tumours and this has been proposed to be, at least partially, a consequence of collagen degradation (Pandhare et al., 2009).

1.12.3 *PRODH* as a tumour suppressor gene

The *PRODH* gene, which has been identified as a *TP53*-induced gene in 1997 (Polyak et al., 1997). *PRODH* contributes to the *TP53* tumour suppressor function. Indeed, through oxidation of proline to P5C, PRODH generates reactive oxygen species (ROS), which enables p53-induced cell cycle arrest and apoptosis (Simon et al., 2000, Phang et al., 2010, Liang et al., 2013, Phang et al., 2008 a,b and Hu et al., 2007).

Importantly, PRODH enzyme could also support tumour progression through ATP generation under nutrient stress conditions, such as glucose deprivation (Pandhare et al., 2009), or under hypoxia (Liu et al., 2012a).

Other potential mechanisms explain *PRODH* tumour suppressor activity. *PRODH* activity suppresses the phosphorylation activation of the three major subtypes of the mitogen-activated protein kinase (MAPK) pathways, namely MEK/ERK, JNK, and p38 (Liu et al., 2006). Moreover, it plays an important role in reducing cyclooxygenase-2 (COX-2) expression, leading to supressed prostaglandin E2 (PGE2) production (Liu et al., 2008b). PGE2 is an important molecule in promoting inflammation and has been shown to contribute to nuclear ß -catenin localization and CRC progression (Castellone and Teramoto, 2005). Indeed, PRODH/POX decreases the Wnt/ß-catenin signalling pathway in CRC cell lines (Liu et al., 2008 a). Finally, the phosphorylation of epidermal growth factor receptor (EGFR) is hindered by the action of PRODH/POX. Interestingly,

the activating mutations and overexpression of EGFR signalling supports the carcinogenesis processes in several neoplasms, including CRC, through the induction of cellular proliferation and inhibition of apoptotic processes (Henson and Gibson, 2006).

Recently, it has been reported that the oncogenic transcriptional factor *c-MYC* is a critical regulator of PRODH/POX through the micro-RNA miR-23b* (Liu and Phang 2013). Using *c-MYC*-inducible human Burkitt lymphoma cells P493 and PC3 human prostate cancer cells, Phang's team was able to show that *c-Myc* upregulates the expression of miR-23b*, which in turn suppresses PRODH/POX protein expression. (Liu et al., 2012b).

In summary, these results demonstrate the importance of proline catabolism via PRODH/POX in human neoplasms (Liu et al., 2012b and Liu and Phang 2013).

1.12.4 The role of proline biosynthesis in cancer

Proline biosynthesis is an important metabolic pathway during the tumorigenesis. Several human cancers display upregulation of enzymes involved in proline biosynthesis, such as P5CS and PYCR1 (Phang et al., 2012). Notably, the oncogene *c-MYC* stimulates the proline biosynthesis from glutamine through increased expression of glutaminase enzymes GLS-1 and 2, as well as upregulation of P5CS and PYCR1 (Wise et al., 2008, Gao et al., 2009, Hu et al., 2008, Liu et al., 2012b, Li and Simon, 2013 and Phang et al., 2015).

Among PYCRs isozymes, PYCR1 is overexpressed in multiple human cancers such as kidney, lung, prostate, ovary, pancreas, melanoma, breast, brain and bone cancers as well as lymphomas and leukemias (Ahn and Metallo, 2015). A recent large-scale comparative analysis of transcriptomic datasets identified PYCR1 was one of the most commonly overexpressed metabolic genes in comparison to normal tissue among 19 different cancer types (Nilsson et al., 2014).

On the contrary to what is observed with PRODH, expression of the oncogene *c-MYC* in human Burkitt lymphoma and prostate cancer cell lines induced an upregulation of PYCR1 and P5CS, resulting in higher levels of intracellular proline (Liu et al., 2012b). In line with this observation, expression of both PYCR1 and PYCR2 was increased in a panel of melanoma cell lines but was undetectable in normal melanocytes (De Ingeniis et al., 2012).

Experiments performed using genetic knockdown have shown that PYCR1 expression promotes tumorigenesis in vitro and in vivo (Possemato et al., 2011 and Loayza-Puch et al., 2016). Multiple mechanisms have been suggested to explain the pro-tumorigenic role of PYCR1. Of course, PYCR1 is chiefly responsible for proline synthesis and Agami's group reported that renal cell carcinoma progression relies on PYCR1-mediated proline production for protein synthesis (Loayza-Puch et al., 2016). In addition, through its NADH-dependent reaction, PYCR1 regulates mitochondrial NADH/NAD+ with important consequences of oxidative phosphorylation and Krebs cycle activity (Liu and Phang, 2013). Interestingly, a recent publication on IDH-mutant gliomas explained that glutamine-derived proline biosynthesis increases through enhanced activity of PYCR1, coupled to NADH oxidation to NAD+ and in this way, PYCR1 keeps the TCA cycle going providing recycling NADH to NAD+ (Hollinshead et al., 2018). PYCR1 has also been shown to prevent oxidative stress via its interaction with ribonucleotide reductase small subunits B (RRM2B). PYCR1 and PYCR2 proteins interact directly with RRM2B to promote its anti-oxidant activity and thereby promoting cell survival (Kuo et al., 2016). In fact, it has been reported that RRM2B protein recombination promotes intrinsic catalase activity converting hydrogen peroxide to water and oxygen (Liu et al., 2008b). In cancer, RRM2B protein has been over-expressed compared to normal tissue leading to decrease intracellular ROS and protecting the mitochondrial membrane potential against hydrogen peroxide (Liu et al., 2008b).

As previously explained, proline is synthesized from glutamate or ornithine via P5C, which is reduced to proline via an NAD (P) H-dependent reaction, catalysed by PYCRs; whereas its degradation involves two oxidative steps catalysed by PRODH and P5CDH within the mitochondria. According to Phang's model, proline metabolism and catabolism are asymmetric: proline synthesis occurs in the cytoplasm, whereas its degradation is, of course, mitochondrial. This proline-P5C cycling results in an unbalanced transfer of reductive equivalents from the cytosol to the mitochondria and has been implicated in supporting ATP production, nucleotide and protein synthesis, anaplerosis of the TCA cycle, and redox balance in cancers (Hagedorn and Phang, 1983 and Phang and Liu, 2012). It should be noted though that the overall physiological relevance of the proline cycle has been called into question, especially after the identification of critical role of mitochondrial proline synthesis from PYCR1 (Tanner et al., 2018 and Elia et al., 2017).

Although the functional advantages provided to cancer cells by modulating proline metabolism are not completely clear, the importance of proline in extracellular matrix proteins (e.g. collagen) could also play a role in supporting tumour progression (Olivares et al., 2017).

Overall, it is evident that the proline metabolism plays a vital role in the regulation of tumorigenesis. This metabolic pathway is indeed reprogrammed in tumour cells via the *c-MYC* oncogene and the *TP53* tumour suppressor (Green et al., 2016 and Polyak et al., 1997). Although the mechanisms through which proline metabolism sustain tumour progression are still unclear, the proline axis is now recognised as one of the most important metabolic pathways involved in tumour formation and progression.

1.13 The *Lgr5-Cre^{ER} Apc$^{fl/fl}$* mice as a genetically engineered mouse model of CRC

Genetically modified mice as a pre-clinical model for human cancers are widely used tools to recapitulate and dissect the tumourigenesis process, and test potential therapies. In the case of CRC, different mouse models have been developed to study the function of genes implicated in tumour development (Jackstadt and Sansom, 2016 and Heindryckx et al., 2009, Heyer et al., 1999 and Tong et al., 2011).

One of the most commonly used methods to recapitulate CRC development in mice is to induce the selective loss of the tumour suppressor *Apc*, thus mimicking the typical aberrations found in most human CRC cases. In 2009, Hans Clevers' team generated the *Lgr5-EGFP-IRES-Cre^{ERT2}/Apc$^{floxed/floxed}$* (*Lgr5-Cre^{ER}/Apc$^{fl/fl}$*) mice that employ the Cre/Lox site-specific recombination system to achieve depletion of *Apc* selectively in the stem cell compartment of the intestine (Shibata et al., 1997, Barker et al., 2009).

Cre technology exploits the ability of the bacteriophage P1 Cre (cyclization recombination) recombinase to recombine DNA material located between two consensus sequences known as *lox*P sites (lox of x (cross)-over) (Steinberg and Hamilton, 1981 and Nafissi and Slavcev, 2014). Each *lox*P site contains two palindromic sequences (13bp) separated by an asymmetrical spacer sequence (8bp) (Figure 1.17) (Missirlis et al., 2006, O'Gorman et al., 1991 and Sauer and Henderson, 1988).

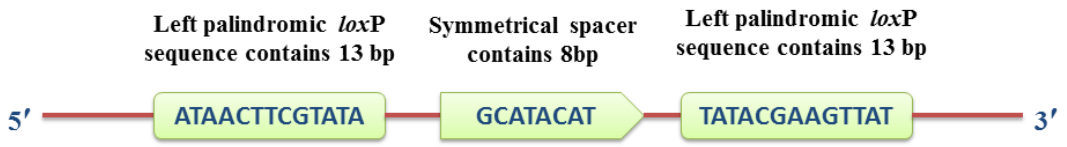

Figure 1.17. The sequences of the *lox*P site. Two 13bp palindromic sequences flank the spacer sequence (8bp); the directionality of *lox*P is given by orientation of the spacer sequence. (Figure taken from Jackson, 2002).

Cre recombinase binding to two consecutive *lox*P sites can result in inversion, translocation or deletion. It is the orientation of the *lox*P sites that determines the outcome of the recombination event. As shown in Figure 1.18, if the sites have the same orientation, then the intermediate DNA is deleted (Shibata, 1997).

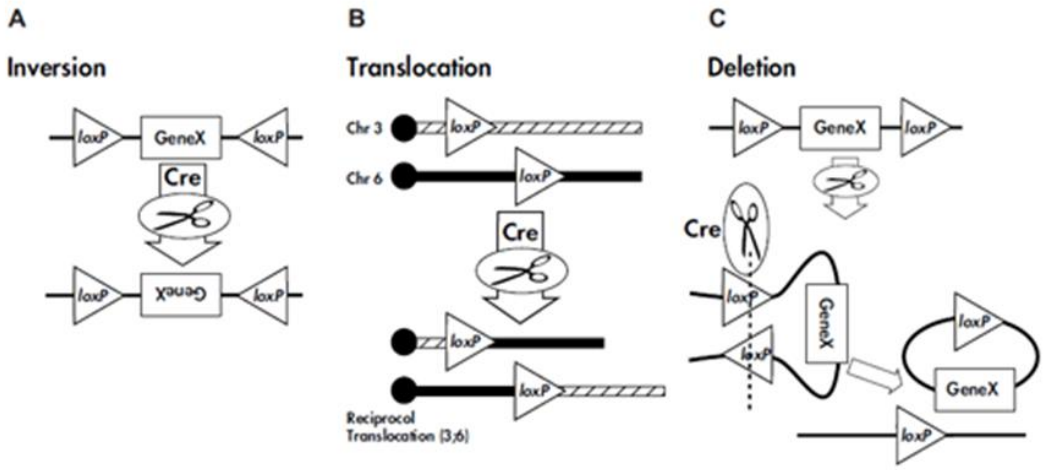

Figure 1.18. The different outcomes of Cre recombinase activity. (A) *lox*P sites located in opposite direction results in Cre-mediated inversion of the floxed sequence. **(B)** When *lox*P sites are located on different chromosome, Cre recombinase activity leads to translocation. **(C)** The deletion of floxed gene takes place when the *lox*P sites are align in the same direction (Figure taken from https://littlesearcher.wordpress.com/2013/02/17/cre-lox-recombination/).

In the case of the *Lgr5-Cre*^{ER}*/Apc*$^{fl/fl}$, model, the Cre gene has been combined with a modified hormone-binding domain of the human oestrogen receptor (ER) to produce a Cre/oestrogen chimeric protein (*Cre*^{ER}). The ER binding domain has being modified in critical residues so that it is able to bind the oestrogen analogue tamoxifen, but not the endogenous mouse hormones (Yaşar et al., 2017). This chimeric protein is retained within the cell cytoplasm, unless animals are injected with tamoxifen which binds to the *Cre*^{ER}, promotes its transient translocation within the nucleus, and enables recombination and deletion of the *Apc* gene (Anastassiadis et al., 2010, Feil et al., 2009 and Metzger and Chambon, 2001) (Figure 1.19).

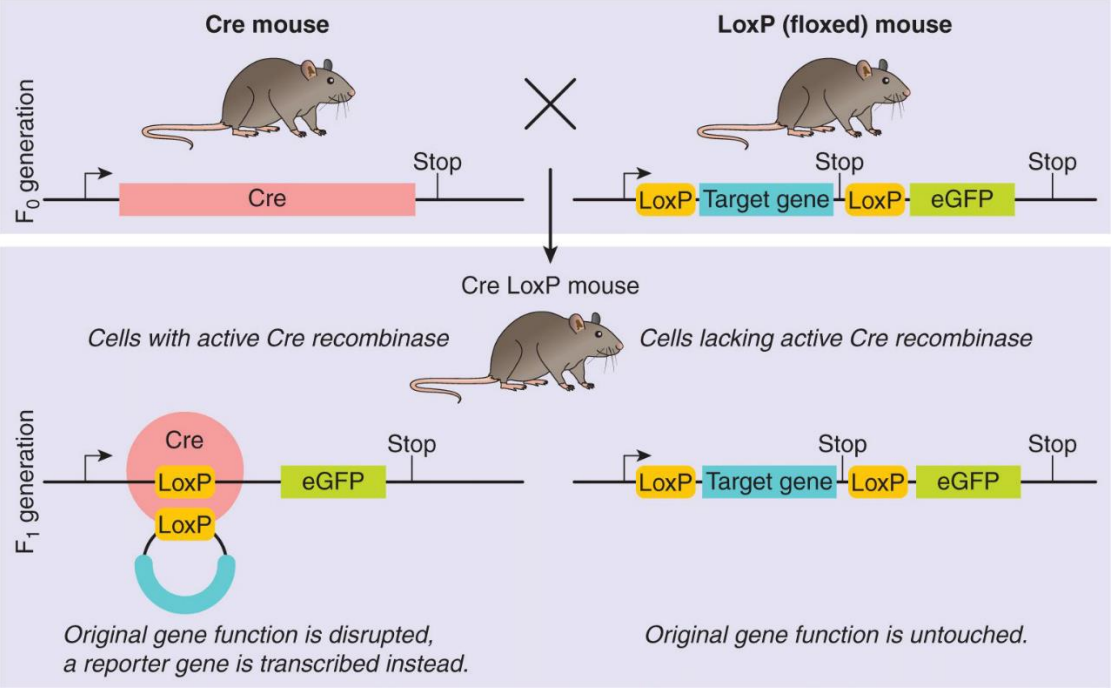

Figure 1.19 Illustration of the experimental Cre-*Lox*P site system. The function of a target gene is disrupted by a conditional knockout achieved by flanking the region of interest with *Lox*P sites for recognition and deletion by the Cre recombinase. Typically, these experiments are performed with a tissue-specific promoter driving the expression of the Cre-recombinase (or with a promoter only active during a distinct time in ontogeny) (Figure taken from https://oncohemakey.com/methods-of-molecular-analysis/).

In fact, the endogenous *Apc* exon 14 has been flanked by two *lox*P sequences within the neighbouring introns 13 and 14 (Shibata et al., 1997). Cre^{ER}-mediated recombination of this region, results in deletion of the *Apc* exon 14 and generation of a truncated, non-functional *Apc* gene (Figure 1.20).

To achieve selective deletion of the *Apc* in the stem cell compartment, Clevers and colleagues integrated an enhanced green fluorescent protein *(EGFP)-IRES-*Cre^{ERT} cassette, within the ATG codon of the endogenous *Lgr5* allele using a knock-in strategy (Clevers et al., 2007, Tetteh et al., 2016, Barker et al., 2007 and Barker et al., 2012). In this way, EGFP and Cre proteins are expressed simultaneously through the IRES (internal ribosomal entry sequence) and are targeted to the stem cell compartment by the endogenous *Lgr5* promoter. (Barker et al., 2007).

Deletion of exon 14 of the *Apc* gene is then achieved by tamoxifen injection. The consequent constitutive activation of Wnt pathway leads to development of adenomas within 4 to 8 weeks from the initial injection of tamoxifen (Barker, 2014).

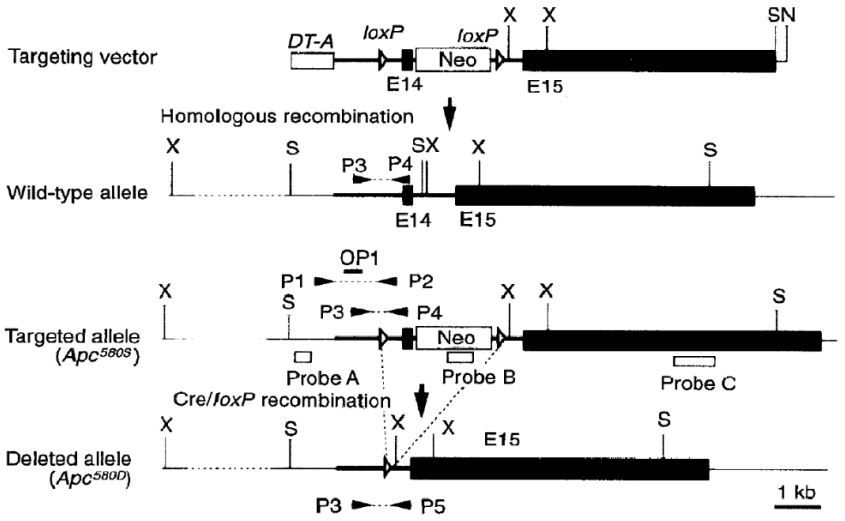

Figure 1.20. Establishment of a mutant mouse line carrying a conditionally targeted *Apc* allele. Structure of the conditionally targeted allele of *Apc* (*Apc580S*) and the mutant *Apc* allele resulting from the deletion mediated by Cre-*lox*P recombination (deleted allele, *Apc580D*). The targeting vector was constructed by inserting one *lox*P site into intron 13 and the other, with a PGKneo cassette (Neo), downstream into intron 14, resulting in exon 14 (E14) flanked by *lox*P sites (open triangles) (Figure taken from Shibata et al., 1997).

1.14 Hypothesis and Aim

Data so far suggest that PRODH/POX contributes to *TP53*-mediated tumour suppressors in CRC cell lines and that *c-Myc* can activate proline biosynthesis (Green et al., 2016, Hu et al., 2010 and Polyak et al., 1997). Moreover, the analysis from Nilsson and colleagues of 19 cancer types, including CRC, identified PYCR1 as one of the most consistently upregulated metabolic genes in cancer (Nilsson et al., 2014). However, the role of proline biosynthesis in CRC remains poorly investigated. Therefore, the overarching hypothesis of this study is that sustained proline biosynthesis fuelled by upregulation of PYCR1 is necessary for CRC progression. In this regard, this project was undertaken to fulfil the following aims:

- To investigate the expression level of PYCR1 enzyme in CRC cell lines, primary cells isolated from CRC patients and tissue microarrays (TMA) of CRC specimens and matched normal colon tissue. To achieve this aim, three main techniques will be employed: western blot (WB), real time (RT)-qPCR and immunohistochemistry (IHC).
- To investigate expression of proline metabolism enzymes in the intestinal tissue isolated from *Lgr5-Cre^{ER}/Apc$^{fl/fl}$* mice to monitor alterations of proline metabolism during early colorectal tumorigenesis. WB, RT-qPCR and IHC will be implemented to achieve this aim.
- To investigate the functional role of PYCR1 expression in tumour progression. Toward this end, knockdown of PYCR1 expression will be accomplished via small-interference (si) RNA technique and the effect of the knockdown on cell proliferation and survival will be assessed. Cytofluorimeter analysis and WB will be used to measure cell proliferation and cell death and to assess expression of biomarkers of cell cycle and apoptosis. To validate PYCR1 as a potential therapeutic target in CRC, we will assess the impact of its knockdown on an immortalized colonic epithelium control cell line (Roig et al., 2010).

Chapter Two: Materials and Methods

Materials and Methods

2.1. Materials

2.1.1. General laboratory consumption

All tissue culture plastic-ware, unless otherwise stated, were purchased from Corning/Life science (Wiesbaden, Germany) or Greiner (Gloucestershire, UK), while Eppendorf tubes were supplied by VWR (Lutterworth, Leicestershire, UK). The 6 cm dishes were obtained from Thermo Scientific (Loughborough, UK). All chemicals and solvents for common laboratory use were from Fisher Scientific (Loughborough, UK) and Sigma (Poole, UK). Cell culture growth medium, trypsin and fetal calf serum (FCS) were purchased from Life Technologies (Paisley, UK). Western blots buffers such as 30% (W/V) Acrylamide: 0.8%(W/V) Bis-Acryl-amide Stock solution (37.5:1), 4X protoGel Resolving buffer and protoGel stacking buffer, were all ordered from Geneflow (Lichfield, UK), in addition to TEMED- (N,N,N',N'- Tetramethylethylenediamine) from Sigma Poole, UK. Additionally, western blot devices and gel casting apparatus were from BIO-RAD Laboratories (Watford, UK).

2.1.2. Buffers

The composition of the buffers used in this project are listed in Table 2.1

Table 2.1 Buffers with their constituent ingredients and procedures of preparation

Buffer Name	Buffer Composition
Running Buffer (Western blot)	Was prepared as 1:10 dilution, adding 100 mL of 0.25M Tris/1.92 M Glycine/1% sodium dodecyl sulfate (SDS) (10X) (Geneflow, Lichfield, UK, Catalogue Number (Cat# B9-0032) in 900mL water.
Transfer Buffer (Western blot)	Was prepared as 1:10 dilution adding 100 mL of 0.25M Tris/1.92M Glycine (Geneflow, Lichfield, UK, Cat# B9-0056) in 700 mL water and 200 mL 100% Methanol (Fisher Scientific , UK, Cat# M/4056/17).
Blocking and Antibody incubation Buffer (Western blot)	**5% blocking buffer** was prepared by dissolving of 2.5 g of milk (Marvel dried skimmed milk, London, UK) in 50 mL of 0.1% PBS-T, **Antibody diluent buffer** was obtained by dissolving 1.5 g of milk or Bovine Serum Albumin (BSA) (Sigma, Poole, UK, Cat# A2153-50G) in 50 mL of 0.1% PBS-TWEEN®20 to get 3% BSA or milk solution for dilution of primary and secondary antibodies.
Cell Lysis Buffer (Western blot)	This buffer was prepared by dissolving 1 taplet complete mini protease inhibitor cocktail and 1 tablet of phosphatase inhibitor in 10 mL of complete lysis–M reagent (Sigma, Roche Diagnostics Sussex, UK, Cat # 04719956001).
10% Ammonium Persulfate (APS) (Western blot)	Was prepared by adding 1 g of Ammonium Persulfate (Sigma, Poole, UK, Cat# A3678-100G) in 10 mL water (10%.w/v ratio). This stock solution was aliquoted and stored at -20 ˚C for long-term storage.
Sample Loading Buffer (Laemmli 2X concentrated buffer) (Western blot)	This buffer contains 4% SDS, 20% Glycerol, 10% 2-Mercaptoethanol, 0.004% Bromophenol blue and 0.125 M Tris HCl, pH adjusted at 6.8 (Sigma, Poole, UK, Cat# s3401).
Enhanced Chemiluminescence Luminol (ECL) reagent to detect of protein (Western blot)	An equal volume of two reagents A and B were mixed together in a 1:1 ratio for 3 min and kept in the dark at room temperature (supplied by Geneflow Ltd, UK, Cat# K1-0174).
Phosphate Buffered Saline (PBS)	Was prepared by dissolving of 10 tablets of PBS (Oxoid, Basingstoke, UK, Cat# BR0014G) in 1000 mL water.
0.1% Phosphate Buffered Saline-TWEEN®20(PBS-T)	Was made by adding 10 tablets of PBS (Oxoid, Basingstoke, UK) to 1000 mL distilled water and mixing

	with 1 mL of TWEEN -20 (Sigma, Poole, UK, Cat# P9416-50 mL).
Antigen Retrieval Buffer (Immunohistochemistry)	10 mM Citrate buffer was prepared by dissolving 2.1 g of citric acid monohydrate (Sigma, Poole, UK, Cat# C7129-500 G) in 1000 mL distilled water, pH was adjusted at 6.0.
Blocking Buffer (Immunohistochemistry)	Blocking buffer was prepared according to Avidin-Biotin Complex (ABC) kit protocol (Thermo Scientific, Loughborough, UK, Cat# 32054) by adding 135µL of Normal Goat Serum to 10 mL PBS. Primary and secondary antibodies were diluted in the same buffer.
Phosphate Buffered saline – Triton (PBS-Triton) (Immunohistochemistry)	Was made by adding 10 tablets of PBS (Oxoid, Basingstoke, UK) to 1000 mL distilled water and mixing with 4 mL of Triton^{TM} X-100 (PBS + 0.4% Triton^{TM} X-100) (Sigma, Poole, UK, Cat# T9284-100mL).
Hydrogen peroxide solution 3% (Immunohistochemistry)	33 mL of 30% Hydrogen peroxide (Sigma, Poole, UK, Cat# H1009-500mL) was diluted in 300 mL of distilled water to obtain a stock of 3% hydrogen peroxide solution.
1%Goat serum in PBS-T (Immunohistochemistry)	1 mL of goat serum (Thermo Scientific, UK, Cat# 32054) was diluted in 100 mL of PBS-T and kept at 4 $^{\circ}$C.
Biotinylated secondary antibody reagent (Immunohistochemistry)	135µL of normal goat serum and 45 µL of the Biotinylated secondary antibody (ABC peroxidase-staining kit, Thermo Scientific, UK, Cat# 32054) were added to 10 ml of PBS and kept in 4 $^{\circ}$C.
ABC Reagent (Immunohistochemistry)	90 µL of reagent A plus 90 µL of reagent B from ABC peroxidase staining kit (Thermo Scientific, UK, Cat# 32054) were mixed and added to 10 mL of PBS and store in 4 $^{\circ}$C
1 X Annexin V Binding Buffer	1 mL of 10-X binding buffer (BD Biosciences, UK, Cat# 556547) was added to 9 mL of distilled water to prepare 1X binding buffer.
1X Click-iT® Saponin-based Permeabilization and Wash Reagent	To prepare 500 mL of 1X Click-iT® Saponin-based Permeabilization and Wash Reagent, 50 mL of 10X Stock Reagent (Fisher Scientific, UK, Cat# 11300962) were added to 450 mL of 1% BSA in PBS. The solution was stored at 4 $^{\circ}$C for a maximum of 4 weeks.
Lipofectamin (Transfection Reagent)	Was ordered from Fisher scientific, UK. The Cat# is13778-150. Store at 4 $^{\circ}$C for long-term use.
Etoposide	25 mM of Etoposide was prepared as 1000X stock solution by dissolving of 14.7 mg of Etoposide powder (Sigma, Poole UK, Cat# E1383-25MG) in 1 mL of sterile PBS, then this stock was aliquoted and stored at -20 $^{\circ}$C.

2.1.3. Antibodies

All antibodies were purchased externally. Origin and dilution used are reported in Table 2.2.

Table 2.2. Antibodies: catalogue number, dilution factor, host and supplier

Antibody	Cat#	Dilution	Host	Supplier
P5CR (WB)	sc-243722	1:1000	Goat	Santa Cruz
PYCR1 (WB)	PA5-26890	1:1000	Rabbit	Thermo Scientific
PYCR1(WB, IHC)	NBP2-20016	1:1000 WB 1:250 IHC	Rabbit	Novus
PYCR1(WB, IHC)	Ab103314	1:1000 WB 1:400 IHC	Rabbit	Abcam
PYCR2 (WB)	Ab103535	1:1000	Rabbit	Abcam
PYCRL (WB)	H00065263-M01	1:1000	Mouse	Abnova
PRODH/POX	PA5-27706	1:1000	Rabbit	Thermo Scientific
p21 (WB)	2947	1:1000	Rabbit	Cell Signalling
Cyclin D1	2978	1:1000	Rabbit	Cell Signalling
Cyclin D3	2936	1:1000	Mouse	Cell Signalling
Cleaved Caspase 3	9664	1:1000	Rabbit	Cell Signalling
Cleaved PARP	5625	1:1000	Rabbit	Cell Signalling
Actin	SC-1616	1:5000	Goat	Santa Cruz
Donkey anti-goat (SA)	SC-2020	1:10000	Donkey	Santa Cruz
Goat anti-rabbit (SA)	SC-2030	1:10000	Goat	Santa Cruz
Goat anti-mouse (SA)	SC-2031	1:10000	Goat	Santa Cruz
Goat anti-Rabbit IgG (H+L) Highly Cross-Adsorbed Secondary Antibody, Alexa Fluor 568	A-11036	1:2000	Goat	Life Technologies

WB: Western Blot, **IHC**: Immunohistochemistry, **SA**: Secondary Antibody, **P5CR/ PYCR**: Δ1-pyrroline-5-carboxylate reductase, **PRODH/POX**: Proline dehydrogenase/ Proline oxidase.

2.1.4. Cell lines

All cell lines were supplied by departmental cell line bank except SW620 that was purchased from ATCC supplier (Middlesex, UK) and CL11 that was purchased from DSMS (Braunschweig, Germany) (Table 2.3). Human colorectal epithelial cells (HCEC) cells were generated as described in Roig et al., 2010. HCECs were immortalized by retroviral delivery of *CDK4* and *hTERT*.

Table 2.3. CRC cell lines and media requirements for growth.

Cell lines	stage	CIMP	MS	*KRAS*	*BRAF*	*P53*	Media Requirements
HCT 116	Dukes' D	+	MSI	p.G13D	wt	wt	McCoy's ™ + 10% Fetal Calf Serum (FCS)
RKO	-	+	MSI	wt	p.V600E	wt	MEM + 10% FCS + 1% Glutamax (1x)
SW480	Dukes' B	-	MSS	p.G12V	wt	p.R273H; p.P309S	DMEM + 10% FCS + 1% Glutamax
HT29	Dukes' C	+	MSS	wt	p.V600E; p.T119Sc	p.R273H	DMEM + 10% FCS + 1% Glutamax (1x)
Caco2	-	-	MSS	wt	wt	p.E204X	MEM + 10% FCS + 1% Glutamax (1x)
CL11	Dukes' C	+	MSS	p.V14I; p.Q61H	wt	p.S215N	DMEM/F12 + 10% FCS + Glutamax (1x)
SW620	Dukes' C	-	MSS	p.G12V	wt	p.R273H; p.P309S	DMEM (1000 mg glucose/L) + 10% FCS + 1% Glutamax (1x)
HCEC	N/A	-	-	-	-	-	DMEM + 10% FCS + 1% Glutamax

WT: Wild Type

N/A: Non applicable

2.1.5. Primary cells

The Leicester Cancer Research Centre at the University of Leicester supplied the intestinal and colorectal tumour primary cells through the Leicester Experimental Cancer Medicine Centres (ECMC). These cells were isolated from tissues of patients undergoing surgical resection of CRC, as part of the 'Development and Application of *Ex Vivo* Assays to Assess Efficacy Biomarkers in the Prevention and Treatment of Cancer' study. The study was approved by the Wales REC 4, reference number 19/H0402145/, PI: Prof. W. Steward.

2.1.6. Coating media composition for HCEC

The coating media was prepared as indicated in the Table 2.4, and sterilised using 0.2 µm syringe filter (VWR, Leicestershire, UK) and stored at 4 °C. Culture flasks were incubated with coating media for 30 minutes prior to cell culture.

Table 2.4. The reagents of coating media and their volume.

Reagent	Volume
DMEM (4500mg glucose/L) (Sigma, Poole, UK)	50 mL
5% (BSA) (Sigma, Poole, UK)	65 µL
Fibronectin (1mg/mL) (Sigma, UK)	125 µL
Collagen (0.1mg/mL) (Sigma, Poole, UK)	500 µL

2.1.7. Tissue microarray slides (TMA)

Two sets of TMA slides with CRC cases and normal intestinal tissues were ordered from Abcam Company (Cambridge, UK, Cat# is ab 178129 and ab 178128) to analyse the expression of PYCR1 enzyme in different CRC cases. Each TMA contained 48 samples, including 16 samples of normal colon tissue control (See appendix section, Tables 8.1 and 8.2).

2.2. Methods

2.2.1 Cell culture and maintenance

CRC cell lines, HCT116, SW480, SW620, Caco2, HT29, RKO and CL11, and HCEC were cultured according to the media requirement showed in table 2.3. All cells were incubated at 37 °C in 5 % carbon dioxide (CO_2). Cells doubling times were 48 hours (hrs) for HCT1161, SW480, HT29 and RKO, 72 hrs for CL11 and SW620, and 96 hrs for Caco2. For HCEC doubling time was between 72 hrs to 84 hrs Cells were tested for Mycoplasma infection every 6 months by dedicated laboratory technicians.

Once resuscitated from liquid nitrogen, cells were cultured in 75 cm^2 flasks in their required growth medium (Table 2.3). Typically, after defrosting, cells were grown for 2-3 passages before being plated for experimental purposes. Cells were utilised for a maximum of 30 passages. For routine maintenance, the cells were grown up to approximately 65-70 % confluency before harvesting and passaging. Cell passaging was done by removing the growth medium, washing twice with 10 mL of sterile PBS, and then adding 3 mL of 2X trypsin/EDTA followed by incubation at 37 °C for 5 minutes. To enable detachment of cells, the flask was gently tapped and the trypsin/EDTA was neutralised with 7 mL of the growth medium containing 10% FCS and the cell suspension was collected in 15 mL falcon tube. The suspension was centrifuged at 1500 rpm for 5 minutes and the pellet was resuspended in 10 mL of the required fresh growth medium. 1 mL of fresh suspension was added to 25 mL of fresh growth medium in 175 cm^2 and incubated at 37 $^{\circ}$C.

For HCEC cell line, the same procedure described above was adapted with exception that cell culture flasks were coated. The coating media was prepared as described in paragraph 2.1.6, and Table 2.4. The medium was utilised to coat the flasks at 37 $^{\circ}$C on gentle rocking for 20 minutes. The coating medium was then removed and the coated flasks used for HCEC culture.

2.2.2. Cell freezing and recovery

Cells were cultured in a 175cm^2 flask to reach to ~80% confluency, then cells were harvested and transferred to a 15 mL falcon tube, centrifuged at 1500 rpm for 5 minutes to get a pellet of cells, which was resuspended in 1 mL of pre-cooled freezing solution (90% FCS, 10% Dimethyl sulfoxide (DMSO). The cells were moved into a cryo tube and

kept directly on ice, then transferred to a -80 °C freezer for 24 hrs. Finally, the tubes were transferred to the liquid nitrogen departmental bank.

For defrosting, cells from liquid nitrogen were directly thawn in a 75cm^2 flask with the required medium and incubated at 37 °C. The day after, the growth medium was replaced with fresh medium. The cell culture was then passaged when the confluency reached to 60-70%.

2.2.3. Cell transfection with siRNA

2.2.3.1. Cell culture plating for siRNA experiments

Cells at suitable confluency (60%-70%) were collected according to standard protocol (see section 2.2.1). 1 mL of cell suspension was added to 9 mL of isotonic solution using coulter counter cup and cells were counted using coulter counter machine (Z2 Coulter Particle Counter with Size Analyser, Beckman Coulter, High Wycombe, UK).

For siRNA transfection, cells were seeded in 6 cm^2 dishes and divided into three groups, untransfected (negative control), siCTRL (scramble negative control) and siPYCR1 (targeted siRNA). For each condition, three 6 cm^2 dishes were prepared.

Three CRC cell lines (HCT116, RKO and SW620) and the immortalized colon epithelial HCEC were used for siRNA experiment. In case of HCT116 cell line, 50000 cells were seeded in 6 cm^2 dishes, while for RKO 100000 cells were seeded and 65000 SW620 and HCEC cells were plated. All cell lines were incubated at 37 °C for 72 hrs prior to transfection. After reaching 30% confluence, cells were transfected for the indicated time with transfection mix as described below.

2.2.3.2. Preparation siRNA solution

ON-TARGET plus smart pool PYCR1 siRNA (siPYCR1) and NON-TARGET pool (siCTRL) arrived as lyophilized 5 nmol vial from Dharmacon (GE Healthcare, Buckinghamshire, UK) and Ambion (Thermo scientific, Loughborough, UK) (Table 2.5). To prepare 20 picomol/µL siRNA pool stock solution, 250 µL of free RNase/DNase distilled water (DEPC-Treated water, Ambion, by Thermo Scientific, Loughborough, UK, Cat# AM9930) was used to make this stock under sterile conditions using laminaire

hood and this stock was aliquoted into 15 µL using RNase/DNase free Eppendorf tubes and stored in -20 °C. The same procedure was followed for Ambion pools, ON-TARGET PYCR1 (siPYCR1) and NON-TARGET pool (siCTRL).

Table 2.5. siRNA pools from Dharmacon and Ambion, catalogue number and sequence.

siRNA pool	Company	Cat#	Sequence
siPYCR1	Dharmacon	L-012349-00-0005	GACCAACACUCCAGUCGUG
siCTRL	Dharmacon	D-001810-10-05	Not available
siPYCR1	Ambion	4390824	TGACGGCATCAATCAGGTCCT
siCTRL	Ambion	AM4611	Not available

2.2.3.3. siRNA transfection protocol

The transfection mix was prepared under the laminaire hood. The transfection medium Opti-MEM® (Life Technologies, Paisley, UK) was pre-warmed using a water bath at 37 °C for 30 minutes prior to transfection mix preparation. The mix was obtained mixing 250 µL of Opti-MEM® with 10 µL of Lipofectamine RNAiMAX (Invitrogen, Life Technology, Paisley, UK) in an Eppendorf tube. In parallel, 250 µL of Opti-MEM® media was mixed with 5 µL (100 picomoles) of siRNA (either siPYCR1 or siCTRL) in a separate 1.5 mL eppendorf. The content of the first eppendorf tube was then mix to the second eppendorf, mix thoroughly and incubated 10 minutes under the hood to enable liposome formation. During the incubation, the cells were refreshed with 3.5 mL of fresh medium. Finally, the transfection mix was added to 6 cm^2 dishes for 48/72 hrs. After incubation, 2 mL of PBS was used to wash the cells for two times. To detach the cells, 0.5 mL of 1X Trypsin/EDTA was added to each dish and incubated at 37 ˚C for 5 minutes. 3.5 mL of fresh growth medium was added to neutralise the trypsin/EDTA effect. Then the cell counting procedure was performed as described in see section 2.2.3.1.

2.2.4. Apoptosis detection via Annexin V/Propidium Iodide assay and flow cytometry.

To detect apoptosis, the FITC-Annexin V Apoptosis Detection kit (BD Biosciences, Oxford, UK) was employed. In healthy cells, the phospholipid phosphatidylserine (PS) is localized on the inner side of the plasma membrane, but flips to the outer layer in the early phases of apoptosis (Martin et al., 1995). The cellular protein Annexin V binds selectively to PS exposed on the external cell surface. In the Apoptosis Detection kit, Annexin V is conjugated with fluorescein isothiocyanate (FITC) and, therefore, can be used to identify early apoptotic cells, using of flow cytometry, fluorescence activated cell sorting (FACS). In addition, the kit provides the DNA dye propidium iodide (PI) for the identification of late apoptotic cells. PI is impermeable to healthy cells with an intact cell membrane, but, in the late phases of apoptosis, the cell membrane is damaged and the PI can enter the cells and stain the DNA. Accordingly, normal living cells are annexin V-FITC and PI negative, early apoptotic cells are annexin V-FITC positive and PI negative here as late apoptotic cells and necroptotic/necrotic cells are annexin V-FITC and PI double positive (Vermes et al., 1995) (Figure 2.1). It is worth mentioning that cell death can also occur by necrosis. During the necrosis, cells die by action of autolytic enzymes (autolysis). Contrary to apoptosis, necrotic cells lose membrane permeability at the early stages and therefore their nucli become immediately positive to PI. The membrane rapture that characterises late stages of necrosis allows Annexin V to stain PS inside the cells, which is why double positivity for Annexin and PI can indicate necrosis as well as apoptosis (Vermes et al., 1995).

HCT116 CRC cell line were transfected as described previously (see 2.2.3. section). After 72 hrs, floating dead cells were collected. The remaining adherent cells were washed two times with cold PBS, trypsinized and then pooled with the floating cells. After centrifugation at 1500 rpm for 5 min, the pooled cells were resuspended in 10 mL fresh growth medium supplemented with FCS. The cell pellet was then resuspended in 500 μL 1X Annexin V Binding Buffer, with the addition of 5 μL FITC-Annexin V and 5 μL of PI (50 mg/mL). The cells were gently vortexed and incubated at room temperature in the dark for 15 min. The percentage of cells undergoing apoptosis was determined by flow cytometry using a FACS Aria II (Becton Dickinson, New Jersey, USA) with the BD FACS Diva analysis software (version 6.1.2). The total number of acquired cells was

10000 and the wavelength for Annexin dye was 488 nm for excitation and 530/30 nm for emission, whereas the wavelength for PI dye was 561 nm for excitation and 610/20 nm for emission. Positive control for apoptosis was obtained treating HCT116 cells with the DNA damaging agent Etoposide. 25 μM Etoposide was added to HCT116 cells for 48 hrs to induce apoptosis.

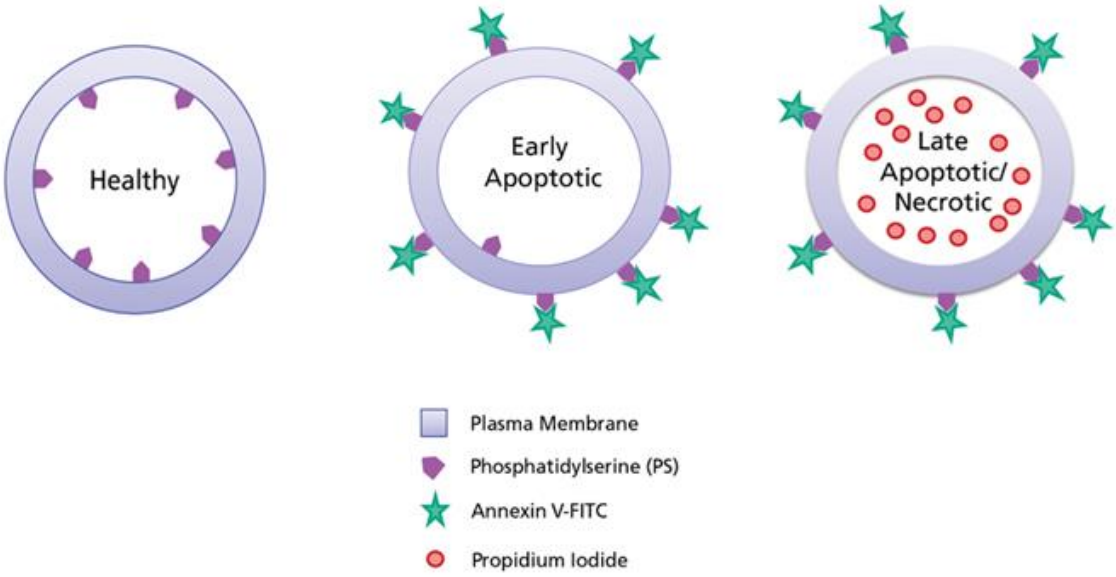

Figure 2.1. Diagram showing how healthy apoptotic and necrotic cells are identified using Annexin V-PI cytofluorimetry (adapted from Hingorani et al., 2011).

2.2.5. Click-iT® EdU Alexa Fluor® 488 Flow Cytometry Assay

EdU (5-ethynyl-2'-deoxyuridine) incorporation assay can be used to quantify active DNA as a quantitative readout of cell proliferation. EdU is a nucleoside analogue of thymidine that is incorporated into cellular DNA during S phase (Salic and Mitchison, 2008). EdU can be fluorescently labelled with click reaction. The click reaction is a copper dependant reaction between an azide and an alkyne. The EdU contains the alkyne group that can react with the fluorescently labelled azide, to form a stable triazole ring (Figure 2.2) (Breinbauer and Köhn, 2003 and Wang et al., 2003). This chemical reaction can be detected and measured using flow cytometry and FACS.

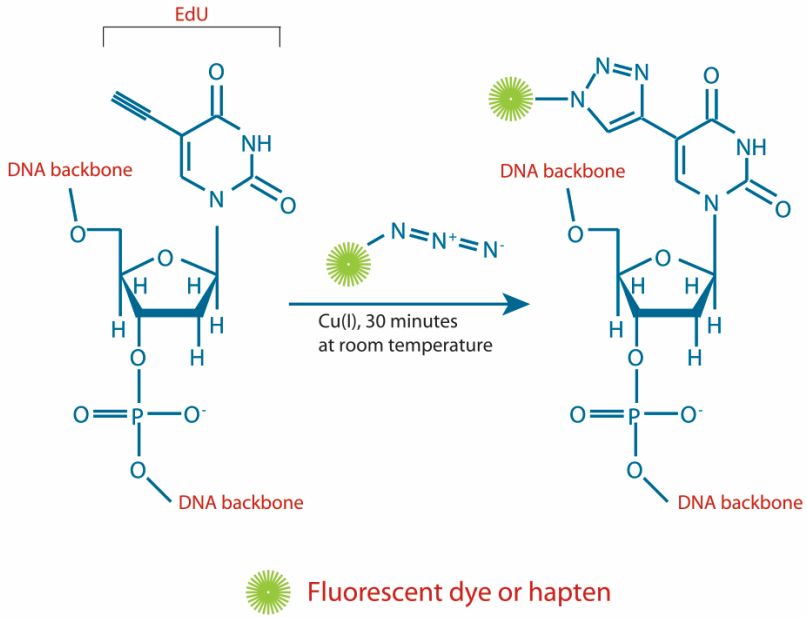

Figure 2.2. Click reaction between EdU and azide-modified dye. (Figure taken from Invitrogen website at https://assets.thermofisher.com/TFS-Assets/LSG/manuals/mp10044.pdf).

Cells were seeded in 6 cm dishes 48 hours before transfection, and then cells were transfected as described in section 2.2.3. After 72 hrs of transfection, cells were pulsed with 10 µM EdU dye for 1 hour at 37 °C, 5% CO2. Cells were collected according to routine tissue culture protocols and washed with 1% BSA in PBS. After a 5 minute centrifugation at 1500 rpm, the cell pellet was resuspended in 100 µL of Click-iT® fixative. Cells were then incubated for 15 minutes at room temperature in the dark, followed by washing with 1% BSA in PBS. Next, the cell pellet was dislodged and cells were resuspended in 100 µL of 1X Click-iT® Saponin based permeabilization and wash reagent. Cells were incubated for 15 min in the dark at room temperature. Right after incubation, a Click-iT® Reaction Cocktail was prepared according to Table 2.6. 500 µL of Click-iT® Reaction Cocktail was added to each tube and thoroughly mixed. Samples were incubated at room temperature for 30 min protected from light. Cells were then washed with 1X Click-iT® Saponin-based Permeabilization and wash reagent once and resuspended in 1 mL 1X ClickiT ® Saponin-based Permeabilization and wash reagent. A total DNA staining was performed by adding 1 µL Fx Cycle™ Violet stain (Life Technologies, Paisley, UK, Cat# F10347) in samples containing 1 mL cell suspension.

After mixing well, samples were incubated for 30 min on ice, protected from light. Samples were analysed with Aria Analyser (BD FACS ARIATM II) using 405 nm excitation and 450/50 band-pass emission for total DNA staining, whereas EdU detection with Alexa Fluor® 488 azide, was achieved with a 488 nm excitation and a green emission filter (530/30 nm). Samples of untreated cells, stained and unstained with EdU or FxCycle™, were also included.

Table 2.6. Click-iT® Reaction Cocktails

Reaction components	Number of reactions	
	2	5
PBS	875 µL	2.19 mL
$CuSO_4$	20 µL	70 µL
Fluorescent dye azide	5 µL	12.5 µL
Reaction Buffer Additive	100 µL	250 µL
Total reaction volume	1 mL	2.5 mL

2.2.6. Preparation of 0.15 mM, 3mM and 5mM proline media

To prepare 0.15 mM proline media, 8.62 mg of proline powder (Sigma, Cat# P5607-100g) was weighted and added to 500 mL of growth media (DMEM), while 3 mM proline media was prepared by dissolving 1.7 g of proline powder (Sigma, Cat# P5607-100g) in 5 mL of culture medium to get 3 M stock of proline medium (1000x stock). 30 µL of 3 M stock was added to 30 mL of culture media to reach to 3 mM final concentration. The medium was then filtered using 0.2 µm syringe filter and kept at 4 °C until use.

Similarly, to generate a 5 mM proline media, 2.8 g of proline powder was dissolved in 5 mL of culture medium to get 5 M stock of proline medium (1000x stock). 30 µL of 5 M stock was added to 30 mL of culture media to reach to 5 mM final concentration. The new concentration media was filtered using 0.2 µm syringe filter and kept at 4 °C until use. Dialyzed fetal bovine serum (10%) (HyClone™, Thermo Scientific, UK, Cat# 12349822) was added to media as supplementary element.

2.2.7. Western blotting analysis

2.2.7.1 Preparation of cell and tissue lysate

Cells were collected following routine tissue culture protocols (see section 2.2.1), and the cell suspension was centrifuged at 1500 rpm for 5 min. The pellets were resuspended with PBS and transferred to 1.5 Eppendorf tubes and spin down at 1500 rpm for 5 minutes. The lysis-M buffer (Roche Diagnostics, Sussex, UK) was used to resuspend the pellets in a 1:2 ratio (w/v) (see Table 2.1 / cell lysis buffer). The lysed cell suspension was incubated on ice for 30 min, and then stored at -20 °C overnight. The day after, the lysate was thawed and centrifuged at 13000 rpm for 10 minutes at 4 ˚C. The supernatant was transferred to a new eppendorf tube, whereas the residual pellet of cell debris was discarded.

In the case of mouse intestinal tissues, the samples were defrosted on ice and 30 to 60 mg collected in sterile Eppendorf tubes. Double amount of lysis-M buffer (60 µL to 120 µL) was added to samples and tissues were homogenized using the tissue homogenizer. The samples were kept on ice for 1 hr and overnight at -20 °C. The next day, samples were thawed on ice and centrifuged at 13000 rpm for 10 minutes at 4 °C. The supernatants were collected and transferred in new eppendorf tubes.

For primary cells, cells were collected directly from liquid nitrogen bank, washed with PBS twice and then lysate with Lysis-M buffer. Samples were then treated as previously described.

2.2.7.2. Bicinchoninic acid (BCA) Protein Assay

To determine the concentration of proteins in lysates, the Pierce BCA protein assay kit (Thermo Scientific, Loughborough, UK) was utilized. The standard curve of protein concentration was prepared by using sequential dilutions of 1 mg/mL BSA from 0 (distilled water) to 1 mg/mL (0, 0.2, 0.4, 0.6, 0.8 and 1 mg/mL) to form the standard BSA stock, distilled water was used to prepare these standard dilutions. Serial dilutions of unknown concentration lysates (1:10, 1:50 and 1:100) were prepared by using distilled water to a final volume 35 µL, 50 µL, and 100 µL, respectively. In 96 well microplate, 10 µL of the distilled water (blank reference), BSA standard solutions and serially diluted lysates were added to separate wells in triplicate. At this point, the BCA working solution

was prepared by mixing 25 mL of BCA Reagent A with 0.5 mL of BCA Reagent B. 200 µL of the BCA working solution was added to each well. The microplate then incubated at 37 °C for 30 min the dark. Next, the microplate was cooled at room temperature for approximately 2 min in the dark before reading the absorbance at 595 nm on a Fluostar Optima plate reader (BMG Labtech Ltd, Aylesbury, UK). The standard curve generated by excel sheet was used to determine the protein concentration of the unknown lysates.

2.2.7.3. Protein denaturation

Appropriate volumes of protein lysate were diluted in water to provide samples of equivalent concentration (30µg for cell lines and intestinal tissue, while 20 µg for primary cells lysate and 50 µg for HCEC cell line) in a final volume of 10µL. An equal volume (10µL) of sample loading buffer (2x Laemmli, Sigma, UK) was added to the protein lysate, making a total loading volume of 20 µL. Samples were then mixed by vortexing and heated for 5 minutes at 100 °C to denature the proteins.

2.2.7.4. SDS – PAGE

The gel casting apparatus (Bio-Rad, mini gel apparatus) was used for preparation of the SDS gels. Stacking and resolving gels were prepared to contain 5 and 10% acrylamide concentration respectively. Volumes for the stacking and resolving gels are indicated in Table 2.7. The stacking gel buffer was prepared and poured on top of the set resolving gel with the addition, a 10 or 15 well comb to enable samples loading. Once set, the comb was removed and the gel cassette placed in the running tank with 1X running buffer (Table 2.1). Samples were loaded into the wells and run at 40 mA for 90 min. 5 µL of benchmark protein ladder (Thermo Scientific, UK, Cat# 26616) as loaded on a separate well.

Table 2.7. Composition of the polyacrylamide gels used in Western blotting

Reagents	5% Stacking Gel	10% Resolving Gel
Distilled water	5.7 mL	8.1 mL
4X ProtoGel Resolving Buffer	-	5 mL
ProtoGel Stacking Buffer	2.5 mL	-
ProtoGel 30 % Acrylamide	1.7 mL	6.7 mL
10 % APS	100 µL	200 µL
TEMED	0.015 mL	0.015 mL
Total volume	10.015 mL	20.015 mL

Volumes are appropriate for two gels. The stacking gel was loaded onto the set resolving gel in the gel cassettes.APS: Ammonium Persulphate. TEMED: N, N, N′, N′ - Tetramethylethylenediamine. Each gel was taken 10 -15 minutes to be solid.

2.2.7.5. Transferring protein samples

Proteins were transferred from the gel onto a nitrocellulose membrane as follows: acrylamide gels were placed into a transfer cassette, which consisted of a sponge, blotting paper (Thermo Scientific, UK, Cat# 88600), the gel, the nitrocellulose membrane (Geneflow Ltd, UK, Cat# 10600104), blotting paper and a final sponge. The transfer cassette was placed into a mini gel holder with colour coding that ensured the correct orientation of the transfer cassette, so that the nitrocellulose membrane was oriented towards the positive pole. All blotting paper, nitrocellulose membrane, and sponges were pre-soaked in 1 X transfer buffer (Table 2.1) before being placed in the transfer cassette. The transfer cassette was then inserted into a tank filled with transfer buffer. Protein transfer was undertaken at 100 V for 2 hrs at room temperature.

2.2.7.6. Blocking and antibody incubations

After proteins transferring, the nitrocellulose membrane was incubated for 2 hrs at room temperature on a shacking platform in blocking buffer (Table 2.1) to prevent non-specific binding. Then, the membrane was washed three times for 10 minutes in PBS-T (Table 2.1) followed by incubation with primary antibody overnight in gentle rocking at 4°C. Dilutions of primary antibodies are reported in table 2.2. The following day, the membrane was washed for 10 minutes three times in PBS-T and incubated for 1 hr at

room temperature with the secondary antibody (Table 2.2). Finally, the membrane was washed three times with PBS-T for 10 minutes followed by a last wash in distilled water for 5 minutes.

2.2.7.7. Detection of proteins

Protein detection was achieved with Enhanced Chemiluminescence Luminol (ECL) solution (Geneflow Ltd, UK) (Table 2.1). After the last wash, the membrane was incubated in the ECL solution for 2 minutes at room temperature. The excess of ECL reagent was poured off and the membrane wrapped in a cling film and placed into an X-ray developing hyper cassette (Amersham, UK). The membrane was exposed to X-ray film (Thermo Scientific, UK, Cat# 4351379) in a dark room for 1-5 minutes and the film was developed using an Agfa Curix 60 developer (AGFA Gevaert N.V, Germany).

Alternatively, the GeneGnome XRQ machine (Syngene, UK) was used to detect the ECL Chemiluminescence signal using the manufacturer's GeneGnome XRQ software.

2.2.7.8. Verifying equal loading

Housekeeping protein actin was used to normalize the protein quantitation. To confirm that proteins were loaded in equal amounts, actin antibody (Santa Cruz, UK) was used to re-probe the membrane overnight at 4 °C. Using the same steps previously described (See sections 2.2.6.6 and 2.2.6.7), Quantitation was performed by measuring the protein band intensities with ImageJ, Ink software version 1.49V.

2.2.8. mRNA expression in cultured cells and tissues

2.2.8.1. RNA extraction and elimination of genomic DNA

The total RNA was isolated either from cells or intestinal tissues using the RNeasy mini kit (Qiagen, Germany), according to the manufacturer’s instructions. For cell cultures, cells were spun down at 1500 rpm for 5 minutes to get pellets that contained approximately 2-4 x106 cells. The pellet was lysed in 350 µL of RLT buffer, which was mixed with beta-mercaptoethanol (10 µL of beta-mercaptoethanol for 1 mL of RLT buffer), and vortexed thoroughly to ensure efficient lysis. The lysate was then loaded on a QIAshredder spin column and homogenized by centrifugation for 2 min at 12000 rpm. 70% ethanol was added in an equal volume to the homogenized lysate and mixed

thoroughly by pipetting. The lysate was then transferred to an RNeasy spin column and centrifuged at 10000 rpm for 30 seconds. The column was then washed with 350 µL of RW1 buffer by centrifugation at 10000 rpm for 30 seconds. In the next step, the column was incubated with 80 µL of DNaseI reagent (Qiagen) for 15 min at room temperature to enable digestion of the genomic DNA. The column was then washed with 350 µL of buffer RW1 and 500 µL of Buffer RPE by centrifugation at 10000 rpm for 30 seconds. Total RNA was eluted in a final volume of 45 µL nuclease-free water (Qiagen) and stored at -80 ˚C until further analysis.

In case of intestinal tissues sample, 10-30 mg of frozen tissue was lysed with 600 µL of RLT buffer/beta-mercaptoethanol. Then the same steps as above were followed to complete the extraction of the RNA.

2.2.8.2. RNA quantification

The NanoDrop spectrophotometer (NanoDrop Technologies, USA) was used to quantify the total concentration of RNA. A volume of 2 µL was used from each sample in duplicate to measure absorbance at 260 nm and the average of two readings was calculated. To assess RNA purity, absorbance ratios at 260/280 nm and 260/230 nm were also recorded. RNA was considered pure when the ratio values were around 2. RNA samples were rejected if the absorbance ratios did not fall within the above value.

2.2.8.3. Reverse transcription

Complementary DNA (cDNA) was obtained through reverse- transcription of RNA using RNA-to-cDNA kit from Applied Biosystems (Thermo Fisher Scientific, Loughborough, UK). As per manufacturer's instructions, two reverse transcriptase reactions (RT reactions) were prepared, RT+ and RT- (i.e., negative control). 2 µg of total RNA was then added to each RT reaction. The RT+ mix was prepared by mixing of 10 µL of 2X RT buffer, 1 µL of 20x enzyme mix, and additional 9 µL made up of 2 µg RNA sample and the necessary quantity of nuclease-free water to reach a final volume of 20 µL. similarly, the RT- mix was composed in a similar manner but the enzyme mix was replaced with 9 µL nuclease-free water. The RT reactions were mixed thoroughly and spin down at 3000 rpm for one minute. The reverse transcriptase reaction was performed

using thermal cycler machine at 37 ˚C for 1 hr and then at 95 ˚C for five min and hold at 4 ˚C. The cDNA was stored at -20 ˚C until ready to use.

2.2.8.4. Reverse transcriptase - quantitative polymerase chain reaction (RT-qPCR).

TaqMan® probe technology from ThermoFisher Scientific, UK was used to analyze gene expression by RT-qPCR. TaqMan® probes are hydrolysis probes, which are designed to bind specifically to the sequence of a target gene (Figure 2.3). They consist of a fluorophore, typically FAM® (6-carboxyfluorescein) or VIC, covalently attached to the 5' end of the nucleotide probe, and a quencher, such as TAMRA® (6-carboxy-terta-methyl-rhodamine) and minor groove binder (MGB) attached to the 3' end. FAM maximum absorbance is 494 nm with emission maximum at 518 nm. VIC has an absorbance maximum of 538 nm and an emission maximum of 554 nm. MGB induces hyper-stabilized duplexes with complementary DNA (cDNA) to allow shorter probes to be used for hybridization- based assays (Kutyavin et al., 2000). The quencher absorbs the emission of the fluorescent reporter dye when they are in close proximity (6 to 10 nucleotides). During the extension stage, the probe is hydrolyzed by the Taq polymerase 5'-3' nuclease activity resulting in separation of fluorophore from quencher and release of detectable fluorescence. Therefore, the degradation of probes during the extension phase on the RT-qPCR reaction, results in increasing fluorescence that is recorded by the PCR machine at the end of each PCR cycle resulting in the formation of an amplification plot (Figure 2.4).

RT- qPCR was carried out using Applied Biosystems Step One PlusTM Real-time PCR System (Life Technologies, Paisley, UK). For each reaction 10 µL of TaqMan® Gene Expression Master Mix (Applied Biosystems, Thermo Fisher Scientific, Loughborough, UK) was mixed with 1 µL of target-specific TaqMan FAM-MGB probe (Life Technologies, UK, see Table 2.7 below), 1 µL of housekeeping endogenous control TaqMan VIC-MGB probe (Life Technologies, see Table 2.7 below), 2 µL of cDNA and 6 µL of PCR water to final volume of 20µL. The reactions were loaded in triplicate in MicroAmp™ 8-Tube Strip (0.2 mL) (Applied Biosystems) with MicroAmp™ 8-Cap Strip cover (Applied Biosystems). The thermal cycling parameters for the qPCR were holding stage 95 ˚C for 20 seconds, followed by 40 cycles at 95 ˚C for 1 seconds and 60 ˚C for 20 seconds. The comparative C_T (cycle threshold) method was used to determine

the fold change in the expression of the target mRNA relative to the control after normalization to the reference genes.

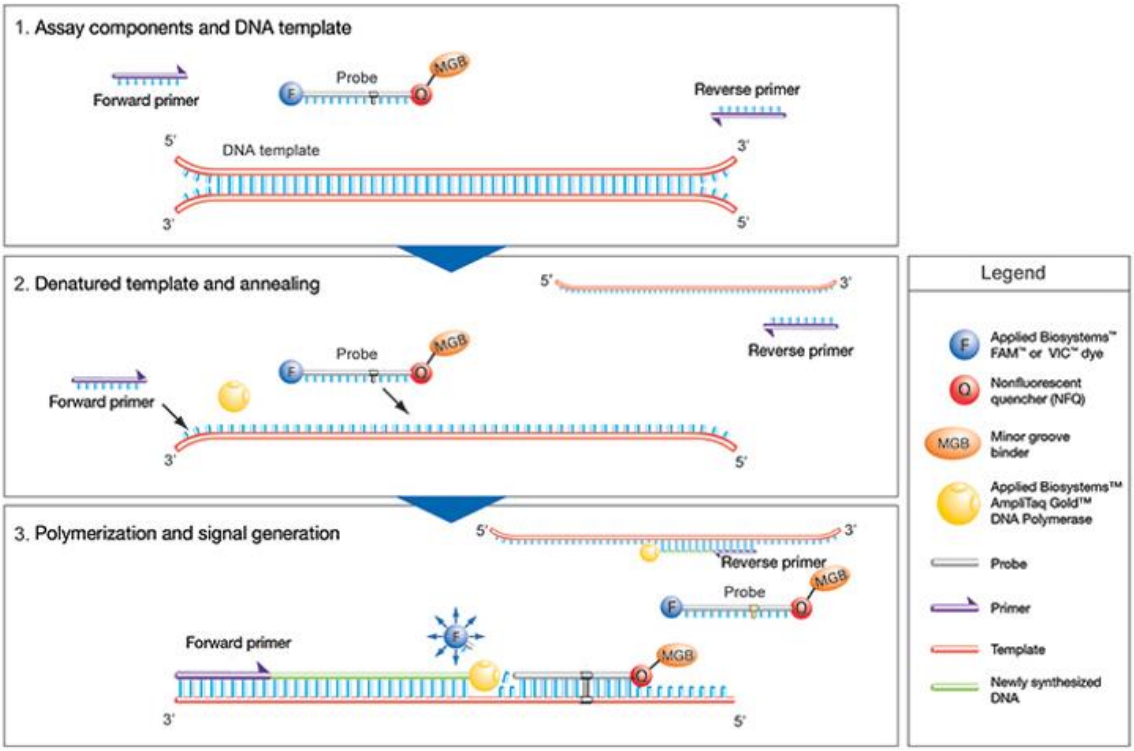

Figure 2.3. TaqMan Gene Expression Assay. The diagram shows the steps of RT-qPCR technique using TaqMan probe (Taken from Thermo Scientific website at https://www.thermofisher.com/uk/en/home/life-science/pcr/real-time-pcr/real-time-pcr-learning-center/real-time-pcr-basics/how-taqman-assays-work.html).

Table 2.8. Amplicon lengths of target genes. TaqMan probes were obtained from Thermo Fisher Scientific, UK.

Gene	Type	Fluorophore	Amplicon Length	Assay ID/Catalogue Number
Human *PYCR1*	Target	FAM	128	Hs01048019_mL/ 4351372
Human *PYCR2*	Target	FAM	107	Hs00371953_mL/ 4331182
Human *PYCRL*	Target	FAM	110	Hs00225031_mL/ 4351372
Human *PRODH/POX*	Target	FAM	136	Hs00275205_mL/ 433118
Human *ACTB* (*Actin*)	Endogenous	VIC	171	Hs99999903_m1/ 4448484
Mouse *Pycr1*	Target	FAM	82	Mm00522674_m1/ 4331182
Mouse *Pycr2*	Target	FAM	58	Mm00505074_m1/ 4331182
Mouse *Pycrl*	Target	FAM	68	Mm01205845_m1/ 4331182
Mouse *Prodh / Pox*	Target	FAM	76	Mm00448398_m1/ 4351372
Mouse *Actb* (*Actin*)	Endogenous	VIC	143	Mm02619580_g1/ 4448484
Mouse *Tbp*	Endogenous	VIC	121	Mm01279310_m1/ 4448484
Mouse *Ywhz*	Endogenous	VIC	70	Mm01722325_m1/ 4448484
Mouse *Gusb*	Endogenous	VIC	93	Mm00446957_m1/ 4448484
Mouse *Pop4*	Endogenous	VIC	116	Mm00546481_m1/ 4448484
Mouse *Efnb2*	Endogenous	VIC	136	Mm01215896_m1/ 4448484
Mouse *Gapdh*	Endogenous	VIC	109	Mm99999915_g1/ 4448484
Mouse *Hprt*	Endogenous	VIC	131	Mm03024075_m1/ 4448484
Mouse *B2m*	Endogenous	VIC	125	Mm00437764_m1/ 4448484

2.2.8.5. Quantification

In RT-qPCR, the relative quantity of amplicons is measured at the end of each cycle using the fluorometric probe. From these measures, a DNA amplification curve is produced (Figure 2.4). The C_T value is determined which represents the cycle number at which the fluorescence signal rises above the fluorescence threshold, that is -a fluorescent signal significantly above the background fluorescence. The C_T is a measure of the amplicon product that has been amplified; this value is inversely proportional to the expression levels of the gene of interest, i.e. the lower C_T value, the higher the expression of the target gene. To quantify the gene of interest (GOI), its C_T value is normalised to an endogenous control (EC) or reference gene using the following equation:

$$\mathbf{\Delta C_T = C_T\ GOI - C_T EC}$$

To ensure the accuracy, the samples are run in triplicate and the mean values of C_T of the GOI and EC are used for calculating the ΔC_T. Here, when analysing mouse tissue, we used 2 different EC (for explanation see section 4.3.3.1), and in this case the geometric mean (GM) was calculated using the mean C_T of each EC. This is then subtracted from the GOI C_T value to obtain the ΔC_T.

To convert ΔC_T to fold change in mRNA expression, the equation $2^{(-\Delta\Delta C_T)}$ is used. The $\Delta\Delta C_T$ value is obtained subtracting the ΔC_T of the sample of interest from the ΔC_T of the control sample.

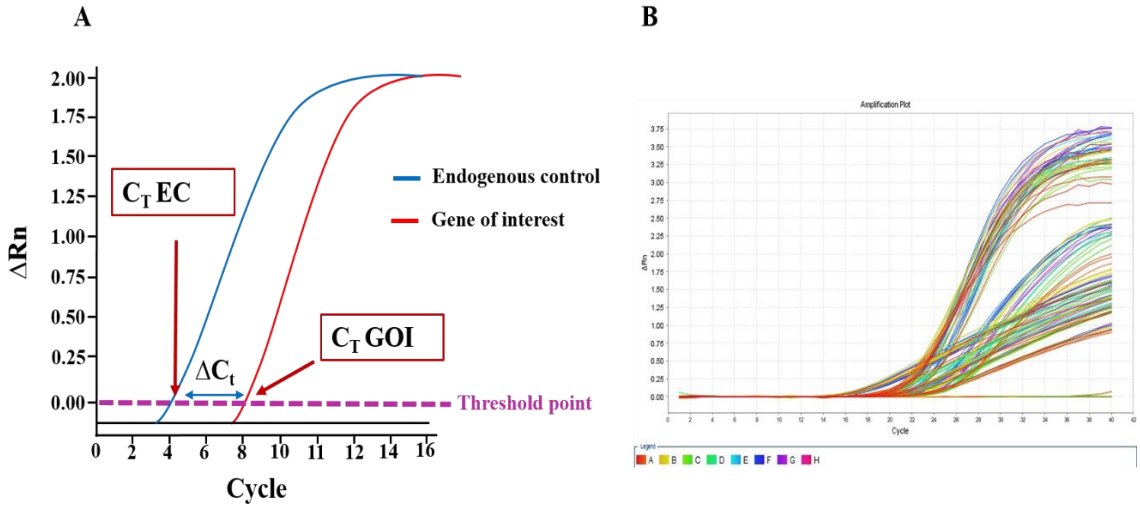

Figure 2.4. The amplification plot of RT-qPCR using StepOnePlus™ real time PCR. (A) A schematic diagram showing the amplification curve for cDNA analysis. The C_T is identified by the purple line. **(B)** An example of amplification plot for PYCR1, PYCR2 and PYCRL mRNAs.

2.2.9. Tissues processing and Haematoxylin and eosin staining

Intestinal mouse tissues were fixed in 10% formalin and transferred to histology facility laboratory (Core Biotechnology Services, University of Leicester) for paraffin embedding and processing, including Haematoxylin and eosin (H&E) staining and provision of tissue slides for immunohistochemical staining on polylysine-coated slides (Thermo Fisher Scientific, UK, Cat# J2800AMNT).

2.2.10. Immunohistochemical staining of mouse intestine

Formalin-fixed, paraffin embedded (FFPE) sections of *Lgr5-Cre^{ER}/Apc$^{fl/fl}$* intestinal mouse tissues were stained using anti-PYCR1 polyclonal antibody (Abcam, Cambridge, UK) (Table 2.2) and ultra- –sensitive ABC peroxidase staining kit (Thermo Scientific, Loughborough, UK) (Table 2.1). For dewaxing, 5 µm thick FFPE sections were incubated at 65 °C for 20 min and then twice in xylene (Genta Medical, York, UK) for 3 min,, followed by re-hydration by immersion in a graded series of industrial methylated spirit (IMS) (Genta Medical, York, UK, Cat# I99050) rinses (99 % twice for 3 min and 95 % twice for 3 min). The slides were then washed in running tap water for 5 min. Antigen retrieval was performed by microwaving the slides on high power in 10 mM citrate buffer (pH 6.0) for 20 min. Slides were then cool down at room temperature. The endogenous

peroxidase activity was inactivated by adding 200 μL of the peroxidase block directly on the sections for 15 min at room temperature.

The slides were washed again in 1% goat serum in PBS-Triton (Table 2.1) before adding 200 μL of the protein block directly on the sections for 20 min to block nonspecific binding. The slides were washed again in 1% goat serum in PBS-Triton followed by incubation of the tissue sections with the PYCR1 antibody (Table 2.2) overnight at 4 °C. The antibody was diluted in blocking buffer (Table 2.1).

The negative control was rabbit immunoglobulin fraction (Dako, Ely, UK, Cat# X0936) diluted to match primary antibody concentration. After overnight incubation, the sections were washed with 1% goat serum in PBS-Triton twice for 10 min. The sections were subsequently incubated for 30 min with a biotinylated secondary antibody (Table 2.1 and 2.2).

The sections were then washed with 1% goat serum in PBS-Triton and followed by incubation with ABC reagent (Table 2.1) for 30 min at room temperature. Slides were then washed with 1% goat serum in PBS-Triton for 10 min twice, followed by 3,3′-diaminobenzidine (DAB) staining (Leica microsystems, UK, Cat# RE7270-K). DAB was prepared by adding 5 μL DAB chromogen to 100 μL Novolink™ DAB substrate buffer and this DAB working solution was added to the sections for 5 min to allow reaction with the peroxidase and precipitation of the DAB brown staining. Following a 5 min wash with running tap water, the sections were counterstained with Mayer's Haematoxylin for 3 min and washed again for 5 min in running tap water.

The sections were finally dehydrated back through the graded IMS and xylene. Coverslips were added to the slides with the help of the DPX (distyrene, a plasticizer and xylene) mounting medium. The slides were visualized under a light microscope (Leica DM 2500 with Leica digital camera, Leica Microsystems, Milton Keynes, UK), and images were acquired using the Hamamatsu NanoZoomer Digital Slide Scanners (Leica).

The non-digital zoomer program (NDP) and ImageScope software were employed to analyse the slide pictures. For each animal, 50 intestinal crypts were randomly selected with ImageScope software. The index of ImageScope program was then used to calculate the H-score of PYCR1 level in stained cryptal area of the intestinal tissues. The H-score

value of ImageScope software was calculated based on the percentage of positive cells using the following formulation : H-score = 1*(% of weak positive)+2*(% of positive)+ 3*(% of strong positive).

2.2.11. Immunohistochemical staining for TMA sections

FFPE sections of human CRC TMA (Abcam, Cambridge, UK) (Section 2.1.7) were immunohistochemically stained according to the above procedure (Section 2.2.10). The PYCR1 staining intensity was scored by pathologist (Prof. Kevin West, Leicester Royal Infirmary, Leicester, UK), and by ImageScope software. According to the pathologist, the level of PYCR1 expression was graded into four grades: 0/1/2/3 dependent on staining intensity, and the H score was calculated by multiply each grade by 100. In the assessed CRC TMAs, the maximum score was 300 (100 x 3), while the minimum score was 10 (0.1 x 100).

2.2.12. Immunofluorescence staining (IF)

IF staining was performed manually using Avidin-Biotin detecting system (ABC). FFPE sections were first sequentially treated with xylene and series of graduated IMS to remove paraffin, and rinsed in tap water as described in section 2.2.10. Heat mediated antigen retrieval was performed in microwave in using 10 mM citrate buffer (pH 6.0) for 20 min. Subsequently, slides were treated blocking buffer with 5 % goat serum in PBS-Triton (Table 2.1). Then, the sections were washed with 1% goat serum in PBS-Triton twice for 10 min. The primary antibody was then applied on the sections and incubated overnight at 4 °C. The sections were then washed with 1% goat serum in PBS-Triton twice for 10 min. Alexa Fluor 568- Goat anti-Rabbit IgG (Life Technologies, Invitrogen, UK) secondary antibody was applied for 1 hr at room temperature in the dark. Slides were then washed in 1% goat serum in PBS-Triton twice for 10 min. Finally, sections were counterstained and mounted with an antifade reagent containing 4′,6-diamidino-2-phenylindole (DAPI) (Thermo Fisher Scientific, UK, Cat# P36931), a blue-fluorescent DNA stain. Slides were incubated at room temperature in dark for 30 min, then sealed with nail polish and stored at 4 °C. Slides were examined with inverted confocal microscope IX81, FV1000 (Olympus, Japan). Filter sets for fluorescent signal detection were blue for DAPI (emission wavelengths 405 nm), and red for Alexa 568 (emission wavelength 559 nm).

2.2.13. *In vivo* study

All animal work was performed under the project licence (PPL) no. 60/4370 and the personal licence (PIL) no. ICB86FB2F, granted by the Home Office/UK. Mice were hosted in the specific-pathogen-free Pre-clinical Research Facility (PRF) at the University of Leicester, under climate-control environment with a 12 hrs day/night cycle. Animals were fed ad libitum with AIN 93 diet (TestDiet, USA, Cat# 5801-G).

2.2.13.1. Tamoxifen preparation

The solution of tamoxifen (15 mg/mL) was prepared by dissolving 0.3 g of tamoxifen powder (Sigma, UK, Cat# T5648) in 2 mL absolute ethanol (100%) (Fisher Scientific, Loughborough, UK) at room temperature. The mixture was consequently vortexed and sunflower oil was used to reach a final volume of 20 mL. The mix was then incubated at 45 ˚C in shaker water bath for 1 hr until it was homogeneous and clear. The solution thus obtained was aliquoted in dark Eppendorf tubes and stored at -20 ˚C for a long-term storage.

2.2.13.2. Mice health monitoring

Health monitoring was performed from the experienced technical staff of the pre-clinical research facility (PRF). Animal body weight was measured weekly. However, in case of sickness, weight was recorded twice a week. The sickness signs typically monitored included loss of body weight, pale feet (indicated to anaemia), droopy eyes and ears, raised fur, animal recumbency, animal segregation and melancholy behaviour. Mice were culled is body weight loss reached 20% of the initial weight. However, this condition was never encountered in the two weeks of this experiment.

2.2.13.3. In vivo study endpoint and intestinal tissues collection

35 *LGR5-Cre+/Apc*$^{fl/fl}$ (with expression of Cre recombinase, Cre+) and *LGR5-Cre-/Apc*$^{fl/fl}$ (with a Cre negative genotype and no Cre expression, Cre-) mice of both sexes aged 2-3 months were used in this study. To induce *lox*P recombination, mice, were intraperitoneally injected 3 mg of tamoxifen (200 µL). Negative control was provided by tamoxifen injected *LGR5-Cre-/Apc*$^{fl/fl}$ control mice. *Apc* deleted and control animals were randomly allocated to three groups and sacrificed at 3 days, 1 week and 2 weeks post

tamoxifen injection. At each time point, mice were sacrificed under terminal anaesthesia and cervical dislocation. The small intestine was harvested, washed with PBS, and then divided into three topographic regions, proximal, middle and distal part. From each portion, two pieces of ~0.5 cm^2 of tissue were collected in cryotubes, snap-frozen in liquid nitrogen and later stored at -80 $^{\circ}$C for RNA and protein purification. The remaining tissues were swiss-rolled and fixed overnight in 10% formalin (Formaldehyde: 10% (3.8-4% v/v), NaCl, Atom Scientific, UK) and transfer to the histology facility laboratory (Core Biotechnological Services, University of Leicester, UK) for downstream processing.

2.2.14. Imaging analysis

All western blotting images were analysed using ImageJ software version 1.51, while the immunohistochemistry images were analysed by Aperio ImageScope version 12.3.2.80.13. For immunofluorescent images, the ImageJ version 1.49 was used for analysis.

2.2.15. Statistical analysis

All statistical analysis was carried out using GraphPad Prism version 7. Student's *t*-test, One-way and Two-way Anova were applied for group comparisons. All changes with p -values equal to or lower than 0.05 were considered statistical significant.

Chapter Three: Characterisation of PYCR1 expression in CRC

3. Introduction

It has been reported that PYCR1 enzyme is upregulated in a wide varieties of cancers, including lung, prostate, B cell lymphoma, melanoma, pancreatic and ovarian cancer (De Ingeniis et al., 2012. , Liu et al., 2012a and Nilsson et al., 2014). Additionally, the upregulation of PYCR1 enzyme is closely related to the oncogene *c-Myc* (Liu et al., 2012b). Data obtained from large-scale comparative analysis of mRNA expression datasets covering 1,981 tumours of 19 different types demonstrated that PYCR1 is one of the most commonly overexpressed genes in cancers when compared to normal tissues (Nilsson et al., 2014). Therefore, the aim of this chapter was to explore the expression of the PYCR1 enzyme in CRC cell lines, primary cells and tissues, and to ascertain whether there were differences between PYCR1 expressions in tumour tissues of patients diagnosed with CRC compared to matched normal tissues from the same patients. The additional aim of this chapter was to examine the expression of the PYCR1 protein in association with different CRC stages. Toward this end, the following objectives were achieved:

1. Analysis of publicly available datasets using on-line software tools.
2. Western blot and RT-qPCR analysis of seven cancer cell lines.
3. Western blot analysis of primary cancer cells isolated from patient with benign and malignant tumours.
4. Analysis of commercially available TMAs, which included normal intestinal tissues and malignant cases of CRC.

3.1. *PYCR1* mRNA expression is upregulated in CRC specimens compared to normal tissue

To understand the relevance of *PYCR1* expression in CRC patients, we enquired the Cancer MA and Oncomine on-line databases and found that the *PYCR1* gene is highly expressed in intestinal adenocarcinoma across different datasets (Figures 3.1. A and B) (Rhodes et al., 2004).

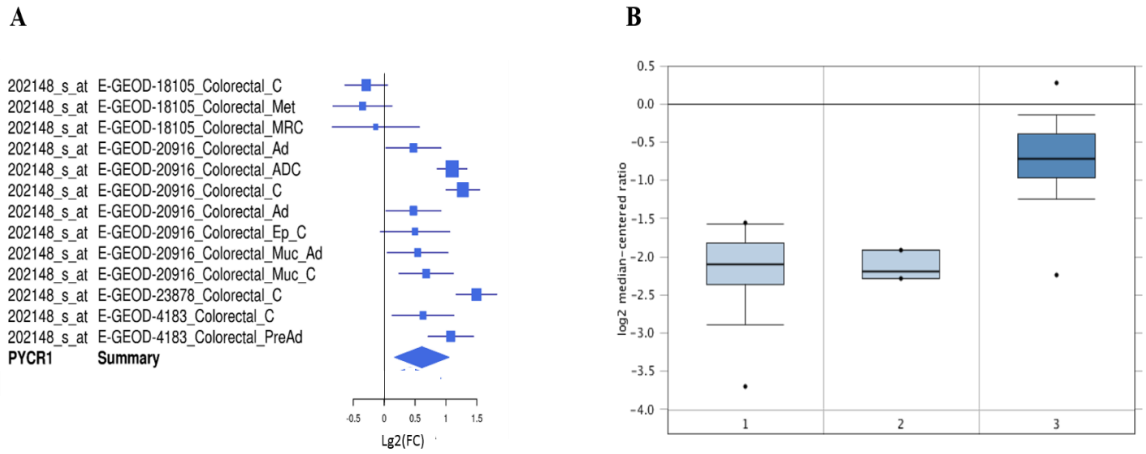

Figure 3.1. *PYCR1* expression in CRC is upregulated in high level compared to normal tissues. (**A**) Meta-analysis of PYCR1 expression in CRC datasets performed using the online tool CancerMA (P<0.001). The Forest plot visualizes the meta-analysis results for PYCR1 gene expression in the indicated CRC datasets. Each dataset is illustrated by a square; the position on the x-axis representing the measure estimate of PYCR1 gene expression (expressed as logarithm of "fold over control tissue", lg2FC ratio), the size of the square being proportional to the weight of the study, and the horizontal line through it reflecting the confidence interval of the estimate. The diamond sign indicates the calculated average *PYCR1* lg2FC ratio and its confidence interval. PYCR1 expression was increased in most datasets analysed. Colorectal_Ad, Colorectal adenoma; Colorectal_ADC, Colorectal adenocarcinoma; Colorectal_C, Colorectal cancer; Colorectal_Ep_C, Colorectal carcinoma, epithelial cells; Colorectal_Met, Colorectal cancer, metastatic; Colorectal_MRC, Colorectal cancer, metastatic recurrence; Colorectal_Muc_Ad, Colorectal adenoma, mucosa; Colorectal_Muc_C, Colorectal carcinoma, mucosa; Colorectal_PreAd, Precancerous adenoma of the colon. (**B**) Box and whisker plots of Oncomine-enabled analysis of PYCR1 expression in normal colorectal tissues versus normal tissues. (1) Normal colon = 19 samples, (2) Normal rectum = 3 samples and (3) Colorectal adenocarcinoma = 101 samples, P value = 1.89E-14.

3.2. Investigation of PYCR1 protein expression in human CRC versus normal tissues using TMAs

To confirm the RNA data, we used TMA to investigate the expression of PYCR1 protein in CRC patients. Two different TMA sets were used in this study (Abcam, see section 2.7 and Appendix Table X). TMA were analysed to check the expression of PYCR1 protein by immunohistochemistry and were scored by a colon cancer pathologist (Professor Kevin West, University Hospitals of Leicester). Additionally, PYCR1 H-score was independently estimated using the Aperio ImageScope software (see section 2.2.10.). As shown in Figure 3.2, the two H-score outcomes were highly correlated and a statistically significant increase in PYCR1 expression in cancer tissues was observed in both TMAs (Figures 3.3. and 3.4). Indeed, 72% of normal tissue specimens showed low expression levels of PYCR1 protein, whereas, malignant tissues displayed strong and moderate positivity for PYCR1 in 53% and 28% of cases, respectively (Figure 3.3.C, Figure 3.4.C and Figure 3.5).

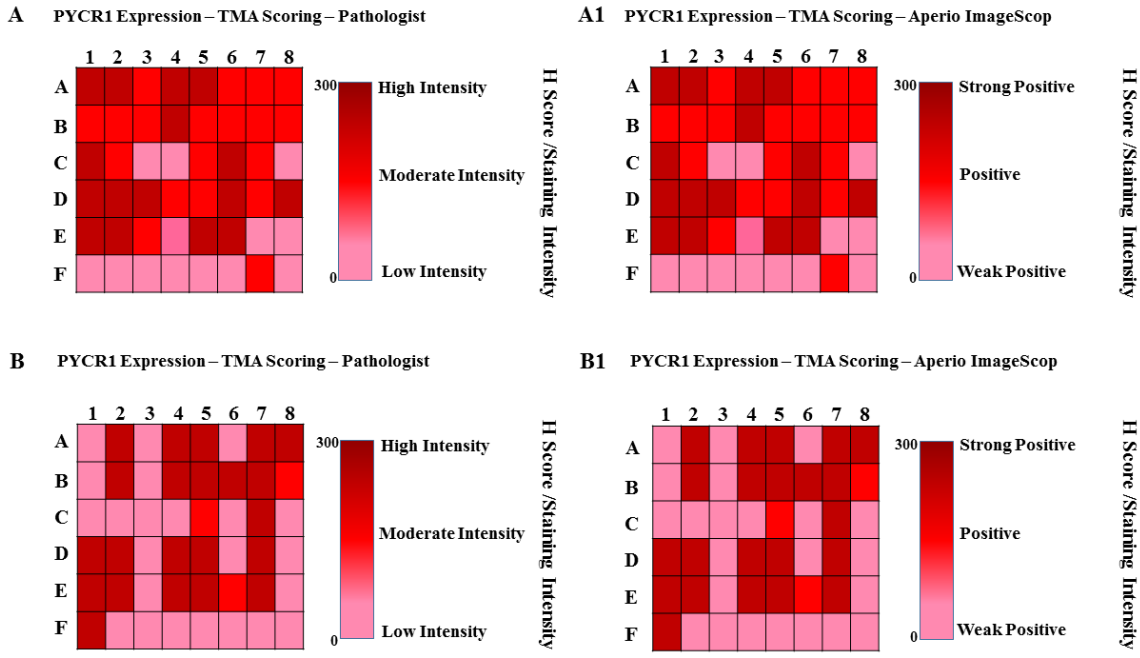

Figure 3.2. Heat maps of PYCR1 protein expression by TMA scoring for CRC patients and normal cases. (**A, A1**) TMA set 1 cores, (**B, B1**) TMA set 2 cores. The results showed different staining levels for PYCR1 expression assessed either by manual scoring (**A, B**) or automated software classification using Aperio ImageScope (**A1, B1**). For each heat map, A, B, D and E rows indicate PYCR1 H-scores in duplicate CRC cores, while, rows C and F represent the PYCR1 expression in normal colon and rectum specimens. The colour key scale represented by dark red colours indicates high stain intensity/strong positive result, bright red colours indicates moderate stain intensity/positive result and pink colours indicates low stain intensity/ weak positive. N=16 normal cases and 16 cancer cases for each TMA.

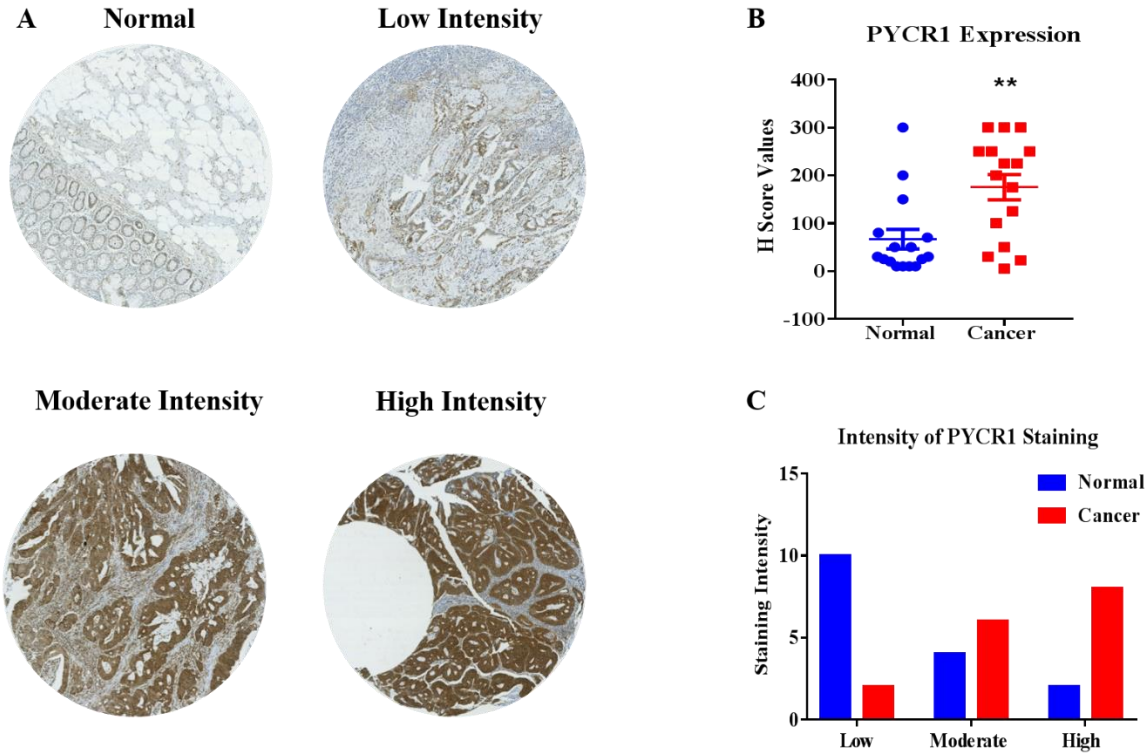

Figure 3.3. PYCR1 expression levels in CRC TMA set 1. (**A**) Representative images of TMA cores stained with PYCR1 antibody. Examples of normal tissue and differentially stained malignant cores are reported. (**B**) H-score analysis of the TMA cohort indicates a significant upregulation of PYCR1 level in cancer tissues compared to normal. Each dot represents a single core for normal specimens and the average of two separate cores for CRC cases. Lines indicate mean ± standard error of mean (S.E.M.). (**C**) PYCR1 intensity staining in normal (**blue**) and cancerous (**red**) tissues in TMA set 1 as assessed by pathologist. Weak intensity is predominant in normal tissue, while malignant cases present with moderate and strong PYCR1 expression. Two tailed student's *t*-test was performed in panel B, n= 16 normal and 16 cancer cases. ** $p < 0.01$.

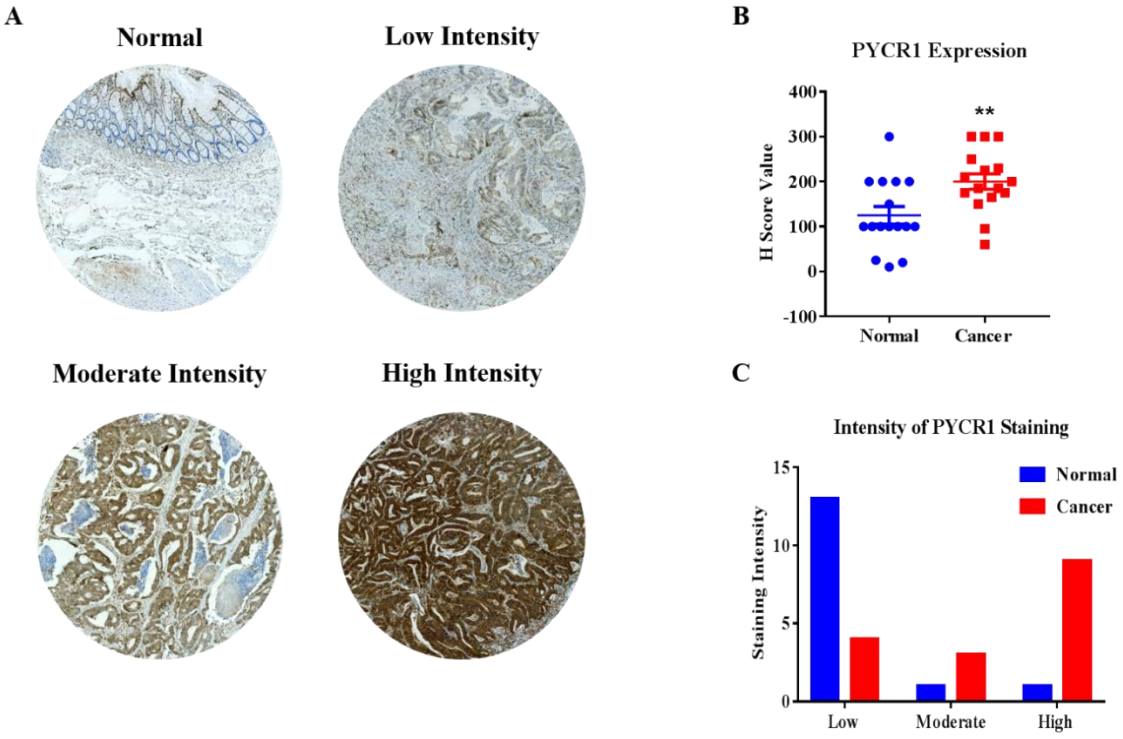

Figure 3.4. PYCR1 expression levels in CRC TMA set 2. (**A**) Representative images of TMA cores stained with PYCR1 antibody. Examples of normal tissue and differentially stained malignant cores are reported. (**B**) H-score analysis of the TMA cohort indicates a significant upregulation of PYCR1 level in cancer tissues compared to normal. Each dot represents a single core for normal specimens and the average of two separate cores for CRC cases. Lines indicate mean ± S.E.M. (**C**) PYCR1 intensity staining in normal (**blue**) and cancerous (**red**) tissues in TMA set 1 as assessed by pathologist. Weak intensity is predominant in normal tissue, while malignant cases present with moderate and strong PYCR1 expression. Two tailed student's *t*-test was performed in panel B, n= 16 normal and 16 cancer cases. ** $p < 0.01$.

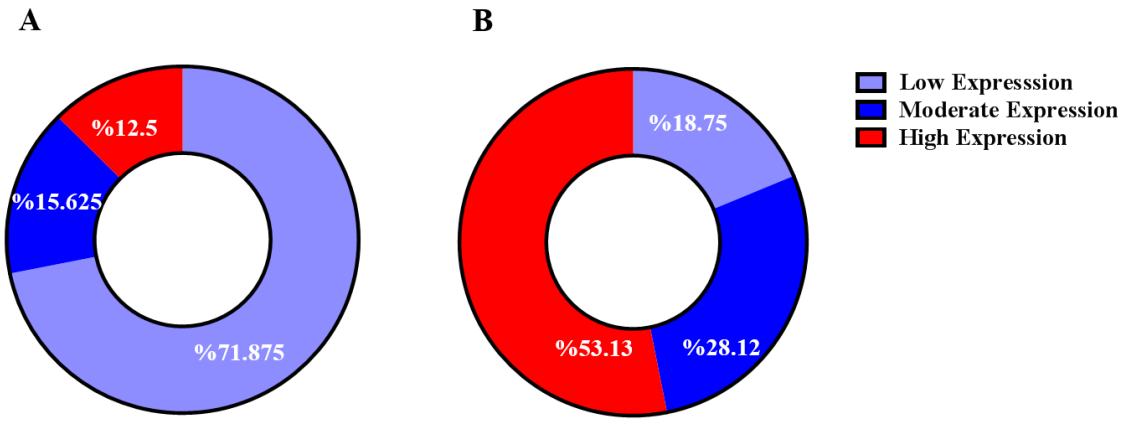

Figure 3.5. PYCR1 expression levels in normal and malignant cases. (**A**) Pie chart showing the low expression of PYCR1 in over 70% of normal intestinal tissue controls. (**B**) Pie chart of PYCR1 expression in CRC specimens showing that 53.13% of CRC cases analysed displayed high expression of PYCR1 protein and that 28.12 % present moderate expression, with only 18.75% of cases having low PYCR1 levels. Data were obtained pulling together both TMA sets, n=32 normal controls and 32 CRC cases.

3.3. Assessment of PYCR1 protein expression in human normal and CRC primary samples

The origin and processing of these human primary samples are described in sections 2.5.1 and 2.2.7.

Out of a total of 40 specimens processed, only 14 provided sufficient amount of protein to investigate the expression of PYCR1 using western blotting. Fortunately, the suitable samples included 5 normal intestinal tissues, 5 colon adenocarcinomas, 3 benign polyps and 1 liver metastasis. In agreement with previous finding, western blotting analysis confirmed that PYCR1 protein was upregulated fourfold in adenocarcinomas and fivefold in benign polyps compared to normal primary cells (Figure 3.6).

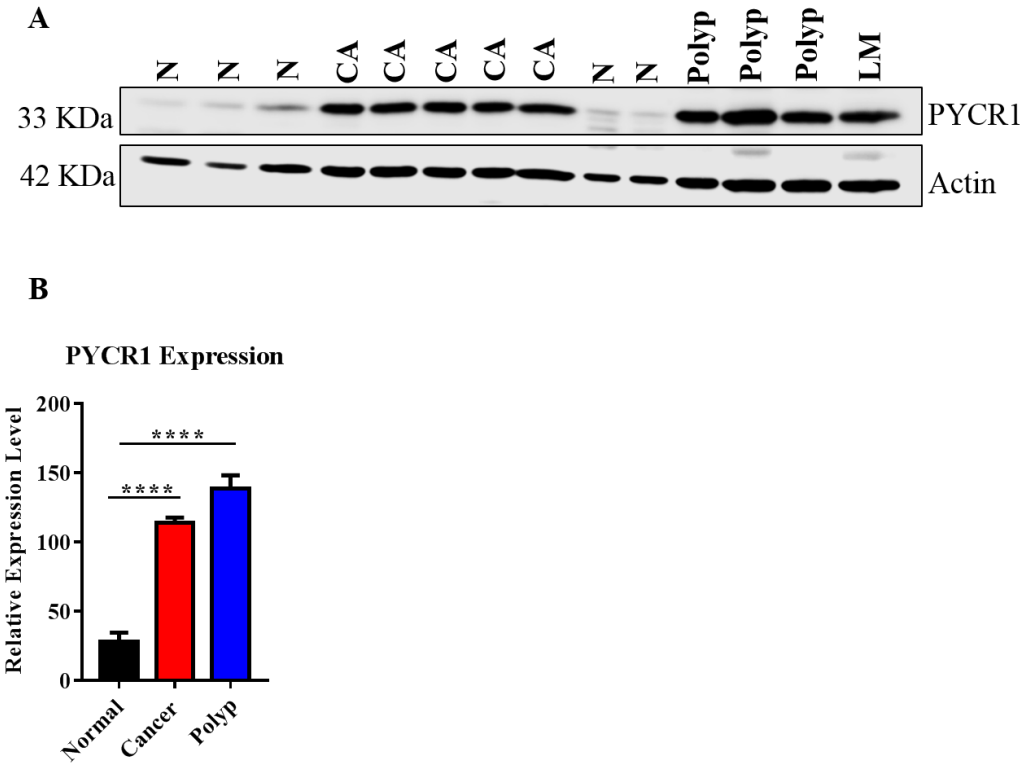

Figure 3.6. Expression of PYCR1 enzyme inhuman primary samples. (**A**) PYCR1 expression was analysed by western blotting. Actin was used performed as endogenous loading control. (**B**) The relative expressions was calculated relative to the normal group using ImageJ software. The p values were measured using Sidak's multiple comparisons One-way Anova test. **** $p < 0.0001$. n=5 normal tissue controls, 6 CRC cases (including 1 liver metastasis) and 3 benign polyps. N = normal, CA = cancer and LM = liver metastasis. The bars indicates mean ± S.E.M.

3.4. mRNA expression of enzymes of proline metabolism in CRC cell lines

3.4.1. Analysis of mRNA expression levels using RT-qPCR

The expression levels of proline metabolism enzymes were measured using RT-qPCR and TaqMan probe-based assays for *PYCR1*, *PYCR2*, *PYCRL* and *PRODH*/*POX* in seven CRC cell lines (HCT116, SW480, HT29, RKO, CL11, Caco2 and SW620).

For the *PYCR1* gene, the results showed that the lowest ΔC_T measurements were recorded for HCT116, SW620 and RKO CRC cell line, which were 0.63 ± 0.06, 1.24 ± 0.22, 1.65 ± 0.11, respectively. At the same time, SW480 and HT29 showed the highest values for PYCR1 mRNA level, (4.64 ± 0.72 and 4.03 ± 0.28, respectively), while the ΔC_T values for both CL11 and Caco2 CRC cell lines revealed intermediate mRNA expression levels (2.73 ± 0.43, 2.01 ± 0.16, respectively) (Figure 3.7 A and B).

In the case of *PYCR2*, the ΔC_T value of HCT116 cells was the lowest (2.62 ± 0.11), while SW480 showed the highest value of 9.47 ± 0.31. The remaining CRC cell lines had comparable ΔC_T values, ranging from 4.03 to 5.36 (Figure 3.8.A and B).

SW480 cells displayed the highest *PYCRL* expression (ΔC_T = 2.81 ± 0.42), whereas Caco2 cells showed the lowest expression, as reflected by the highest ΔC_T value of 10.0 ± 0.32. The remaining CRC cell lines had comparable *PYCRL* mRNA expression levels (Figure 3.9 A and B).

Finally, SW480 showed the highest expression of *PRODH*/*POX* with a ΔC_T value of 2.05 ± 0.20. In contrast, the SW620 cells were at the other end of the spectrum, exhibiting the lowest expression levels of *PRODH/POX* (ΔC_T = 7.24 ± 0.40). The rest of the cell lines had ΔC_T values between 4.16 and 6.92 (Figure 3.10 A and B).

A

	Cell Lines	Endogenous Control (*ACTB*) C_T Mean ± S.E.M	*PYCR1* C_T Mean ± S.E.M	*ΔC_T Mean ± S.E.M
1	HCT116	22.65 ± 0.54	23.28 ± 0.47	0.63 ± 0.06
2	SW480	18.74 ± 0.52	23.38 ± 0.45	4.64 ± 0.72
3	HT29	18.35 ± 0.37	22.38 ± 0.50	4.03 ± 0.28
4	RKO	21.42 ± 0.09	23.07 ± 0.03	1.65 ± 0.11
5	CL11	21.44 ± 0.40	24.17 ± 0.08	2.73 ± 0.43
6	Caco2	21.58 ± 0.33	23.59 ± 0.26	2.01 ± 0.16
7	SW620	23.09 ± 0.40	24.33 ± 0.41	1.24 ± 0.22

B

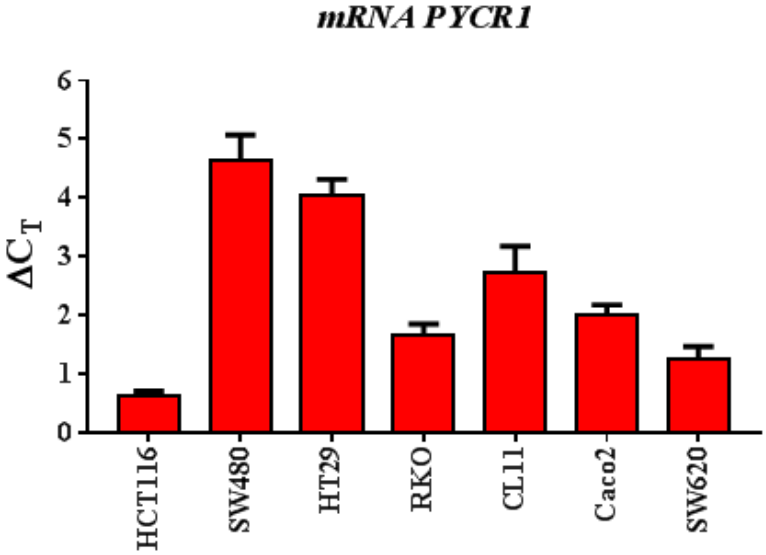

Figure 3.7. *PYCR1* mRNA quantification in CRC cell lines. (**A**) The table lists the C_T means for reference gene (*ACTB*) and C_T means for the gene of interest (*PYCR1*) and the resulting ΔC_T values for PYCR1 mRNA expression in the indicated CRC cell lines. (**B**) The graph shows the levels of PYCR1 mRNA expression (ΔC_T values) in human CRC cell lines. All data represent mean ± SEM, n=5. Of note, a lower ΔC_T value indicates higher expression of the gene.

A

	Cell Lines	Endogenous Control (*ACTB*) C_T Mean ± S.E.M	*PYCR2* C_T Mean ± S.E.M	*ΔC_T Mean ± S.E.M
1	HCT116	21.61 ± 0.39	24.23 ± 0.33	2.62 ± 0.11
2	SW480	16.64 ± 0.21	26.11 ± 0.43	9.47 ± 0.31
3	HT29	18.14 ± 0.28	22.99 ± 0.60	4.85 ± 0.43
4	RKO	21.44± 0.008	26.50 ± 0.17	5.06 ± 0.17
5	CL11	22.54 ± 0.02	26.66 ± 0.36	4.12 ± 0.36
6	Caco2	19.95 ± 0.16	25.31 ± 0.19	5.36 ± 0.27
7	SW620	23.61 ± 0.23	27.64 ± 0.27	4.03 ± 0.20

B

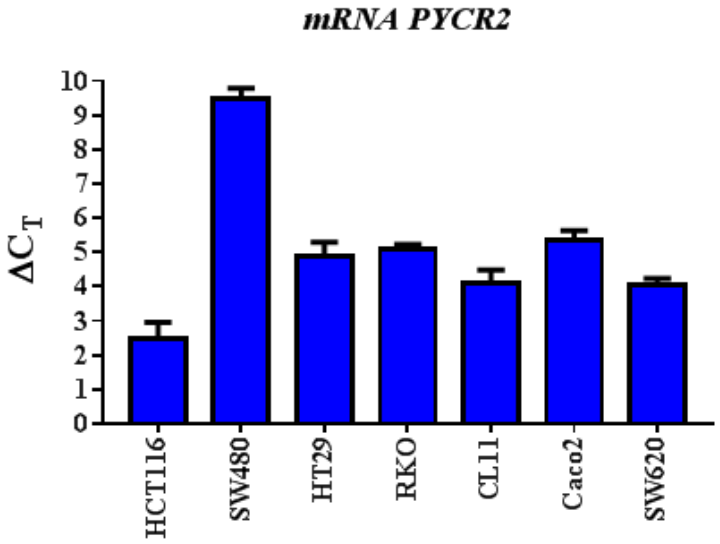

Figure 3.8 *PYCR2* mRNA quantification in CRC cell lines. (**A**) The table lists the C_T means for reference gene (*ACTB*) and C_T means for the gene of interest (*PYCR2*) and the resulting ΔC_T values for *PYCR2* mRNA expression in the indicated CRC cell lines. (**B**) The graph shows the levels of *PYCR2* mRNA expression (ΔC_T values) in human CRC cell lines. All data represent mean ± SEM, n=5. Of note, a lower ΔC_T value indicates higher expression of the gene.

A

	Cell Lines	Endogenous Control (*ACTB*) C_T Mean ± S.E.M	*PYCRL* C_T Mean ± S.E.M	*ΔC_T Mean ± S.E.M
1	HCT116	23.02 ± 0.36	28.27 ± 0.75	5.25 ± 0.27
2	SW480	17.65 ± 0.30	20.46 ± 0.23	2.81 ± 0.42
3	HT29	18.30 ± 0.23	23.33 ± 0.25	5.03 ± 0.14
4	RKO	21.48 ± 0.09	25.96 ± 0.36	4.48 ± 0.38
5	CL11	22.56 ± 0.27	27.16 ± 0.09	4.60 ± 0.30
6	Caco2	20.07 ± 0.14	30.07 ± 0.36	10.00 ± 0.32
7	SW620	24.21 ± 0.12	29.45 ± 0.20	5.24 ± 0.18

B

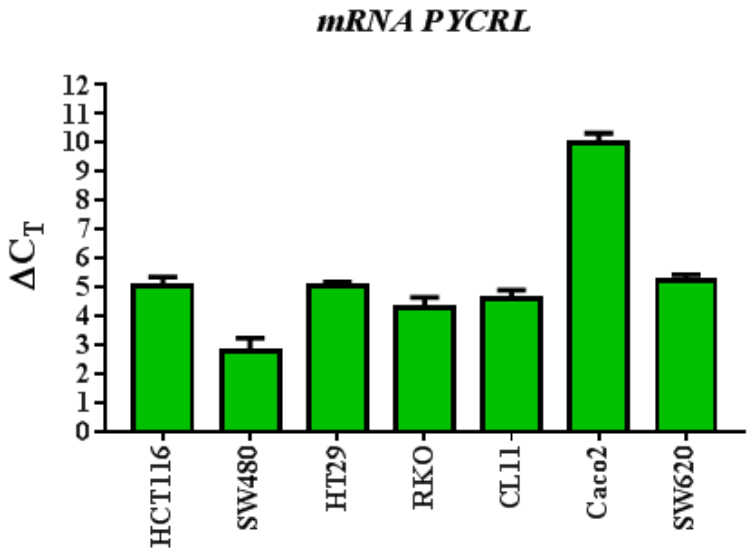

Figure 3.9 *PYCRL* mRNA quantification in CRC cell lines. (**A**) The table lists the C_T means for reference gene (*ACTB*) and C_T means for the gene of interest (*PYCRL*) and the resulting ΔC_T values for *PYCRL* mRNA expression in the indicated CRC cell lines. (**B**) The graph shows the levels of *PYCRL* mRNA expression (ΔC_T values) in human CRC cell lines. All data represent mean ± SEM, n=5. Of note, a lower ΔC_T value indicates higher expression of the gene.

A

	Cell Lines	Endogenous Control (*ACTB*) C_T Mean ± S.E.M	*PRODH/POX* C_T Mean ± S.E.M	*ΔC_T Mean ± S.E.M
1	HCT116	23.41 ± 0.17	28.12 ± 0.41	4.71 ± 0.36
2	SW480	17.36 ± 0.28	19.41 ± 0.46	2.05 ± 0.20
3	HT29	19.65 ± 0.17	23.81 ± 0.50	4.16 ± 0.45
4	RKO	22.03 ± 0.27	28.09 ± 0.27	6.06 ± 0.35
5	CL11	22.69 ± 0.25	29.61 ± 0.51	6.92 ± 0.38
6	Caco2	21.64 ± 0.32	27.92 ± 0.37	6.28 ± 0.36
7	SW620	23.17 ± 0.21	30.41 ± 0.37	7.24 ± 0.40

B

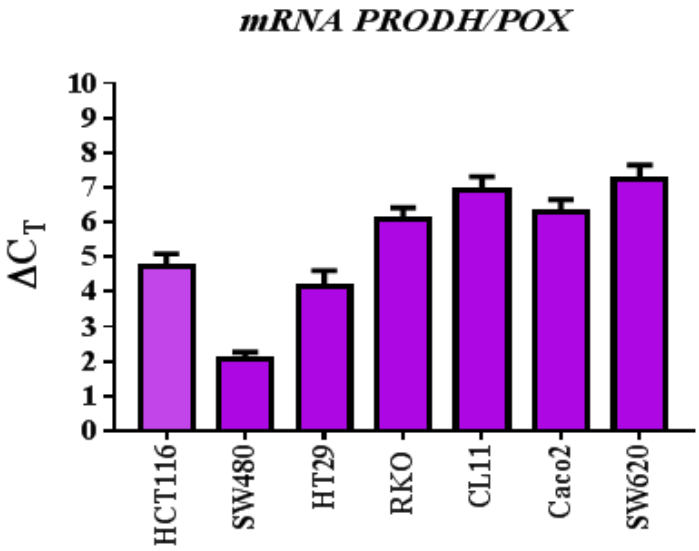

Figure 3.10. *PRODH/POX* mRNA quantification in CRC cell lines. (**A**) The table lists the C_T means for reference gene (*ACTB*) and C_T means for the gene of interest (*PRODH/POX*) and the resulting ΔC_T values for *PRODH/POX* mRNA expression in the indicated CRC cell lines. (**B**) The graph shows the levels of *PRODH/POX* mRNA expression (ΔC_T values) in human CRC cell lines. All data represent mean ± SEM, n=5. Of note, a lower ΔC_T value indicates higher expression of the gene.

3.4.2. Protein expression levels of enzymes of proline metabolism in CRC cell lines

The same CRC cell lines (namely, HCT116, SW40, HT29, RKO, CL11, Caco2 and SW620) were tested to assess protein expression of four enzymes of the proline metabolic pathway: PYCR1, PYCR2, PYCRL and PRODH/POX (Figure 3.11). The results showed that PYCR1 enzyme is poorly expressed in SW480 cell line, but showed robust expression in HCT116, RKO and SW620 (Figure 3.11). With regard to PYCR2, protein expression levels were fairly consistent among the different cell lines. Again, expression levels were highest in HCT116 and lowest in SW480. However, the latter cell line showed the strongest levels of PYCRL. Interestingly, all cell lines, with the exception of SW480, showed undetectable or poor expression of POX/PRODH enzyme (Figure 3.11). These findings seem to suggest that proline metabolism is rewired towards proline biosynthesis in CRC cell lines.

In some cases, measurements from RT-qPCR experiments did not reflect protein expression levels in CRC cells. For instance, in SW480, the RNA expression level of *PYCR1* showed considerable transcriptional value (ΔC_T = 4.64) (Figure 3.7), but we detected only marginal expression of PYCR1 protein (Figure 3.11).

However both RNA and protein data confirmed that SW480 expressed the highest levels of PRODH/POX (Figure 3.10 and Figure 3.11).

These discrepancies between mRNA and protein expression may result from posttranscriptional regulation and differences in mRNA and protein turnover rates (Hack, 2004 and Cox et al., 2005).

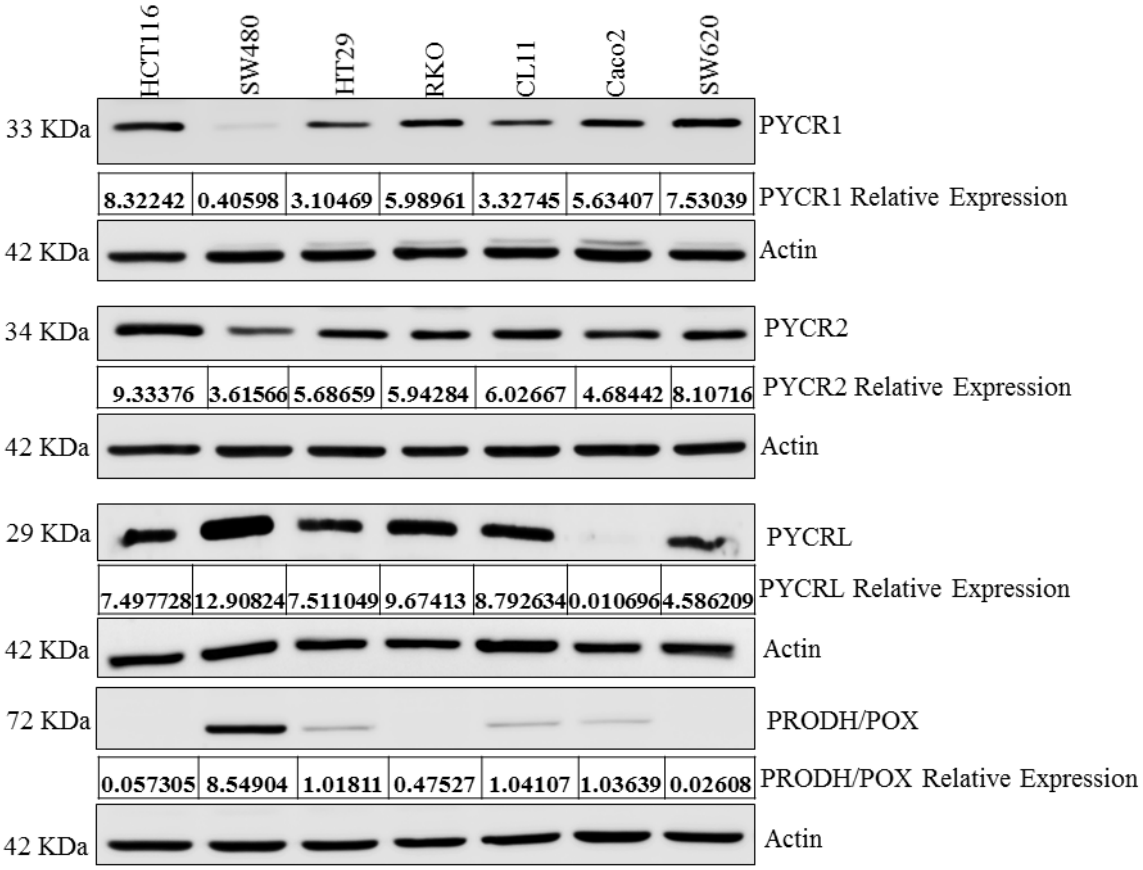

Figure 3.11. Expression of proline metabolism enzymes in CRC cell lines by western blotting. Representative western blot of protein expression levels of PYCR1, PYCR2, PYCRL and PRODH/POX in the indicated CRC cell lines. Actin was used as endogenous loading control. ImageJ software (Version 1.51g) was used to calculate the relative expression values of western blotting bands' intensity. Data were normalized to actin loading control.

Chapter Four: Characterization of proline biosynthesis enzymes in a mouse model of colorectal carcinogenesis

4. Introduction

The aim of this chapter was to assess the expression of PYCR1 and other proline biosynthesis enzymes during the early stages of tumorigenesis using the *Lgr5-Cre^{ER}/Apc$^{fl/fl}$* mouse model of colorectal carcinogenesis. This mouse model has been genetically modified to mimic the aetiology of human CRCs that arise due to *APC* gene mutations (Jackstadt and Sansom, 2016). As described in details in section 1.14, the exon 14 of the mouse *Apc* gene has been floxed and the tamoxifen-inducible Cre^{ER} recombinase expressed under the promoter of the ISC gene *Lgr5* (Barker et al., 2009). Therefore, injection of tamoxifen deletes the *Apc* gene selectively in the ISCs, leading to constitutive activation of Wnt signalling and formation of large adenomas within few weeks. Since the *c-Myc* oncogene, which positively regulates *PYCR1* expression, is a well-characterized target of the Wnt pathway, we hypothesised that PYCR1 levels would be increased in the *Apc*-deleted intestines (Liu et al., 2012b). To prove this, we injected 35 *Lgr5-Cre^{ER}/Apc$^{fl/fl}$* mice of both sexes intraperitoneally with tamoxifen (3 mg/mouse) (Figure 4.1). We culled the animals and harvested tissues 3 days, 1 week and 2 weeks post injection, in order to have a time course analysis of gene expression. The expression of proline biosynthesis enzymes including PYCR1 was assessed using IHC, RT-qPCR, western blotting and immunofluorescence techniques.

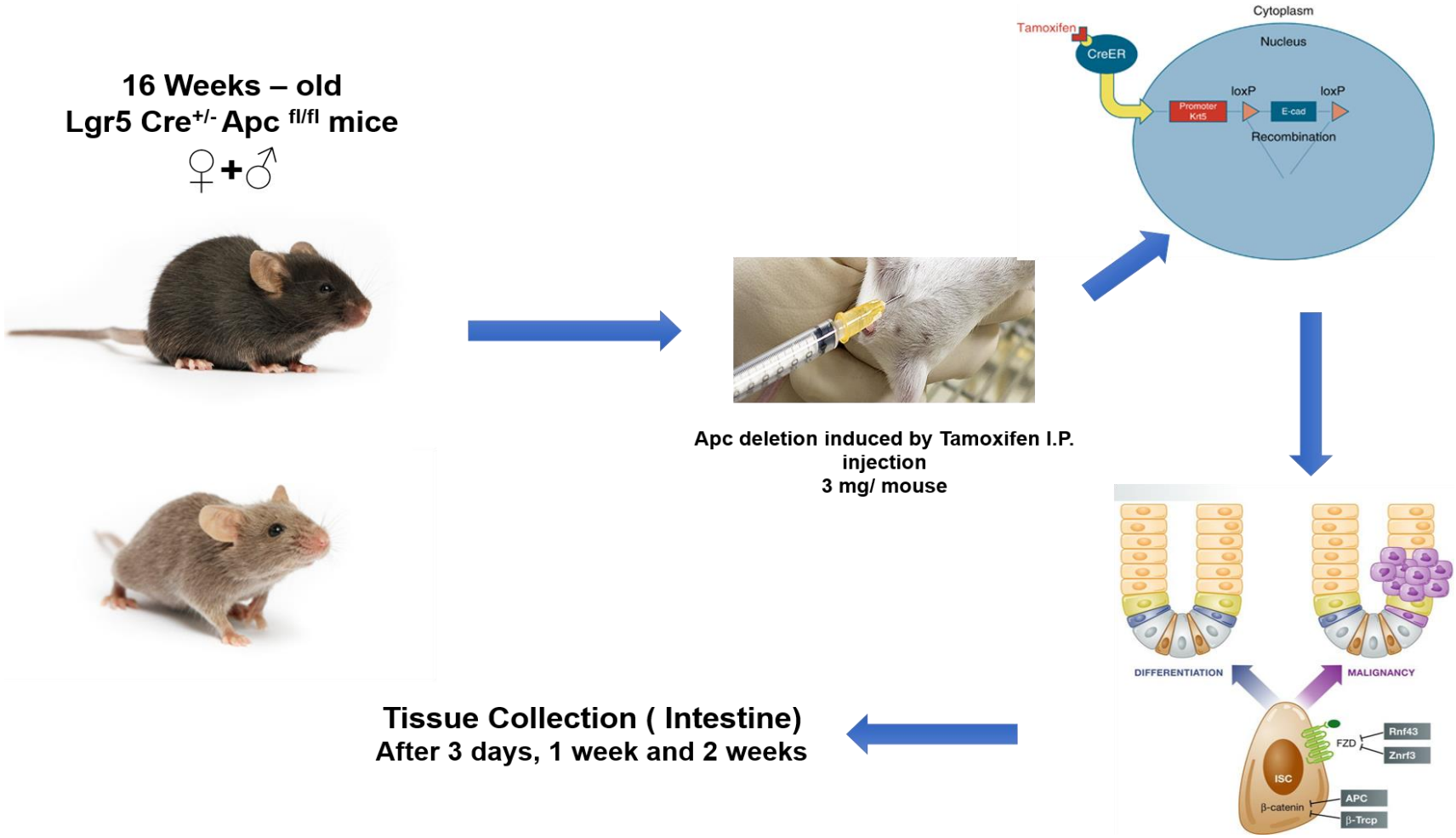

Figure 4.1. Schematic representation of the experimental design implemented in this study. Sixteen- week old *Lgr5-Cre^{ER-}/Apcfl/fl* (Cre negative controls) and *Lgr5-Cre^{ER+}/Apc$^{fl/fl}$* (Cre positive animals) male and female mice were used in this study. Loss of the *Apc* gene was induced by tamoxifen intraperitoneal injection (3 mg/mouse). After three days, one week, and two weeks of Apc gene deletion, the mice were euthanized and intestinal tissues collected for further analysis.

4.1. Experimental animals

As mentioned, 35 *Lgr5-Cre*^{ER}/*Apc*$^{fl/fl}$ mice aged 16 weeks were used. The experimental animals consisted of a control group, Apc-floxed animals without expression of Cre recombinase (*Lgr5-Cre*$^{ER-}$/*Apc*$^{fl/fl}$), and the Apc-deleted group, consitting of *Apc*-floxed, Cre-expressing mice (*Lgr5-Cre*$^{ER+}$/*Apc*$^{fl/fl}$). A summary of mice allocation is reported in Table 4.1. All animals were intraperitoneally injected with 3 mg of tamoxifen to induce deletion of the *Apc* gene in the ISCs and were culled after three days, seven days and lastly 14 days (Figure 4.1). At each time point, mice were euthanized by terminal anaesthesia and the intestines were collected as described in Materials and Methods, section 2.2.13.3.

A

	Mouse ID	Genotype	Sex	Time Point (Days)
Control	6454	Lgr5 Cre -	M	3
	6462	Lgr5 Cre -	M	3
	6486	Lgr5 Cre -	M	3
	6463	Lgr5 Cre -	M	7
	6467	Lgr5 Cre -	M	7
	6476	Lgr5 Cre -	M	7
	6468	Lgr5 Cre -	M	14
	6492	Lgr5 Cre -	M	14

	Mouse ID	Genotype	Sex	Time Point (Days)
Apc Deleted	6453	Lgr5 Cre +	M	3
	6458	Lgr5 Cre +	M	3
	6470	Lgr5 Cre +	M	3
	6457	Lgr5 Cre +	M	7
	6469	Lgr5 Cre +	M	7
	6455	Lgr5 Cre +	M	7
	6481	Lgr5 Cre +	M	14
	6485	Lgr5 Cre +	M	14
	6456	Lgr5 Cre +	M	14

B

	Mouse ID	Genotype	Sex	Time Point (Days)
Control	6459	Lgr5 Cre -	F	3
	6466	Lgr5 Cre -	F	3
	6472	Lgr5 Cre -	F	3
	6460	Lgr5 Cre -	F	7
	6471	Lgr5 Cre -	F	7
	6475	Lgr5 Cre -	F	7
	6490	Lgr5 Cre -	F	14
	6494	Lgr5 Cre -	F	14
	6496	Lgr5 Cre -	F	14

	Mouse ID	Genotype	Sex	Time Point (Days)
Apc Deleted	6453	Lgr5 Cre +	F	3
	6458	Lgr5 Cre +	F	3
	6470	Lgr5 Cre +	F	3
	6457	Lgr5 Cre +	F	7
	6469	Lgr5 Cre +	F	7
	6455	Lgr5 Cre +	F	7
	6481	Lgr5 Cre +	F	14
	6485	Lgr5 Cre +	F	14
	6456	Lgr5 Cre +	F	14

Figure 4.2. Mice used for the in vivo assessment of gene expression of proline metabolism enzymes. Mice IDs, Cre-recombinase genotype, sex and time points for culling after tamoxifen injection are reported in the dedicated columns. (**A**) Tables for male mice. (**B**) Tables for female mice.

4.2. Histopathological analysis of intestinal tissues

H&E staining of small intestine showed no remarkable pathological lesions at three days after *Apc* deletion in both males and females mice (Figure 4.3 and 4.6 respectivley). However, focal hyperplasic and metaplastic lesions were detected in mice at 1 week and 2 weeks after tamoxifen injection for both males and females. Hyperplastic and metaplastic changes manifested as enhanced proliferation of the cryptal epithelium and rounding of the villi (Figures 4.4, 4.5, 4.7 and 4.8). Crypt metaplasia was promptly observed in *Apc*-deleted mice, which displayed increased number of crypts and altered crypt architecture, such that, in some cases, discrete crypts were no longer identifiable (Figures 4.4 B and 4.5 C).

In some cases, precursor adenomatous lesions could be detected in the intestine (Figures 4.4, 4.5. in males and Figure 4.7, 4.8 in females), and dysplastic changes, such as cellular atypia were often detected in the intestinal tissues (Figures 4.5).

Overall, the histological changes identified in the laboratory mice are compatible with precursor CRC lesions (Chen et al., 2001 and Montgomery et al., 2001). Mice from the three day time point and the *Lgr5-Cre*$^{ER-}$*/Apc*$^{fl/fl}$ control mice did not show evident pathological alterations (Figures 4.3 and 4.6).

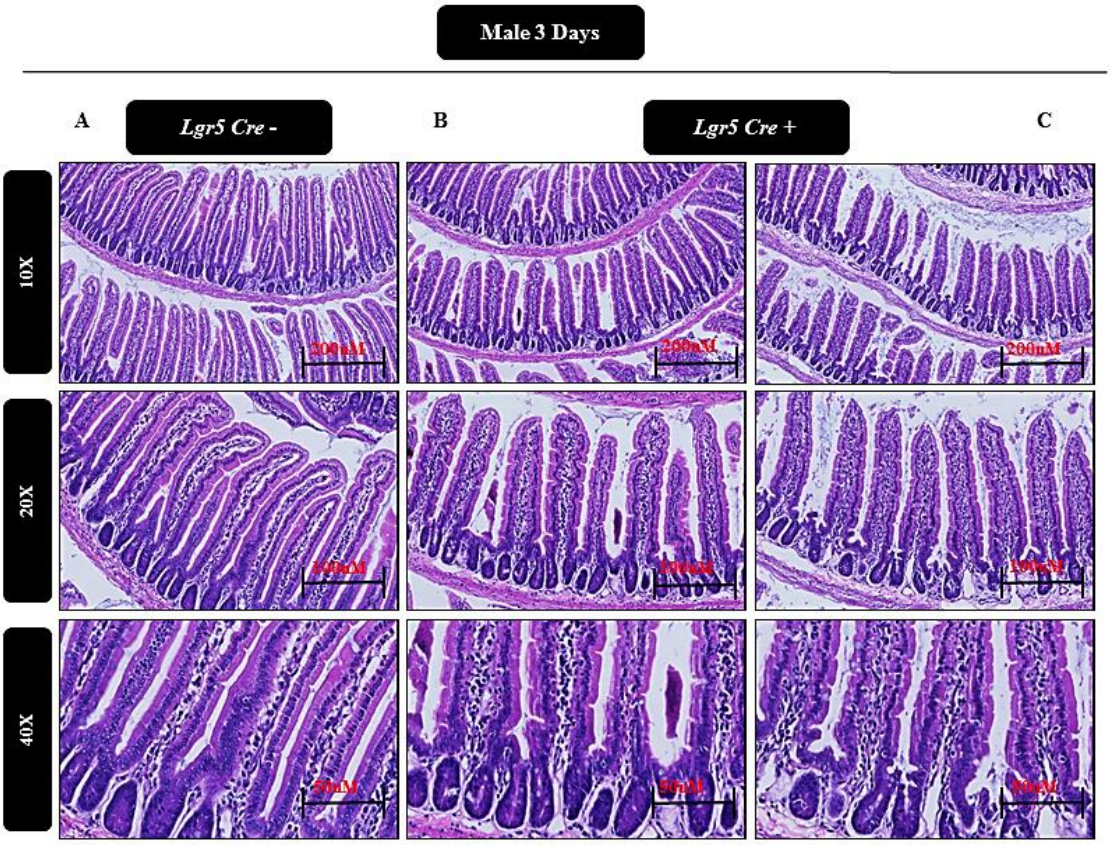

Figure 4.3. Representative histopathological sections of the small intestine of the *Lgr5-Cre^{ER}/Apc$^{fl/fl}$* male mice after three days from tamoxifen injection. H&E stained intestinal sections from control group (**A**) and *Apc*-deleted (**B**) and (**C**) mice at the indicated magnifications. In both control and *Apc*-deleted groups there were no evident pathological lesions. n=6 mice, 3 control and 3 *Apc*-deleted mice. Images were captured using the NanoZoomer-XR digital slide scanner C12000. Insets identify magnified areas. Scale bars are 200µM, 100µM and 50µM, respectively.

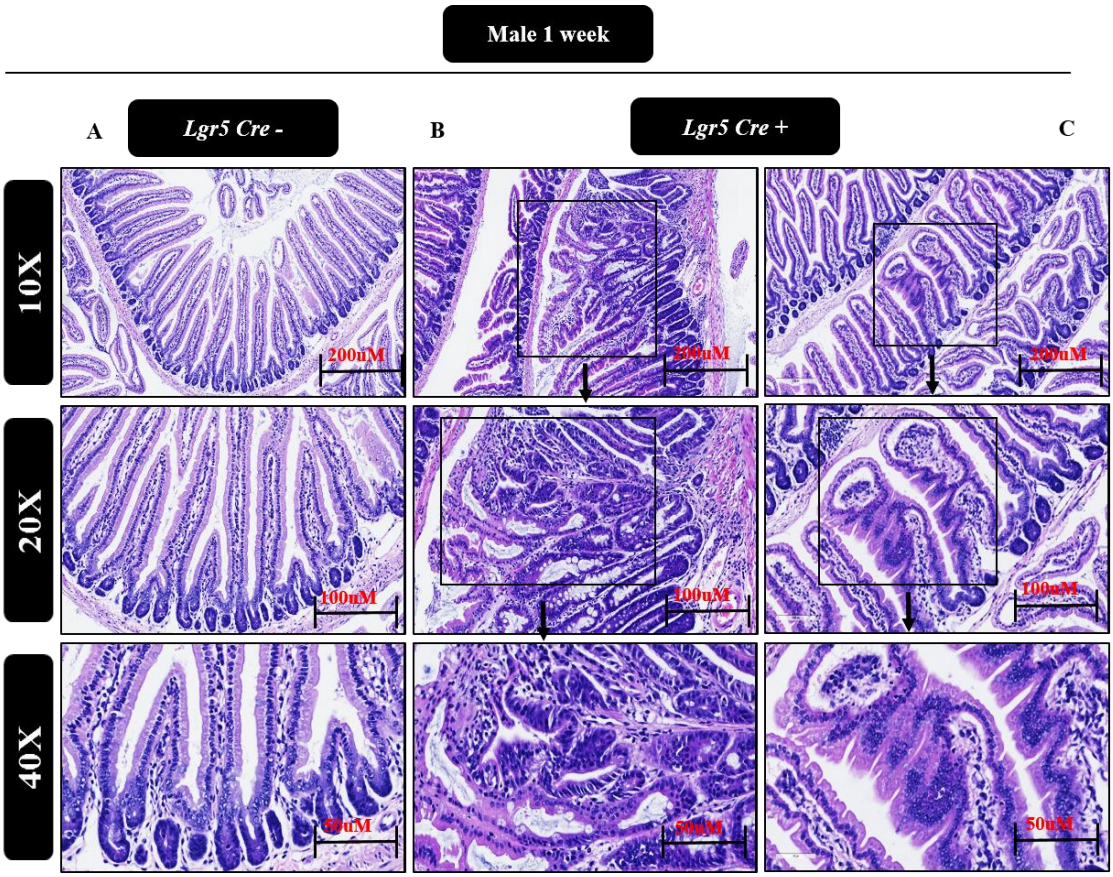

Figure 4.4. Representative histopathological sections of the small intestine of the *Lgr5-Cre^{ER}/Apc$^{fl/fl}$* male mice after one week from tamoxifen injection. H&E stained intestinal sections from control group (**A**) and *Apc*-deleted (**B**) and (**C**) mice at the indicated magnifications. The lesions in (**B**) and (**C**) show that the villi lose their architecture and become crowded with more proliferative cells. The control group did not show any pathological change. n=6 mice, 3 control and 3 *Apc*-deleted mice. Images were captured using the NanoZoomer-XR digital slide scanner C12000. Insets identify magnified areas. Scale bars are 200µM, 100µM, 50µM, respectively.

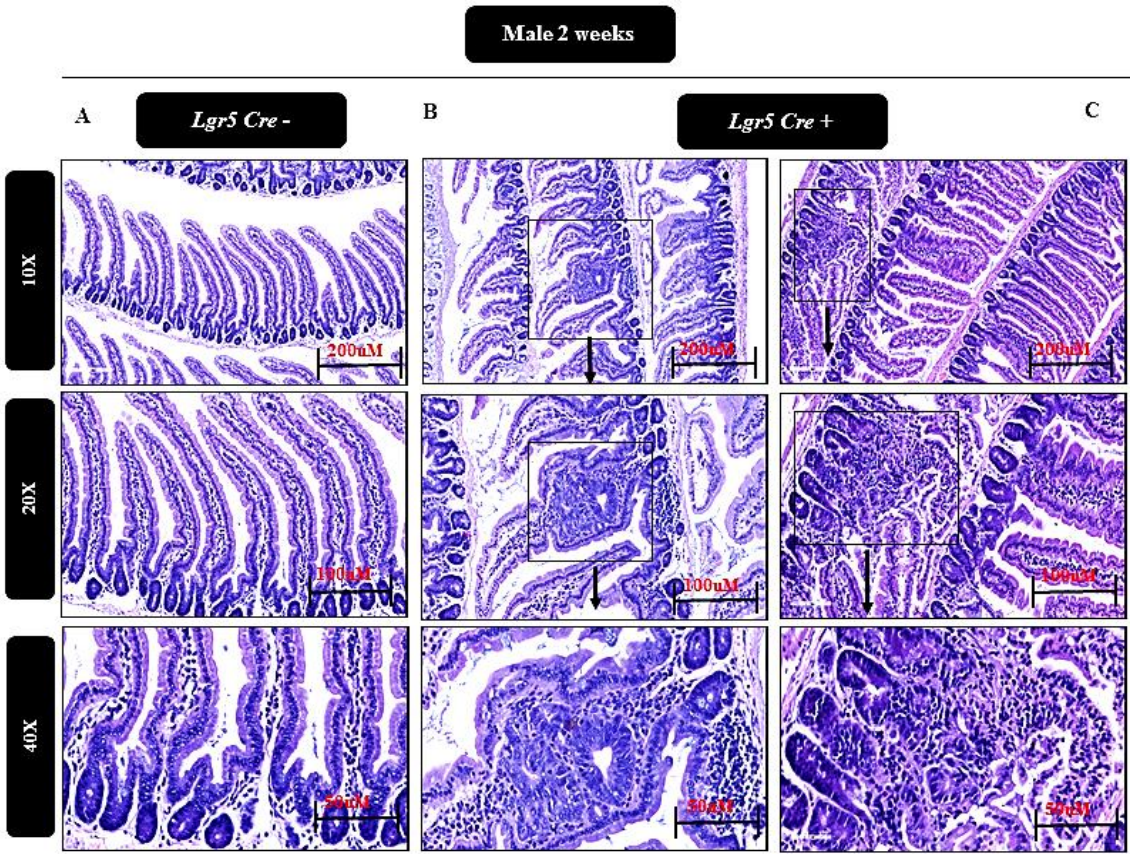

Figure 4.5. Representative histopathological sections of the small intestine of the *Lgr5-Cre^{ER}/Apc$^{fl/fl}$* male mice after two weeks from tamoxifen injection. H&E stained intestinal sections from control group (**A**) and *Apc*-deleted (**B**) and (**C**) mice at the indicated magnifications. A dysplastic villus is evident in (**B**), whereas a dense cellular area with nuclear atypia can be observed in (**C**). The control group did not show any pathological change. n=5 mice, 2 control and 3 *Apc*-deleted mice. Images were captured using the NanoZoomer-XR digital slide scanner C12000. Insets identify magnified areas. Scale bars are 200µM, 100µM and 50µM, respectively.

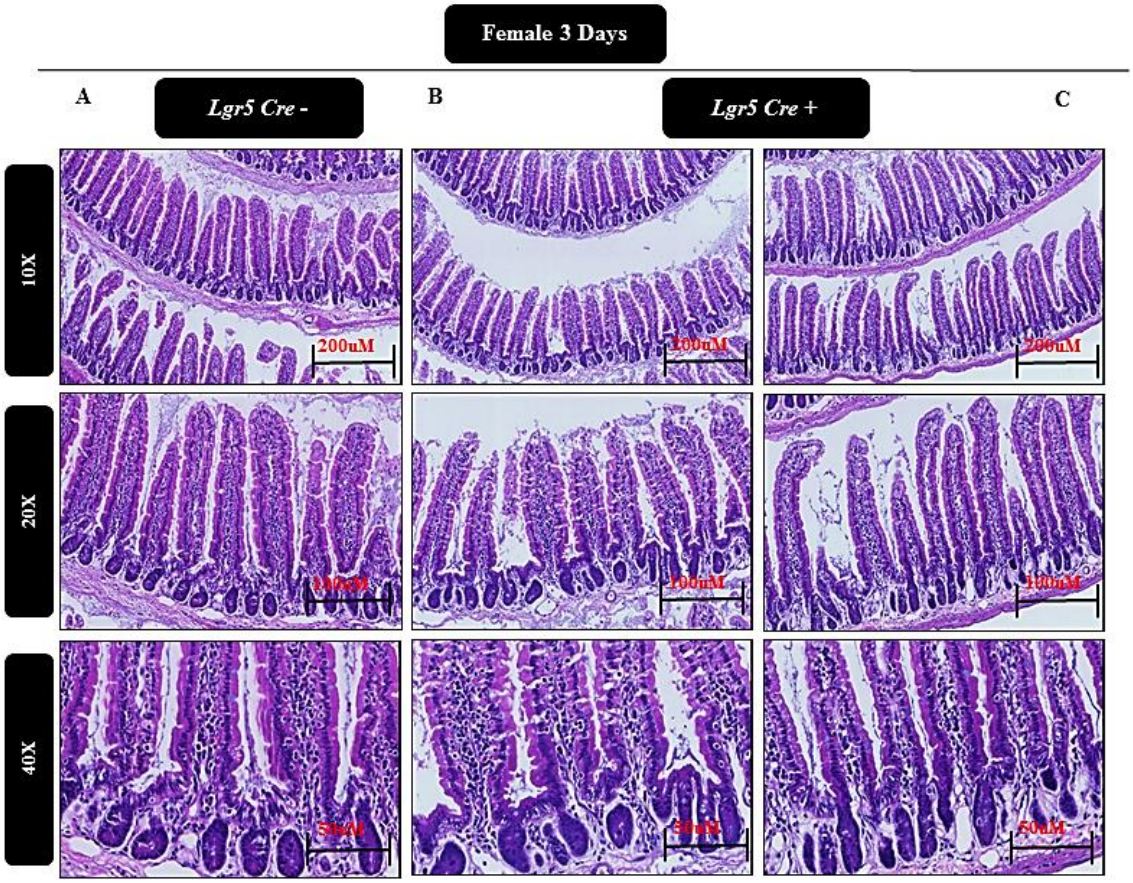

Figure 4.6. Representative histopathological sections of the small intestine of the *Lgr5-Cre^{ER}/Apc$^{fl/fl}$* female mice after three days from tamoxifen injection. H&E stained intestinal sections from control group (**A**) and *Apc*-deleted (**B**) and (**C**) mice at the indicated magnifications. In both control and *Apc*-deleted groups there were no evident pathological lesions. n=6 mice, 3 control and 3 *Apc*-deleted mice. Images were captured using the NanoZoomer-XR digital slide scanner C12000. Insets identify magnified areas. Scale bars are 200µM, 100µM and 50µM, respectively.

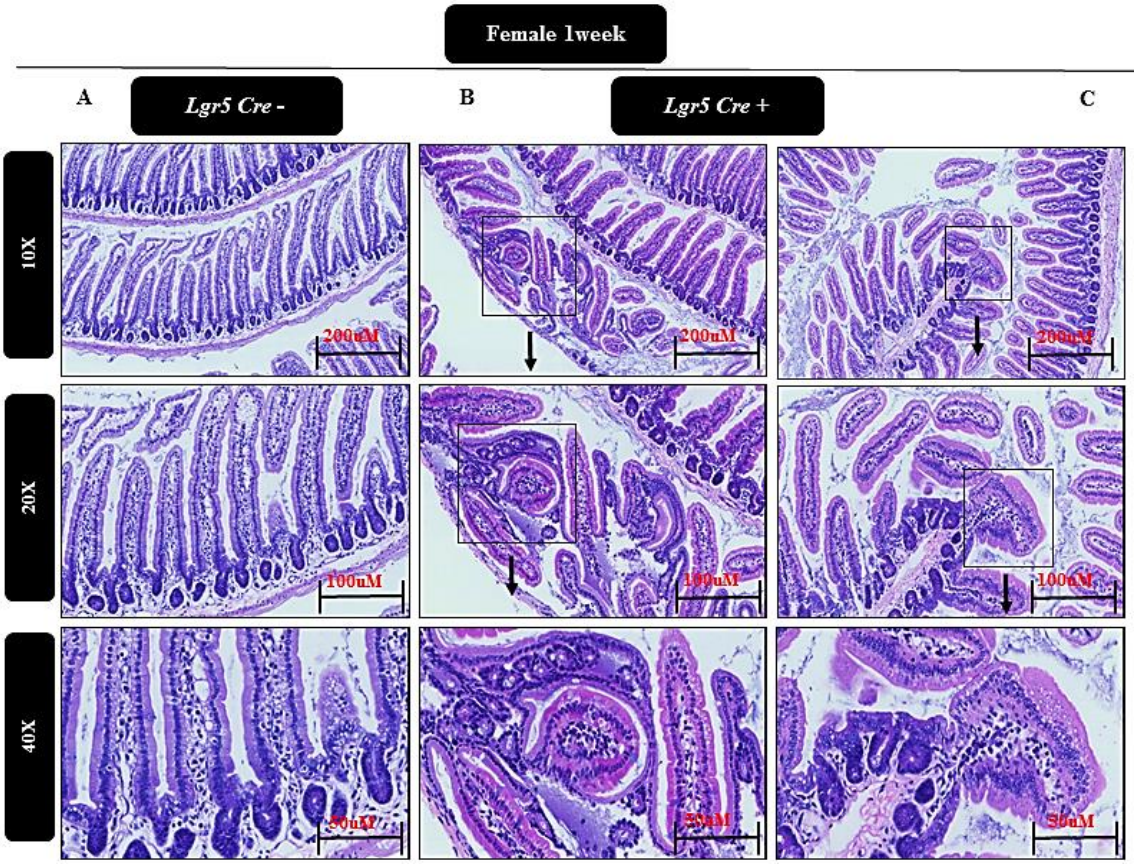

Figure 4.7. Representative histopathological sections of the small intestine of the *Lgr5-Cre^{ER}/Apc$^{fl/fl}$* female mice after one week from tamoxifen injection. H&E stained intestinal sections from control group (**A**) and *Apc*-deleted (**B**) and (**C**) mice at the indicated magnifications. The lesions in (**B**) and (**C**) show distorted villi architecture with crowded and atypical cells reminding of dysplastic polyps. The control group did not show any pathological changes. n=6 mice, 3 control and 3 *Apc*-deleted mice. Images were captured using the NanoZoomer-XR digital slide scanner C12000. Insets identify magnified areas. Scale bars are 200µM, 100µM and 50µM, respectively.

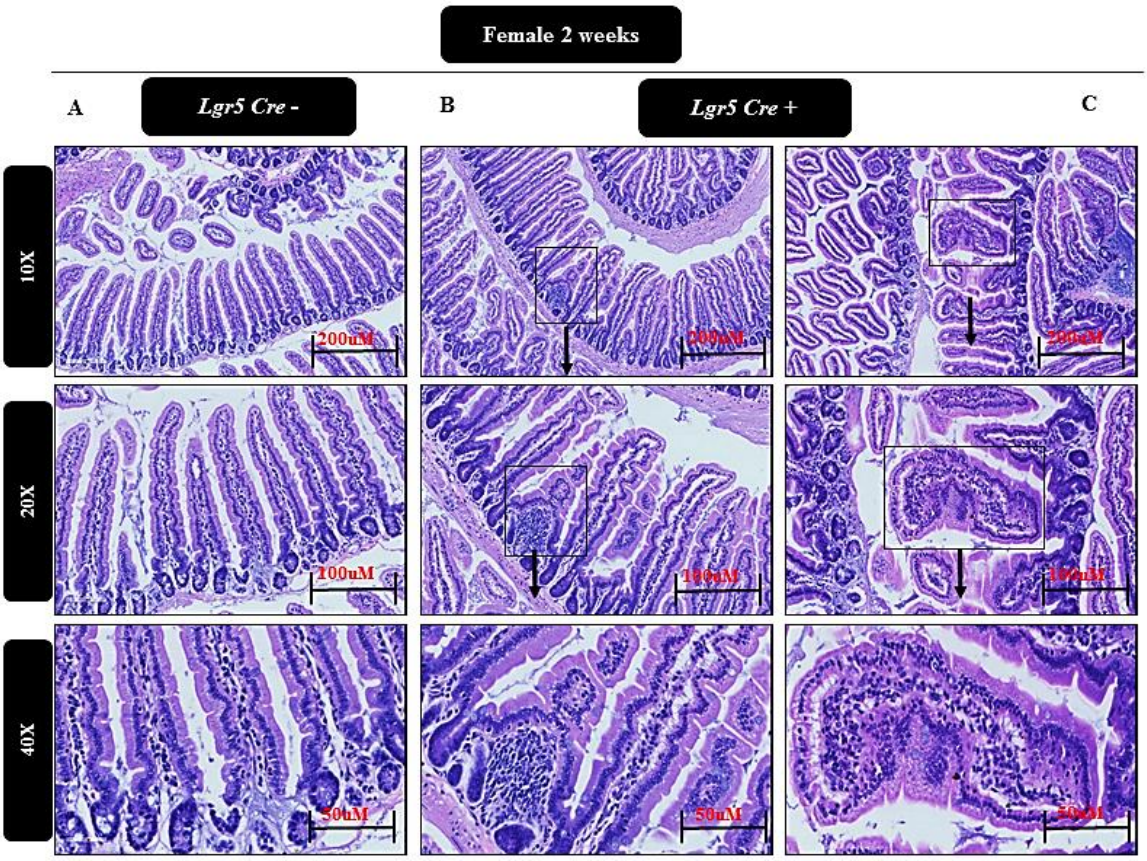

Figure 4.8. Representative histopathological sections of the small intestine of the *Lgr5-Cre* ^{ER}*/Apc*$^{fl/fl}$ female mice after two weeks from tamoxifen injection. H&E stained intestinal sections from control group (**A**) and *Apc*-deleted (**B**) and (**C**) mice at the indicated magnifications. The lesions in (**B**) and (**C**) show focal cell proliferation in villus area with loss of tissue architecture. The control group did not show any pathological changes. n=6 mice, 3 control and 3 *Apc*-deleted mice. Images were captured using the NanoZoomer-XR digital slide scanner C12000. Insets identify magnified areas. Scale bars are 200µM, 100µM and 50µM respectively.

4.3. Investigation the expression of Pycr1 in the mice small intestine

Three techniques have been used to explore the level of Pycr1 expression in the proximal part of the mouse small intestine. IHC has been used to stain the Pycr1 enzyme within intestinal tissue, whereas RT-qPCR has been implemented to investigate the mRNA expression level of the *Pycr1* gene, together with other enzymes of proline metabolism. Finally, western blotting was also employed to measure the expression of Pycr1 protein.

4.3.1. Pycr1 staining in the mice small intestine using immunohistochemistry technique

Previous data from our lab confirmed that, the proximal part of the small intestine presented the highest levels of *Apc* deletion and sustained development of adenomas (not shown). Therefore, this area was selected for staining with an anti-Pycr1 antibody (Table 2.2 in the material section). Pycr1 protein is localized within the mitochondria, with indication of a possible association to the external mitochondrial membrane (Phang et al., 2012). Pycr1 was readily detected in the intestinal crypts in both *Apc*-deleted and control mice (Figures 4.9, 4.10 and 4.11). After three days of tamoxifen injection, there was no difference detected in Pycr1 protein intensity in the mice intestinal crypts (Figure 4.9). Furthermore, the intensity of Pycr1 staining was stronger in the *Apc*-deleted mice, especially in the cryptal area one week and two weeks after tamoxifen injection (Figures 4.10 and 4.11 respectivley).

The scoring of Pycr1 staining intensity was obtained by measuring the intensity of 50 crypts in each mouse intestine in both Cre negative and Cre positive mice. The H-scores of staining intensity were then calculate using Aperio ImageScope software (Figure 4.12). After three days of tamoxifen injection, the H-score did not show any significant difference (p value = 0.7496, Figure 4.12A). However, after one week and two weeks from tamoxifen injection, the H-scores of Pycr1 were significantly increased ($p<0.01$) in the *Apc*-deleted mice compared with control animals (Figure 4.12, B and C).

Here, for the first time, we show that inactivation of the *Apc* gene has a close relation with upregulation of Pycr1 in the mice intestinal crypts compared to the wild-type counterparts. This could be suggestive of the importance of proline biosynthesis in the intestinal tumourigenesis process, especially at the early stages of neoplasia.

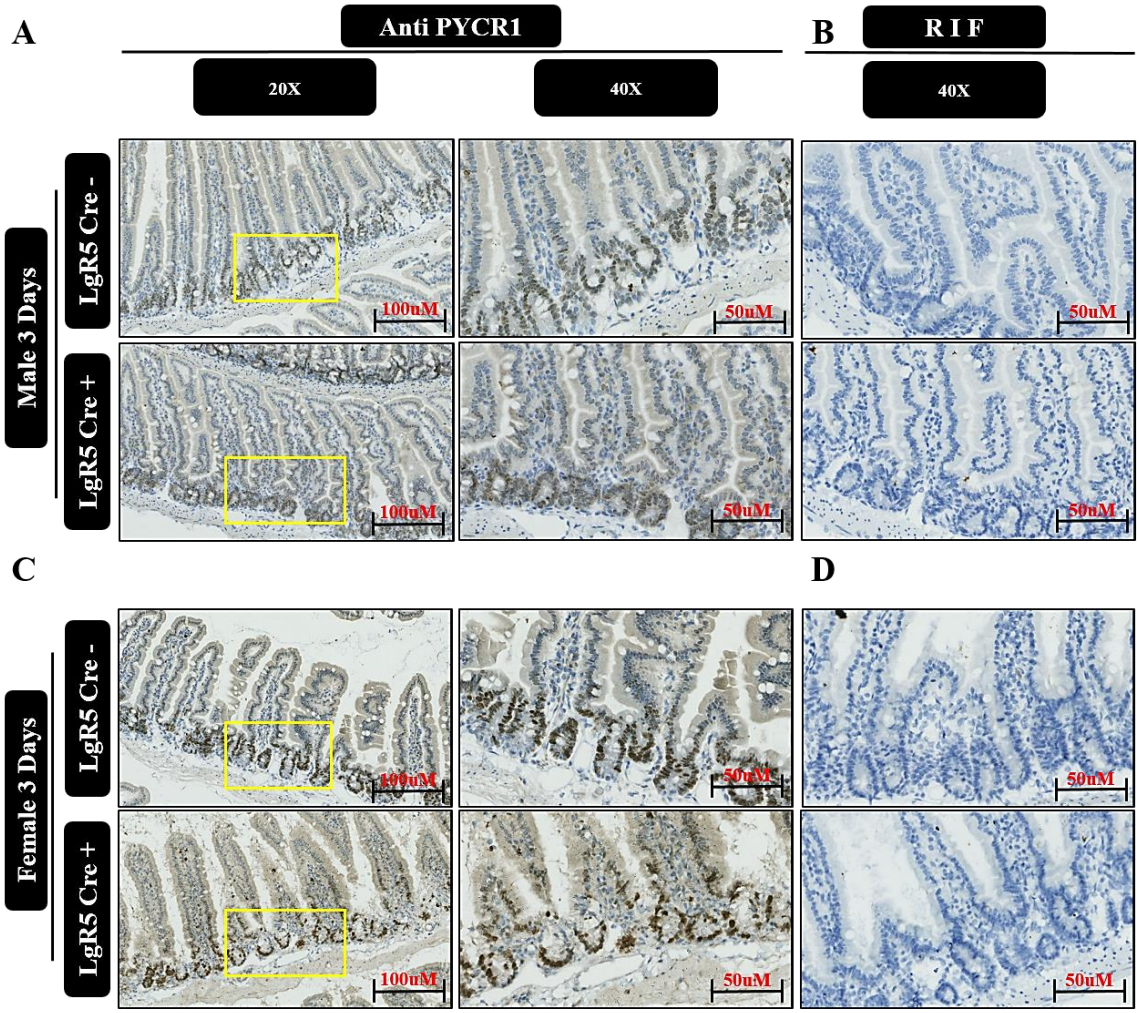

Figure 4.9. Representative Pycr1 IHC staining in the proximal small intestine tissues of the *Lgr5-Cre^{ER}/Apc$^{fl/fl}$* mice three days after tamoxifen injection. (**A**) Images of Pycr1 expression in male mice with Cre negative (Cre-, n=3, upper row) and positive (Cre+, n=3, lower row) genotypes. 20x and 40x magnifications are reported as indicated. (**B**) Examples of negative IHC controls for both Cre negative (upper row) and Cre positive (lower row) male mice. (**C**) Images of Pycr1 expression in female mice with Cre negative (Cre-, n=3, upper row) and positive (Cre+, n=3, lower row) genotypes. (**D**) Examples of negative IHC controls for both Cre negative (upper row) and Cre positive (lower row) female mice. Negative control staining was performed by replacing primary antibody with rabbit immunoglobulin fraction (RIF). The images were taken using the NanoZoomer-XR digital slide scanner. Scale bars are is100µm and 50µm.

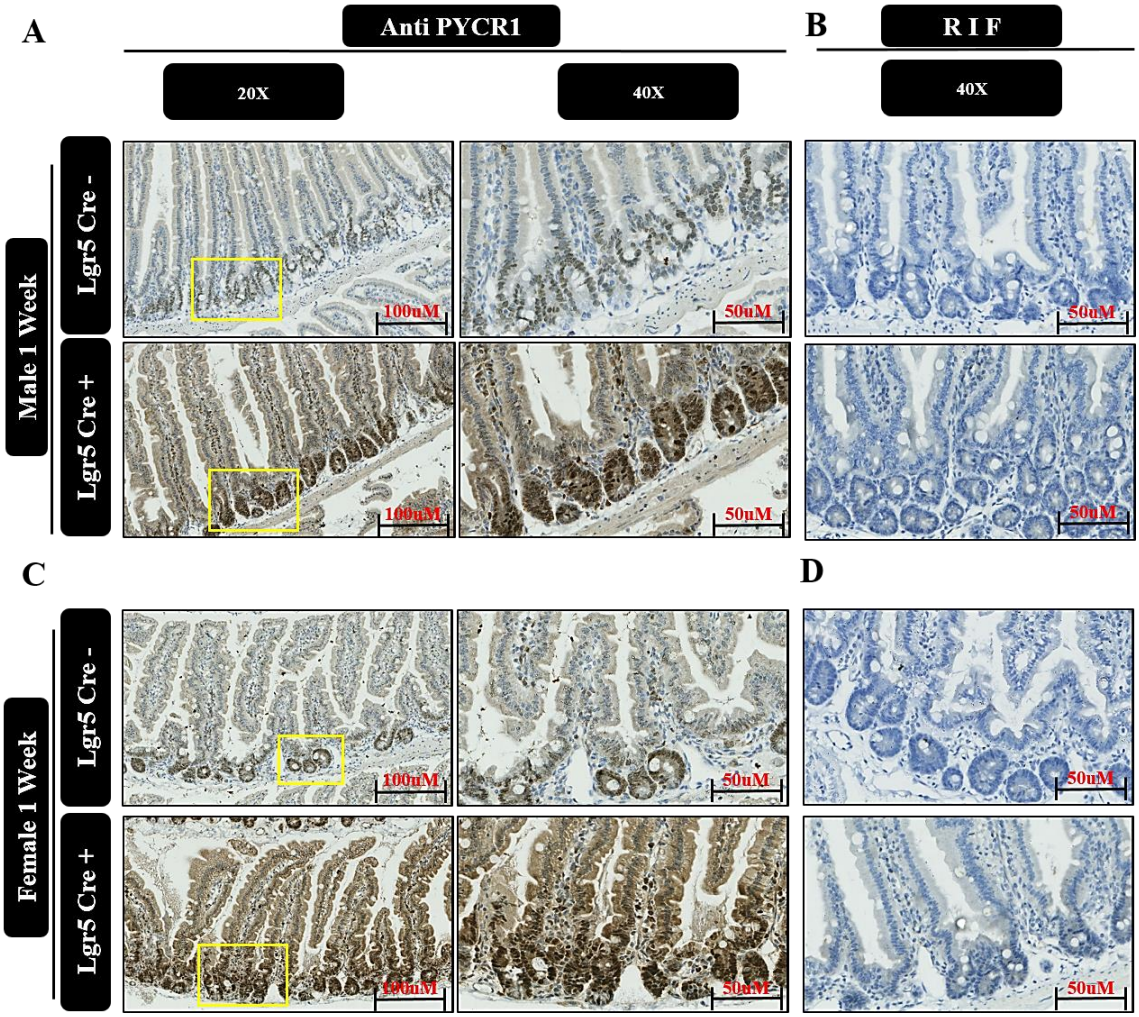

Figure 4.10. Representative Pycr1 IHC staining in the proximal small intestine tissues of the *Lgr5-Cre^{ER}/Apc$^{fl/fl}$* mice one week after tamoxifen injection. (**A**) Images of Pycr1 expression in male mice with Cre negative (Cre-, n=3, upper row) and positive (Cre+, n=3, lower row) genotypes. 20x and 40x magnifications are reported as indicated. (**B**) Examples of negative IHC controls for both Cre negative (upper row) and Cre positive (lower row) male mice. (**C**) Images of Pycr1 expression in female mice with Cre negative (Cre-, n=3, upper row) and positive (Cre+, n=3, lower row) genotypes. (**D**) Examples of negative IHC controls for both Cre negative (upper row) and Cre positive (lower row) female mice. Negative control staining was performed by replacing primary antibody with rabbit immunoglobulin fraction (RIF). The images were taken using the NanoZoomer-XR digital slide scanner. Scale bars are is100µm and 50µm.

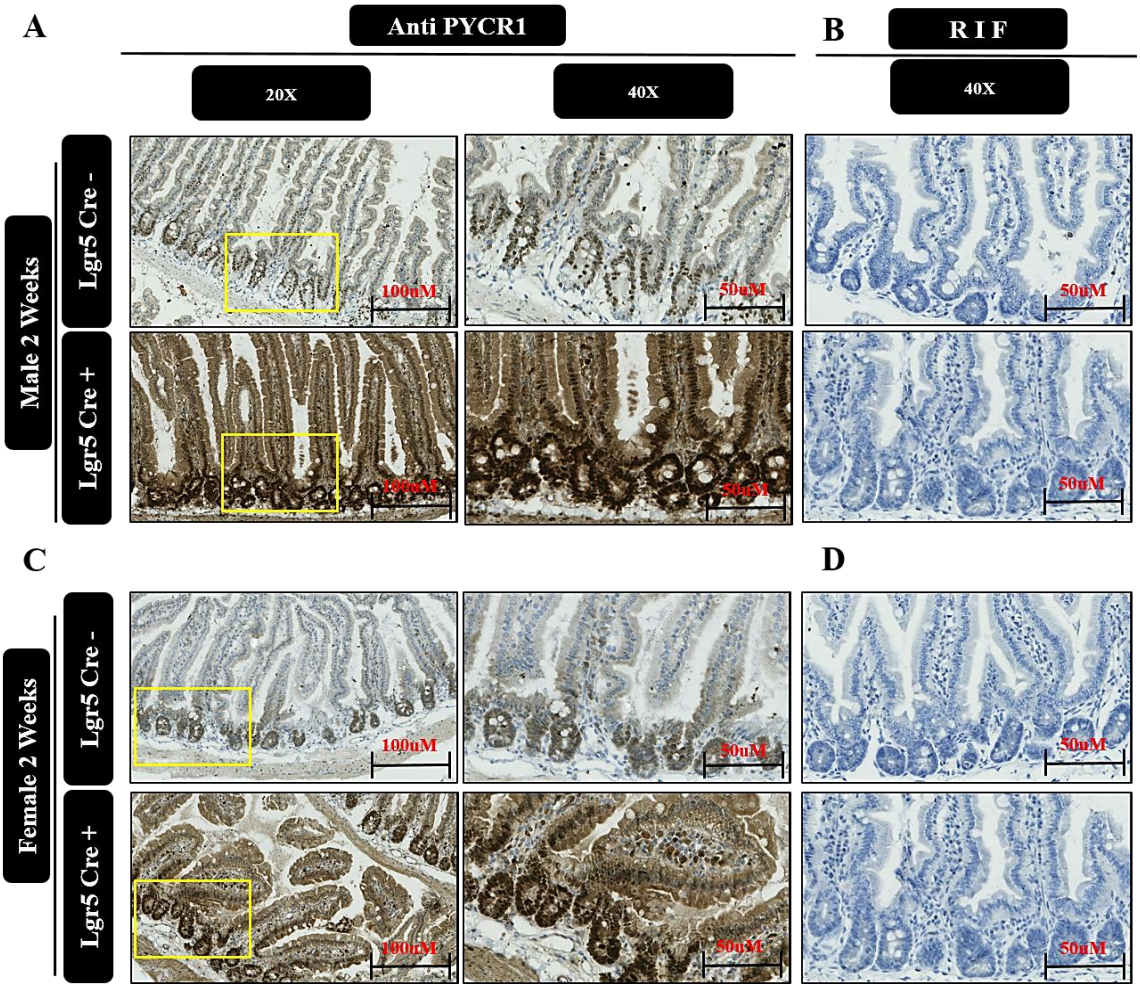

Figure 4.11. Representative Pycr1 IHC staining in the proximal small intestine tissues of the *Lgr5-Cre^{ER}/Apc$^{fl/fl}$* mice two weeks after tamoxifen injection. (**A**) Images of Pycr1 expression in male mice with Cre negative (Cre-, n=2, upper row) and positive (Cre+, n=3, lower row) genotypes. 20x and 40x magnifications are reported as indicated. (**B**) Examples of negative IHC controls for both Cre negative (upper row) and Cre positive (lower row) male mice. (**C**) Images of Pycr1 expression in female mice with Cre negative (Cre-, n=3, upper row) and positive (Cre+, n=3, lower row) genotypes. (**D**) Examples of negative IHC controls for both Cre negative (upper row) and Cre positive (lower row) female mice. Negative control staining was performed by replacing primary antibody with rabbit immunoglobulin fraction (RIF). The images were taken using the NanoZoomer-XR digital slide scanner. Scale bars are is100µm and 50µm.

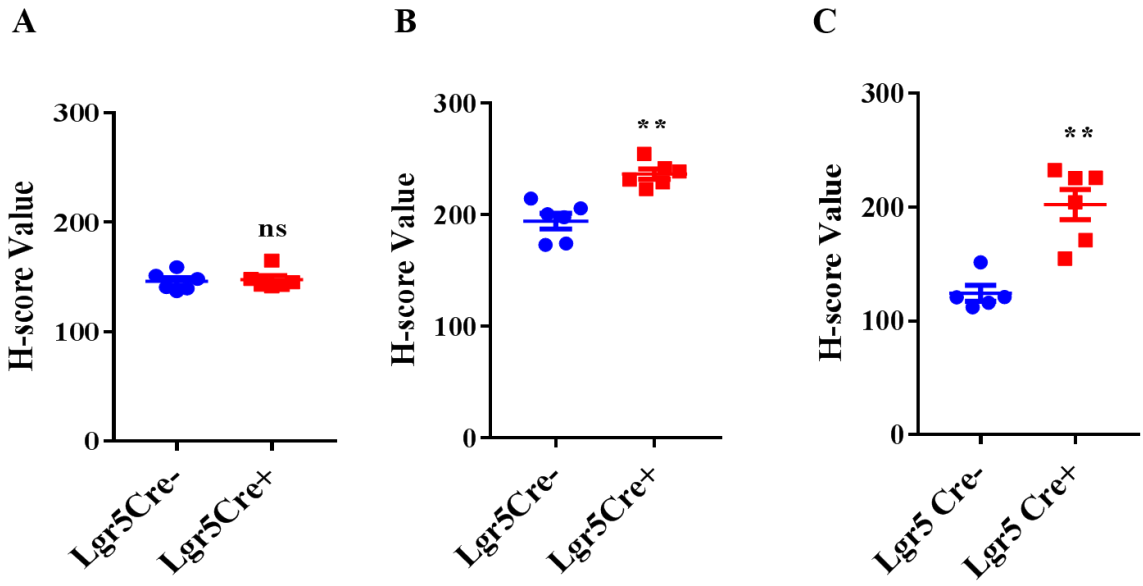

Figure 4.12. The H-score quantification of Pycr1 IHC intensity in the intestinal crypts in *Lgr5-Cre^{ER}/Apc$^{fl/fl}$* mice. The graphs report the H-score values for Pycr1 IHC three days (**A**), one week (**B**) and two weeks (**C**) after tamoxifen injection in Cre+ and control Cre- mice. The H-score was significantly increased in the intestinal crypts of *Apc*-deleted animals two weeks and one week after tamoxifen injection. Each dot represents one mouse, and horizontal bars represent mean ± S.E.M (n=50 crypts were scored for each animal and the average H-score is plotted). Two-tailed student's *t*-test was performed to calculate the p values. ** p <0.01, n=12 (6 control and 6 *Apc*-deleted mice) in (A) and (B); n=11 (5 control and 6 *Apc*-deleted mice) in (C).

4.3.2. Immunofluorescence labelling of intestinal crypts with Pycr1 antibody in representative mice intestinal tissues

Immunofluorescence (IF) and confocal scanning microscopy (CSM) have been used to confirm modulation of Pycr1 expression in intestinal tissue. The two-week specimens used for IHC were utilised for IF-mediated detection of Pycr1. The standard protocol followed to perform this technique is described in the methodology section, paragraph 2.2.11. FFPE tissues were stained with an anti-PYCR1 antibody and a fluorescently labelled with secondary antibody (Alexa Fluor 568).

Nuclei were counterstained with DAPI. To visualize the Pycr1 protein, we used an inverted confocal microscope (IX81, FV1000, Olympus, Japan). The labelling of the intestinal tissue was successful and a clear cytoplasmic staining evident (Figures 4.13 and 4.14). Moreover, increased expression of Pycr1 was confirmed by confocal analysis in the two-week induced mice.

Overall, we used two different labelling techniques to reveal Pycr1 expression in the mouse intestine. Our data indicate that this enzyme is expressed at higher levels in the intestinal crypts compare to villi.

Furthermore, genetic deletion of the *Apc* tumour suppressor gene resulted in increased expression of Pycr1, especially in the highly proliferating intestinal crypts. This suggests that Pycr1 may play an important role in the proliferation processes and sustain tumour progression.

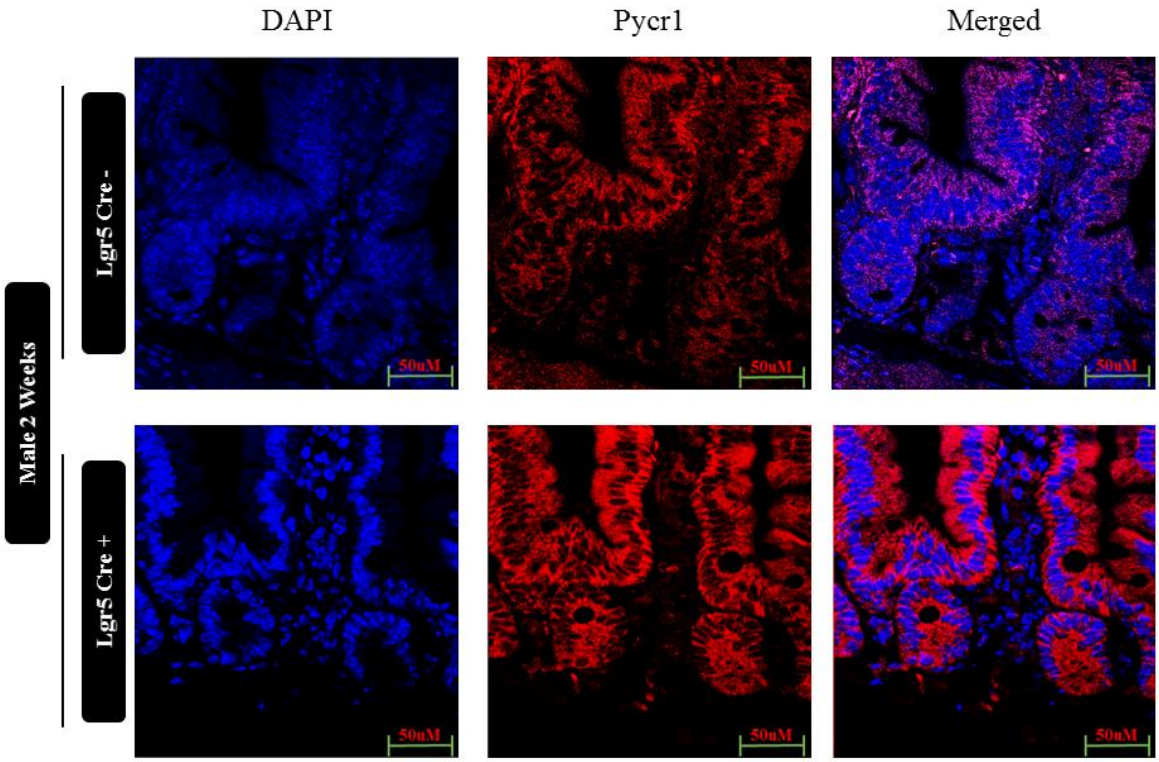

Figure 4.13. IF staining of Pycr1 in of *Lgr5-Cre^{ER}/Apc$^{fl/fl}$* male mice two weeks after tamoxifen injection. Images of Pycr1 fluorescence labelling (middle columns) in Cre negative (Cre-, upper row) and positive (Cre+, lower row) animals. DAPI (blue), on the left, was used to label nuclei. The merged images emphasize the cytoplasmic localization of the Pycr1 protein (right columns). Images were captured at 40x objective lens (scale bar 50µm) using inverted confocal microscope IX81, FV1000 (Olympus, Japan).

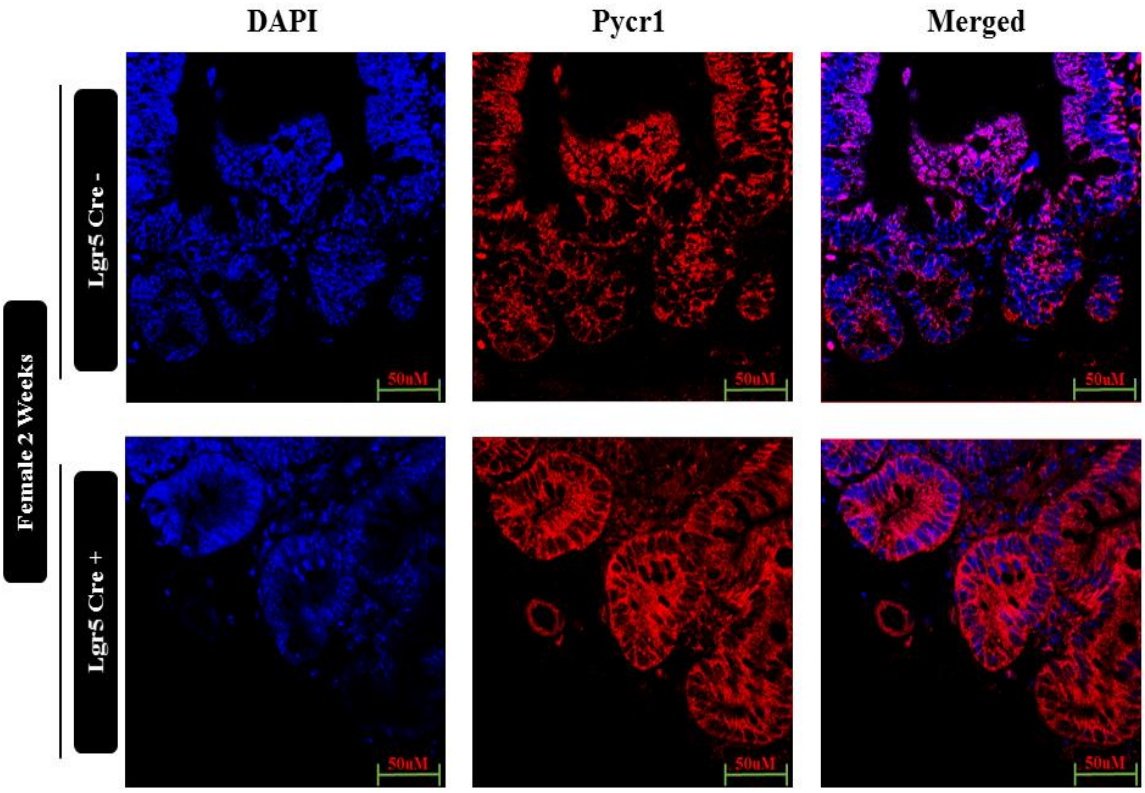

Figure 4.14. IF staining of Pycr1 in of *Lgr5-Cre^{ER}/Apc$^{fl/fl}$* female mice two weeks after tamoxifen injection. Images of Pycr1 fluorescence labelling (middle columns) in Cre negative (upper row) and positive (lower row) animals. DAPI (blue), on the left, was used to label nuclei. The merged images emphasize the cytoplasmic localization of the Pycr1 protein (right columns). Images were captured at 40x objective lens (scale bar 50µm) using inverted confocal microscope IX81, FV1000 (Olympus, Japan).

4.3.3. mRNA levels of proline metabolism enzymes in *Lgr5-Cre^{ER}/Apc$^{fl/fl}$* mice

As described above, the protein levels of Pycr1 is significantly upregulated following deletion of the *Apc* gene. Consequently, to explore whether the changes in protein level stemmed from alterations in the transcription of proline metabolism enzymes, RT-qPCR analysis was performed to investigate the mRNA expression levels of *Pycr1*, *Pycr2* and *Pycrl* genes, together with *Prodh*.

4.3.3.1. The NormFinder® method

A crucial step in RT-qPCR analysis is the identification and validation of the most appropriate reference genes with the aim to verify that treatment, in this case deletion of the *Apc* gene, did not interfere with the expression of reference genes for normalization. Thus, nine potential endogenous reference genes were tested using the Normfinder® algorithm (Andersen et al., 2004). These genes were *Actb*, *Gapdh*, *Ywhaz*, *B2m*, *Gusb*, *Tbp*, *Pop4*, *Hprt1* and *Efnb2*. Three reference genes, *Actb*, *Gapdh* and *Ywhaz*, were excluded because there was an amplification in the non-template control (NTC) samples. NTC samples represent negative controls run in parallel for each sample in which the reverse transcriptase enzyme, which converts mRNA to cDNA, is removed. Amplification events in NTC samples represent genomic DNA contamination.

The Normfinder software estimates the variability in mRNA expression of candidate reference genes between two or more categories to be compared (e.g. treated vs untreated, wild-type vs knockout). To achieve accurate steps of this algorithm, an add-in list of excel sheet program was firstly set-up to be linearized.

Initially the mean C_T values are transformed into relative quantities with the equation: **$RQ = 1/ (2^{C_T \text{ value} - \text{minimum } C_T \text{ value}})$**. The mean C_T value is calculated from all tested samples, independently of their category, and then the mean C_T value is selected to obtain the RQ. Normfinder uses RQ to generate a stability value for each candidate gene. The lower stability value represents the higher stability of the gene in mRNA levels.

Typically, we tested six intestinal specimens, three derived from Cre- control mice and three chosen from the Cre+, *Apc*-deleted mice. The following steps were performed:

First: The mean C_T values of triplicate runs were recorded in the table 4.1, where six candidate reference genes were measured in the six intestinal samples (Columns A to F).

Table 4.1. The first step of NormFinder®

Gene	A	B	C	D	E	F
B2m	**25.5387**	**26.2072**	**22.8085**	**22.1251**	**25.358**	**23.4093**
Gusb	**31.6498**	**33.6612**	**30.843**	**29.8595**	**32.3858**	**30.6074**
Tbp	**34.8603**	**36.0128**	**33.0608**	**31.8004**	**35.3278**	**33.3145**
Pop4	**32.4683**	**33.4627**	**30.6084**	**29.5376**	**32.6545**	**30.9794**
Hprt1	**28.9737**	**30.5097**	**27.9962**	**27.2842**	**28.8694**	**27.4583**
Efnb2	**29.3591**	**30.624**	**27.4679**	**27.9503**	**29.7096**	**28.4533**
	1	**1**	**1**	**2**	**2**	**2**

The two group categories, Cre- (wild type) and Cre+, (*Apc*-deleted) was specified for each sample in order for the NormFinder® software to identify the two categories when estimating variances. To this end, the different columns were allocated a corresponding number: 1 for Cre- and 2 for Cre+, as shown in the last row.

Second : Subsequently, for each reference gene, the minimum mean C_T value was selected and subtracted from the mean C_T values of all other samples for the same reference gene (for example, see Table 4.2 for the calculation relative to the candidate gene).

Table 4.2. The second step of NormFinder®

Pop4 mean C_T Value		Minimum C_T Value	C_T Value – minimum C_T Value
32.4683	**-**	**29.5376**	**2.9307**
33.4627	**-**	**29.5376**	**3.9251**
30.6084	**-**	**29.5376**	**1.0708**
29.5376	**-**	**29.5376**	**0.000**
32.6545	**-**	**29.5376**	**3.1169**
30.9794	**-**	**29.5376**	**1.4418**

Third: Third: The RQ equation **(**1/ ($2^{C_T \text{ Value} - \text{minimum } C_T \text{ Value}}$) **)** was then applied to calculate the values of RQ using the values obtained in the previous step. The RQ values for *Pop4* are shown in the Table 4.3.

Table 4.3. The third step of NormFinder®

RQ Values		
$1/(2^{2.930})$	=	0.131
$1/(2^{3.925})$	=	0.065
$1/(2^{1.070})$	=	0.476
$1/(2^{0.000})$	=	1.000
$1/(2^{3.116})$	=	0.115
$1/(2^{1.441})$	=	0.368

Fourth: The RQ values were then organized in table with the same layout of the initial table with the RT-qPCR C_T values resulting in Table 4.4.

Table 4.4. The fourth step of NormFinder®

Sample	A	B	C	D	E	F
B2m	**0.09385**	**0.05905**	**0.62272**	**1**	**0.10637**	**0.4106**
Gusb	**0.2891**	**0.07171**	**0.50575**	**1**	**0.17358**	**0.59545**
Tbp	**0.11991**	**0.05394**	**0.41741**	**1**	**0.08672**	**0.3501**
Pop4	**0.13115**	**0.06583**	**0.47603**	**1**	**0.11527**	**0.36809**
Hprt1	**0.31004**	**0.10691**	**0.61048**	**1**	**0.33329**	**0.88633**
Efnb2	**0.26958**	**0.11218**	**1**	**0.71579**	**0.21143**	**0.50507**
	1	**1**	**1**	**2**	**2**	**2**

Fifth: The RQ values were finally imputed into NormFinder® add-in software for analysis, using the Log transformation of the data (a screenshot of the software set up is presented in Figure 4.15). The outcome of the NormFinder® analysis is reported in Figure 4.16. The software releases stability value for each reference gene. The lower the stability value, the higher the stability of the gene mRNA levels.

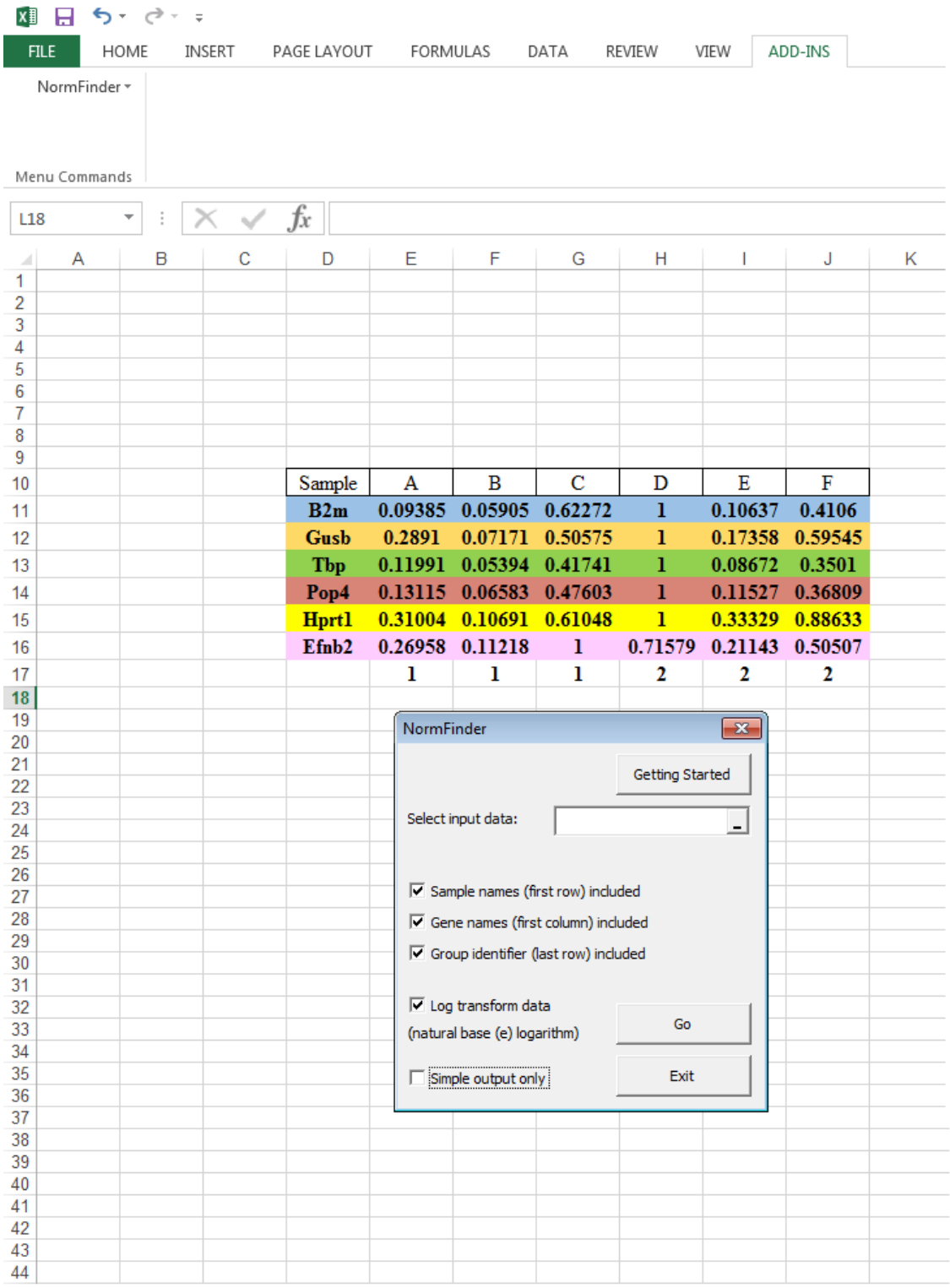

Sample	A	B	C	D	E	F
B2m	0.09385	0.05905	0.62272	1	0.10637	0.4106
Gusb	0.2891	0.07171	0.50575	1	0.17358	0.59545
Tbp	0.11991	0.05394	0.41741	1	0.08672	0.3501
Pop4	0.13115	0.06583	0.47603	1	0.11527	0.36809
Hprt1	0.31004	0.10691	0.61048	1	0.33329	0.88633
Efnb2	0.26958	0.11218	1	0.71579	0.21143	0.50507
	1	1	1	2	2	2

Figure 4.15.The fifth step of NormFinder®

The results of NormFinder® showed that *Pop4* and *Efnb2* were the best genes with stability values of 0.064 and 0.108, respectively (Figure 4.16). Moreover, *Pop4* and *Efnb2*

achieved the best combination stability value (0.063) when combined. Therefore, the geometric mean of C_T values for *Pop4* and *Efnb2* has been used to normalize the RT-qPCR data in the intestinal tissues.

Gene name	Stability value
B2m	0.186
Gusb	0.146
Tbp	0.112
Pop4	**0.064**
Hprt	0.204
Efnb2	**0.108**

Best gene	Pop4
Stability value	0.064
Best combination of two genes	Pop4 and Efnb2
Stability value for best combination of two genes	0.063

Intragroup variation	Wild Type	Apc deleted
Group identifier	1.000	2.000
B2m	0.185	0.046
Gusb	0.143	0.016
Tbp	0.001	0.129
Pop4	**0.001**	**0.038**
Hprt	0.074	0.189
Efnb2	**0.001**	**0.114**

Intergroup variation	Wild Type	Apc deleted
Group identifier	1.000	2.000
B2m	-0.057	0.057
Gusb	-0.015	0.015
Tbp	-0.037	0.037
Pop4	-0.023	0.023
Hprt	-0.080	0.080
Efnb2	**0.212**	**-0.212**

Figure 4.16. The statistical analysis values that generated by NormFinder® process.

4.3.3.2. The transcriptional levels of proline biosynthesis enzymes in *Lgr5-Cre^{ER}/Apc$^{fl/fl}$* mice after tamoxifen injection

The proximal intestinal samples, collected from mice three days, one week and two weeks after tamoxifen injection, were used for RNA extraction. The RNA extraction, quantification, reverse transcription and RT-qPCR protocols were described in section 2.2.8. For the *Pycr1* gene, the results of the RT-qPCR showed significant upregulation of the mRNA in Apc-deleted intestines compared to wild type after two weeks of tamoxifen injection, while there was no significance changes at one week and three days after injection (Figure 4.17).

With regard to the other genes, *Pycr2*, *Pycrl* and *Prodh/Pox*, we did not observe any significant difference in the mRNA levels between the different experimental groups (Figures 4.18, 4.19 and 4.20), suggesting that *Apc* deletion affects selectively expression of the *Pycr1* gene, at least in the very early phase of tissue neoplasia. The C_T, ΔC_T, $\Delta\Delta$ CT, Geometric mean (G mean) and fold changes values are reported in appendix from Table 8.3 to Table 8.32.

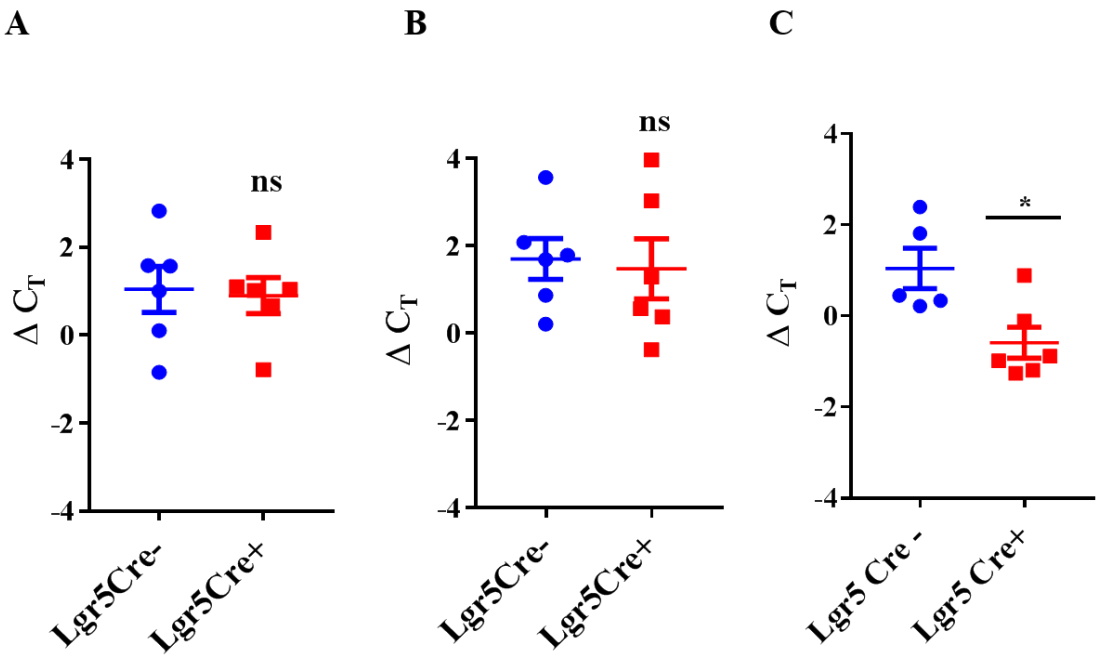

Figure 4.17. *Pycr1* mRNA levels in *Lgr5-Cre^{ER}/Apc$^{fl/fl}$* mice. The scatter blots represent the ΔC_T values for *Pycr1* mRNA levels in *Apc*-deleted mice (Lgr5 Cre+, red) and wild type mice (Lgr5 Cre-, blue) at different time points after tamoxifen injection: (**A**) three days, (**B**) one week and (**C**) two weeks. Each dot represents one mouse, and horizontal bars represent mean ± S.E.M. Normalization was obtained with the geometric mean value obtained from two endogenous housekeeping genes, *Pop4* and *Efnb2*. The lower ΔC_T represents high expression. Two-tailed student's *t*-test was performed to calculate the p values. * $p<0.05$, ns indicates no significant differences, n=12 (6 control and 6 *Apc*-deleted mice) in (**A**) and (**B**); n=11 (5 control and 6 *Apc*-deleted mice) in (**C**). Of note, ΔC_T = C_T mean of gene of interest - C_T mean of endogenous control. The lower ΔCT value indicates higher expression of the gene.

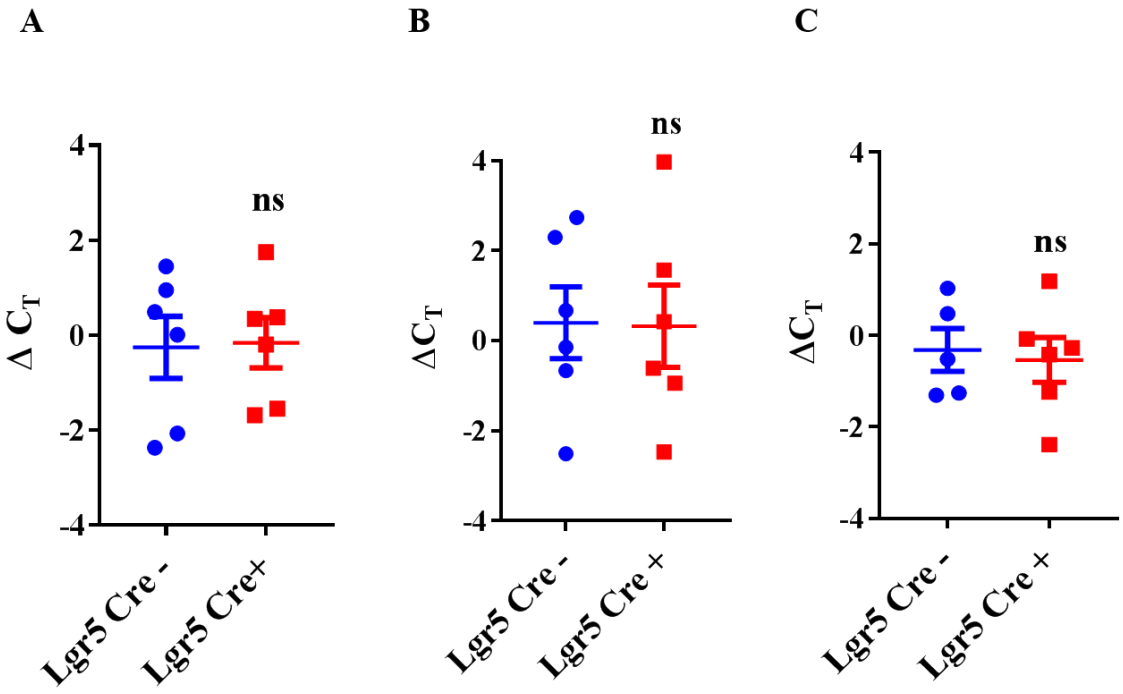

Figure 4.18. ***Pycr2*** **mRNA levels in** ***Lgr5-Cre^{ER}/Apc$^{fl/fl}$*** **mice**. The scatter blots represent the ΔC_T values for *Pycr2* mRNA levels in *Apc*-deleted mice (Lgr5 Cre+, red) and wild type mice (Lgr5 Cre-, blue) at different time points after tamoxifen injection: (**A**) three days, (**B**) one week and (**C**) two weeks. Each dot represents one mouse, and horizontal bars represent mean ± S.E.M. Normalization was obtained with the geometric mean value obtained from two endogenous housekeeping genes, *Pop4* and *Efnb2*. Two-tailed student's *t*-test was performed to calculate the p values, ns indicates no significant differences, n=12 (6 control and 6 *Apc*-deleted mice) in (**A**) and (**B**); n=11 (5 control and 6 *Apc*-deleted mice) in (**C**). Of note, ΔC_T = C_T mean of gene of interest - C_T mean of endogenous control. The lower ΔC_T value indicates higher expression of the gene.

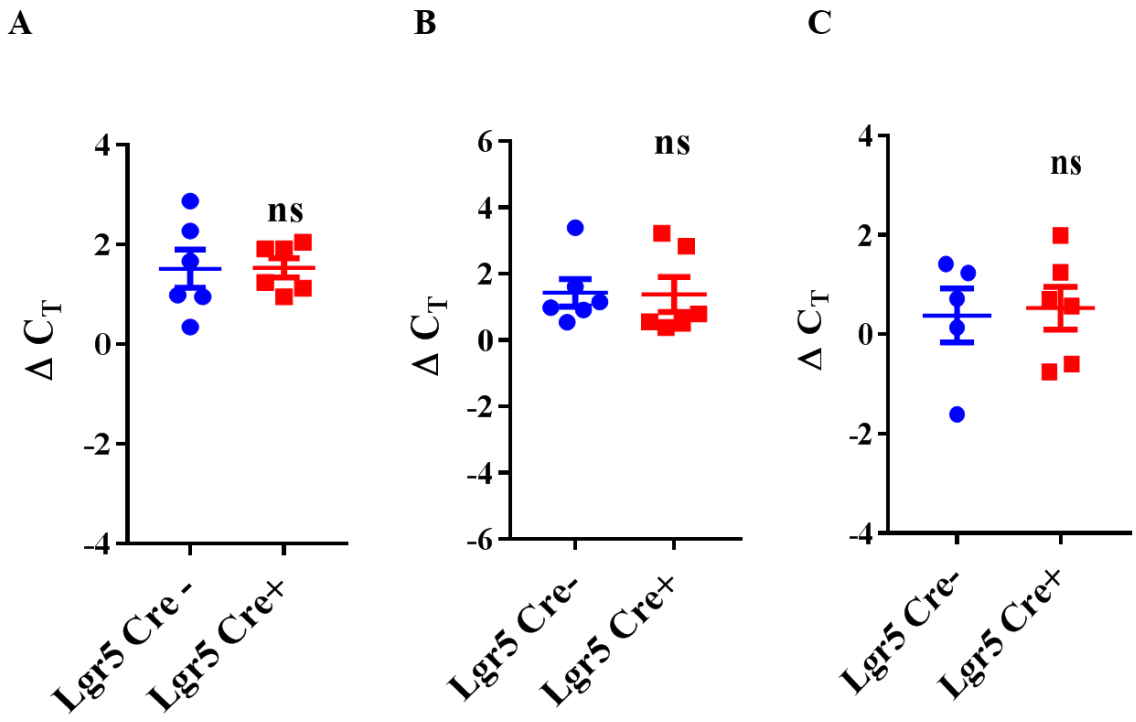

Figure 4.19. ***Pycrl*** **mRNA levels in** ***Lgr5-Cre^{ER}/Apc$^{fl/fl}$*** **mice**. The scatter blots represent the ΔC_T values for *Pycrl* mRNA levels in *Apc*-deleted mice (Lgr5 Cre+, red) and wild type mice (Lgr5 Cre-, blue) at different time points after tamoxifen injection: (**A**) three days, (**B**) one week and (**C**) two weeks. Each dot represents one mouse, and horizontal bars represent mean ± S.E.M. Normalization was obtained with the geometric mean value obtained from two endogenous housekeeping genes, *Pop4* and *Efnb2*. Two-tailed student's *t*-test was performed to calculate the p values, ns indicates no significant differences, n=12 (6 control and 6 *Apc*-deleted mice) in (**A**) and (**B**); n=11 (5 control and 6 *Apc*-deleted mice) in (**C**). Of note, ΔC_T = C_T mean of gene of interest - C_T mean of endogenous control. The lower ΔC_T value indicates higher expression of the gene.

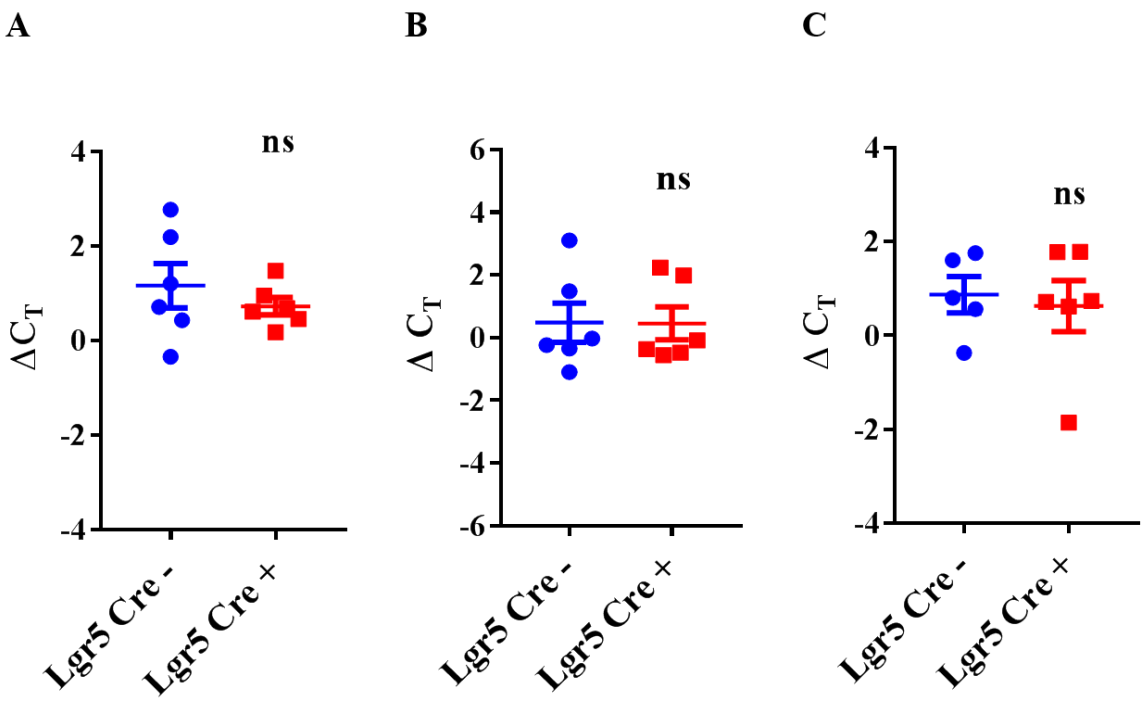

Figure 4.20. *Prodh/Pox* mRNA levels in *Lgr5-Cre^{ER}/Apc$^{fl/fl}$* mice. The scatter blots represent the ΔC_T values for *Prodh/Pox* mRNA levels in *Apc*-deleted mice (Lgr5 Cre+, red) and wild type mice (Lgr5 Cre-, blue) at different time points after tamoxifen injection: (**A**) three days, (**B**) one week and (**C**) two weeks. Each dot represents one mouse, and horizontal bars represent mean ± S.E.M. Normalization was obtained with the geometric mean value obtained from two endogenous housekeeping genes, *Pop4* and *Efnb2*. Two-tailed student's *t*-test was performed to calculate the P values, ns indicates no significant differences, n=12 (6 control and 6 *Apc*-deleted mice) in (**A**) and (**B**); n=11 (5 control and 6 *Apc*-deleted mice) in (**C**). Of note, $\Delta C_T = C_T$ mean of gene of interest - C_T mean of endogenous control. The lower ΔC_T value indicates higher expression of the gene.

4.3.3.3. Expression levels of Pycr1 protein in *Lgr5-Cre^{ER}/Apc$^{fl/fl}$* mice

To investigate Pycr1 protein expression in the experimental mice, intestinal tissue samples were processed for western blot analysis. All the relevant protocols were described in sections 2.2.7 and 2.2.12.3 of methodology chapter.

Unexpectedly, western blot failed to confirm Pycr1 upregulation as detected by IHC and RT-qPCR. Pycr1 protein was indeed promptly detected in all tissue samples and at all time points (Figure 4.21A, C and E). However no differences were discernible between groups when western blots were quantified with image J software (Figure 4.21B, D and F), despite a marginal, and of questionable biologically relevance, increase at the two week time point. The reasons for this discrepancy are unclear. As will be discussed in more detail later, the fact that proteins were isolated from the whole tissue without selecting for the intestinal epithelium or the intestinal crypts might have reduced the ability of western blot to detect differences in Pycr1 expression.

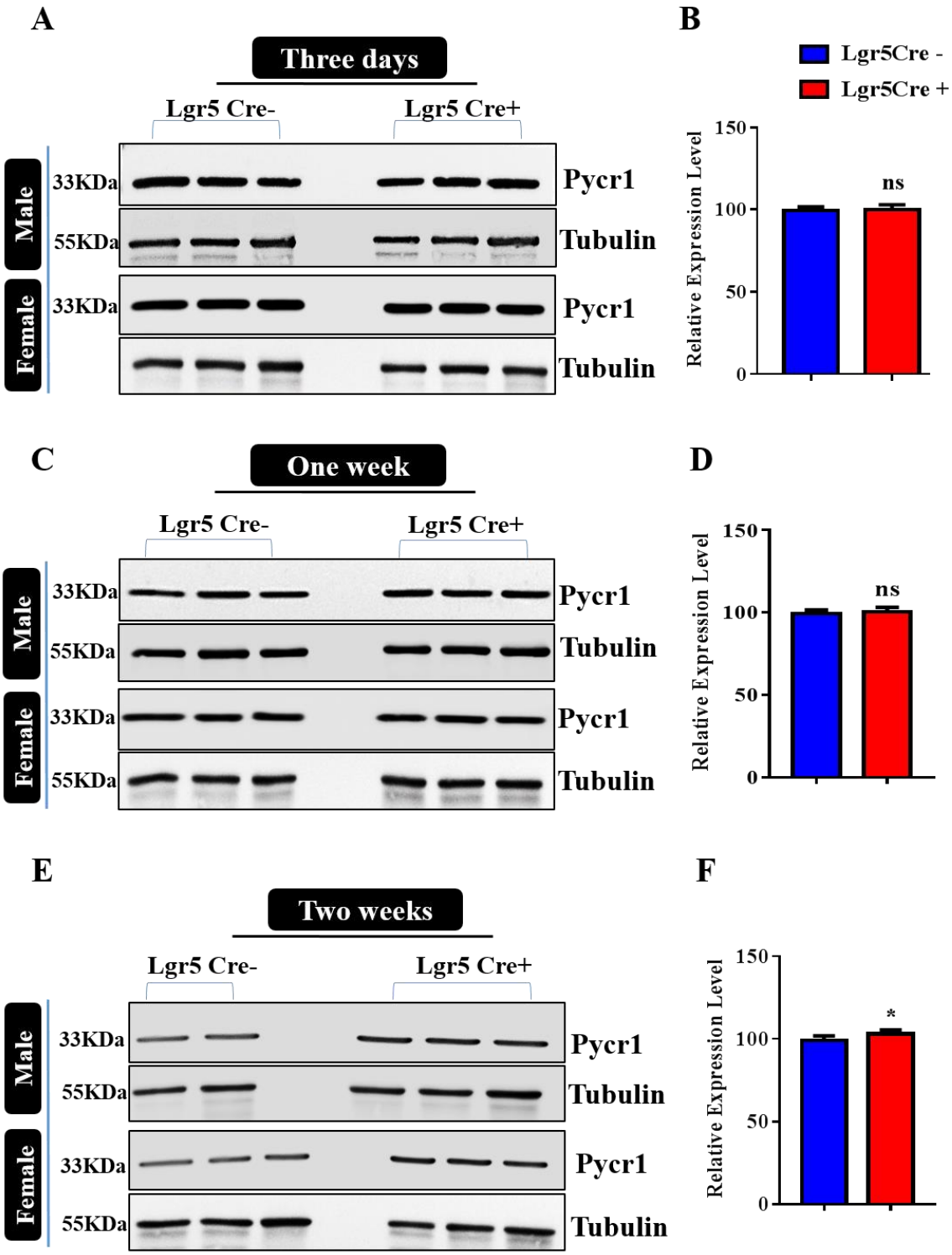

Figure 4.21. Pycr1 protein expression levels in *Lgr5-Cre^{ER}/Apc$^{fl/fl}$* mice after tamoxifen injection. Pycr1protein expression was detected by western blot in Lgr5 Cre- and Lgr5Cre + male and female mice three days (**A, B**) (n=12, 6 males and 6 females), one week (**C**, **D**) (n=12, 6 males and 6 females) and two weeks (**E**, **F**) (n=11, 5 males and 6 females) after tamoxifen injection. Data represents mean ± S.E.M. Tubulin was used as a loading control. p values were calculated using two-tailed student's *t*-test. * $p<0.05$.

Chapter Five: Investigation of the functional role of PYCR1 on growth and proliferation of CRC cell lines

5. Introduction

The results of the two previous chapters provided evidence that the *PYCR1* gene expression is upregulated in human CRC, and in experimental mice following deletion of the *Apc* gene. These results could intimate an important role for this enzyme in the colorectal tumorigenesis process.

Therefore, this chapter was designed to explore the role of PYCR1 enzyme in supporting growth and proliferation of human CRC cell lines. Three cell lines were selected in this study, HCT116, RKO and SW620 and their origin and genetic features were reported in Table 2.3. To address the role of PYCR1 in cell proliferation and survival, small-interference RNA (siRNA) technology was used to knockdown PYCR1 expression.

Overall, the following experiments were performed:

1. siRNA efficacy of knockdown was ascertain by western blotting and RT-qPCR.
2. The functional effect of PYCR1 depletion was assessed by counting cell numbers at 48h and 72h post siRNA transfection.
3. The role of PYCR1 on proliferation was measured using click measured utilizing the Click-iT® EdU Flow Cytometry assay and the expression of the cell cycle markers cyclin D1, cyclin D3 and p21.
4. In addition, effect on cell survival was evaluated by measuring apoptosis using Annexin/PI flow cytometry assay.
5. In the attempt to assess whether the biological effects of loss of PYCR1 expression were caused by compromised proline biosynthesis, different concentrations of exogenous proline were added in the cultured media to investigate whether exogenous proline could rescue PYCR1 deficiency.

5.1. Time course analysis of PYCR1 knockdown

SW620 cells, pleated in 6cm dishes, were transfected with 100 picomoles of Dharmacon^{TM} PYCR1 siRNA pool (siPYCR1) or with non-targeting siRNA scramble pool (siCTRL) as described in section 2.2.7. An additional untransfected control was included. Cells were harvested after 6, 12, 24, 48 and 72 hrs and processed for western blotting. The results showed that, despite a marginal reduction in PYCR1 protein were observed 24 hrs after transfection, 48 and 72 hrs post-transfection were the best time points to achieve robust PYCR1 knockdown, with the highest depletion of PYCR1 protein observed at 72h (Figure 5.1). Additionally, the selectivity of PYCR1 siRNA pool was examined to investigate whether its knockdown is selective for PYCR1 isozyme. The result of western blot analysis showed that PYCR1 knockdown had similar effect on PYCR2 isozyme (Figure 5.1).

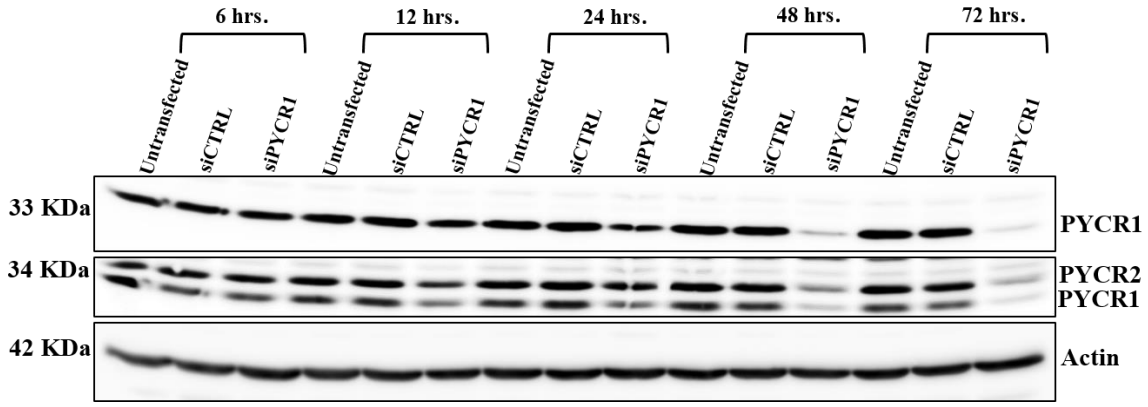

Figure 5.1. Time course of PYCR1 knockdown using siRNA. SW620 cells were transfected with 100 picomoles of PYCR1 targeting siRNA pool (siPYCR1) and non-targeting siRNA pool (siCTRL) from Dharmacon**™**, while another group of cultured cells was left untreated (untransfected). The western blot (WB) panels show the expression levels of PYCR1 protein at the indicated time points following transfection. The PYCR1 siRNA pool results in a clear reduction in the protein levels of both PYCR1 (upper blot) and PYCR2 isozyme (middle blot). Actin was used as loading control.

5.2. mRNA levels of *PYCR* isozymes following siRNA transfection

SW620 cell were transfected with PYCR1 siRNA pool or non-targeting siRNA pool. After 48 and 72 hrs, the cells were harvested and RNA was extracted according to standard protocol (see section 2.2.8) and processed for RT-qPCR-mediated evaluation of *PYCR1*, *PYCR2* and *PYCRL* mRNA expression levels using Taqman assays from Thermo Scientific (see section 2.2.8.4 and Table 2.7).

Knockdown of PYCR1 using DharmaconTM siRNA caused more the 80% reduction in the mRNA level of PYCR1 enzyme after 48 hrs and 72 hrs from siRNA transfection (Table 5.1 and Figure 5.2). Due to the high sequence similarity between the reductase isozymes, we decided to determine whether the commercial PYCR1 siRNA might also affects the expression levels of *PYCR2* and *PYCRL* mRNA. For the PYCR2 isozyme, we detected a 50% reduction in *PYCR2* mRNA levels after transfection with the PYCR1-targeting siRNA. This indicates that knockdown of PYCR1 isozyme results in partial depletion of PYCR2 isozyme (Table 5.1 and Figure 5.2), confirming western blot results in Figure 5.1. In addition to PYCR2 isozyme, the mRNA expression level of *PYCRL* was examined and the results showed no changes at 48 and 72 hrs of PYCR1 knockdown. This indicates that PYCR1 siRNA has no effect on the expression of *PYCRL* gene (Table 5.1 and Figure 5.2). The expression fold change for PYCR isozymes was calculated after PYCR1 knockdown according to standard protocol (see section 2.2.8.5).

		48 hours				72 hours			
		ΔC_T Mean siPYCR1	ΔC_T Mean siCTRL	$\Delta\Delta C_T$	Expression fold-change	ΔC_T Mean siPYCR1	ΔC_T Mean siCTRL	$\Delta\Delta C_T$	Expression fold-change
1	PYCR1	3.23	1.17	2.06	0.23	4.12	1.95	2.17	0.22
2	PYCR2	5.18	4.08	1.1	0.46	5.59	4.24	1.35	0.39
3	PYCRL	5.22	5.41	- 0.19	1.14	5.62	5.83	- 0.21	1.15

Table 5.1. The delta CTs (ΔC_T), delta-delta CTs ($\Delta\Delta C_T$) and fold change values for scramble siRNA (siCTRL) versus PYCRs isozymes after siRNA PYCR1 knockdown in SW620 CRC cell line. Of note, $\Delta\Delta C_T = \Delta C_T$ mean of siPYCR1-ΔC_T mean of siCTRL, fold change = $2^{(-\Delta\Delta CT)}$.

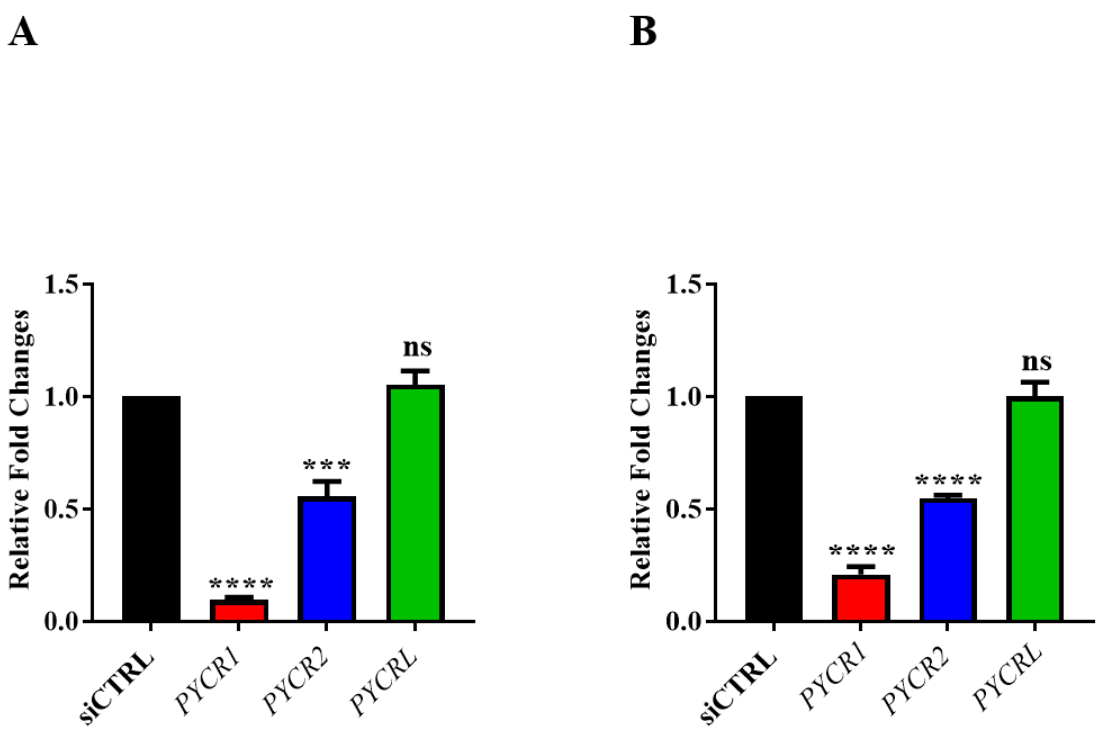

Figure 5.2. Selectivity of PYCR1-targted siRNA knockdown. SW620 cells were cultured in 6 cm2 dishes, and transfected with scramble siRNA (siCTRL) or with PYCR1 targeting siRNA (siPYCR1). Expression of PYCR1, PYCR2 and PYCR3 was then assessed 48hrs (**A**) and 72hrs (**B**) after transfection using TaqMan RT-qPCR assays The graphs show the PYCR isozymes mRNA expression levels expressed as % of siCTRL. The results indicated significant reduction in the mRNA levels of both *PYCR1* and *PYCR2* isozymes following treatment with siRNA for PYCR1, while *PYCRL* mRNA level did not show any significant alteration. Tukey's multiple comparisons One-way Anova was performed to investigate statistical significance. The values are mean ± S.E.M. of three independent experiments (n=3). *** $p < 0.001$, **** $p < 0.0001$. ns indicates no significant change.

5.3. PYCR1 knockdown affects growth of CRC cells

Since, HCT116, RKO and SW620 showed the highest expression of PYCR1 (Figure 3.11), these cell lines were selected to address the functional role of PYCR1 in cell proliferation and survival. Initially, proliferating RKO and HCT116 cell were transfected with Dharmacon siRNA and cell number was assessed 48hrs, and 72hrs post transfection. Moreover, to strengthen the validity of our findings, we used a second commercial siRNA against PYCR1 from Ambion (see section 2.2.3.2 and table 2.5 in methods section).

Interestingly, knockdown of PYCR1 enzyme (siPYCR1) caused reduction in RKO and HCT116 cell number compared with untransfected or scramble siRNA- transfected controls (siCTRL). With regard to HCT116, PYCR1 knockdown significantly reduced cell number by about 50% after 48 hrs (Figures 5.3) and 72 hrs (Figures 5.4) from transfection, with both siRNAs. In RKO cells, PYCR1 knockdown had a clear effect on cell proliferation and after 48 and 72 hrs of enzyme depletion, the reduction in cell growth was around 30% compared to controls (Figures 5.5 and 5.6 respectively), and reached 40% at 96 hrs (Figure 5.7).

Next, PYCR1 siRNA mediated knockdown was carried out on the SW620 CRC cell line to gather additional confirmation of PYCR1 role in cell growth. Moreover, we decided to test the effect of PYCR1 depletion using two different glucose availability (4500 mg/L and 1000 mg/L). Of note, the 1000 mg/L low glucose concentration mirrors the physiological serum levels of circulating glucose. The results, reported in Figure 5.8, showed 26% reduction in cell growth when PYCR1 was knockdown in high glucose condition, which raised to 40 % when using low glucose media. Therefore, the effect of PYCR1 knockdown is exacerbated when cells are grown in physiological glucose.

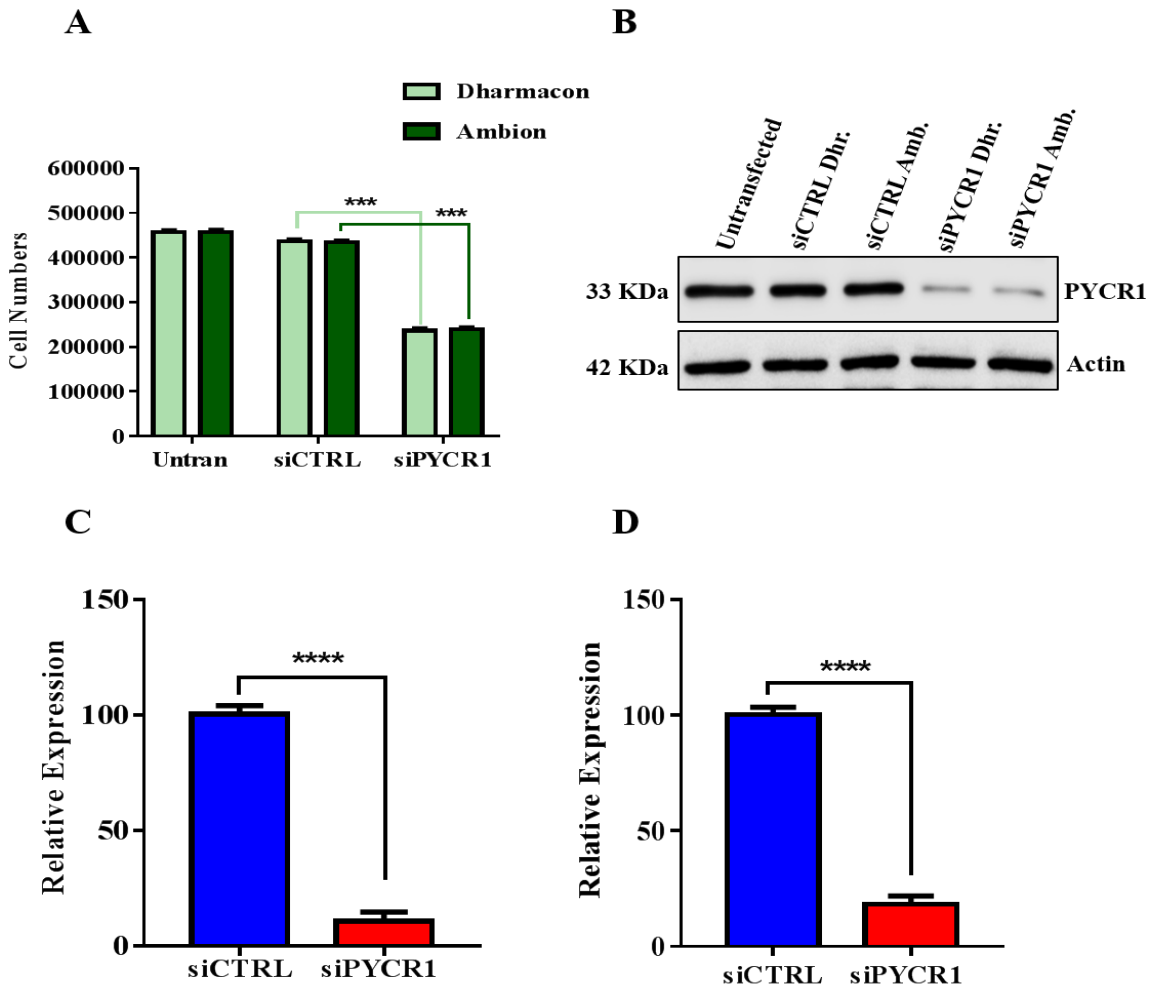

Figure 5.3. Reduced cell growth of HCT116 cells 48 hrs post PYCR1 knockdown. (**A**) The bar graph shows number of cells after 48 hrs transfection with two diverse siRNA targeting PYCR1 (siPYCR1) and scramble siRNA (siCTRL). Untransfected (Untran) indicates control untreated cells. Cells were counted using the Beckman Z2 Coulter Particle Count and Size Analyzer. (**B**) The representative western blot shows the successful PYCR1 protein knockdown in HCT116 cell line with both Dharmacon$^{T.M}$ (Dhr) and Ambion® (Amb) siRNA pools. Actin was used as loading control. (**C** and **D**) The bar graphs show quantification of PYCR1 protein expression from three independent experiments with Dharmacon and Ambion siRNA reagents, respectively. Western blots were quantified using ImageJ software and normalized using actin as endogenous loading control. The bars represent the mean ± S.E.M., n=3 independent experiments. Sidak's multiple comparisons Two-ways Anova test and Two-tailed student's *t*-test were used to calculate p values. *** $p < 0.001$, **** $p < 0.0001$.

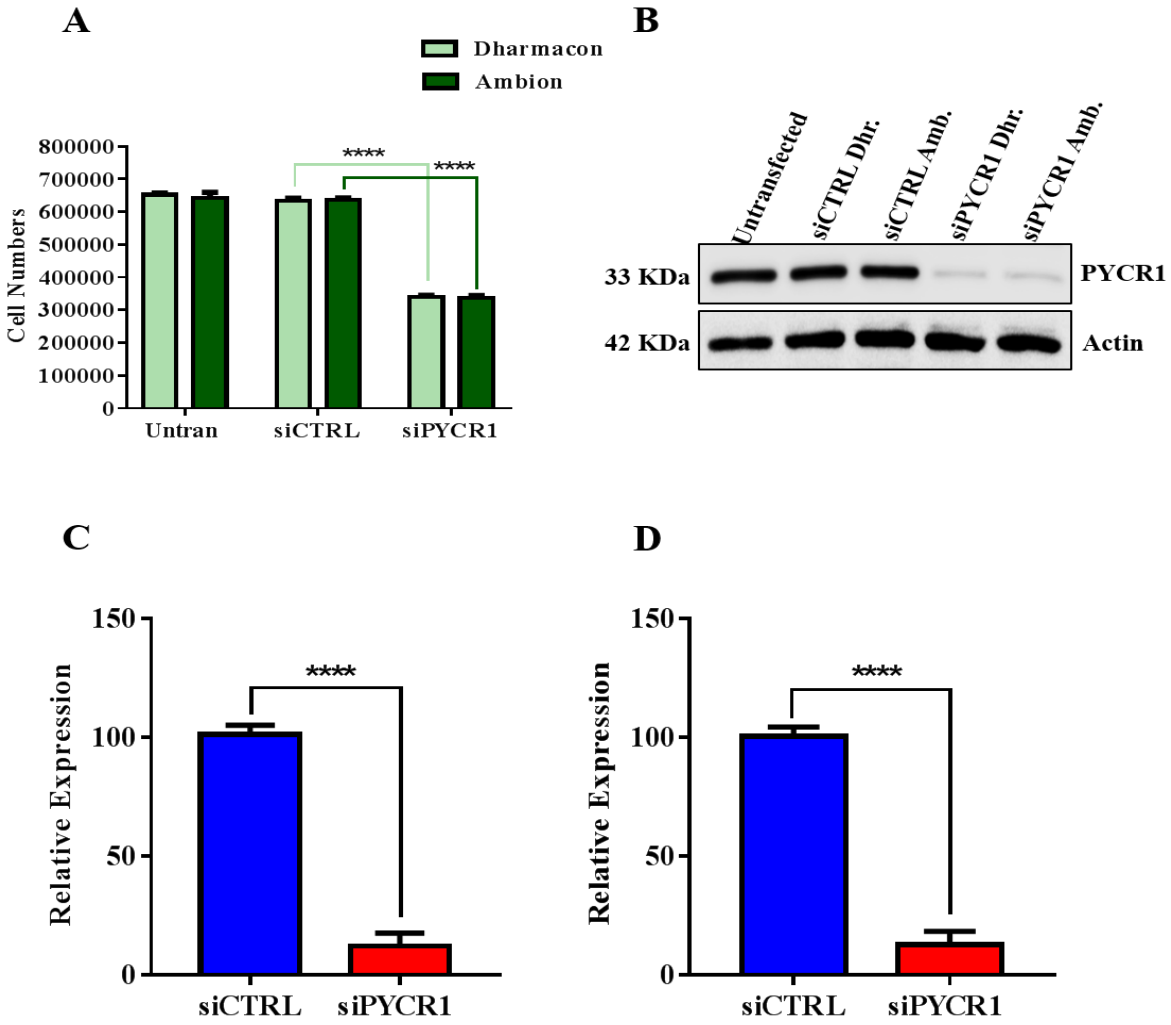

Figure 5.4. Reduced cell growth of HCT116 cells 72 hrs post PYCR1 knockdown. (**A**) The bar graph shows number of cells after 72 hrs transfection with two diverse siRNA targeting PYCR1 (siPYCR1) and scramble siRNA (siCTRL). Untransfected (Untran) indicates control untreated cells. Cells were counted using the Beckman Z2 Coulter Particle Count and Size Analyzer. (**B**) The representative western blot shows the successful PYCR1 protein knockdown in HCT116 cell line with both Dharmacon$^{T.M}$ (Dhr) and Ambion® (Amb) siRNA pools. Actin was used as loading control. (**C** and **D**) The bar graphs show quantification of PYCR1 protein expression from three independent experiments with Dharmacon and Ambion siRNA reagents, respectively. Western blots were quantified using ImageJ software and normalized using actin as endogenous loading control. The bars represent the mean ± S.E.M., n=3 independent experiments. Sidak's multiple comparisons Two-ways Anova test and Two-tailed student's *t*-test were used to calculate p values. **** $p < 0.0001$.

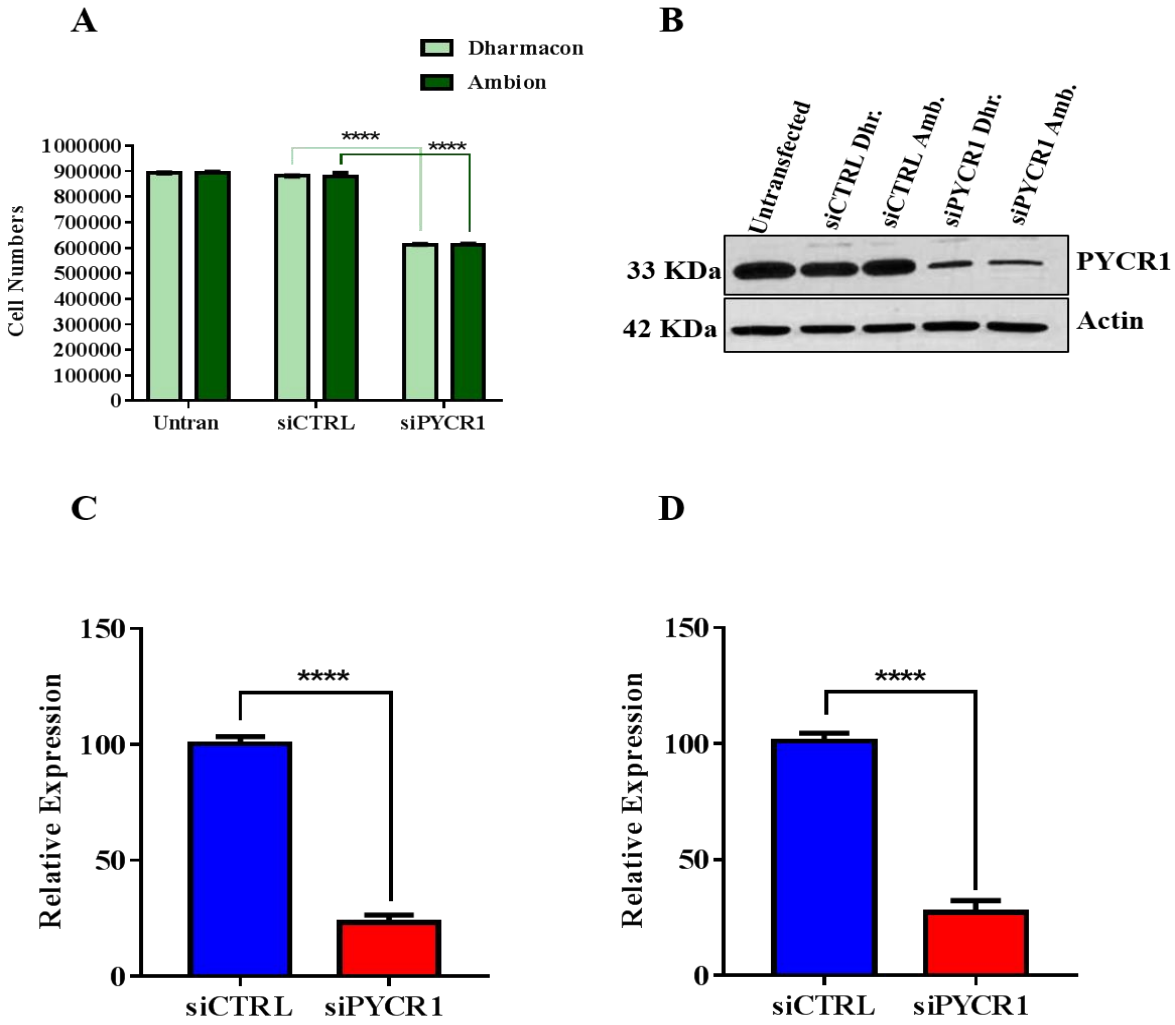

Figure 5.5. Reduced cell growth of RKO cells 48 hrs post PYCR1 knockdown. (**A**) The bar graph shows number of cells after 48 hrs transfection with two diverse siRNA targeting PYCR1 (siPYCR1) and scramble siRNA (siCTRL). Untransfected (Untran) indicates control untreated cells. Cells were counted using the Beckman Z2 Coulter Particle Count and Size Analyzer. (**B**) The representative western blot shows the successful PYCR1 protein knockdown in HCT116 cell line with both Dharmacon$^{T.M}$ (Dhr) and Ambion® (Amb) siRNA pools. Actin was used as loading control. (**C** and **D**) The bar graphs show quantification of PYCR1 protein expression from three independent experiments with Dharmacon and Ambion siRNA reagents, respectively. Western blots were quantified using ImageJ software and normalized using actin as endogenous loading control. The bars represent the mean ± S.E.M., n=3 independent experiments. Sidak's multiple comparisons Two-ways Anova test and Two-tailed student's *t*-test were used to calculate p values. **** $p < 0.0001$.

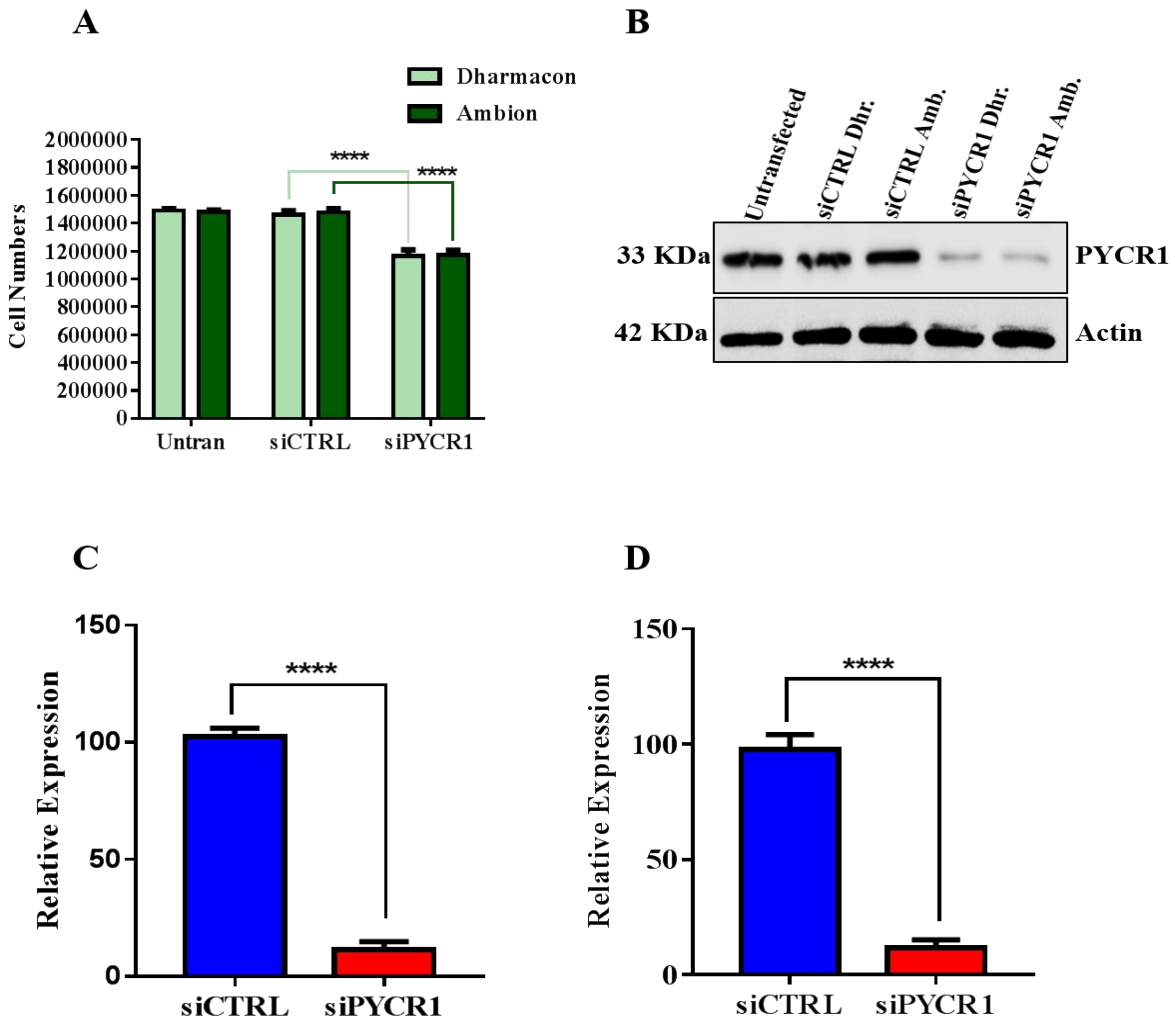

Figure 5.6. Reduced cell growth of RKO cells 72 hrs post PYCR1 knockdown. (**A**) The bar graph shows number of cells after 72 hrs transfection with two diverse siRNA targeting PYCR1 (siPYCR1) and scramble siRNA (siCTRL). Untransfected (Untran) indicates control untreated cells. Cells were counted using the Beckman Z2 Coulter Particle Count and Size Analyzer. (**B**) The representative western blot shows the successful PYCR1 protein knockdown in HCT116 cell line with both Dharmacon$^{T.M}$ (Dhr) and Ambion® (Amb) siRNA pools. Actin was used as loading control. (C and D) The bar graphs show quantification of PYCR1 protein expression from three independent experiments with Dharmacon and Ambion siRNA reagents, respectively. Western blots were quantified using ImageJ software and normalized using actin as endogenous loading control. The bars represent the mean ± S.E.M., n=3 independent experiments. Sidak's multiple comparisons Two-ways Anova test and Two-tailed Student's *t*-test were used to calculate p values. **** $p < 0.0001$.

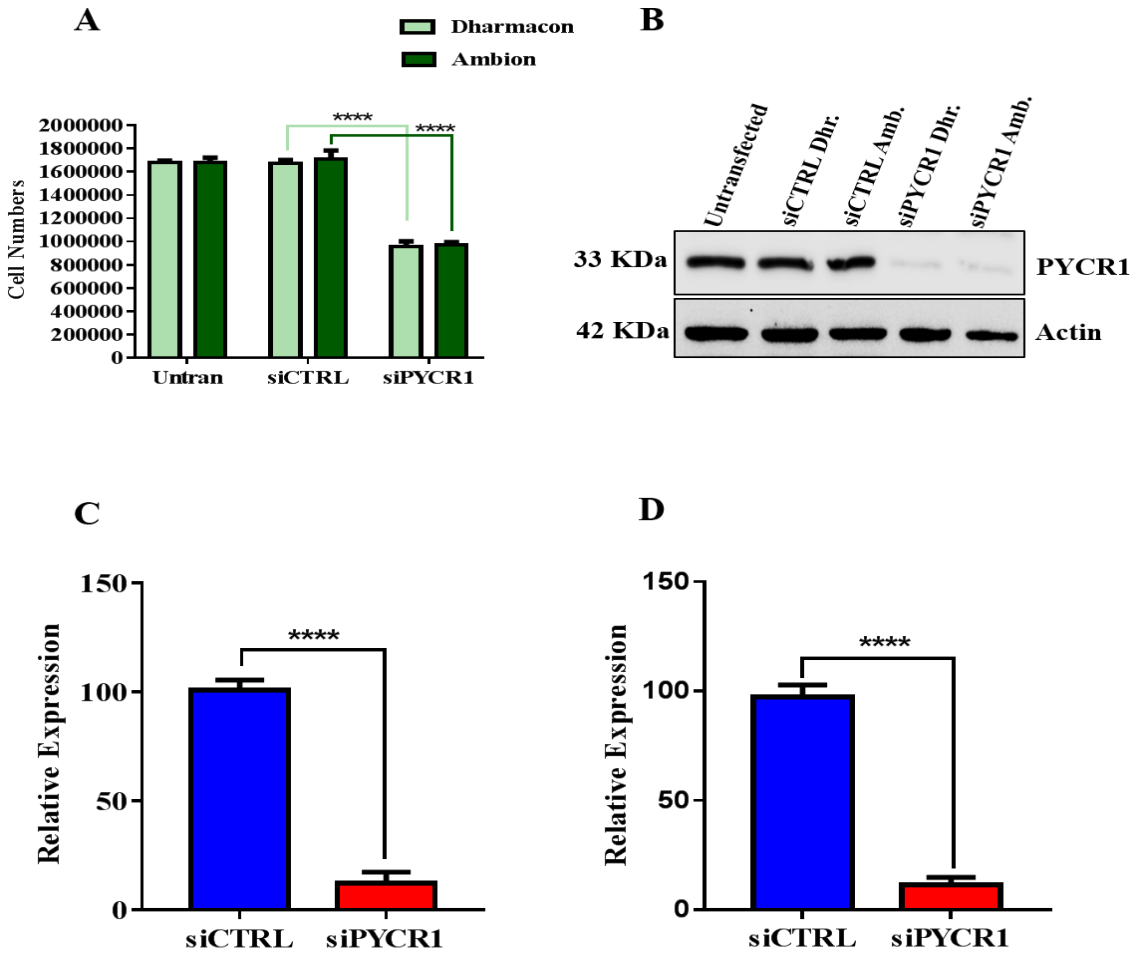

Figure 5.7. Reduced cell growth of RKO cells 96 hrs post PYCR1 knockdown. (**A**) The bar graph shows number of cells after 96 hrs transfection with two diverse siRNA targeting PYCR1 (siPYCR1) and scramble siRNA (siCTRL). Untransfected (Untran) indicates control untreated cells. Cells were counted using the Beckman Z2 Coulter Particle Count and Size Analyzer. (**B**) The representative western blot shows the successful PYCR1 protein knockdown in HCT116 cell line with both Dharmacon$^{T.M}$ (Dhr) and Ambion$^{®}$ (Amb) siRNA pools. Actin was used as loading control. (**C** and **D**) The bar graphs show quantification of PYCR1 protein expression from three independent experiments with Dharmacon and Ambion siRNA reagents, respectively. Western blots were quantified using ImageJ software and normalized using actin as endogenous loading control. The bars represent the mean ± S.E.M., n=3 independent experiments. Sidak's multiple comparisons Two-ways Anova test and Two-tailed student's *t*-test were used to calculate p values. **** p <0.0001.

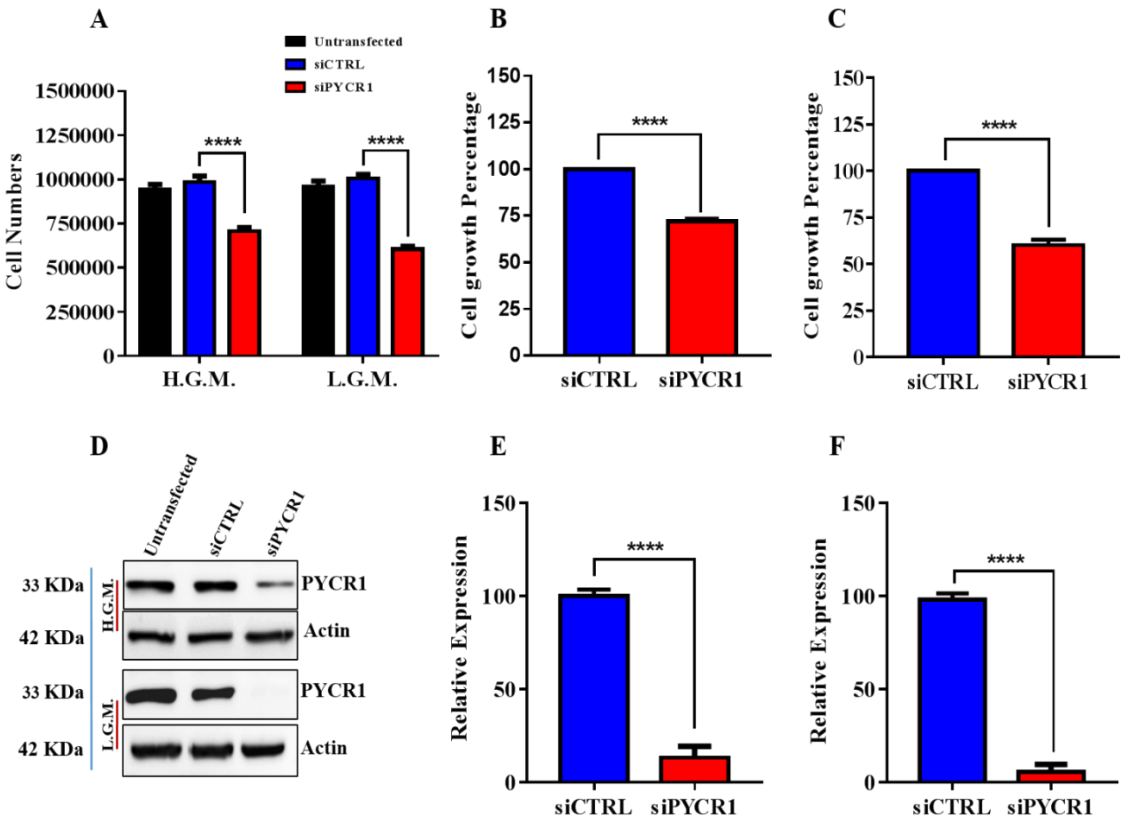

Figure 5.8. Reduced cell growth of SW620 cells following PYCR1 knockdown. PYCR1 knockdown was performed using Dharmacon siRNA and two different glucose concentrations: high (H.G.M., 4500 mg/L) glucose and low (L.G.M., 1000 mg/L) concentration. (**A**) The bar graph shows significant reduction in cellular proliferation 72 hrs after PYCR1 knockdown (siPYCR1), compared with scrambled siRNA (siCTRL) and untransfected (Untran). Cells were counted using Beckman Z2 Coulter Particle Count and Size Analyzer. (**B**) The bar graph shows the percentages of cell growth after PYCR1 knockdown using H.G.M. concentration. (**C**) The bar graph shows the percentages of cell growth after PYCR1 knockdown using L.G.M concentration. (D) The representative western blot shows the successful PYCR1 protein knockdown in both H.G.M and L.G.M conditions. Actin was used as loading control. (**E** and **F**) The bar graphs show quantification of PYCR1 expression quantification after successful knockdown for from three independent experiments. Western blots were quantified using ImageJ software (Version 1.51g) and normalized using actin as endogenous loading control. The results were obtained from three independent experiments (n=3). The values represent the mean ± S.E.M. **** p <0.0001. All p values were obtained by Tukey's multiple comparisons Two-way Anova and Two-tailed student's *t*-test.

5.4. PYCR1 knockdown reduces cell proliferation

The results of cell counting experiments showed a significant reduction in cell growth following PYCR1 knockdown, suggesting that the upregulation of this enzyme in CRC cancer cells could be involved in cell survival and/or cancer cell proliferation. To assess whether PYCR1 knockdown has an effect on CRC cell proliferation and DNA synthesis, Click-iT® EdU Flow Cytometry assay was used to measure the effect of PYCR1 knockdown on the proliferation rate of CRC cell lines. EdU (5‑ethynyl‑2'deoxyuridine) is a thymidine analogue, which is incorporated into the newly synthesized DNA during active DNA synthesis in the S phase of the cell cycle (Mead and Lefebvre, 2014) and can be readily detected using a staining protocol. As shown in Figures 5.9, 5.10 and 5.11, following PYCR1 knockdown, the percentages of EdU incorporation were significantly decreased in the siPYCR1 group compared to both untreated and scramble (siCTRL) control groups in three distinct cell lines.

In both RKO and SW620 cell lines, PYCR1 knockdown led to a 70% reduction in EdU incorporation (Figure 5.9 and 5.10).

Correspondingly, in the HCT116 cell line, we observed a similar dramatic reduction in proliferation as in RKO and SW620. However, the EdU incorporation was indeed significantly diminished in PYCR1 depleted cells, but the reduction was about 25% compared to scramble control (siCTRL) (Figure 5.11). The reported reductions in EdU percentages were accompanied by a decreased cell numbers in all cell lines, as previously reported. Overall, these data suggest that the PYCR1 enzyme sustains proliferation of CRC cells.

In addition, to investigate further the molecular pathways that underlie the impact of PYCR1 on the cell cycle regulation, we assessed expression of the cyclin D1, cyclin D3 and p21 proteins after PYCR1 silencing. The cyclin D family of proteins promote the G1 to S progression during the cell cycle and their deregulation has been extensively reported in human cancers (Musgrove, 2006). p21 protein, encoded by the *CDKN1A* gene, is also known as cyclin-dependent kinase inhibitor 1. p21 is a major p53 target, which triggers cell cycle arrest by inhibiting all cyclin/CDK complexes (Wade et al., 1993, El-Deiry et al., 1993 and Waldman et al., 1995). Therefore, we sought to address whether knockdown of PYCR1 might alter expression of cyclins and p21.

To achieve this, the expression levels of these targets were tested by western blot technique after PYCR1 knockdown in three CRC cell lines, RKO, SW620 and HCT116. In agreement with the reduced cell proliferation observed in the EdU incorporation assay, our data indicated a significant decrease in cyclin D1 and D3 proteins and a concomitant increase in p21 protein after 72 hrs of PYCR1 knockdown in all cell lines tested (Figures 5.12, 5.13 and 5.14).

Based on these results, we can conclude that PYCR1 plays an important role in promoting the cell cycle progression and its genetic depletion compromises cell proliferation and reduces expression of cyclin D1 and cyclin D3 proteins, while increasing the expression of the cell cycle inhibitor p21.

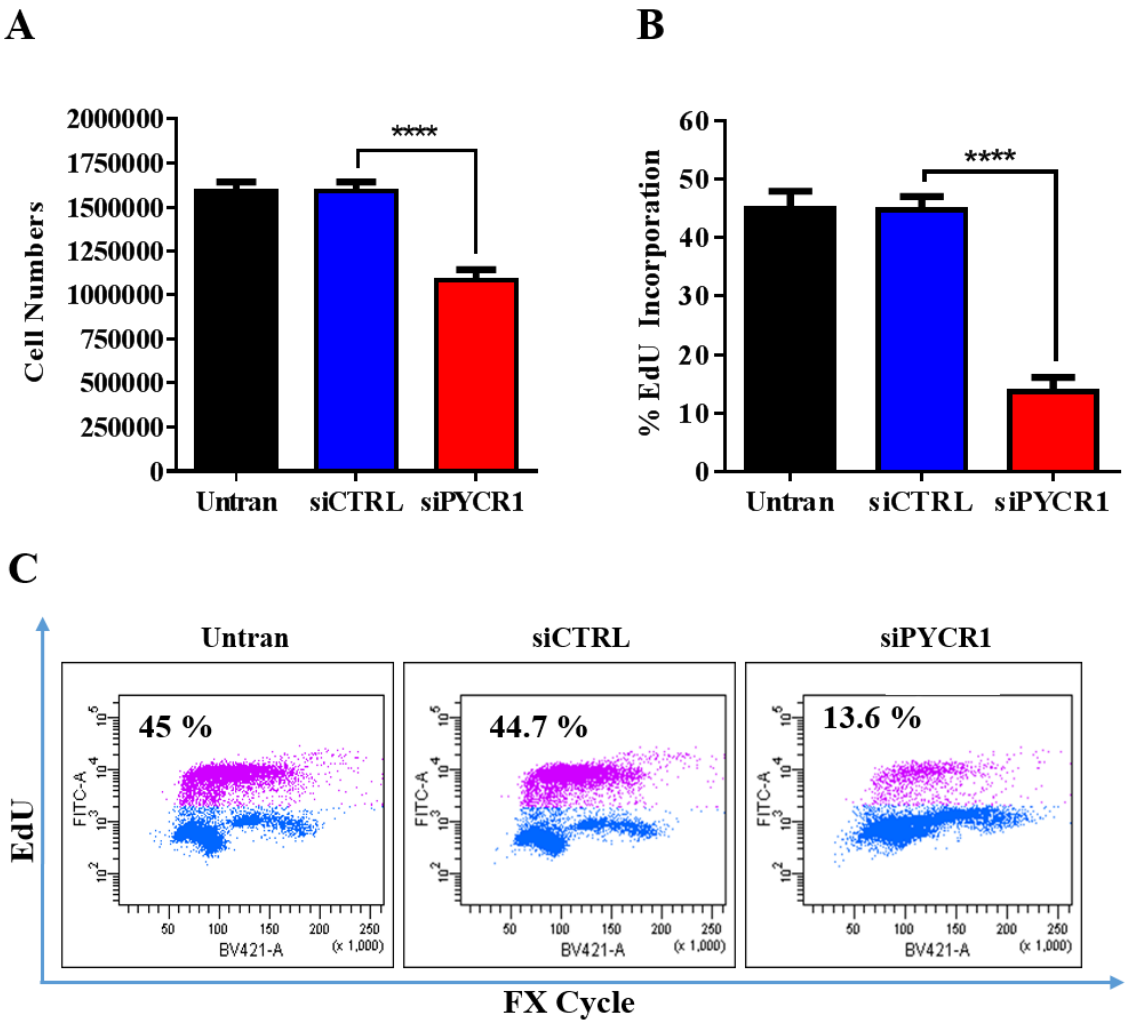

Figure 5.9. Effect of PYCR1 knockdown on cell cycle in RKO cells. (**A**) The bar graph shows significant reduction in number of cells 72 hrs after transfection with Dharmacon siRNA targeting PYCR1 (siPYCR1)**.** Cells were counted using Beckman Z2 Coulter Particle Count and Size Analyzer. (**B**) The bar graph shows the percentage of EdU incorporation in cell transfected with Dharmacon siRNA targeting PYCR1 (siPYCR1) and untransfected (Untran) and scramble transfected controls (siCTRL). (**C**) Representative scatter plots of EdU incorporation in RKO. The cell cycle analysis was performed using FACS technique and Thermo Scientific Click EdU assay. Total DNA content was quantified with FxCycle™ Violet Stain. All values represent the mean ± standard error of mean (S.E.M.) of three independent experiments. **** $p < 0.0001$. All p values were obtained by Sidak's multiple comparisons One-way Anova test.

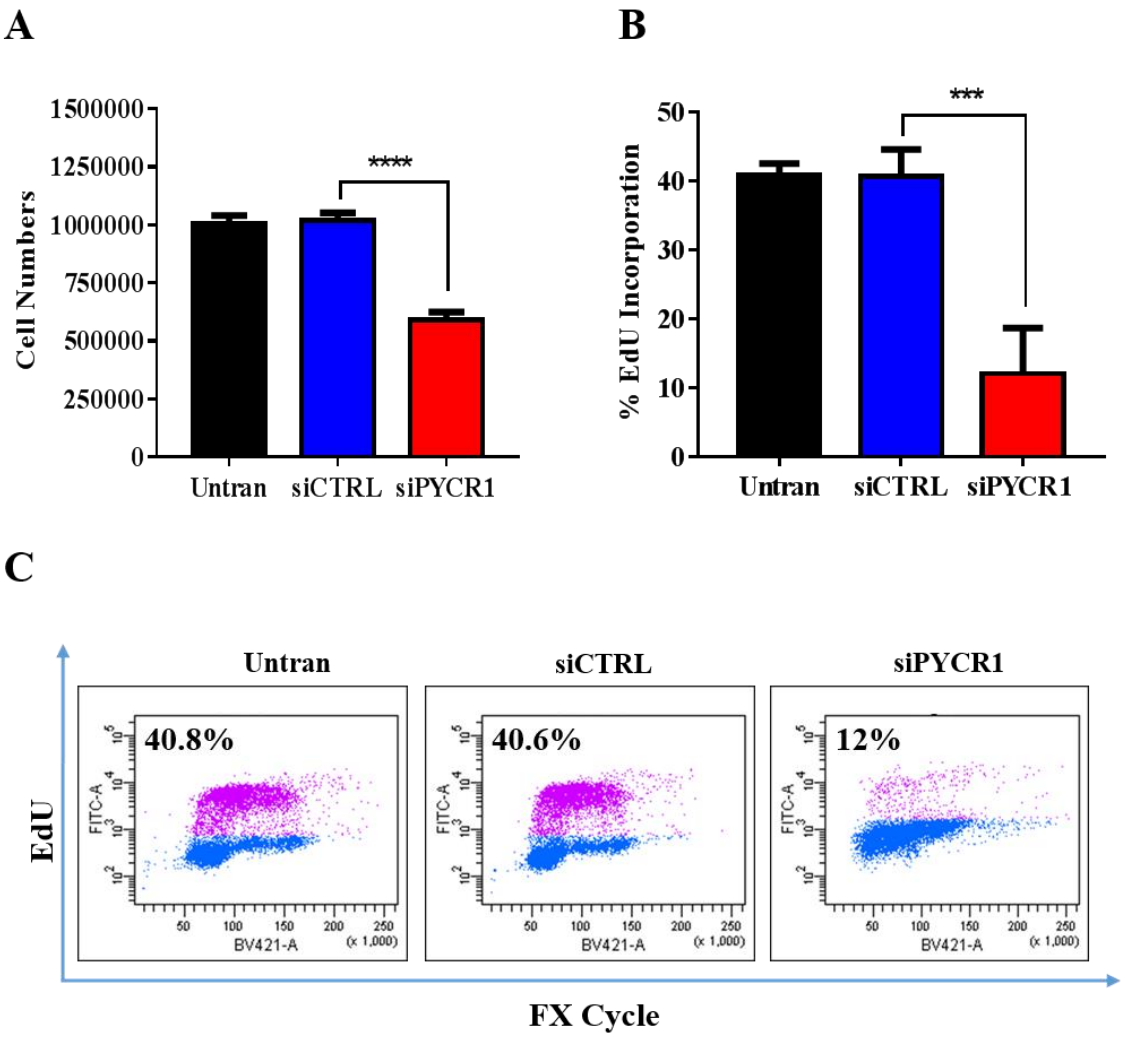

Figure 5.10. Effect of PYCR1 knockdown on cell cycle in SW620 cells. (**A**) The bar graph shows significant reduction in cell number 72 hrs after transfection with Dharmacon siRNA targeting PYCR1 (siPYCR1). Cells were counted using Beckman Z2 Coulter Particle Count and Size Analyzer. (**B**) The bar graph shows the percentage of EdU incorporation in cell transfected with Dharmacon siRNA targeting PYCR1 (siPYCR1) and untransfected (Untran) and scramble transfected (siCTRL) controls. (**C**) Representative scatter plots of EdU incorporation in SW620. The cell cycle analysis was performed using FACS technique and Thermo Scientific Click EdU assay. Total DNA content was quantified with FxCycle™ Violet Stain. All values represent the mean ± S.E.M. of three independent experiments. *** $p<0.001$, **** $p<0.0001$. All p values were obtained by Sidak's multiple comparisons One-way Anova test.

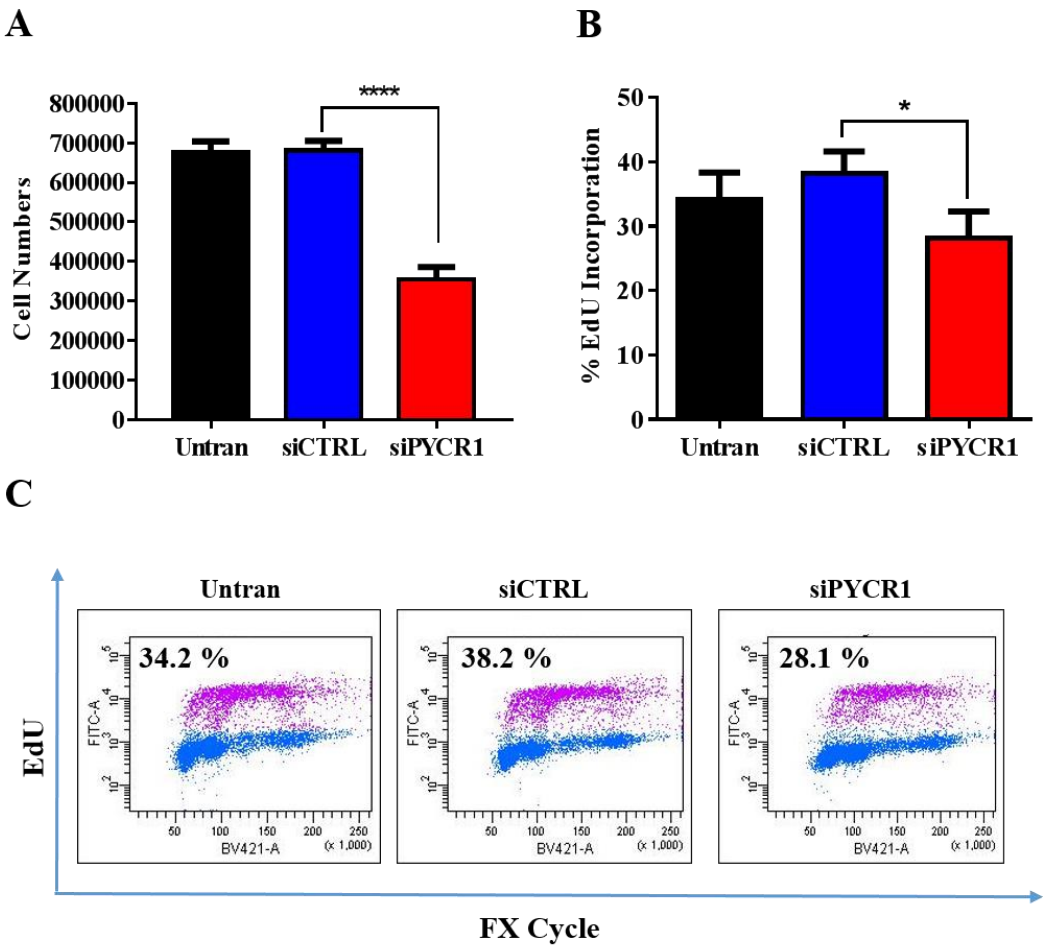

Figure 5.11. Effect of PYCR1 knockdown on cell cycle in HCT116 cells. (**A**) The bar graph shows significant reduction in cell number 72 hrs after transfection with Dharmacon siRNA targeting PYCR1 (siPYCR1). Cells were counted using Beckman Z2 Coulter Particle Count and Size Analyzer. (**B**) The bar graph shows the percentage of EdU incorporation in cell transfected with Dharmacon siRNA targeting PYCR1 (siPYCR1) and untransfected (untran) and scramble transfected (siCTRL) controls. (**C**) Representative scatter plots of EdU incorporation in HCT116. The cell cycle analysis was performed using FACS technique and Thermo Scientific Click EdU assay. Total DNA content was quantified with FxCycle™ Violet Stain. All values represent the mean ± S.E.M. of three independent experiments.* $p < 0.05$. All p values were obtained by Sidak's multiple comparisons One-way Anova test.

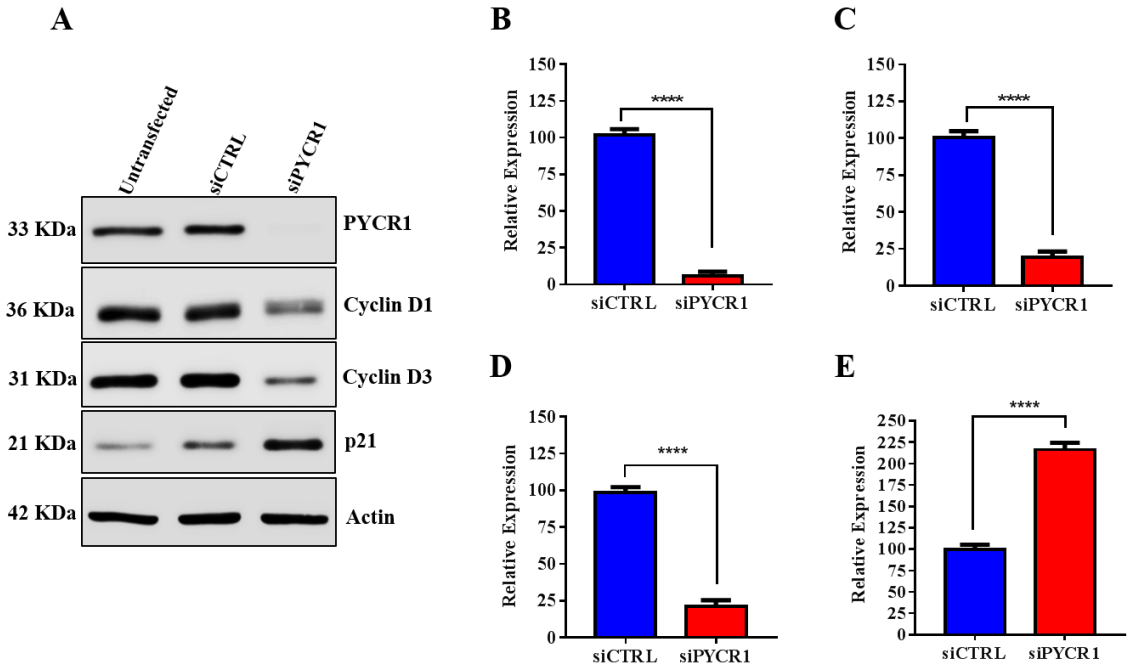

Figure 5.12. Expression of cell cycle proteins following PYCR1 silencing in RKO CRC cell line. (**A**) Representative western blots showing the levels of PYCR1 after siRNA-mediated knockdown and the substantial decrease in cyclin D1, cyclin D3 protein expression together with increased in p21 protein expression upon PYCR1 knockdown. Actin was used as loading control. The bar graphs show the relative expression levels of PYCR1 (**B**), cyclin D1 (**C**), cyclin D3 (**D**) and p21 (**E**) proteins in cells transfected for 72 hrs with Dharmacon siRNA targeting PYCR1 (siPYCR1) relative to scramble transfected (siCTRL) control and normalized to actin loading control. All western blots were quantified using ImageJ software (Version 1.51g). The values represent the mean ± S.E.M. of three independent experiments. **** $p < 0.0001$. All p values were obtained by Two-tailed student's *t*-test.

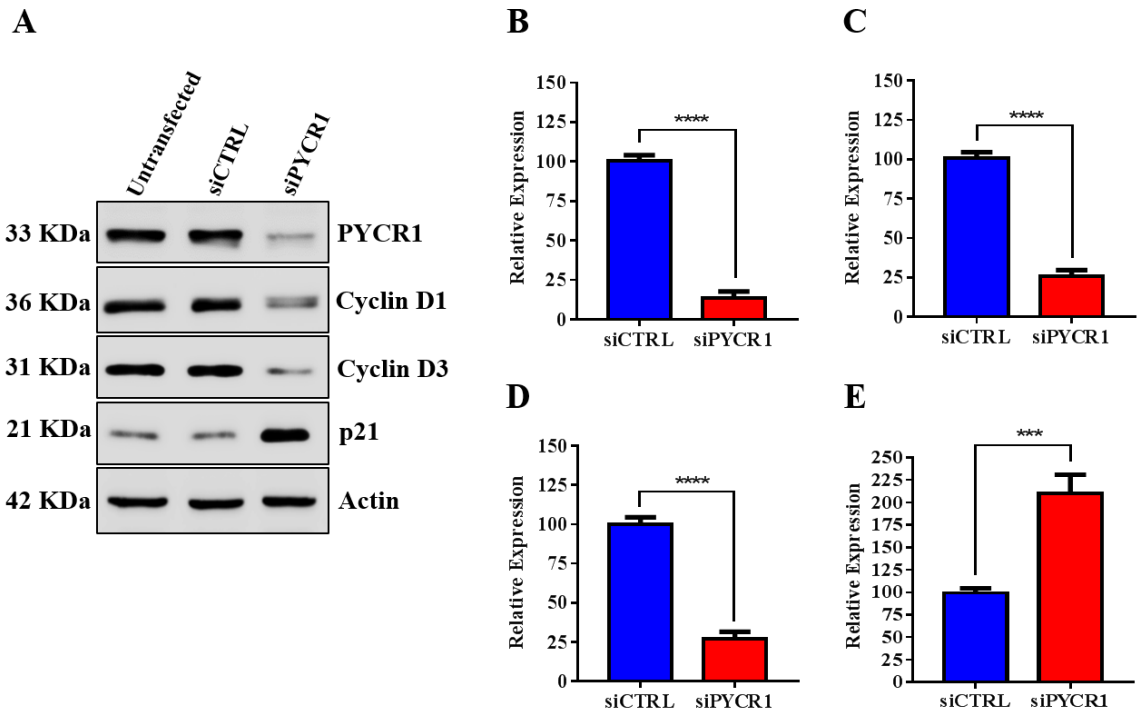

Figure 5.13. Expression of cell cycle proteins following PYCR1 silencing in SW620 CRC cell line. (**A**) Representative western blots showing the levels of PYCR1 after siRNA-mediated knockdown and the substantial decrease in cyclin D1, cyclin D3 protein expression together with increased in p21 protein expression upon PYCR1 knockdown. Actin was used as loading control. The bar graphs show the relative expression levels of PYCR1 (**B**), cyclin D1 (**C**), cyclin D3 (**D**) and p21 (**E**) proteins in cells transfected for 72 hrs with Dharmacon siRNA targeting PYCR1 (siPYCR1) relative to scramble transfected (siCTRL) control and normalized to actin loading control. All western blots were quantified using ImageJ software (Version 1.51g). The values represent the mean ± S.E.M. of three independent experiments. *** $p < 0.001$, **** $p < 0.0001$. All p values were obtained by Two-tailed student's *t*-test.

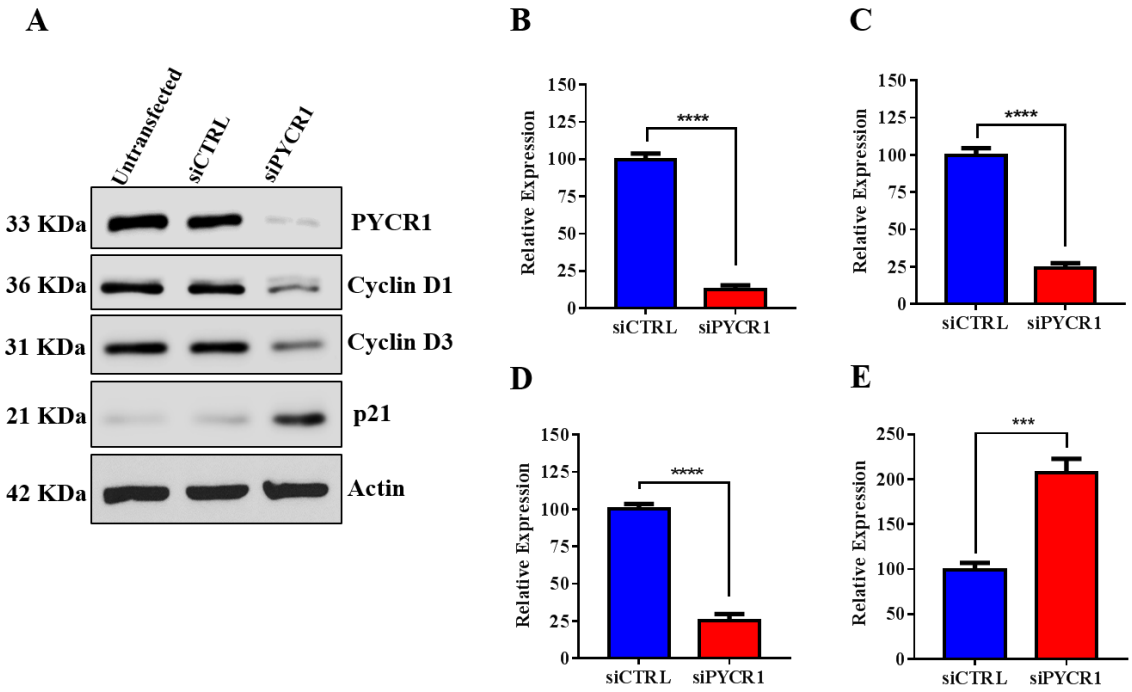

Figure 5.14. Expression of cell cycle proteins following PYCR1 silencing in HCT116 CRC cell line. (**A**) Representative western blots showing the levels of PYCR1 after siRNA-mediated knockdown and the substantial decrease in cyclin D1, cyclin D3 protein expression together with increased in p21 protein expression upon PYCR1 knockdown. Actin was used as loading control. The bar graphs show the relative expression levels of PYCR1 (**B**), cyclin D1 (**C**), cyclin D3 (**D**) and p21 (**E**) proteins in cells transfected for 72 hrs with Dharmacon siRNA targeting PYCR1 (siPYCR1) relative to scramble transfected (siCTRL) control and normalized to actin loading control. All western blots were quantified using ImageJ software (Version 1.51g). The values represent the mean ± S.E.M. of three independent experiments. *** p <0.001, **** p <0.0001. All p values were obtained by Two-tailed student's *t*-test.

5.5. Silencing of PYCR1 induces apoptosis in HCT116 CRC cells

Reduction of apoptosis is the general features of tumorigenesis, and typically, cancer cells tend to be resistant to apoptotic stimuli (Zhivotovsky and Orrenius, 2006 and Hanahan and Weinberg, 2000). Induction of apoptosis is one the most relevant responses to cancer therapeutic agents (Hail, 2005 and Sun et al., 2004).

It has been demonstrated that PYCR1 has a potential role in the inhibition of apoptosis in non-small cell lung cancer and prostate cancer (Cai et al., 2017 and Zeng et al., 2017). Interestingly, we observed numerous floating cells when PYCR1 was silenced in HCT116 cells, suggesting that, in this cell line; proline metabolism might have a role in cell survival. Thus, we examined whether PYCR1 knockdown induces apoptosis in the HCT116 cell line using Annexin V/PI staining. As in previous experiments, HCT116 cells were left untreated, transfected with scrambled siRNA or with siRNA targeting PYCR1. Moreover, the chemotherapeutic drug Etoposide was used as positive control for induction of apoptosis. After 48 hrs of transfection/treatment, floating and adherent cells were collected and stained with annexin V/PI before being analysed by FACS (See section 2.2.4.).

As evident in the representative fluorescence scattergrams (Figure 5.15), the proportions of cells that stained for Annexin V and/or PI increased substantially following PYCR1 knockdown, to levels comparable to Etoposide-treated positive control. Overall, PYCR1 depletion led to a 50% decreased in live cells (Figure 5.16).

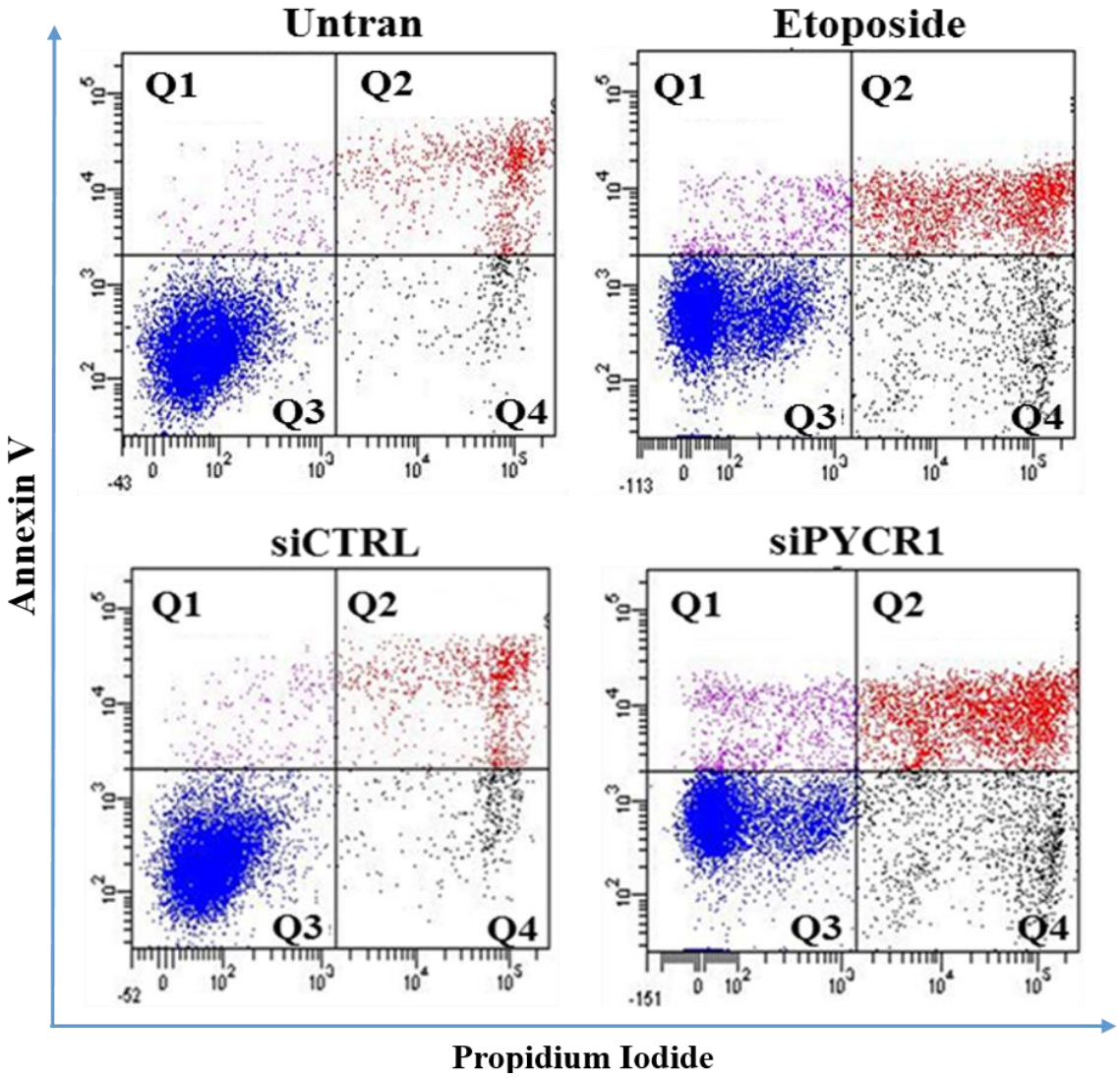

Figure 5.15. Detection of apoptosis in HCT116 following PYCR1 knockdown. Cells were transfected with Dharmacon siRNA targeting PYCR1 (siPYCR1) and with non-targeting scrambled siRNA (siCTRL) for 48 hrs. One group was left without any untreated (Untran.), while Etoposide (25µM) was used as positive control for induction of apoptosis. After 48 hrs, cells were stained with Annexin-FITC and PI according to standard protocol. The figure is a representative cytofluorimeter scattergrams showing live cells that did not stain with either Annexin V or PI (**Q3**) and death cells that stained for Annexin V (early apoptotic, **Q1**), or for both Annexin V and PI (late apoptotic or necrotic, **Q2**). The **Q4** showed the nucli of dead cells that stained with PI only.

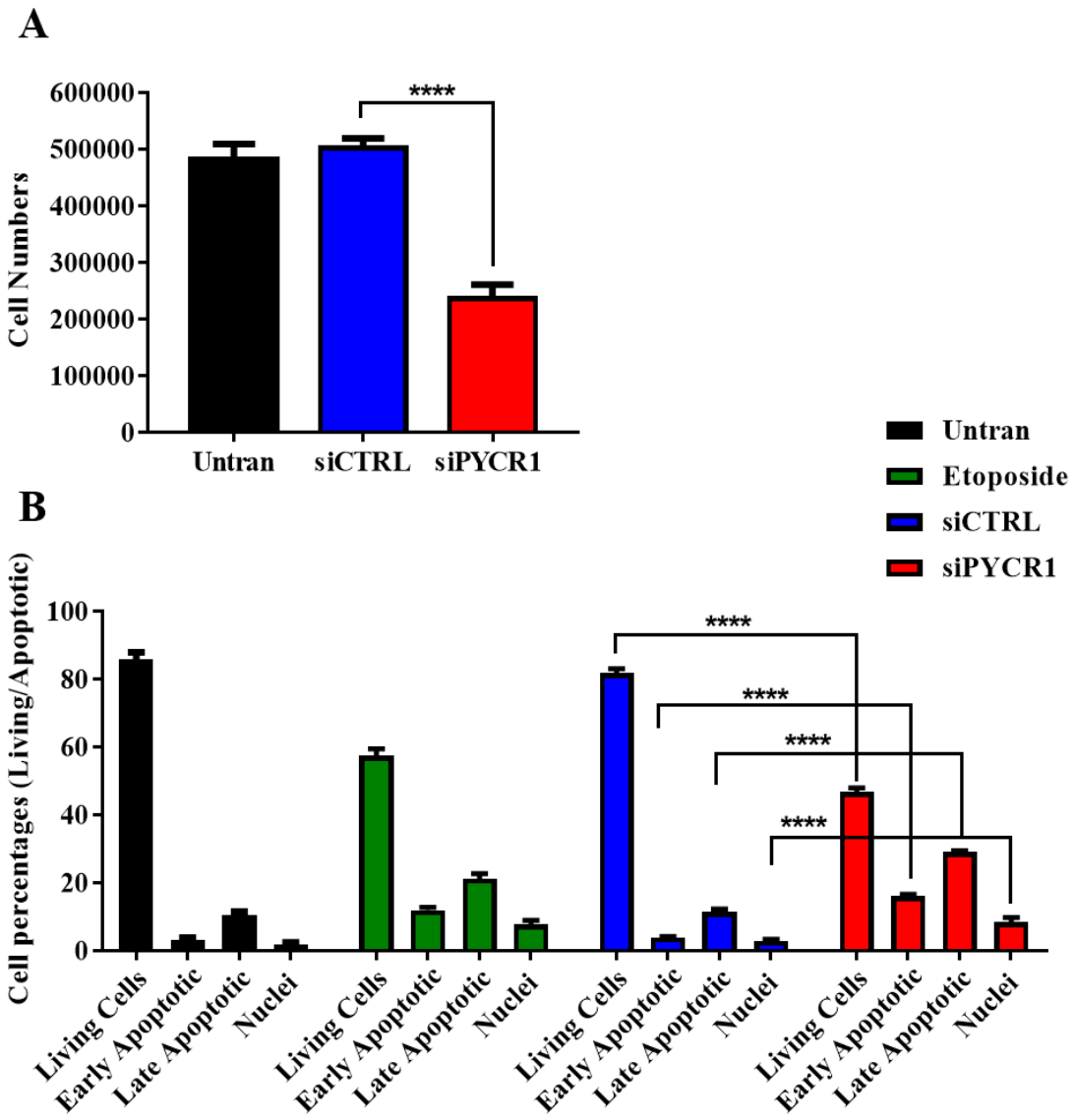

Figure 5.16. Effect of PYCR1 knockdown on the proportion of live, apoptotic and necrotic HCT116 CRC cell line. (**A**) HCT116 cells show significant reduction in growth after 48 hrs of PYCR1 knockdown. Cells were counted using Beckman Z2 Coulter Particle Count and Size Analyzer. (**B**) The bar graph shows live, apoptotic and necrotic cells as percentages of total cell number. Data were plotted as mean ± S.E.M. of three independent experiments, each performed in triplicate. Cell death was assessed using Annexin V/PI staining. Etoposide (25µM) was used as positive control for apoptosis induction. **** p <0.0001. All p values were obtained with Sidak's multiple comparisons One-way Anova test for panel **A** and Tukey's multiple comparisons Two-way Anova test for panel **B**.

5.6. Impact of different extracellular proline concentrations on cell proliferation and survival after PYCR1 knockdown

Since the PYCR1 enzyme mediates the biosynthesis of proline, its depletion might lead to proline deficiency, which, in turn, could be responsible for the observed impairment in proliferation and survival. Moreover, previous results showed that PYCR1 knockdown in CRC cell lines is not selective and leads to concomitant reduction in PYCR2 levels (Figure 5.1). Therefore, PYCR2 cannot compensate for PYCR1 loss in our experimental system.

Thus, we tested the possibility that replenishing culture media with proline could rescue proliferation of PYCR1/2-depleted cells.

It should be noted that HCT116 and RKO's growth media, McCoy's 5A and Eagle's Minimum Essential Medium, respectively, contain a physiological concentrations of proline (0.15mM). Nonetheless, to address the impact of defective proline biosynthesis, we investigated whether the addition of an excess of exogenous proline to the cell cultures could rescue the impaired proliferation triggered by PYCR1 deficiency.

In the HCT116 cell line, the addition of 3mM and 5mM proline led to a general increase in cell numbers compared to the standard medium concentration of proline (Figure 5.17). Nonetheless, exogenous proline failed to rescue fully the growth deficiency in PYCR1-knockdown cells. Indeed, as shown in Figure 5.17, PYCR1 deficiency resulted in 50% decrease in cell number in vehicle treated samples, whereas growth reduction was limited to 25-30% when an excess of proline is provided, but this difference remains statistically significant when compared to scrambled siRNA control. Notably, proline supplementation also failed to rescue expression of cell cycle markers as demonstrated by a dramatic decrease in cyclin D1 and cyclin D3 expression, accompanied by enhanced p21 levels in HCT116 (Figure 5.18)

Similarly, in RKO cell line, an increase in cell number was observed when cells were supplemented with 5mM proline (Figure 5.19), but the overall impact of PYCR depletion remained unaffected, with a comparable decrease in cell number irrespective of proline availability. The cell cycle markers including cyclin D1 and cyclin D3 expression failed to rescue and cell cycle inhibitor p21 showed upregulation level in this cell line (Figure 5.20).

Moreover, whether physiological or supra-physiological proline concentrations have any effect following PYCR1 deficiency was additionally investigated in SW620 cells. These data are of great interest as the formulation of Dulbecco's Modified Eagle's Medium (DMEM), the growth medium of SW620, does not contain proline. Similar to HCT116 and RKO cell lines, the exogenous proline failed to rescue the growth deficiency in PYCR1-depleted SW620 CRC cells, either at physiological concentrations or at 5mM excess (Figure 5.21). Similar to HCT116 and RKO CRC cell lines, in SW620 CRC cells, both cyclin D1 and cyclin D3 showed dramatic decreasing levels while p21 was increased (Figure 5.22). These data suggest that proline biosynthesis is unlikely to underpin PYCR1's role in cell proliferation, although the underling mechanisms remain unknown.

Interestingly, whether exogenous proline has a differential, selective effect on cell survival versus proliferation has not been addressed here. However, a selective rescue of cell death could explain the partial recovery observed in HCT116 and would also be compatible with the inability of exogenous proline to rescue expression of cyclin D1 and cyclin D3 and normalize p21 levels in this cell line.

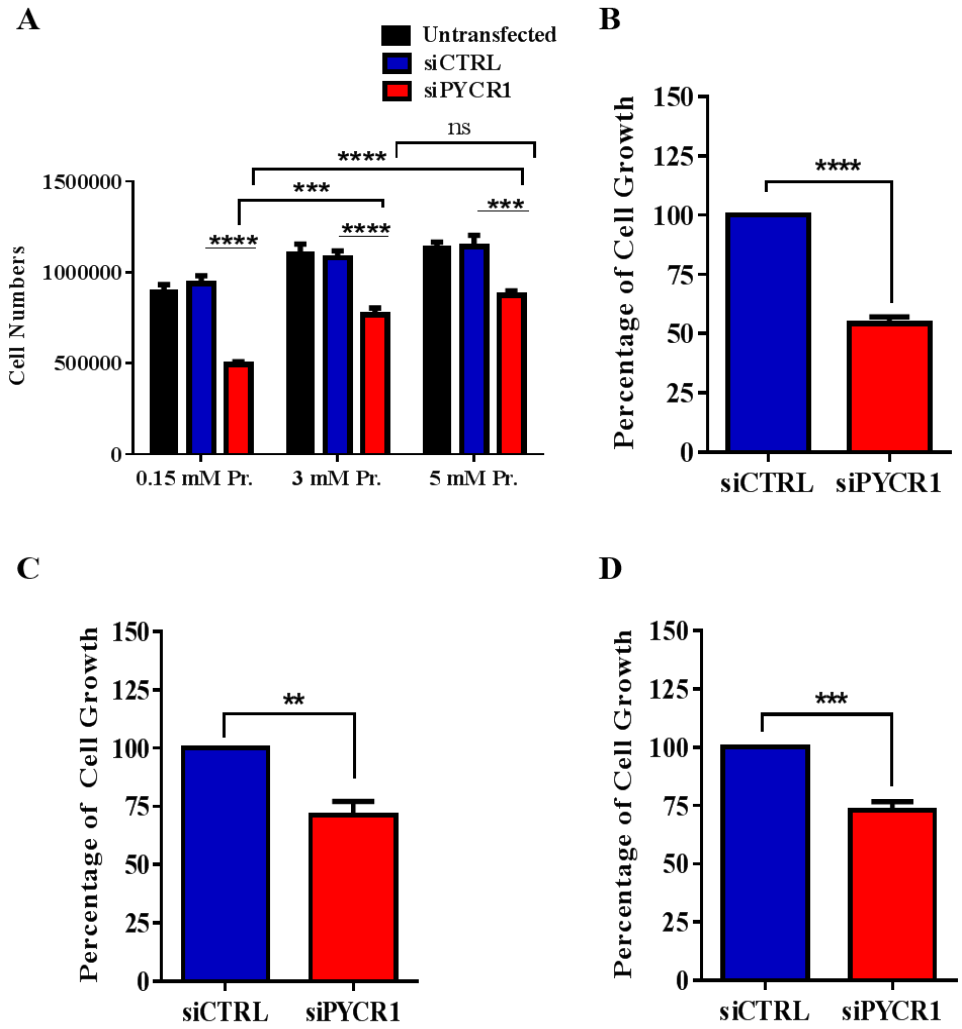

Figure 5.17. Effect of proline supplementation on the growth of HCT116 cell line. (**A**) The bar graph shows the effect of different proline concentrations (0.15mM from McCoy's 5A medium as control, 3 mM and 5mM) on cell growth in PYCR1-knockdown cells (siPYCR1), siRNA scramble-transfected cells (siCTRL) and untransfected cells. Cells were collected 72 hrs after transfection and counted using Beckman Z2 Coulter Particle Count and Size Analyzer. (**B**, **C** and **D**). The graphs show the percentages of cell growth in PYCR1 knockdown (siPYCR1) group compared to scramble (siCTRL) in control medium (0.15mM proline) or medium replenished with 3mM and 5mM proline. The bars represent the mean ± S.E.M. of three independent experiments. ** p <0.01, *** p <0.001 and **** p< 0.0001. All p values were obtained by Tukey's multiple comparisons Two-way Anova test for panel **A** and Two-tailed student's *t*-test for panels **B**, **C** and **D**.

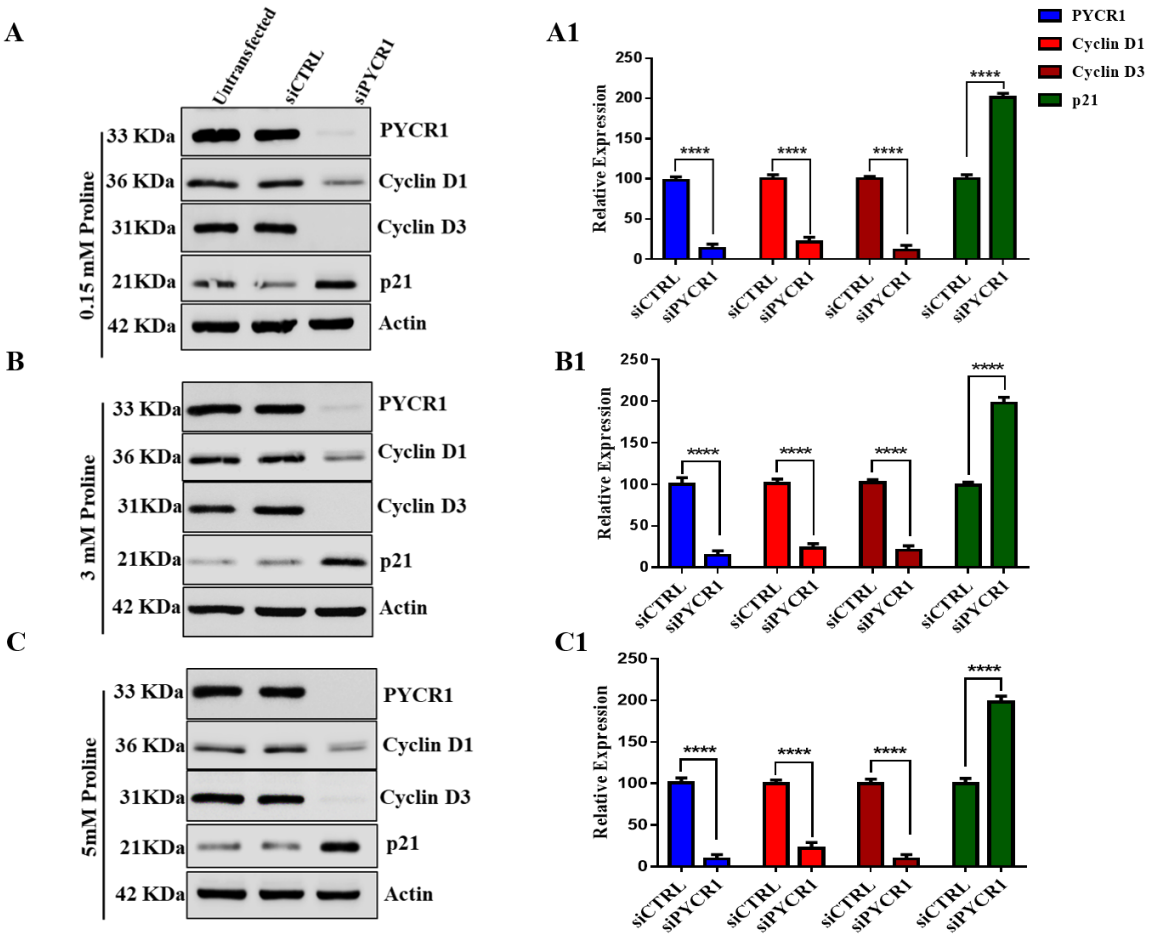

Figure 5.18. Effect of proline supplementation on the expression of proliferation markers in HCT116 cell line. Representative western blots showing decreased expression of cyclin D1 and D3 and increased p21 protein expression after PYCR1 silencing cells using 0.15mM (**A**), 3mM (**B**) and 5mM (**C**) proline-containing media. (**A1**, **B1** and **C1)** The graphs show the quantification of densitometry readings for PYCR1, cyclin D1, cyclin D3 and p21 protein bands relative to scramble control (siCTRL) in the indicated growing media. Western blots were quantified using ImageJ software (Version 1.51g) and normalized using actin as endogenous loading control. The values represent the mean ± S.E.M. of three independent experiments. **** p <0.0001. All p values were obtained using Sidak's multiple comparisons Two-way Anova test.

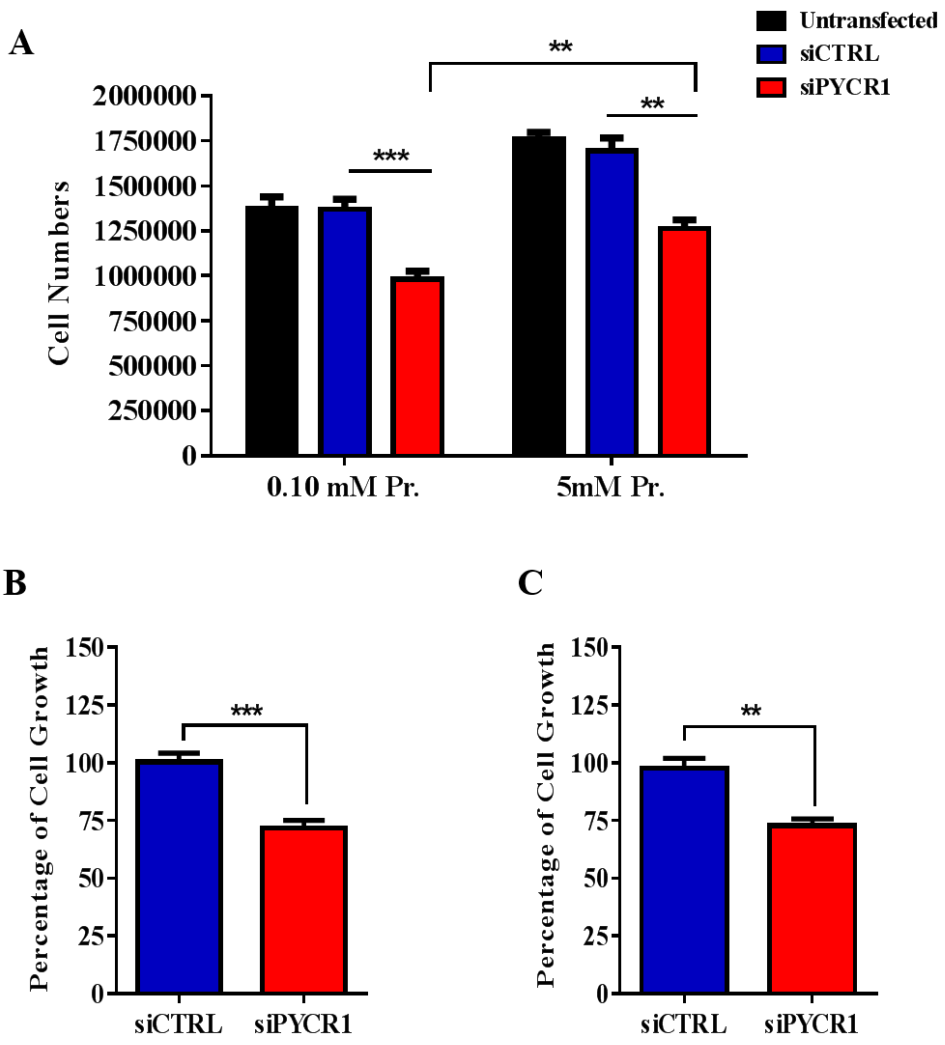

Figure 5.19. Effect of proline supplementation on the growth of RKO cell line. (**A**) The bar graph shows the effect of different proline concentrations (0.10 mM from Minimum Essential Medium Eagle (MEM) as control and 5mM) on cell growth in PYCR1-knockdown cells (siPYCR1), siRNA scramble-transfected cells (siCTRL) and untransfected cells. Cells were collected 72 hrs after transfection and counted using Beckman Z2 Coulter Particle Count and Size Analyzer. (**B** and **C**) The graphs show the percentages of cell growth in PYCR1 knockdown (siPYCR1) group compared to scramble (siCTRL) in control medium (0.15mM proline) or medium replenished with 5mM proline. The bars represent the mean ± S.E.M. of three independent experiments. ** $p < 0.01$ and *** $p < 0.001$. All p values were obtained by Tukey's multiple comparisons Two-way Anova test for panel **A** and Two-tailed student's *t*-test for panels **B** and **C**.

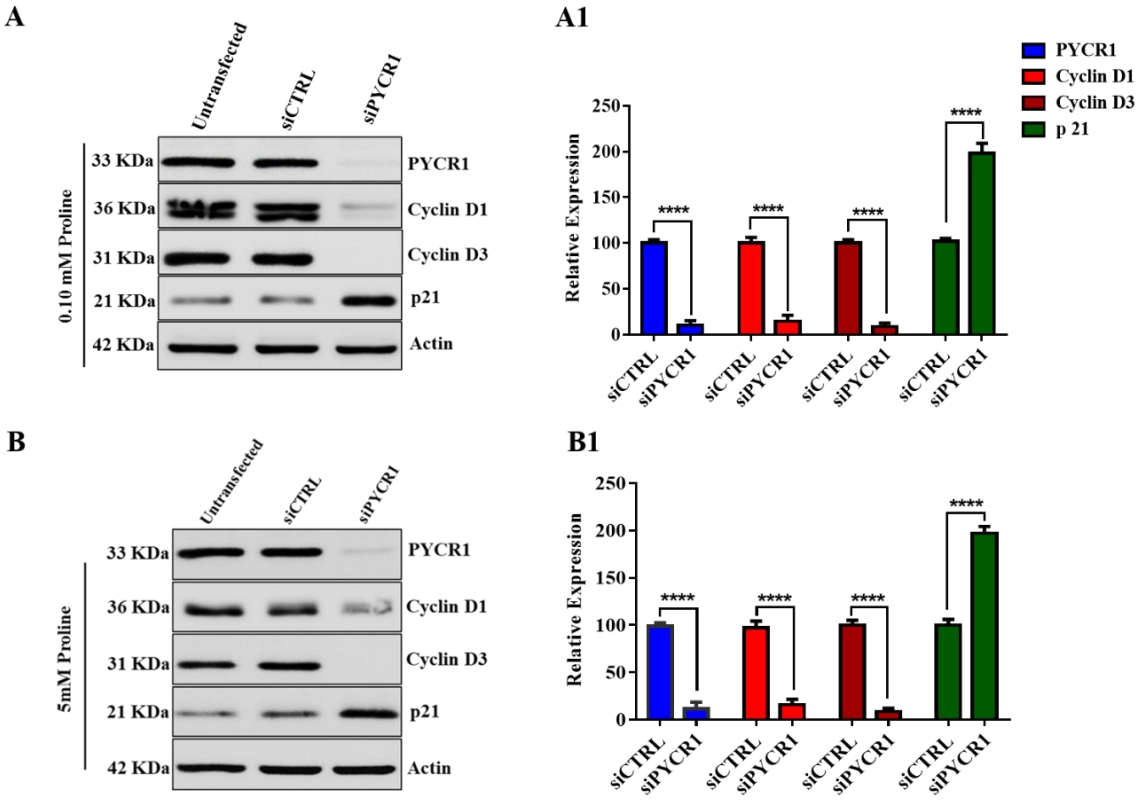

Figure 5.20. Effect of proline supplementation on the expression of proliferation markers in RKO cell line. Representative western blots showing decreased expression of cyclin D1 and D3 and increased p21 protein expression after PYCR1 silencing cells using 0.10mM (**A**), 5 mM (**B**) proline-containing media. (**A1**, **B1** and **C1**) The graphs show the quantification of densitometry readings for PYCR1, cyclin D1, cyclin D3 and p21 protein bands relative to scramble control (siCTRL) in the indicated growing media. Western blots were quantified using ImageJ software (Version 1.51g) and normalized using actin as endogenous loading control. The values represent the mean ± S.E.M. of three independent experiments. **** $p < 0.0001$. All p values were obtained using Sidak's multiple comparisons Two-way Anova test.

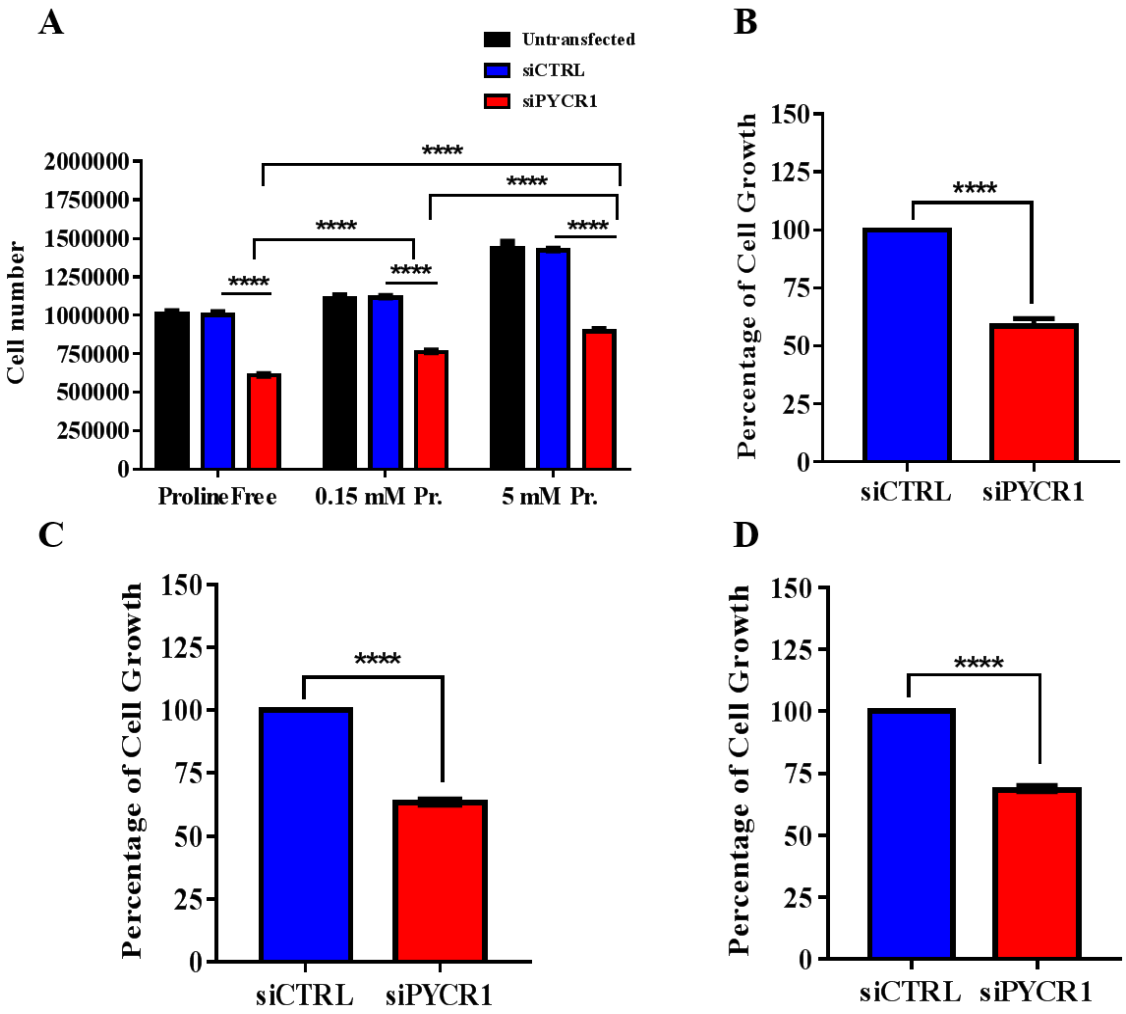

Figure 5.21. Effect of proline supplementation on the growth of SW620 cell line. (**A**) The bar graph shows the effect of different proline concentrations (proline-free from DMEM medium as control, physiological 0.15mM and 5mM) on cell growth in PYCR1-knockdown cells (siPYCR1), siRNA scramble-transfected cells (siCTRL) and untransfected cells. Cells were collected 72 hrs after transfection and counted using Beckman Z2 Coulter Particle Count and Size Analyzer. (**B**, **C** and **D**) The graphs show the percentages of cell growth in PYCR1 knockdown (siPYCR1) group compared to scramble (siCTRL) in control medium (proline-free) or medium replenished with 0.15mM and 5mM proline. The bars represent the mean ± S.E.M. of three independent experiments. **** $p < 0.0001$. All p values were obtained by Tukey's multiple comparisons Two-way Anova test for panel **A** and Two-tailed Student's *t*-test for panels **B**, **C** and **D**.

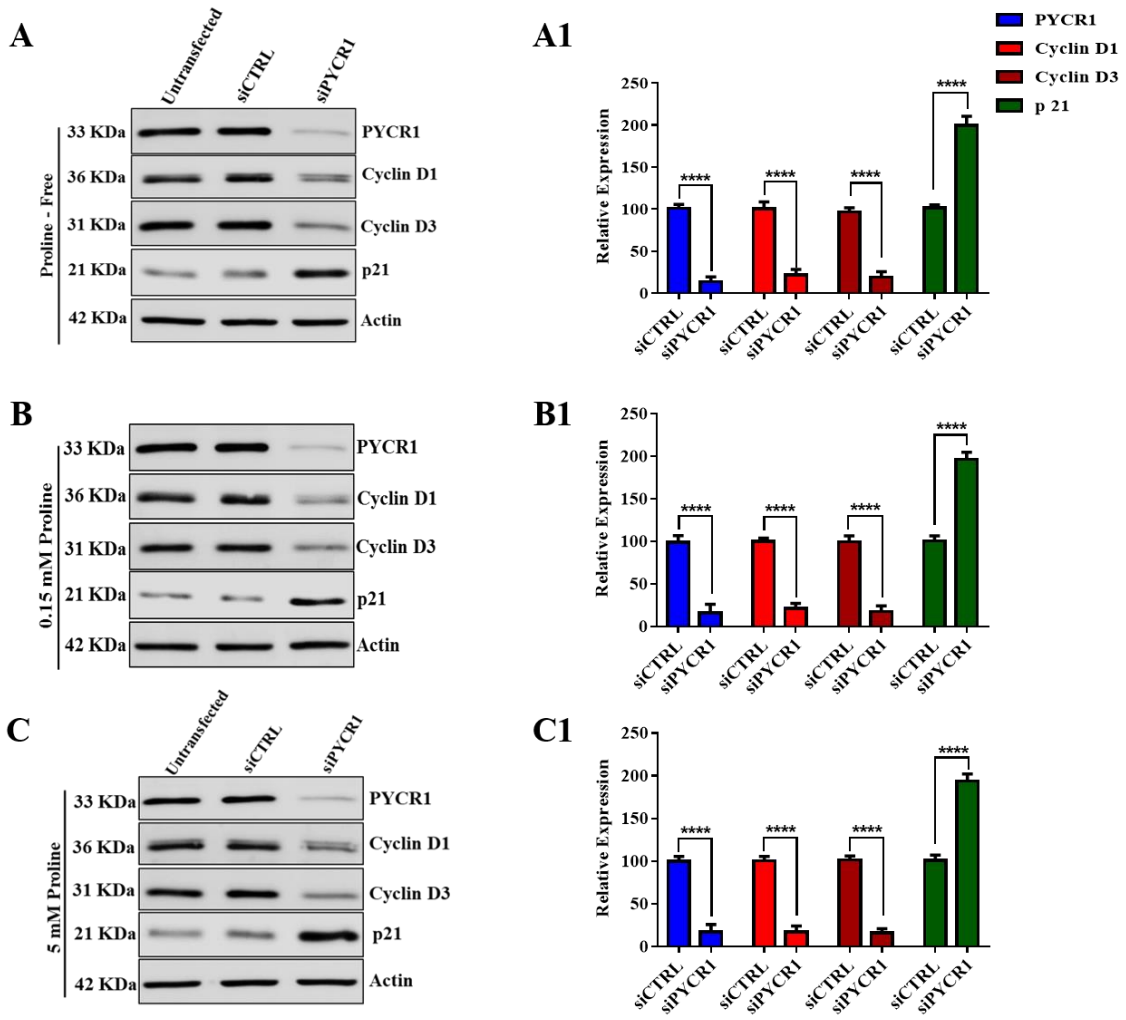

Figure 5.22. Effect of proline supplementation on the expression of proliferation markers in SW620 cell line. Representative western blots showing decreased expression of cyclin D1 and D3 and increased in p21 protein expression after PYCR1 silencing cells using proline free-medium (**A**), 0.15mM (**B**) and 5mM (**C**) proline-containing media. (**A1**, **B1** and **C1**) The graphs show the quantification of densitometry readings for PYCR1, cyclin D1, cyclin D3 and p21 protein bands relative to scramble control (siCTRL) in the indicated growing media. Western blots were quantified using ImageJ software (Version 1.51g) and normalized using actin as endogenous loading control. The values represent the mean ± S.E.M. of three independent experiments. **** p <0.0001. All p values were obtained using Sidak's multiple comparisons Two-way Anova test.

5.7. Expression and functional role of PYCR1 in HCEC cell line

HCEC cells were used to investigate the effect of PYCR1 depletion on non-transformed colon cells. Firstly, the expression of PYCR1 and PRODH/POX proteins cells was evaluated using western blot technique, and the results were compared with CRC cell lines (HCT116, SW480, HT29, RKO, CL11, Caco2 and SW620). The result showed weak expression of PYCR1 in HCEC cells. However, the level of PRODH/POX protein was high (Figure 5.23 A).

The functional effect of PYCR1 was assessed using siRNA, as described previously. Because of low expression of PYCR1 in HCEC cell line, 50 µg of protein concentration was used instead of 30 µg to obtain an adequate signal in western blot (see sections 2.2.3 and 2.2.7). After 72 hrs, siRNA treatment resulted in a robust decrease of PYCR1 expression in HCEC (Figure 5.24 B). However, there was no effect on cell growth as shown in Figure 5.23 C and D

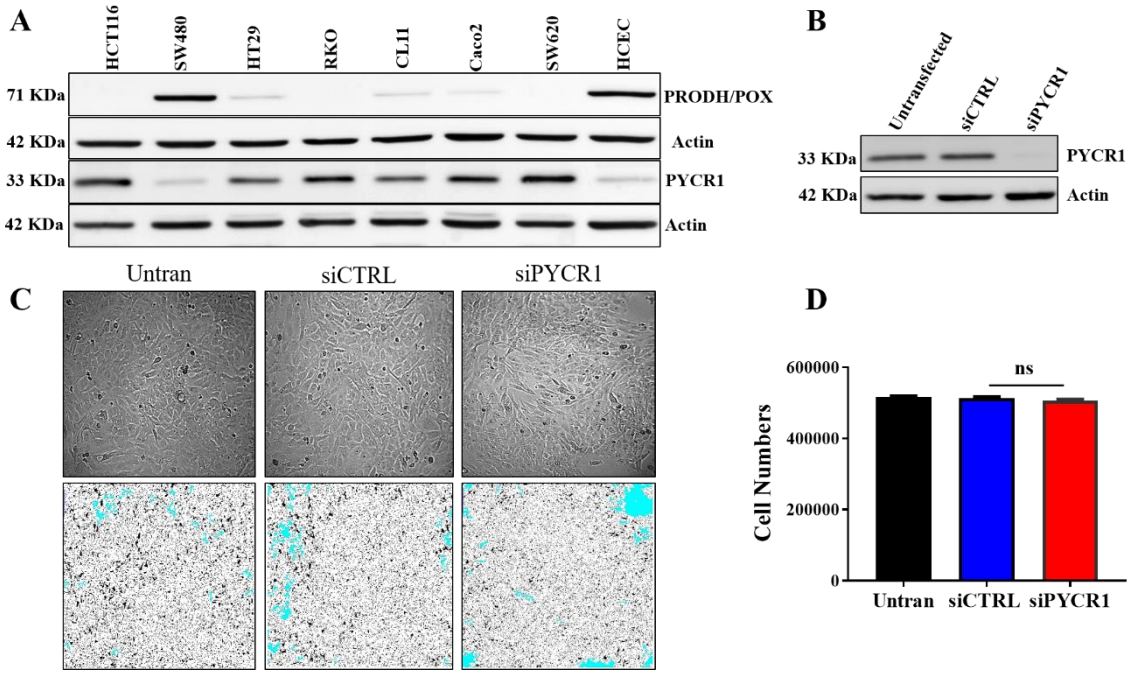

Figure 5.23. Effect of PYCR1 knockdown on the growth of HCEC cells. (**A**) Representative western blots showing low expression of PYCR1 and robust expression of PRODH/POX in HCEC cells compared with other CRC cell lines. Actin ewes used as loading control. (**B**) The representative western blot shows the successful PYCR1 protein knockdown in HCEC cell line using Dharmacon™ siRNA pools. (**C**) Representative microscopic images (upper row) and grey scale images (lower row) for HCEC cell culture after 72 hrs in the indicated conditions. The light blue colour represents the space between cells in cell culture plate. (**D**) The bar graph shows number of cells after 72 hrs of PYCR1 transfection (siPYCR1) in HCEC cell line compared to untransftected control (untran) and scramble control (siCTRL). The results were obtained from three independent experiments. ns represents no significant changes between siPYCR1 and siCTRL groups. Sidak's multiple comparisons One-way Anova test was used to calculate the statistical significances.

Chapter Six: Discussion

CRC is the second leading cause of cancer-related mortality after lung cancer in industrialized countries and it is the third most common cancer worldwide (Greenlee et al., 2001; Jemal et al., 2006). Despite our growing understanding of CRC pathogenesis, treatment option remains limited. Moreover, in addition to the poor survival of individuals with metastatic disease, it has been reported that up to 50% of patients with CRC will develop recurrent disease after surgery (Jemal et al., 2007), indicating that currently, available treatment strategies are not sufficient to control the disease, and there is urgent need of novel therapeutics.

Specific metabolic requirements have been identified in proliferating cancer cells (Vander et al., 2009). For instance, with the purpose of supporting their high rates of proliferation, cancer cells tend to consume avidly nutrients, such as glucose and glutamine, and to channel them into macromolecular biosynthesis pathways (Hosios et al., 2017). Therefore, metabolic pathways are rewired during carcinogenesis in order to balance biosynthetic processes with adequate ATP production and appropriate maintenance of the redox balance (Cairns et al., 2011). Since cancer cells depend on these changes in cellular metabolism, these altered pathways represent attractive therapeutic targets (Tennant et al., 2010). However, since normal proliferating cells rely, to some extent, on the same nutrients as cancer cells, finding a therapeutic window between proliferating cancer cells and proliferating normal cells is arguably the main challenge for the development of successful cancer therapies targeting metabolic pathways (Vander, 2011). Understanding the metabolic rewiring and adaptations that take place during CRC tumorigenesis can potentially identify vulnerabilities and highlight new therapeutic targets (Vander, 2011).

Recently, proline metabolism has received considerable attention (Tanner et al., 2018). The metabolism of proline has a critical importance for promoting cancer cell growth and proliferation. PYCR1, a key mitochondrial enzyme in proline biosynthesis, has been found overexpressed in many cancer types such as, breast, lung, melanoma, human B lymphoma, prostate and kidney cancers (Cai et al., 2018, Craze et al., 2017, De Ingeniis et al., 2012, Liu et al., 2015c, Loayza-Puch et al., 2016 and Elia et al., 2017; Ernst et al., 2002). A meta-analysis covering 1,981 tumours from 19 different types of cancers demonstrated that PYCR1 is one of the most commonly overexpressed genes in cancers (Nilsson et al., 2014).

In addition, proline biosynthesis through PYCRs isozymes is noticeably stimulated by the *c-MYC* oncogene, whereas the degradation of proline is activated by the *TP53* tumour suppressor gene via upregulation of PRODH (Craze et al., 2017 and Phang et al., 2012). The aim of the work described in this thesis was to elucidate the role of proline biosynthesis in CRC.

Firstly, we assessed the expression levels of enzymes of proline metabolism in CRC. Analysis of TMA and primary cells isolated from patients with CRC and colon polyps showed that PYCR1 enzyme is significantly overexpressed in tumours compared to the matched normal. Unfortunately, due to the limited material available, we were only able to assess expression of the PYCR1 enzyme, so investigation of other proline metabolism enzymes is warranted, although attempts in this direction might be hampered by unavailability of suitable antibodies for PYCR2 and PYCRL. Moreover, despite our TMA analysis indicating a statistically significant increase in PYCR1 protein in CRC tissue, the data were obtained from a relatively small cohort (32 CRC cases versus 32 normal intestinal tissues) and therefore an investigation in larger cohorts should be performed in the future.

In addition to TMA and primary cells, seven CRC cell lines were tested via RT-qPCR and western blot to measure the expression levels of proline metabolic enzymes including PYCR1, PYCR2, PYCRL and PRODH/POX. With the noticeable exception of SW480, protein expression data indicate that CRC cell lines express high levels of PYCR1 and relatively low levels of PRODH. The results of mRNA expression levels did not always match protein levels. In particular, *PRODH/POX* gene mRNA expression level was detected in all cell lines, whereas only SW480 protein expression level for this enzyme. Perhaps, post-transcriptional modifications and regulations could account for these differences. Notwithstanding, these data suggest that CRC cancer cells rely on increased PYCRs expression coupled to a concomitant silencing of PRODH/POX enzyme.

The reason for this switch toward proline biosynthesis remains unclear, however it is worth noticing that PRODH/POX was initially described as a p53 target gene necessary for p53-induced apoptosis (Polyak et al., 1997, Simon et al., 2000, Phang et al., 2010, Liang et al., 2013, Phang et al., 2008 a, b and Hu et al., 2007). PRODH/POX enzyme resides in the mitochondria and it is directly coupled to mitochondrial electron transport chain, therefore its induction in response to *TP53* activation has been linked to ROS

production and apoptosis (Liu and Phang, 2013). These data are also in agreement with recent findings showing the oncogene *c-MYC*, which plays a critical role in CRC development (Liu et al., 2012b and Sansom et al., 2007) promotes proline biosynthesis and decreases PRODH-POX expression through regulation of mir23b* (Liu et al., 2012 a and b, Wise et al., 2008, Gao et al., 2009, Hu et al., 2008, Li and Simon, 2013 and Phang et al., 2015).

To corroborate our data on expression of human *PYCR* genes in CRC, we examine the expression level of proline metabolic enzymes in the CRC mouse model, *Lgr5-Cre^{ER}/ Apc$^{fl/fl}$*. This mouse model is genetically engineered to mimic the loss of *APC* observed in CRC patients and deletion of the mouse *Apc* gene in the intestinal epithelium is achieved by intraperitoneal injection of tamoxifen (Barker et al., 2007). As detailed in section 4.1, we tested modulation of proline metabolism at three time points following deletion of *Apc*, three days, one week and two weeks and used Cre negative mice as controls.

Apc-depleted mice showed the typical signs of epithelium hyperplasia and dysplasia. In terms of proline metabolism, mRNA expression data, IHC and IF staining confirmed a significant upregulation of Pycr1 two weeks after *Apc* deletion. However, when we attempted to confirm these findings using western blotting, we failed to observe a similar increase in protein expression. Currently, the reason for this lack of consistency is unclear. Perhaps, results with western blotting have been biased by the fact that we collected and processed the whole intestine and did not enrich for the intestinal mucosa or, especially, epithelium. Ideally, if this experiment could be repeated on isolated crypts or intestinal organoids (Sato et al., 2011), a significant increase in Pycr1 protein levels could be successfully observed. Alternatively, longer time points following depletion of *Apc* could be analysed in order to assess Pycr1 expression in advanced adenomas, since these lesions take 6 to 8 weeks to develop.

The IHC and IF staining for Pycr1 showed that this protein is highly upregulated in the cryptal area of intestine, in line with the Cre recombinase being expressed in the intestinal stem cells. However, currently, we have no evidence to suggest that Pycr1 is expressed on ISC and/or Paneth cells, which could be investigated in the future using cell-specific markers and double staining with different fluorophores.

In the *Lgr5-Cre^{ER}/Apc$^{fl/fl}$* model, intestinal tumourigenesis is driven by activation of the Wnt signalling pathway and is dependent on sustained *c-Myc* activity (Sansom et al., 2007). Therefore, it is tempting to speculate that the increased expression of Pycr1 in the intestine of *Apc*-depleted mice is supported by *c-Myc*, although we cannot currently rule out a direct activation of the *Pyrc1* gene by the Wnt/β-catenin axis. It is also interesting to observe that RNA expression of the other Pycrs is not altered in the mice, at least within the time frame of this experiment. This is in line with most experimental evidence reporting selective upregulation of Pycr1 in tumours (Craze et al., 2017, Cai et al., 2018, Zeng et al., 2017 and Nilsson et al., 2014). Overall, the results obtained using the mouse model confirm, at least partially, the changes observed in human samples and suggest that PYCR1 upregulation might be an early event in colorectal carcinogenesis.

Overall, our results with regard to PYCR upregulation in CRC, suggest that these enzymes might support CRC tumourigenesis. In this regard, in kidney cancer, proline is a limiting amino acid for protein synthesis, and the depletion of PYCR1 expression is sufficient to impair proliferation of cancer cell (Loayza-Puch et al., 2016). Moreover, PYCR1 enzyme is overexpressed in human non-small cell lung carcinoma and prostate cancer, and its knockdown impairs proliferation of cancer cells (Cai et al., 2018, Zeng et al., 2017).

Cancer cell proliferation depends on biomass production, such as DNA from nucleotides, protein from amino acids and lipids from fatty (Elia et al., 2016). Proline biosynthesis has been shown to fuel protein production, which is needed for cell proliferation (Phang, 2017). Moreover, proline derived from collagen has been found to support pancreatic cancer cell proliferation (Olivares et al., 2017). The importance of proline for the proliferation of pancreatic cancer cells resulted not solely from direct incorporation of proline into proteins, but also via proline catabolism with concomitant production of glutamine, glutamate and aspartate, which, in turn, fuel the TCA cycle and precursors of nucleotides and/or proteins (Liu et al., 2012a and Liu et al., 2015c).

Interestingly, proline biosynthesis has also been suggested to contribute to biomass genration of the oxidased redox cofactor NAD(P)+. The resulting increase in NAD(P)+/NAD(P)H ratio stimulates the oxidative arm of pentose phosphate pathway, leading to production of ribose, the sugar constituent of nucleotides. (Liu et al., 2015b). In addition, NADPH/NADP+ ratio is also implicated in the maintenance of reduced

glutathione pool and therefore ROS scavenging. An involvement of PYCRs in regulation of glutathione could link again with a ROS-based model whereby increase proline biosynthesis and decreased catabolism help cancer cells to maintain their redox balance. In keeping, Kuo and colleagues found that mitochondrial PYCRs work as anti-oxidant factors, though direct binding with ribonucleotide reductase small subunit B (RRM2B), a stress response protein that protects cells from oxidative stress (Kuo et al., 2016).

All these findings prompted us to investigate whether the proline biosynthesis pathway is necessary for proliferation of CRC cells. In this study, we used commercially available siRNAs targeting PYCR1 and showed that PYCR1 knockdown has a significant effect on the proliferation of different CRC cell lines.

As revealed by immunoblotting analysis, PYCR1 knockdown triggered a dramatic decrease in Cyclin D1 and D3 levels. D cyclins are necessary for the progression through the G1 phase of the cell cycle (Holnthoner et al., 2002, Sakamaki et al., 2006, Bock et al., 2007 and Liang et al., 2015). During the G1 phase, they are produced rapidly and accumulate in the nucleus where they contribute to progression to S-phase by regulating cyclin-dependent kinases CDK4 and CDK6. The reduction in cyclins expression is therefore a hallmark of cell cycle arrest. Additionally, the cell cycle arrest triggered by PYCR1 depletion was confirmed by other experiments. Indeed, loss of PYCR1 protein also increased the expression of the cell cycle inhibitor p21, a cyclin-dependent kinase inhibitor (CKI) and the main mediator of p53 activity in response to DNA damage and other stressors that cause cell cycle arrest (Xiong et al., 1993, El-Deiry et al., 1993, Waldman et al., 1995 and Bunz, 1998).

Furthermore, when we measure directly DNA synthesis utilizing the Click-iT® EdU assay, we observed that PYCR1-depleted cells showed a significant and robust reduction in the percentage of EdU incorporation, especially RKO and SW60 cell lines. Overall, this is however, the first evidence that PYCR1 expression is necessary to sustain CRC tumorigenesis. It is worth noticing that this arrest in proliferation was observed under acute depletion of PYCR1 expression (72 hrs) and we have no information as to how cells would respond to chronic inactivation of the PYCR enzymes, a condition that would reflect more accurately a therapeutic scenario. Stable knockout of the *PYCR1* gene has been achieved in clear renal cell carcinoma cells using CRISPR/Cas9 technology (Loayza-Puch et al., 2016). In this case, the authors did not observe any growth defect in

vitro, but *PYCR1* knockout cells had delayed growth when xenografted in immunocompromised mice. Generation of CRC cell lines with stable knockdown or knockout of *PYCR1* and analysis of their growth in vivo would be a very interesting and important experiment to perform in the future.

To validate PYCR1 enzyme as a potential target for treatment of CRC, we investigated the effect of its knockdown on immortalized normal colon epithelial cells (HCEC) cell line. First of all, we assessed expression levels of PYCR1 enzyme in this cell type using immunoblotting technique and observed that PYCR1 was expressed at low levels, confirming its specific upregulation in cancer. In addition, PRODH/POX protein was also examined and showed robust expression level. When PYCR1 was knockdown in HCEC we did not observe any effect on cell survival and proliferation. These encouraging results suggest that PYCR1 expression is dispensable for normal epithelial cells. However, HCEC cells do not recapitulate the whole intestinal physiology. These cells were obtained by overexpression of *CDK4* and *hTERT* in human intestinal epithelial cells isolated from colonic crypts (Roig et al., 2010) and therefore were likely derived from stem cells. Therefore, we cannot exclude that PYCR1 is necessary for the normal function of specialized intestinal cells such as Paneth, enterocytes and goblet cells. The observation that this enzyme is expressed in normal human and mouse tissue suggests a role for PYCR1 in intestinal physiology. Additional experiments will be necessary to ascertain this possibility, including the development of knockout mouse models.

Nevertheless, our data seem to indicate that PYCR1 could be a suitable target for the development of anti-cancer therapies. In this case, an apoptotic response is arguably preferable to a cell cycle arrest, which might be only transient. Again, we cannot formally exclude that prolonged loss of PYCR1 might cause cell death in CRC cell lines, however so far we observed considerable apoptosis only in HCT116 cells.

Indeed, upon PYCR1 knockdown in HCT116, we observed a significant increase in apoptotic cells by AnnexinV-PI staining. This result demonstrates that PYCR1 expression is necessary for the survival of HCT116 CRC cell line. Similarly, previous studies have reported that depletion of PYCR1 in non-small cell lung cancer and prostate cancer induces apoptosis (Cai et al., 2018 and Zeng et al., 2017).

It is unclear at the moment, why HCT116 preferentially undergo apoptosis, whereas other cell lines, such as RKO, display cell cycle arrest in response to PYCR1 loss. Possibly, additional cell lines should be tested to understand whether a specific genetic feature is responsible for the observed response. Both HCT116 and RKO display microsatellite instability and CpG island methylation phenotype, but they have different mutations in driver genes (Ahmed et al., 2013). RKO cells have a mutant *BRAF*, whereas HCT116 have a mutation in *KRAS* and *CTNNB1* (the gene encoding for β-catenin) oncogenes (Berg et al., 2017). These differences might potentially explain the diverse responses of these cell lines to PYCR1 inhibition. Alternatively, transcriptomic profiling of cell lines exhibiting difference behaviours could provide insight into underline mechanisms.

Because of the high degree of sequence homology between the different PYCR genes, we investigated the selectivity of the siRNAs using real-time PCR and western blot technique. Robust reduction of PYCR1 expression, was associated with a concomitant decreased in the mRNA and protein levels of PYCR2. This result was not unexpected, given the high homology between these two isozymes (>80%). RNA data showed no changes in the expression of the cytosolic PYCRL isoform. Unfortunately, we were unable to validate this finding at the protein levels, as the most recent batches of PYCRL antibody performed very poorly. Overall, on the light of these results, we cannot rule out that the impact of PYCR1 knockdown on cell growth is at least partially mediated by the concomitant reduced expression of PYCR2. Possibly this issue could be resolved by the use of selective siRNAs designed to target less conserved region of the mRNAs (e.g. 3'UTR) and could discriminate between the two isoforms. Nonetheless, our data convincingly demonstrate that mitochondrial proline reductases are necessary for the proliferation of CRC cells.

One caveat when analysing metabolic pathway in vitro, is that the growth media do not fully mimic physiological nutrient availability (Metallo and Vander Heiden, 2014). For example, most culture media contain supra-physiological levels of glucose (4.5 mg/L vs 1 g/L in blood). This prompted us to investigate whether glucose availability influences dependence on PYCRs expression. Hence, PYCR1 knockdown was examined in SW620 CRC cell line using high (4500 mg/L) and low (1000 mg/L), or rather physiological, glucose Dulbecco′s Modified Eagle′s Medium (DMEM). The results showed a more severe decrease in cell growth when cells were cultured in low glucose media. This

decrease was attributable to reduced proliferation, as indicated by decreased EdU incorporation, lack of Cyclin D1 and D3 expression, and p21 upregulation. It is currently unclear why the phenotype triggered by loss of PYCR1 is exacerbated in low glucose media. Nonetheless, this behaviour is in agreement with evidence linking PYCR1 to the pentose phosphate pathway shunt or ATP production (Tanner et al., 2018). Investigation aimed at measurement of ATP or nucleotide biosynthesis in high versus low glucose conditions should be performed to confirm this link in CRC.

The proline-glucose axis might also help understanding why proline supplementation is unable to restore proliferation in PYCR1-depleted cells. In HCT116 cell line, despite supplemtation with 3 mM and 5 mM proline led to a general increase in cell numbers, it failed to rescue the growth deficiency in PYCR1-knockdown cells. Indeed, PYCR1 deficiency results in 50% decrease in cell number in vehicle treated samples, whereas reduction is limited to 75% when an excess of proline is provided, but this difference remains statistically significant when compared to scrambled siRNA control. It would be interesting to assess whether proline affects survival or proliferation in HCT116 cells, which do undergo apoptosis when PYCR1 is depleted, but also show signs of cell cycle arrest.

A possible-selective effect on cell death is suggested by the fact that proline-supplemented HCT116 cells still show a strong decreased in cyclins expression if PYCR1 is depleted. However, a proper analysis of apoptotic rate should be performed to validate this possibility. Similarly, in RKO and SW620 cells, an increase in cell number was observed when cells were supplemented with 5 mM proline, but the overall impact of PYCR1 depletion on cell number and expression of cell cycle markers remained unaffected.

Overall, these data suggest that proline production is not responsible for PYCR1's role in sustaining cell growth. Again, these findings are consistent with other reports showing that proline biosynthesis via PYCR1 is an important metabolic pathway that provides ATP, macromolecules and regulates the balance of NAD(P)H redox cofactors is association to ROS balance (Tanner et al, 2018 and Phang, 2017). Moreover, as mentioned previously, by generating oxidized NAD(P)+, PYCR1 activity is believed to increase flux through the oxidative arm of the pentose phosphate pathway, which in turn creates ribose precursors for nucleotide biosynthesis (Liu et al., 2015b).

Interestingly, PYCR1 has also been reported to play a fundamental function in the maintenance of mitochondrial integrity and function (Kuo et al., 2016). These findings suggest that depletion of PYCR1 may have a vital effect on cells even in presence of a copious supply of proline. On the other hand, a previous study on kidney cancer reported that addition of exogenous proline rescued loss of PYCR1 and promoted their growth and survival (Loayza-Puch et al., 2016). This might indicate the role of PYCR1 is likely tissue specific. Metabolomics studies and analysis of mitochondrial function following loss of PYCR1 expression will be necessary to shed light on the underlining mechanisms that allow PYCR1 to control cellular proliferation.

Concluding summary

In conclusion, this study clearly demonstrates that PYCR1 protein is highly expressed in CRC cases compared to normal tissue. The findings from the *Lgr5-Cre^{ER}/Apc$^{fl/fl}$* mouse model showed that Pycr1 expression is enhanced after constitutive activation of the Wnt pathway. Additionally, this study also provides convincing evidence that PYCR1 knockdown inhibits CRC cell growth by induction of cell cycle arrest and/or apoptosis and this effect appears to be selective for cancerous cells. Finally, despite the mechanism(s) responsible for PYCR1-mediated growth of CRC cells remains unknown, our data indicate that this function is independent of proline biosynthesis, as exogenous supplementation of excess of proline failed to rescue cancer cells from the consequence of PYCR1 knockdown.

Overall, the findings presented in this dissertation suggest that, potentially, PYCR1 is a novel target for the development of anti-tumour therapy against CRC.

References

Aberle, H., Bauer, A., Stappert, J., Kispert, A. and Kemler, R. (1997). Beta-Catenin is a Target for the Ubiquitin-Proteasome Pathway. *The EMBO Journal*, *16 (13)*, 3797–3804.http://doi.org/10.1093/emboj/16.13.3797.

Adams, E. (1970). Metabolism of proline and of hydroxyproline. Int. Rev. Connect. Tissue Res. 5:1–91.

Adams,E. and Frank, L. (1980). Metabolism of proline and the hydroxyprolines. Annu. Rev. Biochem. 49:1005–61.

Adegboyega, P. A., Mifflin, R. C., DiMari, J. F., Saada, J. I. and Powell, D. W. (2002). Immunohistochemical study of myofibroblasts in normal colonic mucosa, hyperplastic polyps, and adenomatous colorectal polyps. *Archives of Pathology and Laboratory Medicine*, 126 (7), 829-836. http://doi.org/10.1043/00039985 126 < 0829:ISOMIN>2.CO;2.

Ahmed, D., Eide, P. W., Eilertsen, I. A., Danielsen, S. A., Eknæs, M., Hektoen, M. and Lothe, R. A. (2013). Epigenetic and genetic features of 24-colon cancer cell lines. *Oncogenesis*, *2* (424). http://doi.org/10.1038/oncsis.2013.35.

Ahn, C. S. and Metallo, C. M. (2015). Mitochondria as biosynthetic factories for cancer proliferation. *Cancer and Metabolism*, 3(1), 1. http://doi.org/10.1186/s40170-015-0128-2.

Ahuja, N., Mohan, L., Li, Q., Stolker, M., Herman, G., Hamilton, R. and Issa, J. J. (1997). Colorectal Cancer', 3370–3375.

Akkoca, A. N., Yanık, S., Özdemir, Z. T., Cihan, F. G. and Sayar, S. (2014). Original Article TNM and Modified Dukes staging along with the demographic characteristics of patients with colorectal carcinoma, 7(9), 2828–2835.

Alexandrou, C., Al-Aqbi, S. S., Higgins, J. A., Boyle, W., Karmokar, A., Andreadi, C. and Rufini, A. (2018). Sensitivity of Colorectal Cancer to Arginine Deprivation Therapy is shaped by Differential Expression of Urea Cycle Enzymes. *Scientific Reports*, 8 (1), 12096. http://doi.org/10.1038/s41598-018-30591-7.

Almendingen K., H. B. (2001). Does high body fatness increase the risk of presence and growth of colorectal. *American Journal of Gastroenterology*, *96* (7).

American Cancer Society (ACS). (2017). Cancer Facts and Figures 2017,171.http://doi.org/10.1101/gad.1593107.

American Cancer Society (ASC). (2017). Colorectal Cancer Early Detection , Diagnosis , and Staging Can Colorectal Polyps and Cancer Be Found Early.

American Cancer Society (ASC). (2017). Colorectal Cancer Facts and Figures 2017 - 2019. *Atlanta*, 140.https://doi.org/http://dx.doi.org/10.1016/S0140-6736(13)61649-9.

Anastassiadis, K., Glaser, S., Kranz, A., Berhardt, K. and Stewart, A. F. (2010). A practical summary of site-specific recombination, conditional mutagenesis, and tamoxifen induction of CreERT2. *Methods in Enzymology*, 477(C), 109–123. http://doi.org/10.1016/S0076-6879 (10)77007-5.

Anders, R.A. (2011). Functional Histology of the Gastrointestinal Tract. *Johns Hopkins Pathology*, *16* (September), 1–100.

Andersen, C. L., Jensen, J. L., and Ørntoft, T. F. (2004). Normalization of Real-Time Quantitative Reverse Transcription-{PCR} Data: A Model-Based Variance Estimation Approach to Identify Genes Suited for Normalization, Applied to Bladder and Colon Cancer Data Sets TL-64. *Cancer Res*, 64 VN-r (15), 5245–5250. http://doi.org/10.1158/0008-5472.CAN-04-0496.

Armaghany, T., Wilson, J. D., Chu, Q. and Mills, G. (2012). Genetic alterations in colorectal cancer. *Gastrointestinal Cancer Research* : GCR, 5(1), 19–27. Retrieved from.http://www.ncbi.nlm.nih.gov/pubmed/22574233%5Cnhttp://www.pubmedcentral.nih.gov/articlerender.fcgi?artid=PMC3348713.

Asano, T., Katagiri, H., Takata, K., Lin, J. L., Ishihara, H., Inukai, K. and Oka, Y. (1991). The role of N-glycosylation of GLUT1 for glucose transport activity. *Journal of Biological Chemistry*, 266(36), 24632–24636.

Bach, S. P., Renehan, A. G. and Potten, C. S. (2000). Stem cells: the intestinal stem cell as aparadigm. *Carcinogenesis*, *21*(3), 469–476. https://doi.org/DOI10. 1093/carcin / 21.3.469.

Barker, N. (2014). Adult intestinal stem cells: Critical drivers of epithelial homeostasis and regeneration. *Nature Reviews Molecular Cell Biology*, 15(1), 19–33.http://doi.org/10.1038/nrm3721.

Barker, N., Ridgway, R. A., Van Es, J. H., Van De Wetering, M., Begthel, H., Van Den Born, M., and Clevers, H. (2009). Crypt stem cells as the cells-of-origin of intestinal cancer. *Nature*, 457(7229), 608–611. http://doi.org/10.1038/nature07602.

Barker, N., Van Es, J. H., Kuipers, J., Kujala, P., Van Den Born, M., Cozijnsen, M. and Clevers, H. (2007). Identification of stem cells in small intestine and colon by marker gene Lgr5. *Nature,* 449 (7165), 1003–1007. http :// doi.org /10.1038/ nature 06196.

Barker, N., Van Oudenaarden, A., and Clevers, H. (2012). Identifying the stem cell of the intestinal crypt: Strategies and pitfalls. *Cell Stem Cell*, *11*(4), 452460. http://doi.org /10.1016/j.stem.2012.09.009.

Barault, L., Charon-Barra, C., Jooste, V., De La Vega, M. F., Martin, L., Roignot, P. and Piard, F. (2008). Hypermethylator phenotype in sporadic colon cancer: Study on a population-based series of 582 cases. *Cancer Research*, *68*(20), 8541–8546. http://doi.org/10.1158/0008-5472.CAN-08-1171.

Behrens, J., von Kries, J. P., Kühl, M., Bruhn, L., Wedlich, D., Grosschedl, R. and Birchmeier, W. (1996). Functional interaction of β-catenin with the transcription factor LEF1. *Nature* .http://doi.org/10.1038/382638a0.

Bensaad, K., Tsuruta, A., Selak, M. A., Vidal, M. N. C., Nakano, K., Bartrons, R. and Vousden, K. H. (2006). TIGAR, a p53-Inducible Regulator of Glycolysis and Apoptosis. *Cell*, *126*(1), 107–120. http://doi.org/10.1016/j.cell.2006.05.036.

Berg, K. C. G., Eide, P. W., Eilertsen, I. A., Johannessen, B., Bruun, J., Danielsen, S. A. and Lothe, R. A. (2017). Multi-omics of 34 colorectal cancer cell lines - a resource

for biomedical studies. *Molecular Cancer*, *16*(1), 1–16. http:// doi. Org /10 . 1186 / s12943-017-0691-y.

Bertolo, R. F. and Burrin, D. G. (2008). Comparative aspects of tissue glutamine and proline metabolism. *The Journal of Nutrition*, 138(10), 2032S-2039S. http: // doi . org /138/10SI/2032S.

Bhanot, P., Brink, M., Samos, C. H., Hsieh, J.-C., Wang, Y., Macke, J. P., Nusse, R. (1996). A new member of the frizzled family from Drosophila functions as a Wingless receptor. *Nature*. http://doi.org/10.1038/382225a0.

Bock, W. J. (2007). Reproductive Biology and Phylogeny of Birds: Phylogeny, Morphology, Hormones, Fertilization (Volume 6A of Series). *Integrative and Comparative Biology*, *47*(5), 793–794. http://doi.org/10.1093/icb/icm060.

Boyiadzis, M. M., Kirkwood, J. M., Marshall, J. L., Pritchard, C. C., Azad, N. S. and Gulley, J. L. (2018). Significance and implications of FDA approval of pembrolizumab for biomarker-defined disease. *Journal for ImmunoTherapy of Cancer*, *6*(1), 1–7. http://doi.org/10.1186/s40425-018-0342-x.

Brahimi-Horn, M. C., Chiche, J. and Pouysségur, J. (2007). Hypoxia signalling controls metabolic demand. *Current Opinion in Cell Biology*, 19 (2), 223–229. http: // doi. org /10.1016/j.ceb.2007.02.003.

Breinbauer, R., and Köhn, M. (2003). Azide-Alkyne Coupling: A Powerful Reaction for Bioconjugate Chemistry. *ChemBioChem*, 4(11), 11471149. http:// doi . org / 10. 1002 /cbic.200300705.

Browne, D. (2014). Digestive System Module 5: The Small and Large Intestines, 1–13.

Buczacki, S. J. a, Zecchini, H. I., Nicholson, A. M., Russell, R., Vermeulen, L., Kemp, R. and Winton, D. J. (2013). Intestinal label-retaining cells are secretory precursors expressingLgr5. *Nature*, 495(7439), 65–9. http://doi.org/10.1038/nature11965.

Bunz, F. (1998). Requirement for p53 and p21 to Sustain G2 Arrest After DNA Damage. *Science*, 282 (5393), 1497–1501. http: // doi .org / 10. 1126/ science. 282.5393.1497.

Butler, L. M., Sinha, R., Millikan, R. C., Martin, C. F., Newman, B., Gammon, M. D. and Sandler, R. S. (2003). Heterocyclic amines, meat intake, and association with colon cancer in a population-based study. *American Journal of Epidemiology*, 157 (5), 434–445. https://doi.org/10.1093/aje/kwf221.

Cai, F., Miao, Y., Liu, C., Wu, T., Shen, S., Su, X., and Shi, Y. (2018). Pyrroline-5-carboxylate reductase 1 promotes proliferation and inhibits apoptosis in non-small cell lung cancer. *Oncology Letters*, 731–740. http: // doi .org /10. 3892 / ol.2017.7400.

Cai, F., Miao, Y., Liu, C., Wu, T., Shen, S., Su, X., and Shi, Y. (2017). Pyrroline-5-carboxylate reductase 1 promotes proliferation and inhibits apoptosis in non-small cell lung cancer. Oncology Letters, 731–740. http://doi .org /10. 3892 /ol.2017.7400.

Cairns, R. A., Harris, I. S. and Mak, T. W. (2011). Regulation of cancer cell metabolism. *Nature Reviews Cancer*, 11(2), 85–95. http://doi.org/10.1038/nrc2981.

Cancer Research UK (2014), available at: (https://www.cancerresearchuk.org/health-professional/cancer-statistics/statistics-by-cancer-type/bowel-cancer/survival#ref-3).

Cancer Research UK (2015), available at: (http://www.cancerresearchuk.org/health-professional/cancer-statistics/statistics-by-cancer-type/bowel cancer/incidence#headingZero).

Cancer Research UK (2015), available at: (https://www.cancerresearchuk.org/health-professional/cancer-statistics/statistics-by-cancer-type/bowel-cancer/incidence#heading-One).

Cancer Research UK (2016), available at: (https://www.cancerresearchuk.org/health-professional/cancer-statistics/statistics-by-cancer-type/bowel-cancer#heading-One).

Carethers, J. M., and Jung, B. H. (2015). Genetics and genetic biomarkers in sporadic colorectal cancer. *Gastroenterology*, 149 (5), 1177–1190. http:// doi.org /10.1053/j.gastro.2015.06.047.

Carmon, K. S., Gong, X., Lin, Q., Thomas, A., and Liu, Q. (2011). R-spondins function as ligands of the orphan receptors LGR4 and LGR5 to regulate Wnt/ -catenin signaling. *Proceedings of the National Academy of Sciences*, 108(28), 11452–11457. http://doi.org/10.1073/pnas.1106083108

Carulli, A. J., Samuelson, L. C., and Schnell, S. (2014). Unraveling intestinal stem cell behaviour with models of crypt dynamics. *Integrative Biology*, *6* (3), 243. http: // doi. org/10.1039/c3ib40163d.

Castellone, M. D. and Teramoto, H. (2005). Prostaglandin E 2 promotes colon cancer cell growth through a G s -Axin- b -Catenin signaling Axis, 1504–1511.

Cavallo, R. a, Cox, R. T., Moline, M. M., Roose, J., Polevoy, G. a, Clevers, H. and Bejsovec, A. (1998). Drosophila Tcf and Groucho interact to repress Wingless signalling activity. *Nature*, 395 (6702), 604–608. http://doi.org/10.1038/26982.

Cetta, F., Montalto, G., Gori, M., Curia, M. C., Cama, A. and Olschwang, S. (2000). Germline Mutations of the *APC* Gene in Patients with Familial Adenomatous Polyposis-Associated Thyroid Carcinoma: Results from a European Cooperative Study. *The Journal of Clinical Endocrinology and Metabolism*, 85(1), 286–292. http://doi.org/10.1210/jcem.85.1.6254.

Chao, A., Thun, M. J., Connell, C. J., McCullough, M. L., Jacobs, E. J., Flanders, W. D., and Calle, E. E. (2005). Meat consumption and risk of colorectal cancer. *Jama*, 293(2), 172–182. https://doi.org/10.1001/jama.293.2.172.

Chat-Uthai, N., Vejvisithsakul, P., Udommethaporn, S., Meesiri, P., Danthanawanit, C. and Wongchai, Y. and Poungvarin, N. (2018). Development of ultra-short PCR assay to reveal BRAF V600 mutation status in Thai colorectal cancer tissues. *PLoS ONE*, 13 (6), 1–16. http://doi.org/10.1371/journal.pone.0198795.

Chen, X. Y., Van Der Hulst, R. W. M., Shi, Y., Xiao, S. D., Tytgat, G. N. J., and Kate, F. J. W.Ten. (2001). Comparison of precancerous conditions: Atrophy and intestinal metaplasia in Helicobacter pylori gastritis among Chinese and Dutch patients. *Journal of Clinical Pathology*, 54 (5), 367–370. http:// doi. org/ 10. 1136 /jcp. 54.5.367.

Chen, W., Swanson, B. J. and Frankel, W. L. (2017). Molecular genetics of microsatellite-unstable colorectal cancer for pathologists. *Diagnostic Pathology*, 12 (1), 1–12. http://doi.org/10.1186/s13000-017-0613-8.

Christensen, E. M., Patel, S. M., Korasick, D. A., Campbell, A. C., Krause, K. L., Becker, D. F. and Tanner, J. J. (2017). Resolving the cofactor-binding site in the proline biosynthetic enzyme human pyrroline-5-carboxylate reductase 1. *Journal of Biological Chemistry*, 292(17), 7233–7243. http://doi. org/ 10.1074 /jbc. M117. 780288.

Clevers, H. (2013). The intestinal crypt, a prototype stem cell compartment. *Cell*, 154 (2), 274–284. http://doi.org/10.1016/j.cell.2013.07.004.

Clevers, H. and Nusse, R. (2012). Wnt/β-catenin signalling and disease. *Cell*, 149(6), 11921205. http://doi.org/10.1016/j.cell.2012.05.012.

Clevers, H. C. and Bevins, C. L. (2013). Paneth Cells: Maestros of the Small Intestinal Crypts. *Annual Review of Physiology*, 75(1), 289–311. http: //doi. org/ 10.1146/ annurev-physiol030212-183744

Clevers, H., Barker, N., Van Es, J. H., Kuipers, J., Kujala, P., Van Den Born, M and Cozijnsen, M., (2007). Identification of stem cells in small intestine and colon by marker gene Lgr5. *Nature*, 449(7165), 1003–1007. http: //doi .org /10 .1038 / nature 06196.

Cormerais, Y., Massard, P. A., Vucetic, M., Giuliano, S., Tambutté, E., Durivault, J. and Pouyssegur, J. (2018). The glutamine transporter ASCT2 (SLC1A5) promotes tumor growth independently of the amino acid transporter LAT1 (SLC7A5). *Journal of Biological Chemistry*, *293*(8), 2877–2887. http://doi.org /10.1074 /jbc. RA117.001342.

Cox, B., Kislinger, T. and Emili, A. (2005). Integrating gene and protein expression data: Pattern analysis and profile mining. *Methods*, 35 (3 SPEC.ISS.), 303–314. http://doi.org/10.1016/j.ymeth.2004.08.021.

Craze, M. L., Cheung, H., Jewa, N., Coimbra, N. D. M., Soria, D., El-Ansari, R. and Green, A. R. (2017). MYC regulation of glutamine–proline regulatory axis is key in luminal B breast cancer. *British Journal of Cancer*, 118(2), 258–265. http://doi.org/10.1038/bjc.2017.387.

Cunningham, D., Atkin, W., Lenz, H. J., Lynch, H. T., Minsky, B., Nordlinger, B. and Starling, N. (2010). Colorectal cancer. *The Lancet*, 375 (9719), 1030–1047. https:// doi.org / 10.1016/S0140-6736(10)60353-4.

Curi, R., Lagranha, C. J., Doi, S. Q., Sellitti, D. F., Procopio, J., Pithon-Curi, T. C. and Newsholme, P. (2005). Molecular mechanisms of glutamine action. *Journal of CellularPhysiology*, 204 (2), 392–401. http://doi.org/10.1002/jcp.20339.

Dang, C. V. (2012). Links between metabolism and cancer. *Genes and Development*, 26 (9), 877–890. http://doi.org/10.1101/gad.189365.112.

Dang, C. V. (2013). MYC, metabolism, cell growth, and tumorigenesis. *Cold Spring Harbor Perspectives in Medicine*, 3(8), 1–16. http:// doi.org /10. 1101/ cshperspect .a014217.

De Berardinis, R. J. and Chandel, N. S. (2016). Fundamentals of cancer metabolism. *Science Advances*, 2 (5). http://doi.org/10.1126/sciadv.1600200.

De Berardinis, R. J., Lum, J. J., Hatzivassiliou, G. and Thompson, C. B. (2008). The Biology of Cancer: Metabolic Reprogramming Fuels Cell Growth and Proliferation. *Cell Metabolism*, 7 (1), 11–20. http://doi .org/ 10.1016/ j.cmet. 2007. 10.002.

De Ingeniis, J., Ratnikov, B., Richardson, A. D., Scott, D. A., Aza-Blanc, P., De, S. K. and Smith, J. W. (2012). Functional Specialization in Proline Biosynthesis of Melanoma. *PLoS ONE,* 7(9), 1–9. http://doi.org/10.1371/journal.pone.0045190.

De Lau, W., Barker, N., Low, T. Y., Koo, B. K., Li, V. S. W., Teunissen, H., and Clevers, H. (2011). Lgr5 homologues associate with Wnt receptors and mediate R-spondin signalling. *Nature*, 476(7360), 293–297. http:// doi.org /10.1038 /nature 10337.

De Miglio, M. R., Pascale, R. M., Simile, M. M., Muroni, M. R., Virdis, P., Kwong, K. M. T. and Feo, F. (2004). Polygenic control of hepatocarcinogenesis in Copenhagen

X F344 rats. *International Journal of Cancer*, 111(1), 9–16. http://doi.org/10.1002/ijc.20225.

De Sousa E Melo, F., Wang, X., Jansen, M., Fessler, E., Trinh, A., De Rooij, L. P. M. H., Vermeulen, L. (2013). Poor-prognosis colon cancer is defined by a molecularly distinct subtype and develops from serrated precursor lesions. *Nature Medicine*, 19 (5), 614–618. http://doi.org/10.1038/nm.3174.

Derynck, R. and Zhang, Y. E. (2003). Smad-dependent and Smad-independent pathways inTGF-. *Nature*. http://doi.org/10.1038/nature02006.

Deryugina, E. I., and Quigley, J. P. (2006). Matrix metalloproteinases and tumor metastasis.*Cancer and Metastasis Reviews*, 25 (1), 9–34. http:// doi.org /10. 1007/ s10555-006-7886-9.

Dong, S., Lester, L. and Johnson, L. F. (2000). Transcriptional control elements and complex initiation pattern of the TATA-less bidirectional human thymidylate synthase promoter. *Journal of Cellular Biochemistry*, 77(1), 50–64. http:// doi.org/ 10.1002/(SICI)1097-4644(20000401)77:1<50::AID JCB6>3.0.CO;2-C.

Dougherty M., Brandriss, M., C. and Valle, D., K. (1992). Cloning Human Pyrrolin-5-carboxylate Reductase cDNA by Complementation in Saccharomyces cerevisiae. *The Journal of Biological Chemistry*, 267 (2), 871.

Dtxit, S. N., Seyer, J. M., and Kang, A. (1977). Covalent Structure of Collagen . Sequence of Chymo ryptic Peptides from the Garboxyl-Terminal Reg on of a2-CB3 ofChick-Skin Collagen. *Amino Acid*, (607), 599–607.

East, J. E., Vieth, M. and Rex, D. K. (2015). Serrated lesions in colorectal cancer screening: Detection, resection, pathology and surveillance. *Gut*, 64 (6), 991–1000. http://doi.org/10.1136/gutjnl-2014-309041.

El-Deiry, W. S., Tokino, T., Velculescu, V. E., Levy, D. B., Parsons, R., Trent, J. M. and Vogelstein, B. (1993). WAR, a Potential Mediator of 53 Tumor Suppression. *Cell*, 75, 817–825.

Elia, I., Broekaert, D., Christen, S., Boon, R., Radaelli, E., Orth, M. F. and Fendt, S. M. (2017). Proline metabolism supports metastasis formation and could be inhibited to selectively target metastasizing cancer cells. *Nature Communications*, 8, 1–11. http://doi.org/10.1038/ncomms15267.

Elia, I., Schmieder, R., Christen, S., and Fendt, S.-M. (2016) Organ-specific cancer metabolism and its potential for therapy. *Handb Exp Pharmacol*, 233, 321-353.

Erisman, M. D., Rothberg, P. G., Diehl, R. E., Morse, C. C., Spandorfer, J. M. and Astrin, S. M. (1985). Deregulation of c-*Myc* Gene Expression in Human Colon Carcinoma Is Not Accompanied by Amplification or Rearrangement of the Gene. *Molecular and Cellular Biology*, 5 (8), 1969–1976. http:// doi.org/ 10.1128 /MCB .5.8.1969.

Ernst, T., Hergenhahn, M., Kenzelmann, M., Cohen, C. D., Bonrouhi, M., Weninger, A. and Gröne, H. J. (2002). Decrease and gain of gene expression are equally discriminatory markers for prostate carcinoma: A gene expression analysis on total and microdissected prostate tissue. *American Journal of Pathology*, 160 (6), 2169–2180. http://doi.org/10.1016/S0002-9440 (10)61165-0.

Faubert, B., Li, K. Y., Cai, L., Hensley, C. T., Kim, J., Zacharias, L. G. and DeBerardinis, R. J. (2017). Lactate Metabolism in Human Lung Tumors. *Cell*, 171 (2), 358–371. http://doi.org/10.1016/j.cell.2017.09.019.

Fearnhead, N. S. (2001). The ABC of *APC*. *Human Molecular Genetics*, 10 (7), 721–733. http://doi.org/10.1093/hmg/10.7.721.

Fearnhead, N. S. , Wilding, J.L, and Bodmer, W. F. (2002). Genetics of colorectal cancer hereditary: aspects and overview of colorectal tumorigenesis. *British MedicalBulletin*, 64 (1), 27-43. https://doi.org/10.1093/bmb/64.1.27.

Fearon, E. F. and Vogelstein, B. (1990). Colorectal Tumorigenesis. *Cell*, 61 (1), 759–767.

Feil, S., Valtcheva, N., and Feil, R. (2009). Inducible Cre mice. *Methods in Molecular Biology* (Vol. 530). http://doi.org/10.1007/978-1-59745-471-1_18.

Feun, L.G., Kuo, M.T. and Savaraj, N. (2015) Arginine deprivation in cancer therapy. *Curr Opin Clin Nutr Metab Care*, 18 (1):78–82.http://doi: 10.1097 /MCO. 122.

Feun, L. G., Marini, A., Walker, G., Elgart, G., Moffat, F., Rodgers, S. E. and Savaraj, N. (2012). Negative argininosuccinate synthetase expression in melanoma tumours may predict clinical benefit from arginine-depleting therapy with pegylated arginine deiminase. *British Journal of Cancer*, 106 (9), 1481–1485. http://doi.org/10.1038/bjc.2012.106.

Fevr, T., Robine, S., Louvard, D. and Huelsken, J. (2007). Wnt/ -Catenin Is Essential for Intestinal Homeostasis and Maintenance of Intestinal Stem Cells. *Molecular and Cellular Biology*, 27(21), 7551–7559. http://doi.org/10.1128/MCB.01034-07.

Fichman, Y., Gerdes, S. Y., Kovács, H., Szabados, L., Zilberstein, A. and Csonka, L. N. (2015). Evolution of proline biosynthesis: Enzymology, bioinformatics, genetics, and transcriptional regulation. *Biological Reviews*, 90(4), 1065–1099. http://doi.org/10.1111/brv.12146.

Fleming, M., Ravula, S., Tatishchev, S. F., and Wang, H. L. (2012). Colorectal carcinoma: Pathologic aspects. *Journal of Gastrointestinal Oncology*, 3(3), 153–173. http://doi.org/10.3978/j.issn.2078-6891.2012.030

Foekens, J. A., Romain, S., Look, M. P., Martin, P. and Klijn, J. G. M. (2001). Thymidine Kinase and Thymidylate Synthase in Advanced Breast Cancer : Response to Tamoxifen and Chemotherapy. *Cancer Research*, 61, 1421–1425. http://doi.org/PMID: 11245445.

Fre, S., Huyghe, M., Mourikis, P., Robine, S., Louvard, D. and Artavanis-Tsakonas, S. (2005). Notch signals control the fate of immature progenitor cells in the intestine. *Nature*, 435(7044), 964–968. http://doi.org/10.1038/nature03589.

Fredericks, E., Dealtry, G. and Roux, S. (2015). Molecular aspects of ColorectalCarcinogenesis : A Review. *Journal of Cancer Biology and Research*, 3 (1), 1057–1062.

Friedenreich, C. M. and Orenstein, M. R. (2002). On Food, Nutrition and Cancer Physical Activity and Cancer Prevention : *Etiologic Evidence and Biological Mechanisms* 1, 2, (1), 3456-3464.

Fung, M. K. L. and Chan, G. C. F. (2017). Drug-induced amino acid deprivation as strategy for cancer therapy. *Journal of Hematology and Oncology*, 10 (1), 1–18. http://doi.org/10.1186/s13045-017-0509-9.

Furuta, E., Okuda, H., Kobayashi, A. and Watabe, K. (2010). Metabolic genes in cancer: Their roles in tumor progression and clinical implications. *Biochimica et Biophysica Acta - Reviews on Cancer*, 1805(2), 141–152. http:// doi.org /10.1016 /j.bbcan.2010.01.005.

Gao, P., Tchernyshyov, I., Chang, T. C., Lee, Y. S., Kita, K., Ochi, T. and Dang, C. V. (2009). *c-Myc* suppression of miR-23a/b enhances mitochondrial glutaminase expression and glutamine metabolism. *Nature*, 458 (7239), 762–765. http:// doi.org /10.1038/nature07823.

Gassler, N. (2017). Paneth cells in intestinal physiology and pathophysiology. World *Journal of Gastrointestinal Pathophysiology*, 8 (4), 150–160. http://doi.org /10 .4291/wjgp.v8.i4.150.

Gelberg, H. B. (2014). Comparative Anatomy, Physiology, and Mechanisms of Disease Production of the Esophagus, Stomach, and Small Intestine. *Toxicologic Pathology*, (42), 54-66. http:// doi.org/10.1177/0192623313518113.

Gemayel, R., Cho, J., Boeynaems, S. and Verstrepen, K. J. (2012). Beyond junk-variable tandem repeats as facilitators of rapid evolution of regulatory and coding sequences. *Genes*, 3 (3), 461–480. http://doi.org/10.3390/genes3030461.

Giovannucci, E., Stampfer, M. J., Colditz, G. A., Rimm, E. B., Trichopoulos, D., Rosner, B. A. and Willett, W. C. (1993). Folate, Methionine, and Alcohol Intake and Risk of Colorectal Adenoma. *JNCI Journal of the National Cancer Institute*, 85 (11), 875–883. https://doi.org/10.1093/jnci/85.11.875.

Giovannucci, E., Stampfer, M. J., Colditz, G., Rimm, E. B. and Willett, W. C. (1992). Relationship of diet to risk of colorectal adenoma in men. *Journal of the National CancerInstitute*, 84 (2), 91–8. Retrieved from http:// www.ncbi. nlm.nih.gov/ pubmed / 1310511.

Grady, W. M. and Carethers, J. M. (2008). Genomic and Epigenetic Instability in Colorectal Cancer Pathogenesis. *Gastroenterology*, *135* (4), 1079–1099. http:// doi.org/ 10.1053/j.gastro.2008.07.076.

Green, A. R., Aleskandarany, M. A., Agarwal, D., Elsheikh, S., Nolan, C. C., Diez-Rodriguez, M. and Rakha, E. A. (2016). *MYC* functions are specific in biological subtypes of breast cancer and confers resistance to endocrine therapy in luminal tumours. *British Journal of Cancer*, 114 (8), 917–928. http:// doi.org /10.1038 /bjc. 2016.46.

Greenlee, R. T., Hill-Harmon, M. B., Murray, T. and Thun, M. (2001). Cancer Statistics.

Gregorieff, A., Pinto, D., Begthel, H., Destrée, O., Kielman, M. and Clevers, H. (2005). Expression pattern of Wnt signaling components in the adult intestine. *Gastroenterology*, 129 (2), 626–638. http://doi.org/10.1016/j.gastro.2005.06.007.

Guertin, D. A., and Sabatini, D. M. (2007). Defining the Role of mTOR in Cancer. *Cancer Cell*, 12 (1), 9–22. http://doi.org/10.1016/j.ccr.2007.05.008.

Gupta, G. P. and Massagué, J. (2006). Cancer Metastasis: Building a Framework. *Cell*, 127 (4), 679–695. http://doi.org/10.1016/j.cell.2006.11.001.

Hack, C. J. (2004). Integrated transcriptome and proteome data: The challenges ahead. *Briefings in Functional Genomics and Proteomics*, 3 (3), 212–219. http:/ / doi.org / 10.1093/bfgp/3.3.212.

Hagedorn, C. H. and Phang, J. M. (1983).Transfer of reducing equivalents into mitochondria by the interconversions of proline and delta1-pyrroline-5-carboxylate. *Arch.Biochem.Biophys*, 225, 95–101. http://doi.org/10.1016/0003-9861(83)90010-3.

Hail, N. (2005). Mitochondria: A novel target for the chemoprevention of cancer. *Apoptosis*, 10 (4), 687–705. http://doi.org/10.1007/s10495-005-0792-8.

Haines, R. J., Pendleton, L. C. and Eichler, D. C. (2011). Argininosuccinate synthase: At the center of arginine metabolism. *International Journal of Biochemistry and Molecular Biology*, 2 (1), 8–23.

Hanahan, D. and Weinberg, R. A. (2011). Hallmarks of cancer: The next generation. *Cell*, 144(5), 646–674. http://doi.org/10.1016/j.cell.2011.02.013.

Hanahan, D. and Weinberg, R. A. (2000). The hallmarks of cancer. Cell, 100(1), 57-70. http://doi.org/10.1007/s00262-010-0968-0.

Hao, X. P. (2002). The spectrum of *p53* mutations in colorectal adenomas differs from that in colorectal carcinomas. *Gut*, *50*(6), 834–839. http:// doi.org/ 10.1136 /gut. 50.6.834.

Haque, T., Greene, K. G., and Crockett, S. D. (2014). Serrated neoplasia of the colon: What do we really know? *Current Gastroenterology Reports*, 16 (4). http://doi.org/ 10.1007/s11894-014-0380-6.

Haramis, A.-P. G. (2004). De Novo Crypt Formation and Juvenile Polyposis on BMP Inhibition in Mouse Intestine. *Science*, 303 (5664), 1684-1686. http:// doi.org/ 10.1126 /science.1093587.

Hardwick, J. C., Kodach, L. L., Offerhaus, G. J. and van den Brink, G. R. (2008). Bone morphogenetic protein signalling in colorectal cancer. *Nature Reviews Cancer*, 8 (10), 806–812. http://doi.org/10.1038/nrc2467.

Hawkins, N., Norrie, M., Cheong, K., Mokany, E., Ku, S. L., Meagher, A. and Ward, R. (2002). CpG island methylation in sporadic colorectal cancers and its relationship to microsatellite instability. *Gastroenterology*, *122*(5), 1376–1387. http://doi.org/10.1053/gast.2002.32997.

He, T., Sparks, A. B., Rago, C., Hermeking, H., Zawel, L., Costa, L. T., and Kinzler, K. W. (1998). Identification of *c- MYC* as a Target of the *APC* Pathway. *Science*, 281, 1509–1512. http://doi.org/10.1126/science.281.5382.1509.

He, X. C., Zhang, J., Tong, W.-G., Tawfik, O., Ross, J., Scoville, D. H. and Li, L. (2004). BMP signaling inhibits intestinal stem cell self-renewal through suppression of Wnt–β-cateninsignaling. *Nature Genetics*, 36 (10), 1117–1121. http:// doi.org/ 10. 1038/ng1430.

He, X., Tamai, K., Semenov, M., Kato, Y., Spokony, R., Liu, C. and Saint-Jeannet, J.-P. (2000). LDL-receptor-related proteins in Wnt signal transduction. *Nature*, 407 (6803), 530–535. http://doi.org/10.1038/35035117.

Heindryckx, F., Colle, I. and Van Vlierberghe, H. (2009). Experimental mouse models for hepatocellular carcinoma research. *International Journal of Experimental Pathology*, 90 (4), 367–386. http://doi.org/10.1111/j.1365-2613.2009.00656.x.

Heitman, S. J., Ronksley, P. E., Hilsden, R. J., Manns, B. J., Rostom, A., and Hemmelgarn, B. R. (2009). Prevalence of Adenomas and Colorectal Cancer in Average Risk Individuals: A Systematic Review and Meta-analysis. *Clinical Gastroenterology and Hepatology*, 7 (12), 1272–1278. http://doi.org /10.1016/j .cgh.2009.05.032.

Henderson, B. R. (2000). Nuclear-cytoplasmic shuttling of APC regulates beta-catenin subcellular localization and turnover. *Nature Cell Biology*, 2 (9), 653–660. http://doi.org/10.1038/35023605.

Henson, E. S., and Gibson, S. B. (2006). Surviving cell death through epidermal growth factor (EGF) signal transduction pathways: Implications for cancer therapy. *Cellular Signalling*, 18 (12), 2089–2097. http:// doi.org/ 10.1016/ j.cellsig. 2006.05.015.

Heyer, J., Heyer, J., Yang, K., Yang, K., Lipkin, M., Lipkin, M. and Kucherlapati, R. (1999). Mouse models for colorectal cancer. *Oncogene*, 18 (38), 5325–5333. http://doi.org/10.1038/sj.onc.1203036.

Hingorani, R., Deng, J., Elia, J., McIntyre, C. and Mittar, D. (2011). Detection of Apoptosis Using the BD Annexin V FITC Assay on the BD FACSVerse™ System. *BD Biosciences, August*, 1–12. http://doi.org/ 10.1016/j. pestbp.2011. 02.012.Investigations

Hollinshead, K. E. R., Munford, H., Eales, K. L., Bardella, C., Li, C., Escribano-Gonzalez, C. and Tennant, D. A. (2018). Oncogenic *IDH1* Mutations Promote Enhanced Proline Synthesis through PYCR1 to Support the Maintenance of Mitochondrial Redox Homeostasis. *Cell Reports*, 22 (12), 3107–3114. http:// doi.org /10.1016/j.celrep.2018.02.084.

Holnthoner, W., Pillinger, M., Groger, M., Wolff, K., Ashton, A. W., Albanese, C. and Petzelbauer, P. (2002). Fibroblast growth factor-2 induces Lef/Tcf-dependent transcription in human endothelial cells. *The Journal of Biological Chemistry*, 277 (48), 45847–53. http://doi.org/10.1074/jbc.M209354200.

Hong-qi, Z., Croes, A. F. and Linskens, H. F. (1982). Protein synthesis in germinating pollen of Petunia: role of proline. *Planta*, 154(3), 199–203. http:// doi.org /10.1007 /BF00387864.

Horovitz, O. and Paşca, R.-D. (2017). Classification of amino acids by multivariate data analysis, based on thermodynamic and structural characteristics. *Studia Universitatis Babes-Bolyai Chemia*, 62 (2Tom1). http://doi.org/10.24193/ subbchem. 2017.2.02.

Hosios, A. M., Hecht, V. C., Danai, L. V, Johnson, M. O., Jeffrey, C., Steinhauser, M. L. and Vander, M. G. (2017). *HHS Public Access*, 36 (5), 540–549. http:// doi.org/ 10.1016 /j.devcel.2016.02.012.

Howe, G. R., Benito, E., Castelleto, R., Corne, J., Estve, J., Gallagher, R. P., Zheng, S. (1992). Dietary intake of fibre and decreased risk of cancers of the colon and rectum: evidence from the combined analysis of 13 case- control studies. *J.Natl.Cancer Inst.*, 84 (24), 18871896.

Hu, C. A., and Hou, Y. (2014). Mammalian P5CR and P5CDH : Protein Structure and Disease Association, 8–11.

Hu, C. A., Bart Williams, D., Zhaorigetu, S., Khalil, S., Wan, G., and Valle, D. (2008). Functional genomics and SNP analysis of human genes encoding proline metabolicenzymes. *Amino Acids*, 35 (4), 655–664. http://doi.org/10.1007/s00726-008-0107-9.

Hu, C. A., Donald, S. P., Yu, J., Lin, W. W., Liu, Z., Steel, G. and Phang, J. M. (2007). Overexpression of proline oxidase induces proline-dependent and mitochondria-mediated apoptosis. *Molecular and Cellular Biochemistry*, 295 (1–2), 85–92. http://doi.org/10.1007/s11010-006-9276-6.

Hu, W., Zhang, C., Wu, R., Sun, Y., Levine, A. and Feng, Z. (2010). Glutaminase 2, a novel p53 target gene regulating energy metabolism and antioxidant function. *Proceedings of the National Academy of Sciences*, 107 (16), 7455–7460. http:// doi.org/10.1073/pnas.1001006107.

Hui, S., Ghergurovich, J. M., Morscher, R. J., Jang, C., Teng, X., Lu, W. and Rabinowitz, J. D. (2017). Glucose feeds the TCA cycle via circulating lactate. *Nature*, 551 (7678), 115–118. http://doi.org/10.1038/nature24057.

Hursting, S. D., Thornquist, M. and Henderson, M. M. (1990). Types of dietary fat and the incidence of cancer at five sites. *Preventive Medicine*, 19 (3), 242–253. https://doi.org/10.1016/0091-7435(90)90025-F.

Jackson-Grusby, L. (2002). Modeling cancer in mice. *Oncogene*, 21 (35 REV. ISS. 3), 5504-5514. http://doi.org/10.1038/sj.onc.1205603.

Jackstadt, R. and Sansom, O. J. (2016). Mouse models of intestinal cancer. *Journal of Pathology*, 238 (2), 141–151. http://doi.org/10.1002/path.4645.

Jemal, A., Siegel, R., Ward, E., Murray, T., Xu, J. and Thun, J. (2007). Cancer Statistics.

Jemal, A., Siegel, R., Ward, E., Murray, T., Xu, J., Smigal, C. and Thun, M. J. (2006). Cancer Statistics.

Kabiri, Z., Greicius, G., Madan, B., Biechele, S., Zhong, Z., Zaribafzadeh, H., and Virshup. (2014). Stroma provides an intestinal stem cell niche in the absence of epithelial Wnts. Development, 141 (11), 2206–2215. http:// doi.org/ 10.1242 /dev. 104976.

Kakkad, S. M., Solaiyappan, M., O'Rourke, B., Stasinopoulos, I., Ackerstaff, E., Raman, V. and Glunde, K. (2010). Hypoxic Tumor Microenvironments Reduce Collagen I Fiber Density. *Neoplasia*, 12 (8), 608–617. http:// doi.org /10.1593 /neo. 10344.

Kanas, G. P., Taylor, A., Primrose, J. N., Langeberg, W. J., Kelsh, M. A., Mowat, F. S., Poston, G. (2012). Survival after liver resection in metastatic colorectal cancer: review and meta-analysis of prognostic factors. *Clin Epidemiol*, 4, 283–301. http://doi.org/10.2147/clep.s34285.

Kawakami, R., Satomura, T., Sakuraba, H. and Ohshima, T. (2012). L-Proline dehydrogenases in hyperthermophilic archaea: Distribution, function, structure, and application. *Applied Microbiology and Biotechnology*, 93 (1), 83–93. http:// doi.org/10.1007/s00253-011-3682-8.

Keshet, R. and Erez, A. (2018). Arginine and the metabolic regulation of nitric oxide synthesis in cancer. *Disease Models and Mechanisms*, 11 (8), 332-336. http:// doi.org/10.1242/dmm.033332.

Kim, E., Goraksha-Hicks, P., Li, L., Neufeld, T. P. and Guan, K. L. (2008). Regulation of TORC1 by Rag GTPases in nutrient response. *Nature Cell Biology*, 10 (8), 935–945. http://doi.org/10.1038/ncb1753.

Kim, J. W., Tchernyshyov, I., Semenza, G. L. and Dang, C. V. (2006). HIF-1-mediated expression of pyruvate dehydrogenase kinase: A metabolic switch required for cellular adaptation to hypoxia. *Cell Metabolism*, 3 (3), 177–185. http:// doi.org /10.1016/j.cmet.2006.02.002.

Kim, K.-A., Kakitani, M., Zhao, J., Oshima, T., Tang, T., Binnerts, M., and Tomizuka, K. (2005). Materials and Methods Suppl data : Mitogenic influence of human R-spondin1 on the intestinal epithelium. *Science*, 309 (3), 1256–1260.

Knott, S. R. V., Wagenblast, E., Khan, S., Kim, S. Y., Soto, M., Wagner, M. and Hannon, G. J. (2018). Asparagine bioavailability governs metastasis in a model of breast cancer. *Nature*, 554 (7692), 378–381. http://doi.org/10.1038/nature25465.

Korinek, V., Barker, N., Morin, P. J., van Wichen, D., de Weger, R., Kinzler, K. W. and Clevers, H. (1997). Constitutive transcriptional activation by a b-catenin-Tcf complex in *APC*-/- colon carcinoma. *Science*, 275, 1784–1787. http:// doi.org/ 10.1126/science.275.5307.1784.

Korinek, V., Barker, N., Willert, K., Molenaar, M., Roose, J., Wagenaar, G. and Clevers, H. (1998). Two Members of the Tcf Family Implicated in Wnt/β-Catenin Signaling during Embryogenesis in the Mouse. *Molecular and Cellular Biology*, 18 (3), 1248–1256.http://doi.org/10.1128/MCB.18.3.1248.

Kosinski, C., Li, V. S. W., Chan, A. S. Y., Zhang, J., Ho, C., Tsui, W. Y. and Chen, X. (2007). Gene expression patterns of human colon tops and basal crypts and BMP antagonists as intestinal stem cell niche factors. *Proceedings of the National Academy of Sciences of the United States of America*, 104 (39), 15418–23. http://doi.org/10.1073/pnas.0707210104.

Krall, A. S., Xu, S., Graeber, T. G., Braas, D. and Christofk, H. R. (2016). Asparagine promotes cancer cell proliferation through use as an amino acid exchange factor. *Nature Communications*, 7, 1–13. http://doi.org/10.1038/ncomms11457.

Kuhnert, F., Davis, C. R., Wang, H.-T., Chu, P., Lee, M., Yuan, J., and Kuo, C. J. (2004). Essential requirement for Wnt signaling in proliferation of adult small intestine and colon revealed by adenoviral expression of Dickkopf-1. *Proceedings of the National Academy of Sciences*, 101 (1), 266–271. http://doi.org/ 10.1073/ pnas.2536800100.

Kuo, M. L., Lee, M. B. E., Tang, M., Den Besten, W., Hu, S., Sweredoski, M. J. and Yen, and Y. (2016). PYCR1 and PYCR2 Interact and Collaborate with RRM2B to Protect Cells from Overt Oxidative Stress. *Scientific Reports*, 6, 115. http:// doi.org/10.1038/srep18846.

Kuo, M. T., Savaraj, N. and Feun, L. G. (2010). Targeted cellular metabolism for cancer chemotherapy with recombinant arginine-degrading enzymes Abstract : Glycolysis TCA cycle. *Oncotarget*, 1 (4), 246–251. http:// doi.org/ 10.2174/ 138161208784246199.

Kutyavin, I. V, Afonina, I. a, Mills, a, Gorn, V. V, Lukhtanov, E. a, Belousov, E. S., and Hedgpeth, J. (2000). 3'-minor groove binder-DNA probes increase sequence specificity at PCR extension temperatures. *Nucleic Acids Research*, 28 (2), 655–661. http://doi.org/10.1093/nar/28.2.655.

Labuschagne, C. F., van den Broek, N. J. F., Mackay, G. M., Vousden, K. H. and Maddocks, O. D. K. (2014). Serine, but not glycine, supports one-carbon metabolism and proliferation of cancer cells. *Cell Reports*, 7 (4), 1248–1258. http://doi.org/10.1016/j.celrep.2014.04.045.

LaMonte, G., Tang, X., Chen, J. L.-Y., Wu, J., Ding, C.-K., Keenan, M. M. and Chi, J.-T. (2013). Acidosis induces reprogramming of cellular metabolism to mitigate oxidative stress. *Cancer and Metabolism*, 1 (1), 23. http://doi.org/10.1186/2049-3002-1-23.

Lane, A. N., and Fan, T. W. M. (2015). Regulation of mammalian nucleotide metabolism and biosynthesis. *Nucleic Acids Research*, 43 (4), 2466–2485. http://doi.org/10.1093/nar/gkv047.

Le, A., Lane, A. N., Hamaker, M., Bose, S., Gouw, A., Barbi, J. and Dang, C. V. (2012). Glucose-independent glutamine metabolism via TCA cycling for proliferation and survival in b cells. *Cell Metabolism*, 15(1), 110-121. http:// doi.org/10.1016/j.cmet.2011.12.009.

Li, B., and Simon, M. C. (2013). Molecular pathways: Targeting *MYC*-induced metabolic reprogramming and oncogenic stress in cancer. *Clinical Cancer Research,* 19 (21), 5835-5841. http://doi.org/10.1158/1078-0432.CCR-12-3629.

Li, F., Wang, Y., Zeller, K. I., Potter, J. J., Wonsey, D. R., Donnell, K. a O. and Dang, C. V. (2005). *Myc* Stimulates Nuclearly Encoded Mitochondrial Genes and Mitochondrial Biogenesis. *Molecular and Cellular Biology*, 25 (14), 6225–6234. http://doi.org/10.1128/MCB.25.14.6225.

Li, T., Kon, N., Jiang, L., Tan, M., Ludwig, T., Zhao, Y. and Gu, W. (2012). Tumor suppression in the absence of *p53*-mediated cell-cycle arrest, apoptosis, and senescence. *Cell*, 149 (6), 1269–1283. http://doi.org/10.1016/j.cell.2012.04.026.

Liang, D., Xue, H., Yu, Y., Lv, F., You, W. and Zhang, B. (2015). Elevated expression of UHRF1 predicts unfavorable prognosis for patients with hepatocellular carcinoma. *International Journal of Clinical and Experimental Pathology*, 8 (8), 9416–9421. http://doi.org/10.1091/mbc.02

Liang, X., Zhang, L., Natarajan, S. K., and Becker, D. F. (2013). Proline Mechanisms of Stress Survival. *Antioxidants and Redox Signaling*, 19 (9), 998-1011. http:// doi.org/10.1089/ars.2012.5074.

Lichtenstein, P., Holm, N. V. and Verkasalo, P. K. et al. (2000). Environmental and heritable factors in the causation of cancer – analysis of cohorts of twins from Sweden, DenmarkandFinland. *The new England journal of medicine,* 343 (2), 78-85.

Lin, C. Y., Lovén, J., Rahl, P. B., Paranal, R. M., Burge, C. B., Bradner, J. E. and Young, R. A. (2012). Transcriptional amplification in tumor cells with elevated *c-Myc*. *Cell*, 151 (1), 56–67. http://doi.org/10.1016/j.cell.2012.08.026.

Lin, C., Ng, H. L. H., Pan, W., Chen, H., Zhang, G., Bian, Z. and Yang, Z. (2015). Exploring different strategies for efficient delivery of colorectal cancer therapy. *International Journal of Molecular Sciences*, 16 (11), 26936–26952. http:// doi.org /10.3390/ijms161125995.

Liu, L. L., Zhao, H., Ma, T. F., Ge, F., Chen, C. S., and Zhang, Y. P. (2015a). Identification of valid reference genes for the normalization of RT-qPCR expression studies in human breast cancer cell lines treated with and without transient transfection. *PLoS ONE*, 10 (1).1–15. http://doi.org /10.1371/ journal. pone.0117058.

Liu, W. and Phang, J. M. (2013). MiRNA and Proline Metabolism in Cancer. Medicine.Oncology, Oncogene and Cancer - From Bench to Clinic", book editedbyYahwardiah Siregar, ISBN 978-953-51-0858-0. http://doi.org/ 10.5772 /55139.

Liu, W., Glunde, K., Bhujwalla, Z. M., Raman, V., Sharma, A. and Phang, J. M. (2012a). Proline oxidase promotes tumor cell survival in hypoxic tumor microenvironments. *Cancer Research*, 72 (14), 3677–3686. http:// doi.org/ 10.1158/ 0008-5472.CAN-12-0080.

Liu, W., Hancock, C. N., Fischer, J. W., Harman, M. and Phang, J. M. (2015b). Proline biosynthesis augments tumor cell growth and aerobic glycolysis: Involvement of pyridine nucleotides. *Scientific Reports*, 5,1–13. http://doi.org/10.1038/srep17206.

Liu, W., Le, A., Hancock, C., Lane, A. N., Dang, C. V., Fan, T. W. M. and Phang, J. M. (2012b). Reprogramming of proline and glutamine metabolism contributes to the proliferative and metabolic responses regulated by oncogenic transcription factor *c-MYC*. *Proceedings of the National Academy of Sciences*, 109 (23), 89838988. http://doi.org/10.1073/pnas.1203244109.

Liu, Y., Borchert, G. L., Surazynski, A., and Phang, J. M. (2008a). Proline oxidase, a p53induced gene, targets COX-2/PGE2 signaling to induce apoptosis and inhibit tumor growth in colorectal cancers. *Oncogene*, 27(53), 6729–6737. http:// doi.org /10.1038/onc.2008.322.

Liu, Y., Borchert, G. L., Surazynski, A., Hu, C. A., and Phang, J. M. (2006). Proline oxidase activates both intrinsic and extrinsic pathways for apoptosis: The role of ROS/superoxides, NFAT and MEK/ERK signaling. *Oncogene*, 25 (41),5640-5647. http://doi.org/10.1038/sj.onc.1209564.

Liu, X., Xue, L. and Yen, Y. (2008b). Redox property of ribonucleotide reductase small subunit M2 and p53R2. *Methods Mol. Biol*, 477, 195–206.

Loayza-Puch, F., Rooijers, K., Buil, L. C. M., Zijlstra, J., Oude Vrielink, J. F., Lopes, R. and Agami, R. (2016). Tumour-specific proline vulnerability uncovered by differential ribosome codon reading. *Nature*, 530 (7591), 490–494. http://doi.org/10.1038/nature16982.

Lobo, C. , Ruiz-Bellido, M.A. , Aledo, J.C. , Márquez, J. , Núñez De Castro, I., and Alonso, F.J. (2000). Inhibition of glutaminase expression by antisense mRNA decreasesgrowthand tumourigenicity of tumour cells. *The Biochemical journal*, 348 (2), 257-261.

Locasale, J. W., Grassian, A. R., Melman, T., Lyssiotis, C. A., Mattaini, K. R., Bass, A. J. and Vander Heiden, M. G. (2011). Phosphoglycerate dehydrogenase diverts

glycolytic flux and contributes to oncogenesis. *Nature Genetics*, 43 (9), 869–874. http://doi.org/10.1038/ng.890.

Locasale, J. W. (2013). NIH Public Access. *Nature Rev Cancer*, 13 (8), 572–583. http://doi.org/10.1038/nrc3557.

MacDonald, B. T., Tamai, K., and He, X. (2009). Wnt/β-Catenin Signaling: Components, Mechanisms, and Diseases. *Developmental Cell*, 17 (1), 9–26. http://doi.org/10.1016/j.devcel.2009.06.016.

Madan, E., Gogna, R., Bhatt, M., Pati, U., Kuppusamy, P. and Mahdi, A. A. (2011). Regulation of glucose metabolism by p53: Emerging new roles for the tumor suppressor. *Oncotarget*, 2 (12), 948–957. http://doi.org/10.18632/oncotarget.389

Mannava, S., Moparthy, K. C., Wheeler, L. J., Leonova, K. I., Wawrzyniak, J. A., Bianchi-Smiraglia, A. and Nikiforov, M. A. (2012). Ribonucleotide reductase and thymidylate synthase or exogenous deoxyribonucleosides reduce DNA damage and senescence caused by C-MYC depletion. *Aging*, 4 (12), 917–922. http://doi.org/10.18632/aging.100512.

Markert, E. K. and Vazquez, A. (2015). Mathematical models of cancer metabolism. *Cancer & Metabolism*, 3 (14), 1-13. http://doi.org/ 10.1186/s40170-015-0140-6.

Markowitz, S., Wang, J., Myeroff, L., Parsons, R., Sun, L., Lutterbaugh, J., Willson, J. K. V. (1995). Inactivation of the type II TGF-beta receptor in colon cancer cellswithmicrosatellite instability. *Science*, 268 (5215),1336-1338.

Martin, S. J. (1995). Early redistribution of plasma membrane phosphatidylserine is a general feature of apoptosis regardless of the initiating stimulus: inhibition by overexpression of Bcl-2 and Abl. *Journal of Experimental Medicine*,182 (5), 1545-1556. http://doi.org/10.1084/jem.182.5.1545.

McCain, J. (2013). The MAPK (ERK) Pathway: Investigational Combinations for the Treatment of *BRAF*-Mutated Metastatic Melanoma. *P and T : A Peer-Reviewed Journal for Formulary Management*, 38 (2), 96–108. Retrieved from

http://www.pubmedcentral.nih.gov/articlerender.fcgi?artid=3628180&tool=pmcentrez&rendertype=abstract.

McFate, T., Mohyeldin, A., Lu, H., Thakar, J., Henriques, J., Halim, N. D. and Verma, A. (2008). Pyruvate dehydrogenase complex activity controls metabolic and malignant phenotype in cancer cells. *Journal of Biological Chemistry*, 283 (33), 22700–22708. http://doi.org/10.1074/jbc.M801765200.

Mead, T. J., and Lefebvre, V. (2014). Skeletal Development and Repair, 1130, 1–10. http://doi.org/10.1007/978-1-62703-989-5.

Medema, J. P. and Vermeulen, L. (2011). Microenvironmental regulation of stem cells in intestinal homeostasis and cancer. *Nature*, 474 (7351), 318326. http:// doi.org /10.1038/nature10212.

Mehansho, H., Hagerman, a, Clements, S., Butler, L., Rogler, J. and Carlson, D. M. (1983). Modulation of proline-rich protein biosynthesis in rat parotid glands by sorghums with high tannin levels. *Proceedings of the National Academy of Sciences of the United States of America*, 80 (13), 3948–3952. http: //doi.org /10. 1073/pnas.80.13.3948.

Menendez, J. A. and Lupu, R. (2007). Fatty acid synthase and the lipogenic phenotype in cancer pathogenesis. *Nature Reviews Cancer*, 7 (10), 763–777. http:// doi.org/ 10.1038/nrc2222.

Menon, S. and Manning, B. D. (2009). Common corruption of the mTOR signalling network in human tumors. *Oncogene*, 27 (S2), S43–S51. http://doi.org /10. 1038/onc.2009.352.

Metallo, C. M. and Vander Heiden, M. G. (2014). Understanding metabolic regulation and its influence on cell physiology. *Molecular Cell*, 49 (3), 388–398. http://doi.org/10.1016/j.molcel.2013.01.018.

Metzger, D., and Chambon, P. (2001). Site- and time-specific gene targeting in the mouse. *Methods*, 24 (1), 71–80. http://doi.org/10.1006/meth.2001.1159.

Miller, A.B., Howe, G.R., Jain, M., Craib, K.J. and Harrison, L. (1983). Food items and food groups as risk factors in a case-control study of diet and colorectal cancer. *IntJCancer*,32 (2), 155-161.

Missirlis, P. I., Smailus, D. E., and Holt, R. A. (2006). A high-throughput screen identifying sequence and promiscuity characteristics of the loxP spacer region in Cre-mediated recombination. *BMC Genomics*, 7, 1–13. http://doi.org/10. 1186/1471-2164-773.

Mohan, H. (2010). Text book of Pathology, 6th Edition. New Delhi, India. Jitendar P Vij, Jaypee Brothers Medical Publishers (P) Ltd.

Montgomery, E., Bronner, M. P., Goldblum, J. R., Greenson, J. K., Haber, M. M., Hart, J., and Washington, K. (2001). Reproducibility of the diagnosis of dysplasia in Barrett esophagus: A reaffirmation. *Human Pathology*, 32 (4), 368–378. http://doi.org/10.1053/hupa.2001.23510.

Mori, T. (2010). A comparison of the new (Planned) TNM classification and Japanese general rule for staging colorectal cancer. *Cancer Investigation*, 28 (4), 387-392. http://doi.org/10.3109/07357900903287055.

Murcia, O., Juárez, M., Hernández-Illán, E., Egoavil, C., Giner-Calabuig, M., Rodríguez-Soler, M. and Jover, R. (2016). Serrated colorectal cancer: Molecular classification, prognosis, and response to chemotherapy. *World Journal of Gastroenterology*, 22 (13), 3516–3530. http://doi.org/10.3748/wjg.v22.i13.3516.

Murphy, K. M., Zhang, S., Geiger, T., Hafez, M. J., Bacher, J., Berg, K. D. and Eshleman, J. R. (2006). Comparison of the microsatellite instability analysis system and the Bethesda panel for the determination of microsatellite instability in colorectal cancers. *Journal of Molecular Diagnostics*, 8 (3), 305–311. http:// doi.org/10.2353/jmoldx.2006.050092.

Musgrove, E. A. (2006). Cyclins: Roles in mitogenic signaling and oncogenic transformation. Growth Factors, 24 (1), 13–19. http://doi.org/10.1080 /08977190500361812.

Nafissi, N., and Slavcev, R. (2014). Bacteriophage recombination systems and biotechnical applications. *Applied Microbiology and Biotechnology*, 98 (7), 28412851. http://doi.org/10.1007/s00253-014-5512-2.

Nebot-Bral, L., Brandao, D., Verlingue, L., Rouleau, E., Caron, O., Despras, E. and Kannouche, P. L. (2017). Hypermutated tumours in the era of immunotherapy: The paradigm of personalised medicine. *European Journal of Cancer*, 84, 290–303. http://doi.org/10.1016/j.ejca.2017.07.026.

Nilsson, R., Jain, M., Madhusudhan, N., Sheppard, N. G., Strittmatter, L., Kampf, C. and Mootha, V. K. (2014). Metabolic enzyme expression highlights a key role for MTHFD2 and the mitochondrial folate pathway in cancer. *Nature Communications*, 5,110.http://doi.org/10.1038/ncomms4128.

Nocek, B., Chang, C., Li, H., Lezondra, L., Holzle, D., Collart, F. and Joachimiak, A. (2005). Crystal structures of Δ1-pyrroline-5-carboxylate reductase from human pathogens Neisseria meningitides and Streptococcus pyogenes. *Journal of Molecular Biology*, 354 (1), 91–106. http://doi.org/10.1016/j.jmb.2005.08.036.

Nosho, K., Irahara, N., Shima, K., Kure, S., Kirkner, G. J., Schernhammer, E. S. and Ogino, S. (2008). Comprehensive biostatistical analysis of CpG island methylator phenotype in colorectal cancer using a large population-based sample. *PLoS ONE*, 3 (11). http://doi.org/10.1371/journal.pone.0003698.

Nöthlings, U., Yamamoto, J. F., Wilkens, L. R., Murphy, S. P., Park, S. Y., Henderson, B. E. and Le Marchand, L. (2009). Meat and heterocyclic amine intake, smoking, NAT1 and NAT2 polymorphisms, and colorectal cancer risk in the multiethnic cohort study.*CancerEpidemiology Biomarkers and Prevention*, 18 (7), 2098–2106.

Novak, A. and Dedhar, S. (1999). Signaling through beta-catenin and Lef/Tcf. Cellular and Molecular Life Sciences : CMLS, 56 (5–6), 523–537.

O'Gorman, S., Fox, D. and Wahl, G. (1991). Recombinase-mediated gene activation and site-specific integration in mammalian cells. *Science*, 251 (4999),1351-1355.http://doi.org/10.1126/science.1900642.

Obrocea, F., Sajin, M., Marinescu, E. C., and Stoica, D. (2011). Colorectal cancer and the 7th revision of the TNM staging system: Review of changes and suggestions for uniform pathologic reporting. *Romanian Journal of Morphology and Embryology*, 52 (2), 537–544.http://doi.org/520211537544.

Ogino, S. and Goel, A. (2008). Molecular classification and correlates in colorectal cancer. *Journal of Molecular Diagnostics*, 10 (1), 13–27 . http://doi.org /10.2353/ jmoldx.2008.070082.

Ohno, H. (2015). Intestinal M cells. *Journal of Biochemistry*, 159 (2), 151–160. http://doi.org/10.1093/jb/mvv121.

Olivares, O., Mayers, J. R., Gouirand, V., Torrence, M. E., Gicquel, T., Borge, L. and Vasseur, S. (2017). Collagen-derived proline promotes pancreatic ductal adenocarcinoma cell survival under nutrient limited conditions. *Nature Communications*, 8. http://doi.org/10.1038/ncomms16031.

Pancione, M., Remo, A. and Colantuoni, V. (2012). Genetic and epigenetic events generate multiple pathways in colorectal cancer progression. *Pathology Research International*. http://doi.org/10.1155/2012/509348.

Pandhare, J., Donald, S. P., Cooper, S. K., and Phang, J. M. (2009). Regulation and function of proline oxidase under nutrient stress. *Journal of Cellular Biochemistry*, 107 (4), 759768. http://doi.org/10.1002/jcb.22174.

Papandreou, I., Cairns, R. A., Fontana, L., Lim, A. L. and Denko, N. C. (2006). HIF-1 mediates adaptation to hypoxia by actively downregulating mitochondrial oxygen consumption. *Cell Metabolism*, 3 (3), 187–197. http:// doi.org/ 10.1016 /j.cmet. 2006.01.012.

Passardi, A., Canale, M., Valgiusti, M. and Ulivi, P. (2017). Immune checkpoints as a target for colorectal cancer treatment. *International Journal of Molecular Sciences*, 18 (6). http://doi.org/10.3390/ijms18061324.

Patai, Á. V., Molnár, B., Tulassay, Z., and Sipos, F. (2013). Serrated pathway: Alternative route to colorectal cancer. *World Journal of Gastroenterology*, 19 (5), 607–615. http://doi.org/10.3748/wjg.v19.i5.607.

Phang, J. M. (1985). The Regulatory Functions of Proline and Pyrroline-5-carboxylic Acid. *Current Topics in Cellular Regulation* (Vol. 25). Academic press, inc. http://doi.org/10.1016/B978-0-12-152825-6.50008-4.

Phang, J. M. (2017). Proline metabolism in cell regulation and cancer biology: Recent advances and hypotheses. *Antioxidants and Redox Signaling*. http://doi.org /10.1089/ars.2017.7350.

Phang, J. M., Donald, S. P., Pandhare, J., and Liu, Y. (2008 a). The metabolism of proline, a stress substrate, modulates carcinogenic pathways. *Amino Acids,* 35 (4), 681–690.http://doi.org/10.1007/s00726-008-0063-4.

Phang, J. M., Liu, W., and Zabirnyk, O. (2010). Proline Metabolism and Microenvironmental Stress. *Annual Review of Nutrition,* 30 (1), 441–463. http://doi.org/10.1146/annurev.nutr.012809.104638.

Phang, J. M., Liu, W., Hancock, C. N., and Fischer, J. W. (2015). Proline metabolism and cancer: Emerging links to glutamine and collagen. *Current Opinion in Clinical Nutrition and Metabolic Care*, 18 (1), 71–77. http://doi.org/10.1097/MCO. 121.

Phang, J. M., Liu, W., Hancock, C. and Christian, K. J. (2012). The Proline Regulatory Axis and Cancer. *Frontiers in Oncology*, 2, 1–12. http:// doi.org/ 10.3389/fonc .2012.00060.

Phang, J. M. and Liu, W. (2012). Proline metabolism and cancer. Metabolism and Cancer Susceptibility Section, Laboratory of Comparative Carcinogenesis. Centre for Cancer Research, National Cancer Institute at Frederick, Frederick, MD 21702, USA. 1835–1845.

Phang, J. M., Pandhare, J. and Liu, Y. (2008 b). The metabolism of proline as microenvironmental stress substrate. *The Journal of Nutrition*, 138 (10), 2008S–2015S. http://doi.org/138/10S-I/2008S.

Phillips, M. M., Sheaff, M. T. and Szlosarek, P. W. (2013). Targeting arginine-dependent cancers with arginine-degrading enzymes: Opportunities and challenges. *Cancer Research and Treatment*, 45 (4), 251–262. http:// doi.org/10 .4143/crt.2013.45.4.251.

Pierotti M.A. , Sozzi G. and Croce, C.M. (2003). Mechanisms of oncogene activation. In: Kufe DW, Pollock R.E, Weichselbaum R.R, et al., editors. Holland-Frei Cancer Medicine. 6th edition. Hamilton (ON): BC Decker. Available from: https://www.ncbi.nlm.nih.gov/books/NBK12538/.

Pinheiro, C., Penna, V., Morais-Santos, F., Abrahão-Machado, L. F., Ribeiro, G., Curcelli, E. C. and Baltazar, F. (2014). Characterization of monocarboxylate transporters (MCTs) expression in soft tissue sarcomas: Distinct prognostic impact of MCT1 sub-cellular localization. *Journal of Translational Medicine*, 12 (1), 1-11.http://doi.org/10.1186/1479-5876-12-118.

Pino, M. S., and Chung, D. C. (2010). The Chromosomal Instability Pathway in Colon Cancer. *Gastroenterology*, 138(6), 2059–2072. http:// doi.org/10.1053/ j.gastro. 2009.12.065.

Pino, M. S. and Chung, D. C. (2014). The chromosomal instability pathway in colon, *NIH Public Access*, 138 (6), 2059–2072. http://doi.org/10.1053 /j.gastro. 2009.12.065.

Pinson, K. I., Brennan, J., Monkley, S., Avery, B. J. and Skarnes, W. C. (2000). An LDL-receptor-related protein mediates Wnt signalling in mice. *Nature*, 407 (6803), 535–538.http://doi.org/10.1038/35035124.

Pinto, D. and Clevers, H. (2005). Wnt control of stem cells and differentiation in the intestinal epithelium. *Experimental Cell Research*, 306 (2), 357–363. http://doi.org/ 10.1016/j.yexcr.2005.02.022

Polyak, K., Xia, Y. and Zweier, J. L. (1997). letters to nature Ref. NO. : 569 A model for *p53*-induced apoptosis. *Nature*, 389, 300–305.

Possemato, R., Marks, K. M., Shaul, Y. D., Pacold, M. E., Kim, D., Birsoy, K. and Sabatini, D. M. (2011). Functional genomics reveal that the serine synthesis pathway

is essential in breast cancer. *Nature*, 476(7360), 346–350. http://doi.org/10.1038/nature10350.

Potten, C. S. (1977). Extreme sensitivity of some intestinal crypt cells to X and γ irradiation. *Nature,* (269), 518-521. http://doi:10.1038/269518a0.

Potten, C. S., Kellett, M., Roberts, S. a, Rew, D. A. and Wilson, G. D. (1992). Measurement of in vivo proliferation in human colorectal mucosa using bromodeoxyuridine. *Gut,* 33 (1), 71–78.https://doi.org/10.1136/gut.33.1.71.

Powell, D. W., Mifflin, R. C., Valentich, J. D., Crowe, S. E.,Saada, J. I. and West, A. B. (1999). Myofibroblasts. II. intestinal subepithelial myofibroblasts. *American Journal of Physiology - Cell Physiology*, 277(2), 183-201.

Powell, D. W., Pinchuk, I. V., Saada, J. I., Chen, X. and Mifflin, R. C. (2011). Mesenchymal Cells of the Intestinal Lamina Propria. Annual Review of Physiology, 73(1), 213–237. http:// doi.org/10.1146 /annurev.physiol. 70.113006. 100646.

Qiao, L. and Wong, B. C. Y. (2009). Role of notch signaling in colorectal cancer. *Carcinogenesis*, 30 (12), 1979–1986. http://doi.org/10.1093/carcin/bgp236.

Rad, R., Cadianos, J., Rad, L., Varela, I., Strong, A., Kriegl, L., Bradley, A. (2013). A Genetic Progression Model of BrafV600E-Induced Intestinal Tumorigenesis Reveals Targets for Therapeutic Intervention. *Cancer Cell*, 24 (1), 15–29. http://doi.org/10.1016/j.ccr.2013.05.014.

Rao, C. V., Hirose, Y., Indranie, C. and Reddy, B. S. (2001). Modulation of experimental colon tumorigenesis by types and amounts of dietary fatty acids. *Cancer Research*, 61(5), 1927–1933.

Rennoll, S. (2015). Regulation of MYC gene expression by aberrant Wnt/β-catenin signaling in colorectal cancer. *World Journal of Biological Chemistry*, 6 (4), 290. http://doi.org/10.4331/wjbc.v6.i4.290.

Resnick, M. A. and Inga, A. (2003). Functional mutants of the sequence-specific transcription factor p53 and implications for master genes of diversity.

Proceedings of the National Academy of Sciences of the United States of America, 100 (17), 9934–9. http://doi.org/10.1073/pnas.1633803100.

Rex, D. K., Ahnen, D. J., Baron, J. A., Batts, K. P., Burke, C. A., Burt, R. W. and Church, J. (2012). Serrated lesions of the colorectum: Review and recommendations from an expert panel. *American Journal of Gastroenterology*, 107 (9), 1315–1329. http://doi.org/10.1038/ajg.2012.161.

Rhodes DR, Yu J, Shanker K, Deshpande N, Varambally R, Ghosh D, Barrette T, Pandey A, Chinnaiyan AM (2004). A cancer microarray database and integrated data-mining platform. Oncomine: *Neoplasia, Jan-Feb;* 6 (1):1-6.

Riccio, O., van Gijn, M. E., Bezdek, A. C., Pellegrinet, L., van Es, J. H., Zimber-Strobl, U., Radtke, F. (2008). Loss of intestinal crypt progenitor cells owing to inactivation of both Notch1 and Notch2 is accompanied by derepression of CDK inhibitors p27Kip1 and p57Kip2. *EMBO Reports*, 9 (4), 377–383. http://doi.org/10.1038/embor.2008.7.

Richards, N. G. and Schuster, S. M. (1998). Mechanistic issues in asparagine synthetase catalysis. *Adv. Enzymol*, 72, 145–198. https://doi.org/10.1002/9780470123188.ch5.

Richards, N. G. J. and Kilberg, M. S. (2006). Asparagine Synthetase Chemotherapy. *Annual Review of Biochemistry*, 75 (1), 629–654. http://doi.org/10.1146 /annurev.biochem. 75.103004.142520.

Richman, S. (2015). Deficient mismatch repair: Read all about it. *International Journal of Oncology*, 47 (4), 1189–1202. http://doi.org/10.3892/ijo.2015.3119.

Robinson, M. M., Mcbryant, S. J., Tsukamoto, T., Rojas, C., Ferraris, D. V., Hamilton, S. K. and Curthoys, N. P. (2007). Novel mechanism of inhibition of rat kidney-type glutaminase by bis-2-(5-phenylacetamido-1,2,4-thiadiazol-2-yl)ethyl sulfide (BPTES). *Biochemical Journal*, 406 (3), 407–414. http://doi.org/ 10.1042/ BJ20070039.

Roig, A. I., Eskiocak, U., Hight, S. K., Kim, S. B., Delgado, O., Souza, R. F. and Shay, J. W. (2010). Immortalized Epithelial Cells Derived From Human Colon Biopsies

Express Stem Cell Markers and Differentiate In Vitro. *Gastroenterology*, 138 (3), 1012–1021.e5. http://doi.org/10.1053/j.gastro.2009.11.052

Sailaja, B. S., He, X. C., and Li, L. (2016). The regulatory niche of intestinal stem cells. *Journal of Physiology*, 594 (17), 4827–4836. http://doi.org/10.1113/JP271931.

Sakamaki, T., Casimiro, M. C., Ju, X., Quong, A. A., Katiyar, S., Liu, M. and Pestell, R. (2006). Cyclin D1 Determines Mitochondrial Function In Vivo. *Molecular and Cellular Biology*, 26 (14), 5449–5469. http://doi.org/10.1128/MCB.02074-05

Salic, A., and Mitchison, T. J. (2008). A chemical method for fast and sensitive detection of DNA synthesis in vivo. *Proceedings of the National Academy of Sciences of the United States of America, 105(7),* 2415–2420. http:// doi.org /10.1073/pnas.0712168105.

Samowitz, W. S., Albertsen, H., Herrick, J., Levin, T. R., Sweeney, C., Murtaugh, M. A. and Slattery, M. L. (2005). Evaluation of a large, population-based sample supports a CpG island methylator phenotype in colon cancer. *Gastroenterology*, 129 (3), 837–845. http://doi.org/10.1053/j.gastro.2005.06.020.

Sancak, Y., Bar-Peled, L., Zoncu, R., Markhard, A. L., Nada, S. and Sabatini, D. M. (2010). Ragulator-rag complex targets mTORC1 to the lysosomal surface and is necessary for its activation by amino acids. *Cell*, 141(2), 290–303. http://doi.org/10.1016/j.cell.2010.02.024.

Sansom, O. J., Meniel, V. S., Muncan, V., Phesse, T. J., Wilkins, J. A., Reed, K. R. and Clarke, A. R. (2007). *Myc* deletion rescues *Apc* deficiency in the small intestine. *Nature*, *446*(7136), 676–679. http://doi.org/10.1038/nature05674.

Satia-Abouta, J., Galanko, J. A., Martin, C. F., Ammerman, A. and Sandler, R. S. (2004). Food groups and colon cancer risk in African-Americans and Caucasians. *International Journal of Cancer*, *109 (5),* 728–736. https:// doi.org /10.1002 /ijc. 20044.

Sato, T., Van Es, J. H., Snippert, H. J., Stange, D. E., Vries, R. G., Van Den Born, M., and Clevers, H. (2011). Paneth cells constitute the niche for Lgr5 stem cells in intestinal crypts. *Nature*, 469 (7330), 415–418. http://doi.org/10.1038/nature09637.

Sauer, B. and Henderson, N. (1988). Site-specific DNA recombination in mammalian cells by the Cre recombinase of bacteriophage P1. *Proceedings of the National Academy of Sciences*, 85 (14), 5166–5170.http://doi.org/10.1073/pnas.85.14.5166.

Schneider, K. (2001). Cell Biology and Cancer. *Counseling about Cancer: Strategies for Genetic Counseling*, 1–17.

Scott, L., Lamb, J., Smith, S. and Wheatley, D. N. (2000). Single amino acid (arginine) deprivation: Rapid and selective death of cultured transformed and malignant cells. *British Journal of Cancer*, 83(6), 800–810. http://doi.org/10.1054/bjoc.2000.1353.

Semenza, G. L. (2010a). Defining the role of hypoxia-inducible factor 1 in cancer biology and therapeutics. *Oncogene*, 29 (5), 625–634. http://doi.org/10 .1038/onc .2009.441.

Semenza, G. L. (2010b). HIF-1: upstream and downstream of cancer metabolism. *Current Opinion in Genetics and Development*, 20 (1), 51–56. http://doi.org / 10. 1016/j.gde.2009.10.009.

Semenza, G. L. (2011). Regulation of metabolism by hypoxia-inducible factor 1. *Cold Spring Harbor Symposia on Quantitative Biology*, 76, 347–353. http:// dx. Doi .org /10.1101/sqb. 2011.76.010678.

Shackelford, D. B., and Shaw, R. J. (2009). The LKB1-AMPK pathway: Metabolism and growth control in tumour suppression. *Nature Reviews Cancer*, 9 (8), 563–575. http://doi.org/10.1038/nrc2676.

Shah, B. D. and Zuckerman, K. S. (2011). Normal and Malignant Hematopoiesis. *Advances in Malignant Hematology*, 1–30. http: //doi.org /10.1002 /9781444394016.ch1.

Shaw, R. J., and Cantley, L. C. (2006). Ras, PI(3)K and mTOR signalling controls tumour cell growth. *Nature*, *441*(7092), 424–430. http://doi.org /10. 1038 / nature 04869.

Shen, L., Toyota, M., Kondo, Y., Lin, E., Zhang, L., Guo, Y. and Issa, J.-P. J. (2007). Integrated genetic and epigenetic analysis identifies three different subclasses of colon cancer. *Proceedings of the National Academy of Sciences*, *104*(47), 18654–18659. http://doi.org/10.1073/pnas.0704652104.

Sherr, C. J. (1996). Cancer cell cycles. *Science*, (New York, N.Y.), 274(5293), 1672–1677.http://doi.org/10.1126/science.274.5293.1672.

Shi, Y. and Massagué, J. (2003). Mechanisms of TGF-beta signaling from cell membrane to the nucleus. *Cell, 113(6),* 685–700.http://doi.org/10.1016/S0092-8674 (03)00432-X.

Shibata, H., Toyama, K. and Noda, T. (1997). Rapid Colorectal Adenoma Formation Initiated by Conditional Targeting of the Apc Gene. *Science*, 278, 120.

Shussman, N., and Wexner, S. D. (2014). Colorectal polyps and polyposis syndromes. *Gastroenterology Report*, 2 (1), 1–15. http://doi.org/10.1093/gastro/got041.

Simon, H.-U., Haj-Yehia, A., and Levi-Schaffer, F. (2000). Role of reactive oxygen species (ROS) in apoptosis induction. *Apoptosis*, 5 (5), 415–418. http:// doi.org/ 10.1023/A:1009616228304.

Snippert, H. J., van der Flier, L. G., Sato, T., van Es, J. H., van den Born, M., Kroon-Veenboer, C., and Clevers, H. (2010). Intestinal crypt homeostasis results from neutral competition between symmetrically dividing Lgr5 stem cells. *Cell*, 143 (1), 134–144.http://doi.org/10.1016/j.cell.2010.09.016.

Sonveaux, P., Végran, F., Schroeder, T., Wergin, M. C., Verrax, J., Rabbani, Z. N. and Dewhirst, M. W. (2008). Targeting lactate-fueled respiration selectivelt kills hypoxic tumor cells in mice. *The Journal of Clinical Investigation*, 118 (12), 1–13. http://doi.org/10.1172/JCI36843.

Spano, D., Heck, C., De Antonellis, P., Christofori, G., and Zollo, M. (2012). Molecular networks that regulate cancer metastasis. *Seminars in Cancer Biology*, 22 (3), 234–249.https://doi.org/10.1016/j.semcancer.2012.03.006.

Sreedhar, A. and Zhao, Y. (2017). Dysregulated metabolic enzymes and metabolic reprogramming in cancer cells (Review). *Biomedical Reports*, 3–10. http://doi.org/10.3892/br.2017.1022.

Stallings, M.M. and Radisky, D. (2007). Matrix metalloproteinase-induced malignancy in mammary epithelial cells. *Cells Tissues Organs*, 185, 104-110.https://doi.org/10.1159/000101310.

Steck, S. E., Butler, L. M., Keku, T., Antwi, S., Galanko, J., Sandler, R. S. and Hu, J. J. (2014). Nucleotide excision repair gene polymorphisms, meat intake and colon cancer risk. *Mutation Research - Fundamental and Molecular Mechanisms of Mutagenesis*, 762 (1), 24–31.https://doi.org/10.1016/j.mrfmmm.2014.02.004.

Steinberg, N. and Hamilton, D. (1981). Bacteriophage P1 site-specific recombination. II. Recombination between loxP sites. *J. Mol. Biol*, *150*, 467–486.

Stevenson, R. A., Zemtsov, R. K., Wallace, M. T. and Manuscript, A. (2013). Matrix Metalloproteinase Induction of Rac1b, a Key Effector of Lung Cancer Progression. *NIH Public Access*, 5 (2), 124–136.http://doi.org/10.1002/aur.1222.

Suehiro, Y., Wong, C. W., Chirieac, L. R., Kondo, Y., Shen, L., Renee Webb, C. and Hamilton, S. R. (2008). Epigenetic-genetic interactions in the APC/WNT, RAS/RAF, and P53 pathways in colorectal carcinoma. *Clinical Cancer Research*, 14 (9), 2560–2569. http://doi.org/10.1158/1078-0432.CCR-07-1802.

Sun, L., Song, L., Wan, Q., Wu, G., Li, X., Wang, Y. and Zhang, H. (2015). *c-Myc*-mediated activation of serine biosynthesis pathway is critical for cancer progression under nutrient deprivation conditions. *Cell Research*, 25 (4), 429–444. http://doi.org/10.1038/cr.2015.33.

Sun, S.-Y., Hail, N. and Lotan, R. (2004). Apoptosis as a Novel Target for Cancer Chemoprevention. *JNCI Journal of the National Cancer Institute*, 96 (9), 662–672. http://doi.org/10.1093/jnci/djh123.

Sun, W. Y., Kim, H. M., Jung, W. H. and Koo, J. S. (2016). Expression of serine/glycine metabolism-related proteins is different according to the thyroid cancer subtype.

Journal of Translational Medicine, 14 (1), 1–12. http://doi.org/10.1186/s12967-016-0915-8.

Tanner, J. J. (2008). Structural biology of proline catabolism. *Amino Acids*, 35 (4), 719–730.http://doi.org/10.1007/s00726-008-0062-5.

Tanner, J. J. (2017). Structural biology of proline catabolic enzymes. *Antioxidants and Redox Signalling*.

Tanner, J. J., Fendt, S. M. and Becker, D. F. (2018). The Proline Cycle as a Potential Cancer Therapy Target. *Biochemistry*, 57 (25), 3433–3444. http://doi.org/10.1021/acs.biochem.8b00215.

Tennant, D. A., Durán, R. V. and Gottlieb, E. (2010). Targeting metabolic transformation for cancer therapy. *Nature Reviews Cancer*, 10 (4), 267–277. http://doi.org/10.1038/nrc2817

Tetsu, O. and McCormick, F. (1999). Beta-catenin regulates expression of cyclin D1 in colon carcinoma cells. *Nature*, 398 (6726), 422–426.http://doi.org/10.1038/18884.

Tetteh, P. W., Basak, O., Farin, H. F., Wiebrands, K., Kretzschmar, K., Begthel, H., and Clevers, H. (2016). Replacement of Lost Lgr5-Positive Stem Cells through Plasticity of Their Enterocyte-Lineage Daughters. *Cell Stem Cell*, 18 (2), 203–213. http://doi.org/10.1016/j.stem.2016.01.001.

Tiemersma, E. W., Wark, P. A., Ocke, M. C., Bunschoten, A., Otten, M. H., Kok, F. J., and Kampman, E. (2003). Alcohol consumption, alcohol dehydrogenase 3 polymorphism, and colorectal adenomas. *Cancer Epidemiol. Biomarkers Prev.*, 12 (5), 419–425.

Tong, X., Zhao, F. and Thompson, C. B. (2009). The molecular determinants of de novo nucleotide biosynthesis in cancer cells. *Current Opinion in Genetics and Development*, 19 (1), 32–37. http://doi.org/10.1016/j.gde.2009.01.002

Tong, Y., Yang, W. and Koeffler, H. P. (2011). Mouse Models of colorectal cancer. *Chin J Cancer*, 30 (7), 450–462.http://doi.org/10.5732/cjc.011.10041.

Toyota, M., Ahuja, N., Ohe-Toyota, M., Herman, J. G., Baylin, S. B. and Issa, J.-P. J. (1999). CpG island methylator phenotype in colorectal cancer. *Medical Sciences*, 96, 8681–8686. http://doi.org/10.11569/wcjd.v24.i4.558.

Tsun, Z. Y. and Possemato, R. (2015). Amino acid management in cancer. *Seminars in Cell and Developmental Biology*, 43, 22–32. http://doi.org/10.1016 /j.semcdb. 2015.08.002.

Turyn, J., Schlichtholz, B., Dettlaff-Pokora, A., Presler, M., Goyke, E., Matuszewski, M. and Swierczynski, J. (2003). Increased Activity of Glycerol 3-phosphate Dehydrogenase and Other Lipogenic Enzymes in Human Bladder Cancer. *Hormone and Metabolic Research*, 35 (10), 565–569. http://doi.org/10.1055/s-2003-43500.

Vander Heiden, M. G. (2011). Targeting cancer metabolism: A therapeutic window opens. *Nature Reviews Drug Discovery*, 10 (9), 671–684. http://doi.org /10.1038/ nrd3504.

Van de Wetering, M., Sancho, E., Verweij, C., De Lau, W., Oving, I., Hurlstone, A. and Clevers, H. (2002). The β-catenin/TCF-4 complex imposes a crypt progenitor phenotype on colorectal cancer cells. *Cell*, 111 (2), 241–250. http://doi.org/10. 1016/S0092-8674 (02)01014-0.

Vander Heiden, M. G., Cantley, L. C., Thompson, C. B., Mammalian, P., Exhibit, C. and Metabolism, A. (2009). Understanding the Warburg Effect : Cell Proliferation. *Science*, 324, 1029. http://doi.org/10.1126/science.1160809.

Van der Flier, L. G., Haegebarth, A., Stange, D. E., van de Wetering, M. and Clevers, H. (2009). OLFM4 Is a Robust Marker for Stem Cells in Human Intestine and Marks a Subset of Colorectal Cancer Cells. *Gastroenterology*, 137 (1), 15–17. http://doi.org/10.1053/j.gastro.2009.05.035.

Van Rijnsoever, M., Grieu, F., Elsaleh, H., Joseph, D., and Iacopetta, B. (2002). Characterisation of colorectal cancers showing hypermethylation at multiple CpG islands. *Gut*, 51(6), 797–802. http://doi.org/10.1136/gut.51.6.797.

Vaupel, P., Thews, O. and Hoeckel, M. (2001). Treatment resistance of solid tumors: Role of hypoxia and anemia. *Medical Oncology*, 18 (4), 243–259. http://doi.org/10.1385/MO:18:4:243.

Vermes, I., Haanen, C., Steffens-Nakken, H. and Reutelingsperger, C. (1995). A novel assay for apoptosis. Flow cytometric detection of phosphatidylserine expression on early apoptotic cells using fluorescein labelled Annexin V. *J Immunol Methods*, 184: 39-51.

Vermeulen, L., De Sousa E Melo, F., Van Der Heijden, M., Cameron, K., De Jong, J. H., Borovski, T. and Medema, J. P. (2010). Wnt activity defines colon cancer stem cells and is regulated by the microenvironment. *Nature Cell Biology*, 12 (5), 468–476. http://doi.org/10.1038/ncb2048.

Vučetić, M., Cormerais, Y., Parks, S. K. and Pouysségur, J. (2017). The Central Role of Amino Acids in Cancer Redox Homeostasis: Vulnerability Points of the Cancer Redox Code. *Frontiers in Oncology*, *7*. http://doi.org/10.3389/fonc.2017.00319.

Wade Harper, J., Adami, G. R., Wei, N., Keyomarsi, K. and Elledge, S. J. (1993). The p21 Cdk-interacting protein Cip1 is a potent inhibitor of G1 cyclin-dependent kinases. *Cell*, 75 (4), 805–816. http://doi.org/10.1016/0092-8674(93)90499-G.

Waldman, T., Kinzler, K. W. and Vogelstein, B. (1995). p21 is necessary for the p53-mediated G1 arrest in human cancer cells. *Cancer research*, 55, 5187–5190.

Walther, A., Johnstone, E., Swanton, C., Midgley, R., Tomlinson, I. and Kerr, D. (2009). Genetic prognostic and predictive markers in colorectal cancer. *Nature Reviews Cancer*, 9 (7), 489–499. http://doi.org/10.1038/nrc2645.

Wang, J. Bin, Erickson, J. W., Fuji, R., Ramachandran, S., Gao, P., Dinavahi, R. and Cerione, R. A. (2010). Targeting mitochondrial glutaminase activity inhibits oncogenic transformation. *Cancer Cell*, 18 (3), 207–219. http://doi.org/10.1016/j.ccr.2010.08.009.

Wang, Q., Chan, T. R., Hilgraf, R., Fokin, V. V., Sharpless, K. B., and Finn, M. G. (2003). Bioconjugation by copper(I)-catalyzed azide-alkyne cycloaddition. *Journal of the*

American Chemical Society, 125 (11), 3192–3193. http: //doi.org/10. 1021/ ja021381e.

Warburg O. (1956). On the origin of cancer cells. *Science, 123(3191)*,309-14.

Ward, P. S. and Thompson, C. B. (2012). Metabolic Reprogramming: A Cancer Hallmark Even Warburg Did Not Anticipate. *Cancer Cell*, 21(3), 297–308. http://doi.org/10.1016/j.ccr.2012.02.014.

Whissell, G., Montagni, E., Martinelli, P., Hernando-Momblona, X., Sevillano, M., Jung, P., Batlle, E. (2014). The transcription factor GATA6 enables self-renewal of colon adenoma stem cells by repressing BMP gene expression. *Nature Cell Biology*, 16 (7), 695–707.http://doi.org/10.1038/ncb2992.

Wise, D. R., DeBerardinis, R. J., Mancuso, A., Sayed, N., Zhang, X.-Y., Pfeiffer, H. K., and Thompson, C. B. (2008). *Myc* regulates a transcriptional program that stimulates mitochondrial glutaminolysis and leads to glutamine addiction. *Proceedings of the National Academy of Sciences*, 105(48), 18782–18787. http://doi.org/10.1073/pnas.0810199105.

Woolf, E. C., Syed, N. and Scheck, A. C. (2016). Tumor Metabolism, the Ketogenic Diet and β-Hydroxybutyrate: Novel Approaches to Adjuvant Brain Tumor Therapy. *Frontiers in Molecular Neuroscience*, 9, 1–11. http://doi.org/10 .3389 /fnmol.2016.00122

World Health Organization (WHO, 2009): available at (http://www.who.int/nmh/publications/fact_sheet_cancers_en.pdf).

World Health Organization (WHO, 2015): available at (http://www.who.int/cancer/en/).

World Health Organization (WHO, 2015): available at (http://www.who.int/features/qa/cancer-red-meat/en/).

Worthley, D.-L. and Leggett, B.-A. (2010). Colorectal cancer: molecular features and clinical opportunities. *The Clinical Biochemist.* Reviews / Australian Association of Clinical Biochemists, 31 (2), 3138. Retrieved from: http:// eutils. ncbi. nlm. nih. gov/entrez/eutils/elink. fcgi?dbfrom = pubmed&id= 20498827 and retmode =

ref&cmd = prlinks %5 Cnpapers 2://publication/uuid/8C22FA3D-04DC-4725-BE51-5944DE4C08E1.

Wu, G., Bazer, F. W., Datta, S., Johnson, G. A., Li, P., Satterfield, M. C. and Spencer, T. E. (2008). Proline metabolism in the conceptus: Implications for fetal growth and development. *Amino Acids*, 35 (4), 691–702. http://doi.org/10.1007/s00726-008-0052-7.

Wu, G., Huang, H., Abreu, J. G., and He, X. (2009). Inhibition of GSK3 phosphorylation of β-catenin via phosphorylated PPPSPXS motifs of Wnt coreceptor LRP6. *PLoS ONE*, 4 (3).http://doi.org/10.1371/journal.pone.0004926.

Xing, Y., Clements, W. K., Kimelman, D. and Xu, W. (2003). Crystal structure of a beta-catenin/axin complex suggests a mechanism for the beta-catenin destruction complex. *Genes and Development, 17(22)*, 2753–64. http://doi.org/10 .1101/gad. 1142603.

Xiong, Y., Hannon, G. J., Zhang, H., Casso, D., Kobayashi, R. and Beach, D. (1993). p21 is a universal inhibitor of cyclin kinases. *Nature*, 366 (6456), 701–704. http://doi.org/10.1038/366701a0.

Yamagishi, H., Kuroda, H., Imai, Y. and Hiraishi, H. (2016). Molecular pathogenesis of sporadic colorectal cancers. *Chinese Journal of Cancer*, 35 (1), 1–8. http://doi.org/10.1186/s40880-015-0066-y.

Yamane, L., Scapulatempo-Neto, C., Reis, R. M. and Guimarães, D. P. (2014). Serrated pathway in colorectal carcinogenesis. *World Journal of Gastroenterology*, 20 (10), 2634–2640. http://doi.org/10.3748/wjg.v20.i10.2634.

Yaşar, P., Ayaz, G., User, S. D., Güpür, G. and Muyan, M. (2017). Molecular mechanism of estrogen–estrogen receptor signaling. *Reproductive Medicine and Biology*, 16 (1), 4–20. http://doi.org/10.1002/rmb2.12006.

Zeng, T., Zhu, L., Liao, M., Zhuo, W., Yang, S., Wu, W., and Wang, D. (2017). Knockdown of PYCR1 inhibits cell proliferation and colony formation via cell cycle

arrest and apoptosis in prostate cancer. *Medical Oncology*, 34 (2). http://doi.org/10.1007/s12032-016-0870-5.

Zhang, J., Fan, J., Venneti, S., Cross, J. R., Takagi, T., Bhinder, B. and Thompson, C. B. (2014). Asparagine plays a critical role in regulating cellular adaptation to glutamine depletion. *Molecular Cell*, 56 (2), 205–218. http://doi.org/10. 1016/j.molcel.2014.08.018.

Zhang, Y., Pizzute, T., and Pei, M. (2014). A review of crosstalk between MAPK and Wnt signals and its impact on cartilage regeneration. *Cell and Tissue Research*, 358 (3), 633–649. http://doi.org/10.1007/s00441-014-2010-x.

Zhivotovsky, B., and Orrenius, S. (2006). Carcinogenesis and apoptosis: Paradigms and paradoxes. *Carcinogenesis*, 27 (10), 1939–1945. http://doi.org/10.1093/carcin /bg l035.

Zoncu, R., Efeyan, A. and Sabatini, D. M. (2011). MTOR: From growth signal integration to cancer, diabetes and ageing. *Nature Reviews Molecular Cell Biology*, 12 (1), 21–35. http://doi.org/10.1038/nrm3025.

Appendix

Table 8.1. Colon cancer tissue array, set 1, ab178128.

Array position	Age	Sex	Anatomic site	Nature	Pathology	Grade	Stage (TNM)
A01	60	F	Intestine, Colon	Malignant	Adenocarcinoma	I~II	T2N1M0
A02	85	F	Intestine, Colon	Malignant	Adenocarcinoma	I~II	T2N0M0
A03	43	F	Intestine, Colon	Malignant	Adenocarcinoma	I~II	T2N0M0
A04	51	M	Intestine, Colon	Malignant	Adenocarcinoma	II	T2N0M0
A05	65	M	Intestine, Colon	Malignant	Adenocarcinoma	II	T3N0M0
A06	48	F	Intestine, Colon	Malignant	Adenocarcinoma	II~III	T3N0M0
A07	74	F	Intestine, Colon	Malignant	Adenocarcinoma	II	T2N1M0
A08	43	F	Intestine, Colon	Malignant	Adenocarcinoma	II~III	T4N1M0
B01	60	F	Intestine, Colon	Malignant	Adenocarcinoma	I~II	T2N1M0
B02	85	F	Intestine, Colon	Malignant	Adenocarcinoma	I~II	T2N0M0
B03	43	F	Intestine, Colon	Malignant	Adenocarcinoma	I~II	T2N0M0
B04	51	M	Intestine, Colon	Malignant	Adenocarcinoma	II	T2N0M0
B05	65	M	Intestine, Colon	Malignant	Adenocarcinoma	II	T3N0M0
B06	48	F	Intestine, Colon	Malignant	Adenocarcinoma	II~III	T3N0M0
B07	74	F	Intestine, Colon	Malignant	Adenocarcinoma	II	T2N1M0
B08	43	F	Intestine, Colon	Malignant	Adenocarcinoma	II~III	T4N1M0
C01	60	F	Intestine, Colon	Normal	Uninvolved colon of A1,B1	-	-
C02	85	F	Intestine, Colon	Normal	Uninvolved colon of A2,B2	-	-
C03	43	F	Intestine, Colon	Normal	Uninvolved colon of A3,B3	-	-
C04	51	M	Intestine, Colon	Normal	Uninvolved colon of A4,B4	-	-
C05	65	M	Intestine, Colon	Normal	Uninvolved colon of A5,B5	-	-
C06	48	F	Intestine, Colon	Normal	Uninvolved colon of A6,B6	-	-
C07	74	F	Intestine, Colon	Normal	Uninvolved colon of A7,B7	-	-
C08	43	F	Intestine, Colon	Normal	Uninvolved colon of A8,B8	-	-
D01	36	M	Intestine, Colon	Malignant	Adenocarcinoma	III	T3N0M0
D02	47	M	Intestine, Colon	Malignant	Adenocarcinoma	III	T3N1M0
D03	53	F	Intestine, Colon	Malignant	Adenocarcinoma	III	T3N1M0
D04	53	F	Intestine, Colon	Malignant	Adenocarcinoma	III	T3N2M0
D05	72	M	Intestine, Colon	Malignant	Adenocarcinoma	III	T2N0M0
D06	36	M	Intestine, Colon	Malignant	Adenocarcinoma	III~IV	T2N0M0
D07	60	F	Intestine, Colon	Malignant	Adenocarcinoma	II~III	T3N0M0
D08	35	M	Intestine, Colon	Malignant	Adenocarcinoma	III~IV	T4N2M1
E01	36	M	Intestine, Colon	Malignant	Adenocarcinoma	III	T3N0M0
E02	47	M	Intestine, Colon	Malignant	Adenocarcinoma	III	T3N1M0
E03	53	F	Intestine, Colon	Malignant	Adenocarcinoma	III	T3N1M0
E04	53	F	Intestine, Colon	Malignant	Adenocarcinoma	III	T3N2M0
E05	72	M	Intestine, Colon	Malignant	Adenocarcinoma	III	T2N0M0
E06	36	M	Intestine, Colon	Malignant	Adenocarcinoma	III~IV	T2N0M0
E07	60	F	Intestine, Colon	Malignant	Adenocarcinoma	II~III	T3N0M0
E08	35	M	Intestine, Colon	Malignant	Adenocarcinoma	III~IV	T4N2M1
F01	36	M	Intestine, Colon	Normal	Uninvolved colon of D1,E1	-	-
F02	47	M	Intestine, Colon	Normal	Uninvolved colon of D2,E2	-	-
F03	53	F	Intestine, Colon	Normal	Uninvolved colon of D3,E3	-	-
F04	53	F	Intestine, Colon	Normal	Uninvolved colon of D4,E4	-	-
F05	72	M	Intestine, Colon	Normal	Uninvolved colon of D5,E5	-	-
F06	36	M	Intestine, Colon	Normal	Uninvolved colon of D6,E6	-	-
F07	60	F	Intestine, Colon	Normal	Uninvolved colon of D7,E7	-	-
F08	35	M	Intestine, Colon	Normal	Uninvolved colon of D8,E8	-	-

Table 8.2. Colon cancer tissue array, Set 2, ab178129.

Array position	Age	Sex	Anatomic site	Nature	Pathology	Grade	Stage (TNM)
A01	64	F	Intestine, Colon	Malignant	Adenocarcinoma	I~II	T3N0M0
A02	73	F	Intestine, Colon	Malignant	Adenocarcinoma	I~II	T3N1M0
A03	61	M	Intestine, Colon	Malignant	Adenocarcinoma	I~II	T3N0M0
A04	62	F	Intestine, Colon	Malignant	Adenocarcinoma	I~II	T3N0M0
A05	44	M	Intestine, Colon	Malignant	Adenocarcinoma	I~II	T2N0M0
A06	75	F	Intestine, Colon	Malignant	Adenocarcinoma	I~II	T2N1M0
A07	41	F	Intestine, Colon	Malignant	Adenocarcinoma	II	T3N0M0
A08	49	M	Intestine, Colon	Malignant	Adenocarcinoma	II	T2N0M0
B01	64	F	Intestine, Colon	Malignant	Adenocarcinoma	I~II	T3N0M0
B02	73	F	Intestine, Colon	Malignant	Adenocarcinoma	I~II	T3N1M0
B03	61	M	Intestine, Colon	Malignant	Adenocarcinoma	I~II	T3N0M0
B04	62	F	Intestine, Colon	Malignant	Adenocarcinoma	I~II	T3N0M0
B05	44	M	Intestine, Colon	Malignant	Adenocarcinoma	I~II	T2N0M0
B06	75	F	Intestine, Colon	Malignant	Adenocarcinoma	I~II	T2N0M0
B07	41	F	Intestine, Colon	Malignant	Adenocarcinoma	II	T3N0M0
B08	49	M	Intestine, Colon	Malignant	Adenocarcinoma	II	T2N0M0
C01	64	F	Intestine, Colon	Normal	Uninvolved colon of A1,B1	-	-
C02	73	F	Intestine, Colon	Normal	Uninvolved colon of A2,B2	-	-
C03	61	M	Intestine, Colon	Normal	Uninvolved colon of A3,B3	-	-
C04	62	F	Intestine, Colon	Normal	Uninvolved colon of A4,B4	-	-
C05	44	M	Intestine, Colon	Normal	Uninvolved colon of A5,B5	-	-
C06	75	F	Intestine, Colon	Normal	Uninvolved colon of A6,B6	-	-
C07	41	F	Intestine, Colon	Normal	Uninvolved colon of A7,B7	-	-
C08	49	M	Intestine, Colon	Normal	Uninvolved colon of A8,B8	-	-
D01	85	M	Intestine, Colon	Malignant	Adenocarcinoma	II	T2N0M0
D02	40	M	Intestine, Colon	Malignant	Adenocarcinoma	II	T3N1M0
D03	49	M	Intestine, Colon	Malignant	Adenocarcinoma	II	T3N0M0
D04	70	M	Intestine, Colon	Malignant	Adenocarcinoma	II~III	T3N0M0
D05	80	M	Intestine, Colon	Malignant	Adenocarcinoma	II~III	T3N1M0
D06	54	F	Intestine, Colon	Malignant	Adenocarcinoma	II~III	T3N2M0
D07	65	F	Intestine, Colon	Malignant	Adenocarcinoma	II~III	T3N1M0
D08	80	M	Intestine, Colon	Malignant	Adenocarcinoma	III	T3N1M0
E01	85	M	Intestine, Colon	Malignant	Adenocarcinoma	II	T2N0M0
E02	40	M	Intestine, Colon	Malignant	Adenocarcinoma	II	T3N1M0
E03	49	M	Intestine, Colon	Malignant	Adenocarcinoma	II	T3N0M0
E04	70	M	Intestine, Colon	Malignant	Adenocarcinoma	II~III	T3N0M0
E05	80	M	Intestine, Colon	Malignant	Adenocarcinoma	II~III	T3N1M0
E06	54	F	Intestine, Colon	Malignant	Adenocarcinoma	II~III	T3N2M0
E07	65	F	Intestine, Colon	Malignant	Adenocarcinoma	II~III	T3N1M0
E08	80	M	Intestine, Colon	Malignant	Adenocarcinoma	III	T3N1M0
F01	85	M	Intestine, Colon	Normal	Uninvolved colon of D1,E1	-	-
F02	40	M	Intestine, Colon	Normal	Uninvolved colon of D2,E2	-	-
F03	49	M	Intestine, Colon	Normal	Uninvolved colon of D3,E3	-	-
F04	70	M	Intestine, Colon	Normal	Uninvolved colon of D4,E4	-	-
F05	80	M	Intestine, Colon	Normal	Uninvolved colon of D5,E5	-	-
F06	54	F	Intestine, Colon	Normal	Uninvolved colon of D6,E6	-	-
F07	65	F	Intestine, Colon	Normal	Uninvolved colon of D7,E7	-	-
F08	80	M	Intestine, Colon	Normal	Uninvolved colon of D8,E8	-	-

Table 8.3. C_T Values and fold of change in *Pycr1* mRNA level in mice females after two weeks of tamoxifen injection

	C_T *Pycr*1	G Mean	ΔC_T	ΔC_T Mean	$\Delta\Delta C_T$	Fold Change
FNA	33.43	31.04	2.39	1.47	-1.60	3.03
FNB	33.49	31.68	1.81			
FNC	33.86	33.65	0.21			
FDA	33.02	34.20	-1.18	-0.13		
FDB	34.97	34.09	0.88			
FDC	35.75	35.85	-0.10			

Table 8.4. C_T Values and fold of change in *Pycr1* mRNA level in mice males after two weeks of tamoxifen injection

	C_T *Pycr*1	G Mean	ΔC_T	ΔC_T Mean	$\Delta\Delta C_T$	Fold Change
MNA	33.36	32.92	0.44	0.38	-1.42	2.68
MNB	33.43	33.10	0.33			
MDA	33.00	33.98	-0.98			
MDB	33.03	33.91	-0.88	-1.04		
MDC	33.99	35.25	-1.26			

Table 8.5. C_T Values and fold of change in *Pycr1* mRNA level in mice females after one week of tamoxifen injection

	C_T *Pycr1*	G Mean	ΔC_T	ΔC_T Mean	$\Delta\Delta C_T$	Fold Change
FNA	33.15	31.07	2.08	1.84	-0.21	1.16
FNB	32.26	30.58	1.68			
FNC	35.18	33.40	1.78			
FDA	35.60	34.31	1.29	1.63		
FDB	36.92	32.95	3.97			
FDC	35.88	36.25	-0.37			

Table 8.6. C_T Values and fold of change in *Pycr1* mRNA level in mice males after one week of tamoxifen injection

	C_T *Pycr1*	G Mean	ΔC_T	ΔC_T Mean	$\Delta\Delta C_T$	Fold Change
MNA	32.52	32.32	0.20	1.54	-0.22	1.16
MNB	33.77	32.90	0.87			
MNC	34.03	30.47	3.56			
MDA	36.33	35.96	0.37	1.32		
MDB	35.57	35.01	0.56			
MDC	36.63	33.60	3.03			

Table 8.7. C_T Values and fold of change in *Pycr1* mRNA level in mice females after three days of tamoxifen injection

	C_T *Pycr1*	G Mean	ΔC_T	ΔC_T Mean	$\Delta\Delta C_T$	Fold Change
FNA	31.91	30.33	1.58	0.77	-0.32	1.24
FNB	32.52	30.95	1.57			
FNC	33.84	34.68	-0.84			
FDA	32.80	31.76	1.04	0.45		
FDB	33.31	32.22	1.09			
FDC	33.49	34.27	-0.78			

Table 8.8. C_T Values and fold of change in *Pycr1* mRNA level in mice males after three days of tamoxifen injection

	C_T *Pycr1*	G Mean	ΔC_T	ΔC_T Mean	$\Delta\Delta C_T$	Fold Change
MNA	32.49	29.67	2.82	1.30	0.03	0.97
MNB	32.91	31.91	1.00			
MNC	35.23	35.13	0.10			
MDA	31.34	30.33	1.01	1.33		
MDB	32.72	30.39	2.33			
MDC	34.12	33.45	0.67			

Table 8.9. C_T Values and fold of change in *Pycr2* mRNA level in mice females after two weeks of tamoxifen injection

	C_T *Pycr2*	G Mean	ΔC_T	ΔC_T Mean	$\Delta\Delta C_T$	Fold Change
FNA	32.07	31.04	1.03	0.33	-0.05	1.03
FNB	32.15	31.68	0.47			
FNC	33.14	33.65	-0.51			
FDA	35.38	34.20	1.18	0.28		
FDB	34.02	34.09	-0.07			
FDC	35.58	35.85	-0.27			

Table 8.10. C_T Values and fold of change in *Pycr2* mRNA level in mice males after two weeks of tamoxifen injection

	C_T *Pycr2*	G Mean	ΔC_T	ΔC_T Mean	$\Delta\Delta C_T$	Fold Change
MNA	31.67	32.92	-1.25	-1.27	-0.06	1.04
MNB	31.8	33.10	-1.30			
MDA	32.75	33.98	-1.23	-1.34		
MDB	33.5	33.91	-0.41			
MDC	32.87	35.25	-2.38			

Table 8.11. C_T Values and fold of change in *Pycr2* mRNA level in mice females after one week of tamoxifen injection

	C_T *Pycr2*	G Mean	ΔC_T	ΔC_T Mean	$\Delta\Delta C_T$	Fold Change
FNA	33.80	31.07	2.73	1.62	-0.1	1.07
FNB	32.87	30.58	2.29			
FNC	33.26	33.40	-0.14			
FDA	35.87	34.31	1.56	1.52		
FDB	36.91	32.95	3.96			
FDC	35.31	36.25	-0.94			

Table 8.12. C_T Values and fold of change in *Pycr2* mRNA level in mice males after one week of tamoxifen injection

	C_T *Pycr2*	G Mean	ΔC_T	ΔC_T Mean	$\Delta\Delta C_T$	Fold Change
MNA	31.66	32.32	-0.66	-0.83	-0.05	1.03
MNB	30.4	32.90	-2.5			
MNC	31.14	30.47	0.67			
MDA	33.49	35.96	-2.47	-0.88		
MDB	34.41	35.01	-0.6			
MDC	34.02	33.60	0.42			

Table 8.13. C_T Values and fold of change in *Pycr2* mRNA level in mice females after three days of tamoxifen injection

	C_T *Pycr2*	G Mean	ΔC_T	ΔC_T Mean	$\Delta\Delta C_T$	Fold Change
FNA	31.28	30.33	0.95	- 0.21	0.16	0.89
FNB	31.43	30.95	0.48			
FNC	32.62	34.68	-2.06			
FDA	33.5	31.76	1.74	- 0.04		
FDB	32.03	32.22	-0.19			
FDC	32.59	34.27	-1.68			

Table 8.14. C_T Values and fold of change in *Pycr1* mRNA level in mice males after three days of tamoxifen injection

	C_T *Pycr2*	G Mean	ΔC_T	ΔC_T Mean	$\Delta\Delta C_T$	Fold Change
MNA	31.11	29.67	1.44	-0.30	0.03	0.97
MNB	31.91	31.91	0			
MNC	32.77	35.13	-2.36			
MDA	30.67	30.33	0.34	-0.27		
MDB	30.76	30.39	0.37			
MDC	31.91	33.45	-1.54			

Table 8.15. C_T Values and fold of change in *Pycrl* mRNA level in mice females after two weeks of tamoxifen injection

	C_T *Pycrl*	G Mean	ΔC_T	ΔC_T Mean	$\Delta\Delta C_T$	Fold Change
FNA	31.75	31.04	0.71	-0.25	0	1
FNB	31.81	31.68	0.13			
FNC	32.04	33.65	-1.62			
FDA	33.45	34.20	-0.75	-0.25		
FDB	33.5	34.09	-0.59			
FDC	36.42	35.85	0.57			

Table 8.16. C_T Values and fold of change in *Pycrl* mRNA level in mice males after two weeks of tamoxifen injection

	C_T *Pycrl*	G Mean	ΔC_T	ΔC_T Mean	$\Delta\Delta C_T$	Fold Change
MNA	34.15	32.92	1.23	1.32	-0.01	1
MNB	34.51	33.10	1.41			
MDA	34.68	33.98	0.70	1.31		
MDB	35.89	33.91	1.98			
MDC	36.50	35.25	1.25			

Table 8.17. C_T Values and fold of change in *Pycrl* mRNA level in mice females after one week of tamoxifen injection

	C_T *Pycrl*	G Mean	ΔC_T	ΔC_T Mean	$\Delta\Delta C_T$	Fold Change
FNA	31.98	31.07	0.91	1.22	0.03	0.97
FNB	32.19	30.58	1.61			
FNC	34.55	33.40	1.15			
FDA	34.69	34.31	0.38	1.25		
FDB	35.78	32.95	2.83			
FDC	36.8	36.25	0.55			

Table 8.18. C_T Values and fold of change in *Pycrl* mRNA level in mice males after one week of tamoxifen injection

	C_T *Pycrl*	G Mean	ΔC_T	ΔC_T Mean	$\Delta\Delta C_T$	Fold Change
MNA	32.87	32.32	0.55	1.64	-0.13	1.09
MNB	33.89	32.90	0.99			
MNC	33.86	30.47	3.39			
MDA	36.48	35.96	0.52	1.51		
MDB	35.8	35.01	0.79			
MDC	36.82	33.60	3.22			

Table 8.19. C_T Values and fold of change in *Pycrl* mRNA level in mice females after three days of tamoxifen injection

	C_T *Pycrl*	G Mean	ΔC_T	ΔC_T Mean	$\Delta\Delta C_T$	Fold Change
FNA	32.6	30.33	2.27	2.03	-0.07	1.05
FNB	33.82	30.95	2.87			
FNC	35.63	34.68	0.95			
FDA	33.8	31.76	2.04	1.95		
FDB	34.13	32.22	1.91			
FDC	36.18	34.27	1.91			

Table 8.20. C_T Values and fold of change in *Pycrl* mRNA level in mice males after three days of tamoxifen injection

	C_T *Pycrl*	G Mean	ΔC_T	ΔC_T Mean	$\Delta\Delta C_T$	Fold Change
MNA	30.66	29.67	0.99	1	0.1	0.92
MNB	32.25	31.91	0.34			
MNC	36.8	35.13	1.67			
MDA	31.28	30.33	0.95	1.1		
MDB	31.52	30.39	1.13			
MDC	34.69	33.45	1.24			

Table 8.21 C_T Values and fold of change in *Prodh*/*Pox* mRNA level in mice females after two weeks of tamoxifen injection

	C_T *Prodh*/*Pox*	G Mean	ΔC_T	ΔC_T Mean	$\Delta\Delta C_T$	Fold Change
FNA	31.60	31.04	0.56	1.30	-0.23	1.17
FNB	33.28	31.68	1.60			
FNC	35.40	33.65	1.75			
FDA	34.91	34.20	0.71	1.07		
FDB	35.86	34.09	1.77			
FDC	36.58	35.85	0.73			

Table 8.22. C_T Values and fold of change in *Prodh*/*Pox* mRNA level in mice males after two weeks of tamoxifen injection

	C_T *Prodh*/*Pox*	G Mean	ΔC_T	ΔC_T Mean	$\Delta\Delta C_T$	Fold Change
MNA	32.55	32.92	-0.37	0.21	-0.03	1.02
MNB	33.9	33.10	0.80			
MDA	32.13	33.98	-1.85	0.18		
MDB	35.69	33.91	1.78			
MDC	35.86	35.25	0.61			

Table 8.23. C_T Values and fold of change in *Prodh*/*Pox* mRNA level in mice females after one week of tamoxifen injection

	C_T *Prodh*/*Pox*	G Mean	ΔC_T	ΔC_T Mean	$\Delta\Delta C_T$	Fold Change
FNA	30.84	31.07	-0.23	0.59	0	1
FNB	33.68	30.58	3.1			
FNC	32.31	33.40	-1.09			
FDA	33.95	34.31	-0.36	0.59		
FDB	35.18	32.95	2.23			
FDC	36.17	36.25	-0.08			

Table 8.24. C_T Values and fold of change in *Prodh*/*Pox* mRNA level in mice males after one week of tamoxifen injection

	C_T *Prodh*/*Pox*	G Mean	ΔC_T	ΔC_T Mean	$\Delta\Delta C_T$	Fold Change
MNA	31.98	32.32	-0.34	0.37	-0.05	1.03
MNB	32.88	32.90	-0.02			
MNC	31.95	30.47	1.48			
MDA	35.41	35.96	-0.55	0.32		
MDB	34.54	35.01	-0.47			
MDC	35.58	33.6	1.98			

Table 8.25. C_T Values and fold of change in *Prodh*/*Pox* mRNA level in mice females after three days of tamoxifen injection

	C_T *Prodh*/*Pox*	G Mean	ΔC_T	ΔC_T Mean	$\Delta\Delta C_T$	Fold Change
FNA	33.09	30.33	2.76	1.53	-0.67	1.59
FNB	33.14	30.95	2.19			
FNC	34.34	34.68	-0.34			
FDA	32.44	31.76	0.68	0.86		
FDB	33.69	32.22	1.47			
FDC	34.72	34.27	0.45			

Table 8.26. C_T Values and fold of change in *Prodh*/*Pox* mRNA level in mice males after three days of tamoxifen injection

	C_T *Prodh*/*Pox*	G Mean	ΔC_T	ΔC_T Mean	$\Delta\Delta C_T$	Fold Change
MNA	30.87	29.67	1.2	0.77	-0.2	1.15
MNB	32.62	31.91	0.71			
MNC	35.55	35.13	0.42			
MDA	30.94	30.33	0.61	0.57		
MDB	31.33	30.39	0.94			
MDC	33.62	33.45	0.17			

Table 8.27. The geometric mean values of *Pop4* and *Efnb2* housekeeping gene in mice females at two weeks' time course

	C_T*Pop4*	C_T*Efnb2*	G Mean
FNA	31.85	30.26	31.04
FNB	32.29	31.09	31.68
FNC	34.44	32.88	33.65
FDA	35.24	33.21	34.20
FDB	35.39	32.84	34.09
FDC	36.79	34.95	35.85

Table 8.28. The geometric mean values of *Pop4* and *Efnb2* housekeeping gene in mice males at two weeks' time course

	C_T*Pop4*	C_T*Efnb2*	G Mean
MNA	33.74	32.12	32.92
MNB	33.51	32.69	33.10
MDA	34.17	33.79	33.98
MDB	34.51	33.33	33.91
MDC	35.72	34.79	35.25

Table 8.29. The geometric mean values of *Pop4* and *Efnb2* housekeeping gene in mice females at one week time course

	C_T *Pop4*	C_T*Efnb2*	G Mean
FNA	30.85	31.29	31.07
FNB	30.48	30.69	30.58
FNC	33.28	33.52	33.40
FDA	34.49	34.13	34.31
FDB	32.77	33.13	32.95
FDC	36.64	35.87	36.25

Table 8.30. The geometric mean values of *Pop4* and *Efnb2* housekeeping gene in mice males at one week time course

	C_T*Pop4*	C_T*Efnb2*	G Mean
MNA	34.19	30.55	32.32
MNB	33.65	32.18	32.90
MNC	29.76	31.19	30.47
MDA	38.12	33.93	35.96
MDB	37.51	32.67	35.01
MDC	38.77	29.12	33.60

Table 8.31. The geometric mean values of *Pop4* and *Efnb2* housekeeping gene in mice females at three days' time course

	C_T*Pop4*	C_T*Efnb2*	G Mean
FNA	31.08	29.60	30.33
FNB	31.77	30.14	30.95
FNC	34.61	34.75	34.68
FDA	32.23	31.30	31.76
FDB	32.76	31.68	32.22
FDC	34.63	33.92	34.27

Table 8.32. The geometric mean values of *Pop4* and *Efnb2* housekeeping gene in mice males at three days' time course

	C_T*Pop4*	C_T*Efnb2*	G Mean
MNA	29.19	30.16	29.67
MNB	31.24	32.61	31.91
MNC	35.53	34.74	35.13
MDA	29.70	30.96	30.33
MDB	30.31	30.47	30.39
MDC	33.10	33.81	33.45